Dissertation

Submitted to the
Combined Faculty of Mathematics,
Engineering and Natural Sciences
Heidelberg University, Germany
for the degree of
Doctor of Natural Sciences (Dr. rer. nat.)

presented by
M. Sc. Mina Ebrahimi
Oral examination: February 07th, 2025

Folate-Conjugated Fluorescent Probes for Enhanced Selective Labelling of Cancer Cells

Referee: Prof. Dr. Roland Krämer

Referee: Prof. Dr. Peter Comba

I would like to express my gratitude to Prof. Dr. Krämer for proposing such a stimulating research topic and for his continuous support and guidance throughout my studies. His valuable insights and encouragement were decisive in the completion of this work.

The experimental studies for this work were conducted between February 2021 and October 2024 in the research group of Prof. Dr. R. Krämer at the Institute of Inorganic Chemistry, Heidelberg University.

Abstract

This study focuses on creating enhanced folate-conjugated fluorescent probes designed to target folate receptors, such as FRα, which are overexpressed in various cancers, including ovarian, breast, and lung. Such probes play a crucial role in fluorescence-guided surgery, a technique that enhances tumor visibility during operations. By improving tumor visualization, surgeons can more accurately remove cancerous tissue while preserving healthy structures, thereby improving cancer treatment outcomes.

In the first probe type, the dye fluorescein was coupled to folate using an O-aminoserine linker for a facile oxime click reaction. Next, we synthesized probes with a disulfide linker that respond to elevated glutathione levels in cancer cells by disulfide cleavage, facilitating targeted fluorophore release and resulting in notable fluorescence enhancement within the cells. Finally, we prepared probes with very short linkers via the direct coupling of folate to 5- and 6-aminofluorescein.

The photophysical properties and photostability of these probes were thoroughly evaluated. Cellular experiments demonstrated cancer-specific targeting, with a very high fluorescence intensity observed in cancerous (HeLa) cells compared to very low fluorescence in non-cancerous HDFa cells. Notably, the direct coupling of folic acid to 5-aminofluorescein resulted in a probe that displays particularly strong quenching in biological media if not bound to cancer cells, a desirable feature for reducing the signal-to-noise ratio in imaging applications. Furthermore, confocal microscopy demonstrated the effectiveness of the synthesized probes, achieving high-quality visualization of cancer cells and highlighting their potential for further preclinical evaluation in fluorescence-guided surgery.

Kurzzusammenfassung

Diese Studie konzentriert sich auf die Entwicklung optimierter Fluoreszenzsonden, die mit Folat konjugiert sind. Ziel ist das spezifische Targeting von Folat-Rezeptoren wie FRα die in mehreren Krebsarten (z.B. Eierstock, Brust, Lunge) überexprimiert sind. Diese Sonden spielen eine entscheidende Rolle bei der fluoreszenzgestützten Chirurgie, einer Methodik zur Optimierung der intraoperativen Tumorvisualisierung. Durch die bessere Sichtbarkeit des Tumors können Chirurgen Krebsgewebe präziser entfernen und gleichzeitig gesunde Strukturen erhalten, wodurch das Behandlungsergebnis verbessert werden.

Beim ersten Sondentyp wurde der Farbstoff Fluorescein mit Hilfe eines O-Aminoserin-Linkers über eine einfache Oxim-Klick-Reaktion an Folat gekoppelt. Anschließend synthetisierten wir Sonden mit einem Disulfid-Linker, der auf erhöhte Glutathion-Konzentrationen in Krebszellen anspricht. Durch die Spaltung der Disulfide wird der Fluorophor gezielt freigesetzt, was zu einer deutlichen Verstärkung der Fluoreszenz in den Zellen führt. Schließlich haben wir Sonden mit sehr kurzen Linkern durch die direkte Kopplung von Folat an 5- und 6-Aminofluorescein hergestellt.

Die photophysikalischen Eigenschaften und die Photostabilität der Sonden wurden eingehend untersucht. Zellbasierte Experimente zeigten eine stark erhöhte Fluoreszenzintensität in Krebszellen (HeLa) im Vergleich zu einer sehr geringen Fluoreszenz in gesunden Zellen (HDFa). Insbesondere die direkte Kopplung von Folsäure an 5-Aminofluorescein resultierte in einer Sonde, die in biologischen Medien eine starke Fluoreszenzlöschung zeigt, solange sie nicht an Krebszellen gebunden ist. Diese vorteilhafte Eigenschaft reduziert das Signal-Rausch-Verhältnis bei bildgebenden Anwendungen. Konfokale Mikroskopieaufnahmen bestätigen die Effizienz der synthetisierten Sonden bei der Visualisierung von Tumorzellen und unterstreichen deren Potenzial für weiterführende präklinische Untersuchungen im Kontext der fluoreszenzgestützten Chirurgie.

Contents

List of Abbreviations

βAla - Beta Alanine

5AF - 5-Aminofluorescein

6AF - 6-Aminofluorescein

α-FBA - Alpha Fluorobenzylamine

βAla-5AF - Beta Alanine conjugated to 5-Aminofluorescein

BP - Blood Plasma

CBM - Communication Bus Module

COSY - Correlation Spectroscopy

CTO - Column Temperature Oven

DAPI - 4',6-Diamidino-2-Phenylindole

DIPEA - N,N-Diisopropylethylamine

DMEM - Dulbecco's Modified Eagle's Medium

DMF - Dimethylformamide

DMSO - Dimethyl Sulfoxide

DMTMM - 4-(4,6-Dimethoxy-1,3,5-triazin-2-yl)4-methylmorpholinium chloride

DGU - Degasser Unit

EC17 - Folate-FITC (Fluorescent Probe)

EDTA - Ethylenediaminetetraacetic acid

EMEM - Eagle’s Minimal Essential Medium

ESI - Electrospray Ionization

FA - Folic Acid

FBA - 4-Fluorobenzylamine

FCS - Fetal Calf Serum

FDA - Food and Drug Administration

FDAc - Fluorescein Diacetate

FITC - Fluorescein Isothiocyanate

FP - Fluorescent Probe

FR - Folate Receptor

FRα - Folate Receptor Alpha

FRβ - Folate Receptor Beta

FRγ - Folate Receptor Gamma

FRσ - Folate Receptor Sigma

GSH - Glutathione

HDFa - Human Dermal Fibroblast

HeLa - Human Epithelial Adenocarcinoma Cell Line

HMBC - Heteronuclear Multiple Bond Correlation

HPLC - High-Performance Liquid Chromatography

HR-ESI - High-Resolution Electrospray Ionization

HSQC - Heteronuclear Single Quantum Coherence

LC - Liquid Chromatography

MALDI-TOF - Matrix-Assisted Laser Desorption/Ionization Time of Flight

MeCN - Acetonitrile

mL – Mililiter

mg - Miligram

MS - Mass Spectrometry

nM- Nanomolar

NMR - Nuclear Magnetic Resonance

OTL38 – Pafolacianin (Folate-based Near-Infrared Fluorescent Probe)

PBS - Phosphate Buffered Saline

PET - Positron Emission Tomography

PMMA - Polymethylmethacrylate

RPMI - Roswell Park Memorial Institute Medium

RP-HPLC - Reverse-Phase High-Performance Liquid Chromatography

s, d, t, q, m, br - Singlet, Doublet, Triplet, Quartet, Multiplet, Broad (NMR signal multiplicities)

SPD - Spectral Detector

5 (6)-TAMRA – 5 (6)-Carboxytetramethylrhodamine

TBTU - O-(Benzotriazol-1-yl)-N,N,N',N'-Tetramethyluronium Tetrafluoroborate

TEAA - Triethylammonium Acetate

TEAB - Triethylammonium Bicarbonate

TFA - Trifluoroacetic Acid

UV/Vis - Ultraviolet-Visible Spectroscopy

1 Introduction

1.1 Folate receptors as targets for fluorescent probes in cancer imaging

Folate-conjugated fluorescent probes are innovative compounds designed for use in fluorescence-guided surgery (FGS), offering immense potential to develop tumor resection procedures. These probes exploit the overexpression of folate receptors on the surface of various cancer cells to achieve targeted imaging. By conjugating folate, a vitamin essential for nucleotide synthesis, with fluorescent dyes, these probes selectively bind to cancer cells, providing highly specific labeling for visualization under fluorescence imaging systems. [1-5]

Folate receptors (FRα, FRβ, FRγ, and FRσ) are cysteine-rich cell-surface glycoproteins that bind folate with high affinity, facilitating folate cellular uptake. Due to the increased demand for folate, these receptors are overexpressed in cancer cells, including those of ovarian, breast, lung, and kidney cancers. Folate is essential for DNA synthesis and cell division, processes that are particularly active in rapidly proliferating cancer cells. The overexpression of folate receptors allows cancer cells to efficiently uptake folic acid, supporting their growth and survival. The over expression of folate receptors, especially FRα, makes them an excellent target for selective cancer cell imaging and targeted drug delivery.[6-8]

1.1.1 Folic acid and its structural implications in probe development

Folic acid, also known as vitamin B9, is essential for numerous functions, including DNA synthesis and repair, cell division, and cell growth.[9-11] Its structural composition includes a pteridine ring, para-aminobenzoic acid (PABA), and a glutamic acid residue, **Figure 1**. This unique structure allows folic acid to form regioisomers through its α- and γ-carboxyl groups, which can be linked to other molecules, to create derivatives with varying properties.[12-14]

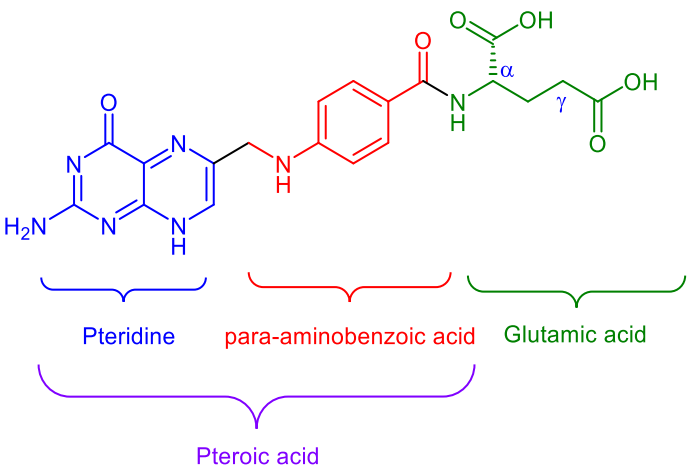

***Figure 1**: Chemical structure of folic acid*

In the study by Chen et al. in 2013, researchers explored the crystal structure of the human folate receptor alpha bound to folic acid.[15] This study offers important insights into how folates bind so strongly to their receptors. The researchers found that FRα has a round shape that is held together by eight disulfide bonds. It also features a deep, open pocket specifically designed to bind folic acid tightly. Within this pocket, the pteroate part of folic acid is compactly held, while the glutamate part is left exposed to the surrounding environment, **Figure 2**. This exposure allows the glutamate to connect with therapeutic agents without losing its binding strength.[15]

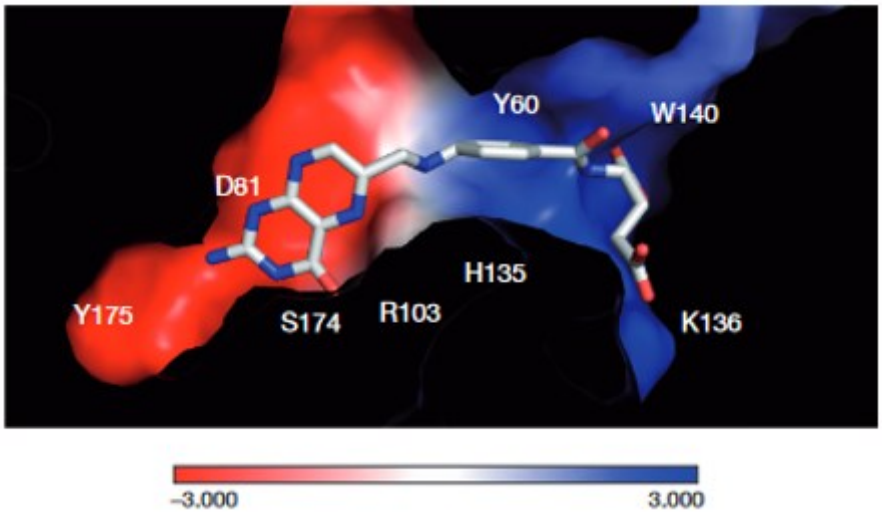

***Figure 2**: Charge distribution on the surface of the folate receptor α, focusing on the entrance to the ligand-binding pocket and the structure of folic acid inside the folate receptor packet. The carbon atoms in folic acid are colored grey, nitrogen atoms are blue, and oxygen atoms are red. The color-coded bar at the bottom indicates the electrostatic potential scale of the folate receptor ranging from -3 to +3 eV. Reproduced with permission from Springer Nature, copyright (2013).[15]*

Folic acid, as illustrated in **Figure 1**, has two carboxylic moieties that serve as potential conjugation sites for the coupling of various compounds such as drugs or fluorophores. These distinct coupling positions give rise to two regioisomers, designated as α and γ. Research by Chen et al. (2013) has elucidated the binding mechanism of folic acid to folate receptors through crystallographic analysis.[15] Their findings indicate that the pteroic acid moiety of folic acid occupies the receptor's binding pocket, while the glutamic acid portion remains unbound. This structural configuration suggests that conjugation at either the α or γ position should not significantly alter the binding affinity of folic acid derivatives to the folate receptors.

1.1.2 Evaluating the binding affinity of α- and γ-folate conjugates

Bettio et al. [16] conducted a comprehensive study comparing the binding affinities of α- and γ-folic acid conjugated to 4-fluorobenzylamine (FBA) with those of unmodified folic acid, using competition binding assays with ^{3}H-labeled folic acid as the reference standard, **Figure 3**. This study systematically explored the differential binding characteristics between folate receptors and the α- and γ-carboxyl groups of folic acid when these functional groups are covalently linked to a prosthetic moiety, such as FBA.[16] Quantitative analysis revealed that both the α- and γ-isomers exhibited comparable binding affinities to the folate receptor, with no statistically significant divergence observed between the two regioisomers. The in vitro binding assays determined the affinity constants (Kd) for α- and γ-FBA-folates to be 71 and 62 nmol/L, respectively, in comparison to 41 nmol/L for unmodified folic acid. This similarity in binding affinity suggests that the conjugation of FBA to either the α- or γ-carboxyl group does not substantially bother the ligand-receptor interaction.[16]

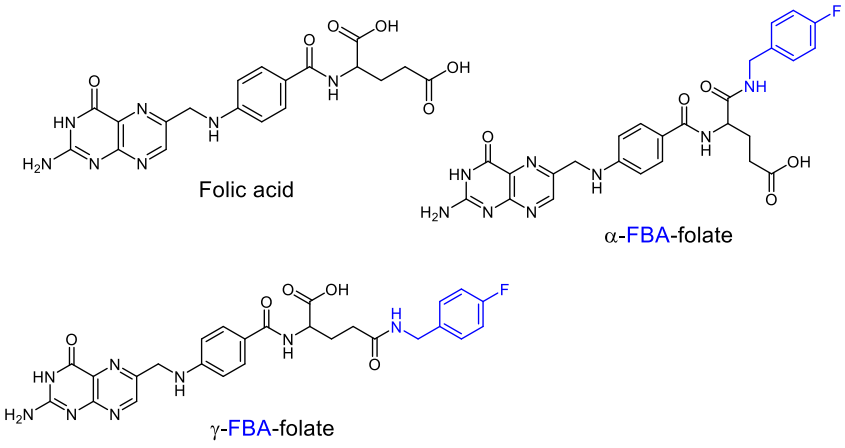

***Figure 3**: Chemical structure of native folic acid, γ-FBA-folate and α-FBA folate*

In the subsequent phase of the study by Bettio et al., folic acid was conjugated to ^{18}F-labelled 4-fluorobenzylamine (FBA) for positron emission tomography imaging applications.[16] In vivo studies demonstrated that both α- and γ-isomers effectively targeted folate receptor-positive tumors, resulting in significant uptake within malignant cells. While minor differences in regioisomeric behavior were observed, with a slight predominance of the γ-isomer, both conjugates proved efficacious for PET imaging due to their comparable affinity for the folate receptor. These findings imply that the chemical modification of folic acid at either the α- or γ-carboxyl position does not inhibit receptor-mediated endocytosis or overall tumor accumulation. Consequently, both derivatives represent possible candidates for targeted molecular imaging of folate receptor-positive tumors.

1.2 Folate receptor-mediated endocytosis for targeted drug delivery in cancer therapy

The binding affinity of folic acid to folate receptors is used also for the purpose of tumor-targeted drug delivery systems. The folate receptor facilitates the uptake of folate into cells through a highly specific and efficient process known as receptor-mediated endocytosis.[1, 17, 18] The folate of the folate-conjugated drugs on the cell surface binds strongly to the folate receptor, particularly the FRα. When the folate binds to receptor, the complex is taken into the cell through a process where the cell membrane folds inward, creating a pocket that eventually separates to form an early endosome inside the cell, as shown in **Figure 4**. Inside this endosome, the acidic environment induces a conformational change in the receptor, causing the folate to detach from the receptor. The late endosome then fuses with a lysosome, where the enzymatic activity leads to the degradation of the conjugate and release of the drug into the cytosol. The free drug can then exert its therapeutic effect, typically leading to cell death in cancerous cells. Meanwhile, the folate receptor is recycled back to the cell surface, ready to mediate further rounds of folate conjugated drug uptake. This efficient recycling and high affinity for folate make the folate receptor a potent target for delivering therapeutics specifically to cancer cells.[19, 20]

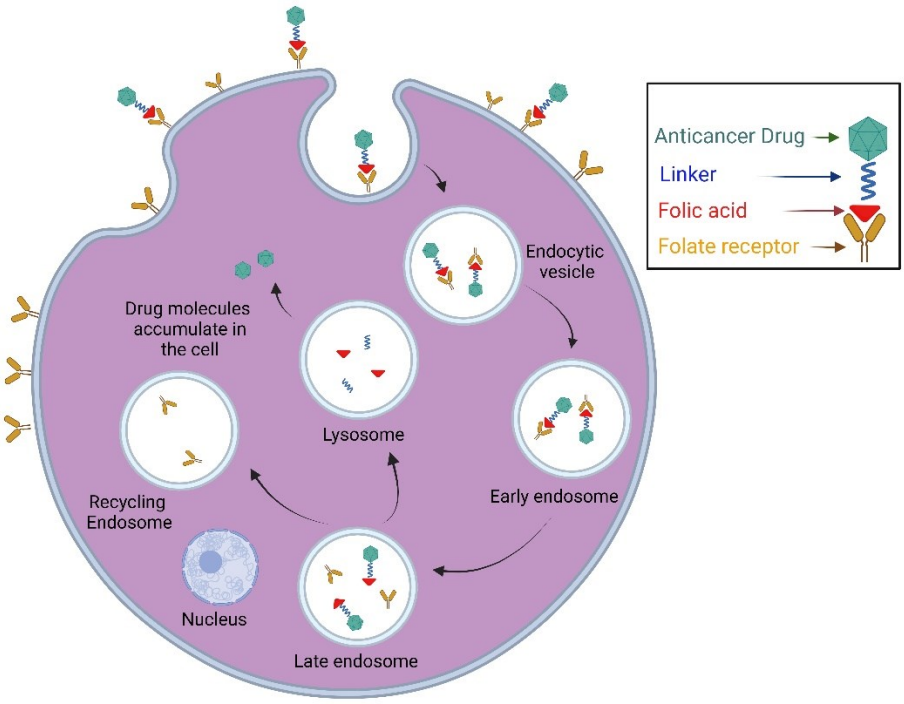

***Figure 4**: Receptor-mediated endocytosis of a folate conjugated drug: Binding to FRα forms an early endosome. pH drop releases the drug, which is then degraded in the lysosome. Folate receptors are recycled to the surface.*

1.3 Folate-conjugated fluorescent probes for cancer detection

Folate-conjugated fluorescent probes have become invaluable tools in the detection and surgical treatment of cancers, particularly those that overexpress the folate receptor alpha (FRα).

These probes are designed to target and bind specifically to cancer cells with high levels of folate receptors α, a receptor commonly overexpressed in various malignancies such as ovarian, breast, and lung cancers. The conjugation of folate to fluorescent dyes allows for precise imaging of tumor tissues, enhancing the visibility of cancerous areas during surgery. The schematic representation of ovarian cancer targeting is illustrated in **Figure 5**.

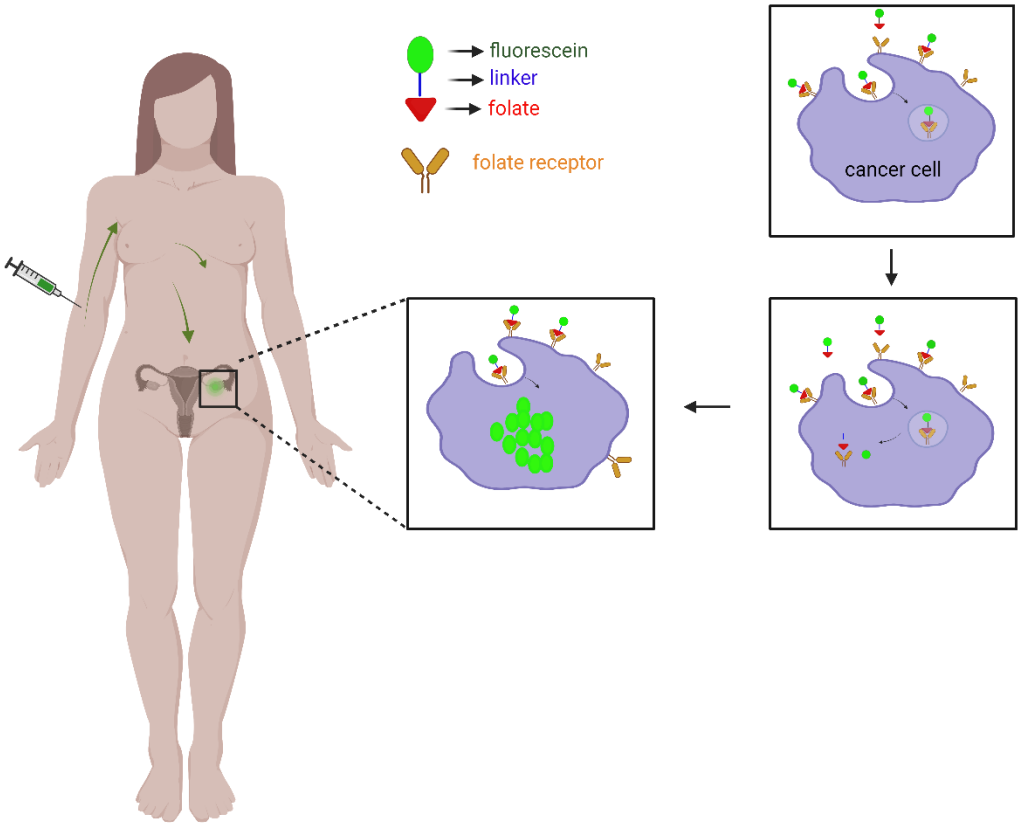

***Figure 5**: Schematic representation of ovarian cancer targeting: Folate-conjugated fluorescein selectively binds to FR-α receptors on cancer cells, facilitating internalization and delivering the fluorescent probe into the cytoplasm.*

Two important examples of folate-conjugated fluorescent probes are folate-FITC and OTL38. These probes have shown great promise in improving the detection of tumors and ensuring complete removal of cancerous cells.

Folate-FITC, or EC17, is a folate-conjugated fluorescent probe currently undergoing phase 2 clinical trials for Food and Drug Administration (FDA) approval. This probe specifically targets cancers that express folate receptor alpha (FRα). EC17 is a folate linked to fluorescein isothiocyanate (FITC), which provides a high tumor-to-background ratio, **Figure 6**. This characteristic enhances the detection of small tumor deposits during fluorescence-guided surgery.[21, 22]

However, the limitations of EC17 became evident during phase 2 clinical trials. At higher dosages, some patients experienced mild abdominal side effects. Furthermore, the probe's visible emission at 520 nm compromised its penetration depth, presenting

significant challenges. Additionally, nonspecific binding of the probe to collagen-rich tissues led to autofluorescence, resulting in false-positive lesions.[23-25]

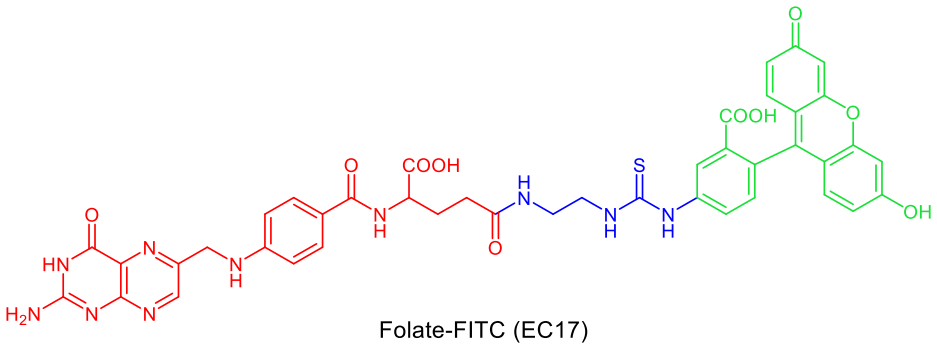

***Figure 6**: Chemical structure of folate-FITC (EC17).*

OTL38, another significant advancement in the field of folate-conjugated fluorescent probes has completed phase III clinical trials and received FDA approval in November 2021 for use in fluorescence-guided surgery for ovarian cancer. This probe consists of a folate analog linked to a near-infrared fluorescent dye, **Figure 7**, allowing deeper tissue penetration and reduced autofluorescence from biological tissues. Clinical trials have shown OTL38's effectiveness in identifying FRα-positive tumors in various cancers, including ovarian, lung, stomach, and kidney. The probe aids in achieving more precise resections by clearly distinguishing malignant tissues from healthy ones, thus potentially reducing residual disease and recurrence rates.[23, 26]

Despite its advantages, OTL38 has some limitations observed during clinical trials. Patients reported mild abdominal side effects, particularly at higher dosages. There were also cases of nonspecific binding or uptake in non-target tissues, leading to background fluorescence that could complicate imaging results. Additionally, the cost of production may limit its widespread use. The variability in achieving high tumor-to-background ratios across different tissue types and patient conditions also presents a challenge. Nonetheless, the overall clinical success and FDA approval of OTL38 underscore its importance and utility in improving surgical outcomes for cancer patients.[27]

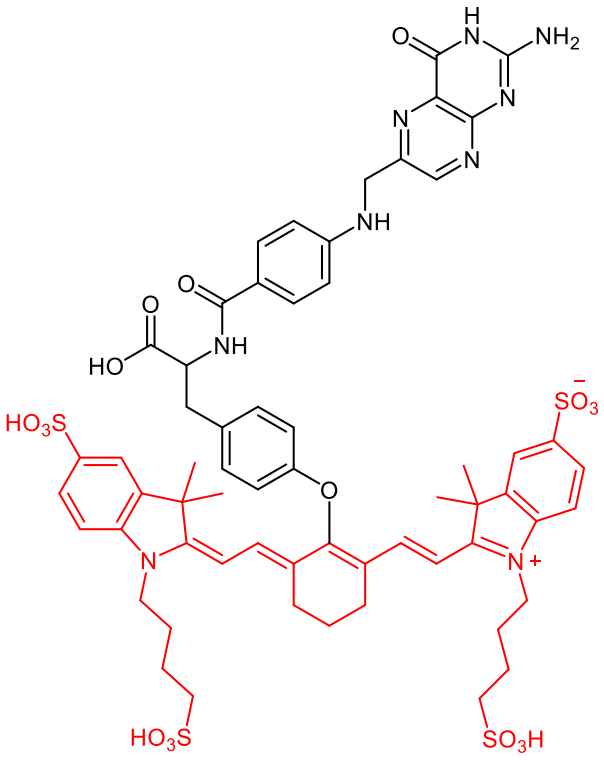

OTL38

***Figure 7**: Chemical structure of OTL38*

1.4 Folate-conjugated fluorescent probes with disulfide linkers in cancer imaging and therapy

Folate-conjugated fluorescent probes with disulfide linkers represent a significant advancement in targeted cancer imaging and diagnosis. This innovative approach combines the specificity of folate receptor targeting with the controlled release mechanism of disulfide bonds, offering enhanced precision in tumor detection and visualization.[28, 29] The incorporation of disulfide linkers in these probes introduces a smart release mechanism that enhances their effectiveness. In the bloodstream, the disulfide bond remains intact, preventing early release of the fluorophore. However, upon internalization into cancer cells, the higher concentration of reducing agents, such as glutathione, cleaves the disulfide bond, resulting in the specific release of the fluorescent probe within the target cells.[28-33]

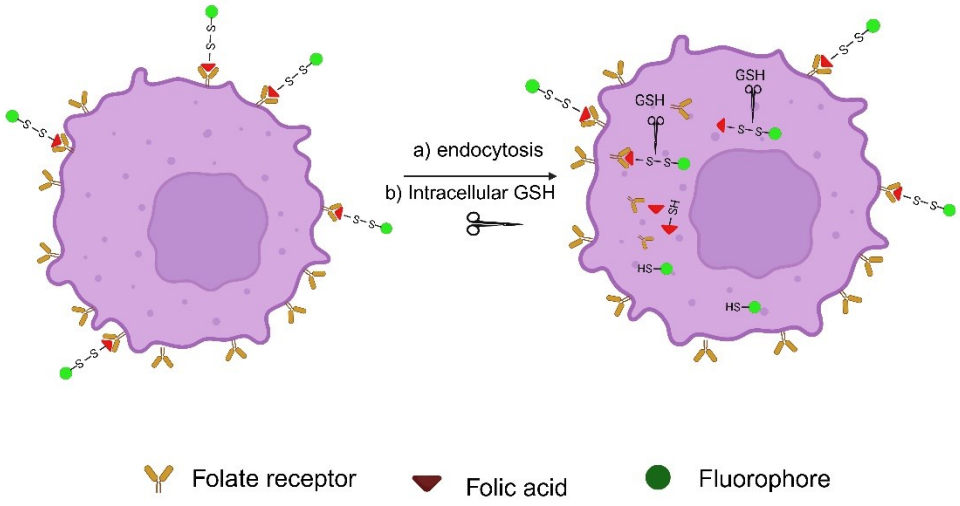

***Figure 8**: Illustration of folic acid-conjugated fluorophore targeting through the folate receptor pathway. Folic acid binds to folate receptors on the cell surface, leading to receptor-mediated endocytosis. Inside the cell, glutathione (GSH) reduces the disulfide linker, releasing the attached fluorophore.*

1.5 Fluorescence

Fluorescence is a photophysical process in which specific molecules, known as fluorophores, absorb photons of light at a characteristic wavelength, causing their electrons to transition from the ground electronic state (S_0) to an excited singlet state (S_1, S_2, etc.). Following excitation, these molecules rapidly undergo vibrational relaxation, dissipating excess energy without emitting radiation and settling into the lowest vibrational level of the excited state within 10^{-13} seconds. The molecule can then return to the ground state by emitting a photon, a process known as fluorescence, which occurs on a timescale of 10^{-9} to 10^{-7} seconds, **Figure 9.** Additionally, the molecule may undergo internal conversion (IC), a non-radiative process in which it transitions between electronic states of the same spin multiplicity, typically from a higher excited singlet state (e.g., S_2) to a lower excited singlet state (e.g., S_1). Furthermore, the molecule can also experience intersystem crossing, a process where it converts from an excited singlet state to an excited triplet state (T_1) due to a spin state change, which can lead to phosphorescence if the molecule returns to the singlet ground state from the triplet state.[34, 35]

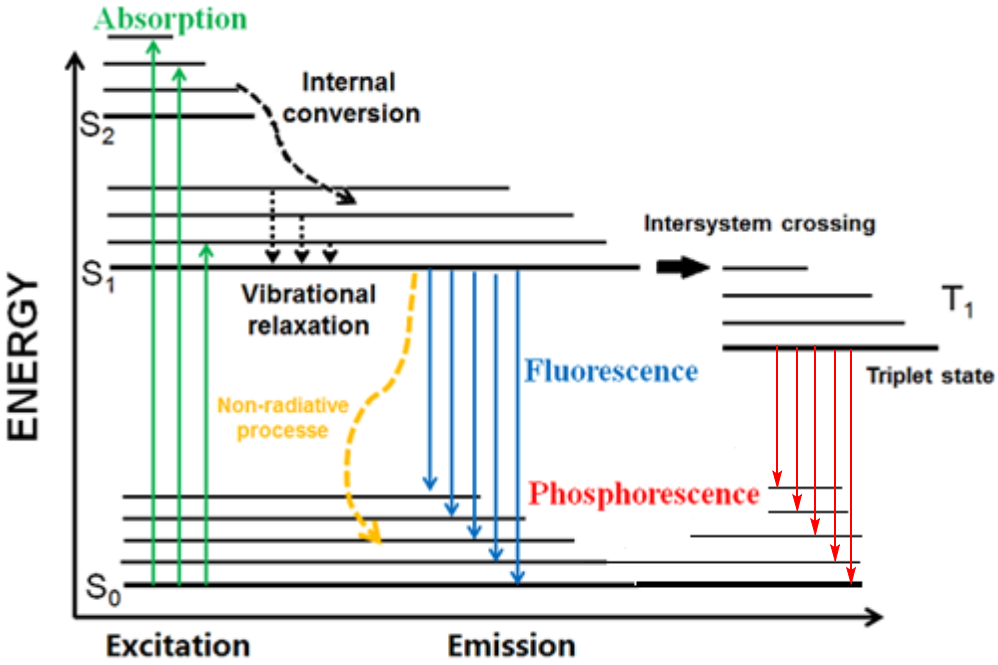

***Figure 9**: Jablonski diagram of fluorescence and phosphorescence.*[36]

The efficiency of the fluorescence process is described by the quantum yield, defined as the ratio of the number of photons emitted to the number of photons absorbed. Fluorescence quenching, on the other hand, refers to the process by which the fluorescence intensity of a fluorophore is decreased due to various interactions with other molecules or environmental factors. Quenching mechanisms, such as dynamic quenching, static quenching, Photoinduced Electron Transfer, and Förster Resonance Energy Transfer (FRET), reduce the number of photons emitted, thereby directly impacting the fluorescence quantum yield.[35]

When quenching occurs, the pathways for non-radiative decay are enhanced, resulting in a lower quantum yield. For instance, in dynamic quenching, collisions between the fluorophore and quencher increase non-radiative decay rates. In static quenching, the formation of non-fluorescent complexes reduces the number of fluorophores available to emit light. PET involves electron transfer that competes with fluorescence emission, and FRET transfers energy from a donor to an acceptor, reducing the donor's fluorescence output.[35]

1.6 Fluorophores for advanced biological imaging

Organic fluorophores are small, carbon-based molecules known for their fluorescence and versatility. They are widely used due to their ability to be easily conjugated to

different biomolecules, such as proteins, nucleic acids, and lipids. Common examples include fluorescein, rhodamine, and cyanine dyes, **Figure 10**. Organic fluorophores are preferred for their high quantum yield and relatively low toxicity, making them suitable for live-cell imaging. However, a major drawback of such organic fluorophores is photobleaching, the irreversible destruction of a fluorophore under prolonged light exposure, which decreases fluorescence intensity and compromises the accuracy of fluorescence-based measurements.[37, 38]

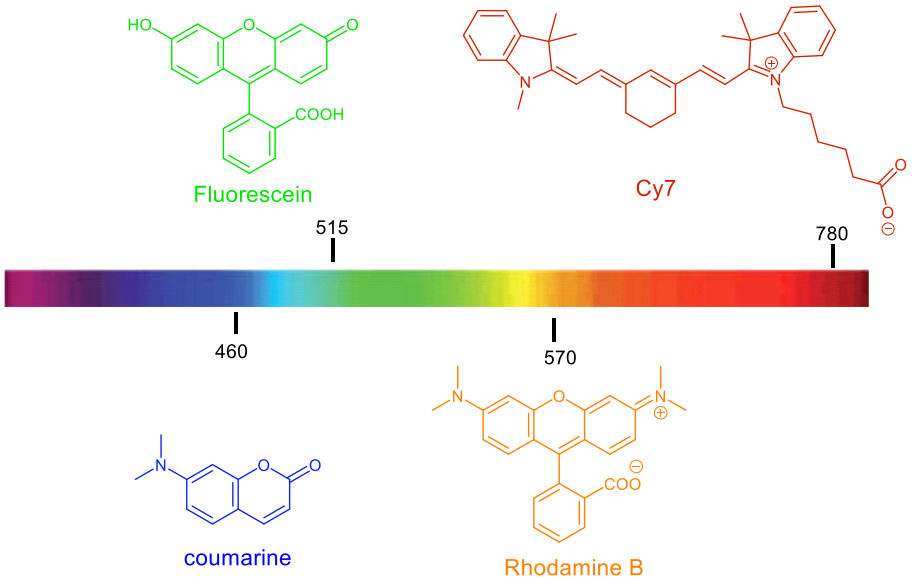

***Figure 10**: Emission regions and chemical structures of commonly used organic fluorophores.*

To overcome these limitations, scientists are developing new fluorescent dyes with enhanced photostability to mitigate photobleaching and extend imaging duration. New materials such as photostable organic fluorescent probes, photoswichable probes, and quantum dots which exhibit superior photostability and brightness, have been developed to overcome these problems, providing more reliable and long-term imaging.[37, 39-41]

Photostable organic fluorescent probes are designed to provide high photostability and brightness, making them ideal for longer lasting fluorescence signals and various demanding applications in biological and medical research. These probes, such as Alexa dyes, maintain their fluorescence intensity over extended periods, even under continuous illumination. Their high quantum yield ensures bright and clear signals, which are crucial for sensitive detection and quantification of biomolecules. However, they can be costly and may involve complex synthesis or conjugation procedures. The

chemical structure of Alexa dyes with the emission wavelength of 488 nm, 532 nm and 647 nm are illustrated in **Figure 11**.[42]

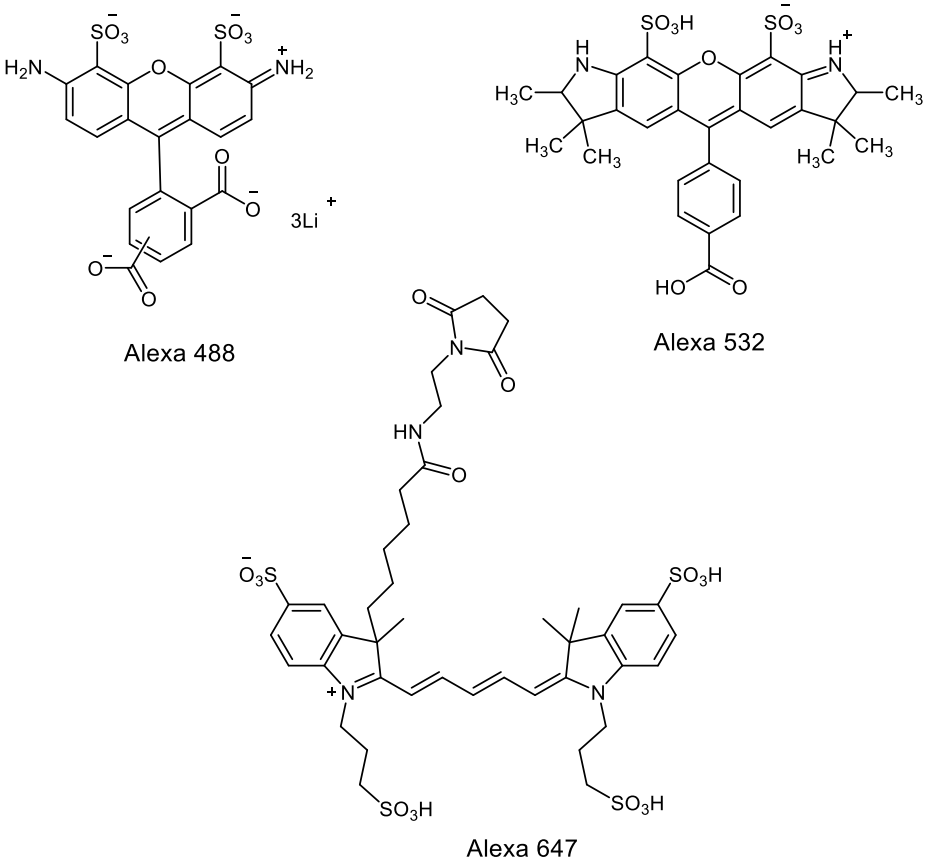

***Figure 11**: Chemical structure of Alexa dyes*

1.7 Photoswitchable probes

In recent years, the limitations of traditional organic fluorophores, particularly their susceptibility to photobleaching, have driven the development of more advanced fluorescent probes. Among these, photoswitchable dyes have emerged as a powerful tool in fluorescence microscopy, offering solutions to many of the challenges faced by conventional fluorophores. Photoswitchable fluorophores are characterized by their ability to switch reversibly between fluorescent and non-fluorescent states upon exposure to light of specific wavelengths. This unique property not only mitigates the issue of photobleaching but also enables super-resolution microscopy techniques. Methods such as Photoactivated Localization Microscopy (PALM), Stochastic Optical Reconstruction Microscopy (STORM), and Stimulated Emission Depletion Microscopy (STED) rely on the precise control of fluorophore activation or deactivation to achieve nanometer-scale resolution. While PALM and STORM utilize stochastic activation of

individual fluorophores, STED employs a fundamentally different mechanism by selectively deactivating excited fluorophores in a controlled manner using a depletion laser.[43, 44]

Several classes of photoswitchable dyes have been developed, each with distinct structures and properties. Diarylethenes switch between open and closed (non-fluorescent) forms upon irradiation with different wavelengths of light, **Figure 12**. Diarylethenes are known for their thermal stability, resistance to losing their character over multiple switching cycles, and rapid switching kinetics.[45, 46] Another class of photoswitchable dyes are spiropyran dyes. The spiropyran form is typically non-fluorescent, while the merocyanine form is fluorescent. This transformation is accompanied by a large spectral shift, making spiropyrans particularly useful for applications requiring distinct "on" and "off" states. Rhodamine spiroamides are another class of photoswitchable fluorophores that are highly valued in biological imaging due to their brightness, good photostability, and compatibility with living systems, **Figure 12**.[47-51]

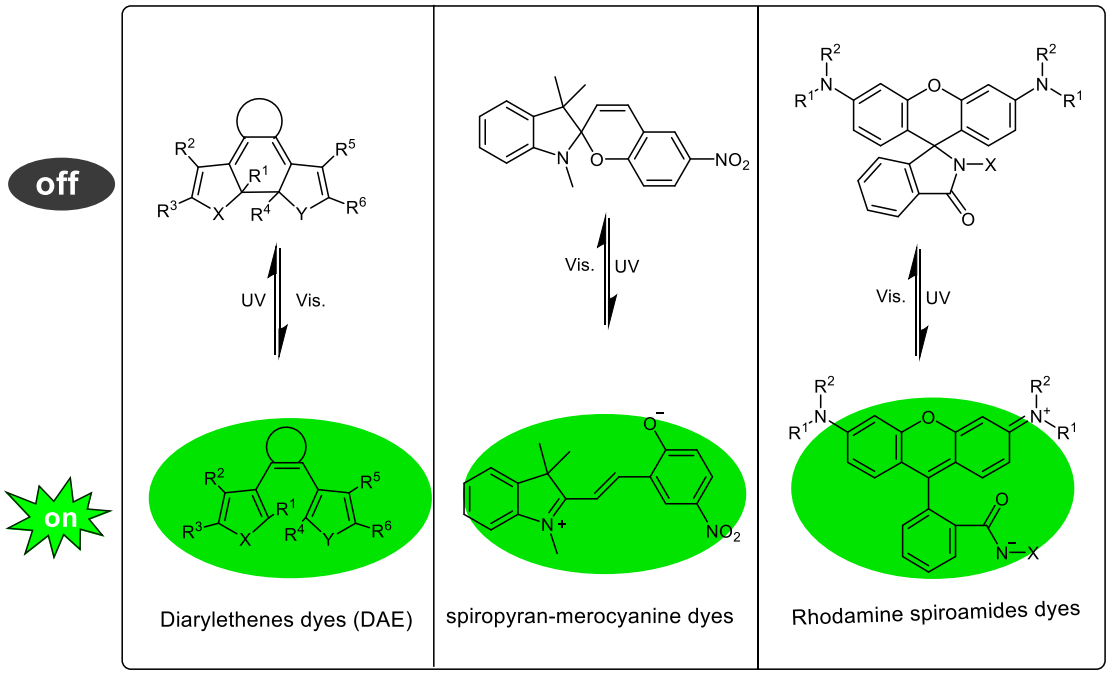

***Figure 12**: Chemical structures of photoswitchable dyes: Diarylethenes, Spiropyran-Merocyanines, and Rhodamine Spiroamides, exhibiting reversible isomerization under UV/Vis light with tunable optical properties*

1.7.1 Quantum Dots

Quantum dots (QDs) are nanoscale semiconductor particles that have emerged as powerful fluorescent probes in biological and medical research. Compared with organic dyes, QDs have strong fluorescence intensity, high stability, and strong resistance ability to photobleaching. Due to their broad absorption spectra and narrow, tunable emission spectra, QDs can be excited by a wide range of wavelengths while emitting highly specific colors. Such versatility enables a technique known as multiplexed imaging, where researchers can label and visualize multiple targets simultaneously using distinct colors. Despite their numerous advantages, QDs can pose significant limitations. Their relatively large size (10- 30 nm) can interfere with cellular processes, potentially altering the behavior of the molecules being tracked. High production costs and potential toxicity are the other limitations of quantum dots.[52-56]

2. Research Objectives

The primary objective of this study was to develop advanced folate-conjugated fluorescein probes that specifically target cancer cells overexpressing folate receptors for a potential use in fluorescence-guided surgery. A significant challenge in this work has been designing probes capable of achieving a high fluorescence contrast between cancerous cells and their microenvironment including non-cancerous cells. This requires strong intramolecular fluorescence quenching by the folate moiety when the probe is not bound to folate receptors, ensuring minimal signal in non-cancerous cells and biological fluids. However, upon binding to the folate receptors and internalization in cancer cells, the probe must show a sharp and substantial increase in fluorescence intensity, enabling precise imaging of tumor cells.

Along with this, simplifying the rather challenging synthetic process for the folate-conjugated fluorescein by reducing the complexity of the organic linker moiety was an important task. Long, complex linkers, used for example to improve solubility, can interfere with the fluorescence quenching efficiency of the folic acid on the fluorescein moiety. This reduces the probe’s desired ability to remain quenched before binding to folate receptors and internalization into cancer cells. By minimizing the linker (and ultimately creating "linker-free" probes directly from readily available precursors), we aimed to enhance the probe's quenching properties while ensuring the synthesis remains straightforward and efficient.

To evaluate the performance of the newly developed probes, the photophysical properties should be investigated in various media including biological fluids, and the labeling efficiency tested with folate-receptor overexpressing cancer cells and compared with non-cancerous cells. Folate-FITC (the conjugate between folate and fluorescein isothiocyanate) was used as a reference, since it is well-established in targeting cancer cells due to its ongoing use in clinical trials, making it an ideal standard for comparison.

.

3. Results and discussion

3.1 Fluorescent probe with O-aminoserine linker

3.1.1 Synthesis of fluorescent probe with O-aminoserine linker

In designing this novel fluorescent probe, we aimed to incorporate a negatively charged short linker between folate and the fluorophore. This approach aligns with previous findings from doctoral research in our group, which established that introducing negatively charged substituents in the linker region between folic acid and the fluorophore improves the probe's uptake efficiency.[57] However, it was also found that a larger or more complex linker reduces the quenching effect of the folate on the fluorophore.

For the synthesis of **FP 2**, we began by opening the ring of D-cycloserine and coupling it to the aldehyde group of fluorescein monoaldehyde via a straightforward oxime-click reaction. The amine group of **1** was then conjugated to folic acid through an amide coupling reaction using TBTU as the coupling reagent, as shown in **Figure 13**.

Purification was carried out using preparative RP-HPLC, yielding **FP 2** as a mixture of both γ and α isomers, **Figure 14**.

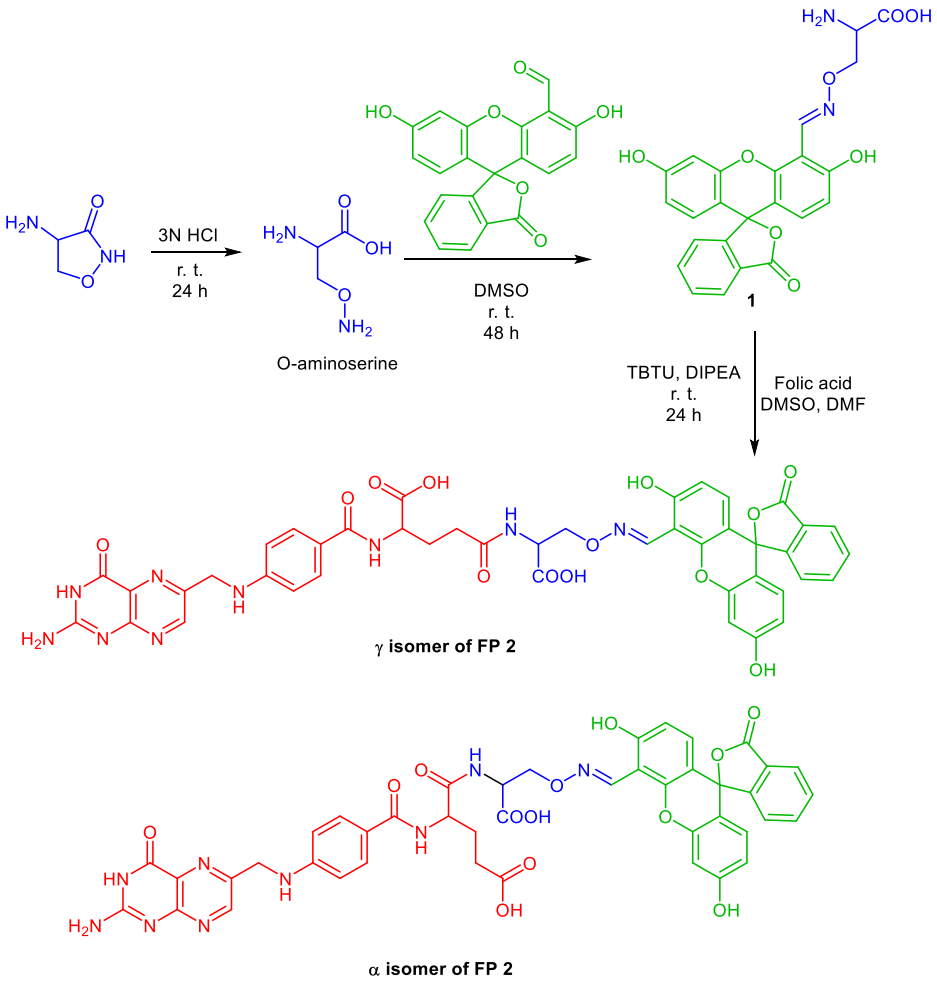

***Figure 13**: Schematic synthesis of FP 2*

Initially, we attempted to synthesize fluorescent probe **FP 2** by coupling D-cycloserine to folic acid, followed by ring-opening using 3 M HCl. The amide coupling of cycloserine to folic acid proceeded efficiently; however, the subsequent ring-opening with 3 M HCl did not proceed as expected.

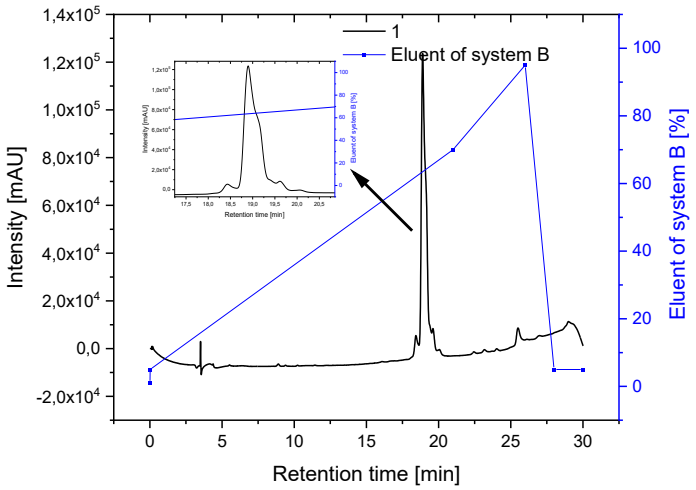

***Figure 14**: Chromatogram of the analytical HPLC of FP 2, showing a mixture of both isomers. The peak shoulder indicates the presence of the second isomer. The inset highlights a zoomed-in region of the main peak.*

3.1.2 Photophysical properties of FP 2

The photophysical properties of **FP 2** were evaluated and compared with those of folate-FITC and fluorescein. Folate-FITC, currently in phase 2 clinical trials for Food and Drug Administration (FDA) approval, served as a benchmark for evaluating our synthesized probes. All measurements were conducted in PBS (pH = 7.4) using 1 mL PMMA cuvettes. The maximum absorption (λ_{abs}) and emission (λ_{em}) wavelengths were recorded, allowing for the calculation of the Stokes shift, and the molar extinction coefficient (ε) was determined using the Lambert-Beer law.

The fluorescence quantum yield was determined using the comparative method, with fluorescein as the reference (φ_R = 0.85 in PBS).[58] In this method, the quantum yield is calculated from the slopes of the linear plots of integrated fluorescence intensity versus absorbance (m_{FP}). The slope of the linear fit for the reference fluorophore (m_R) and its quantum yield (φ_R) is used to calculate the quantum yield of the fluorescent probe (ϕ_{FP}) according to the equation:

$$\phi_{FP} = \phi_R \left(\frac{m_{FP}}{m_R}\right)\left(\frac{\eta_{FP}^2}{\eta_R^2}\right) \quad (1)$$

η_{FP} and η_R : refractive indices of the solvent for fluorescent probe and reference.

Table 1 summarizes the key photophysical parameters of **FP 2** compared to fluorescein and folate-FITC.

***Table 1**: Photophysical properties of 1 µM of FP 2, folate-FITC, and fluorescein in PBS (pH 7.4) using 1 mL PMMA cuvettes, with an excitation wavelength of 480 nm and detector voltage of 520 V.*

Compound	$\lambda_{max\ (Abs)}$[nm]	$\lambda_{max\ (Em)}$[nm]	Stokes shift [nm]	ε [M^{-1} cm^{-1}] 10^4	Quantum yield in PBS (pH=7.4)
Fluorescein	490	515	25	7.90	0.85
Folate-FITC	496	516	20	7.84	0.08
FP 2	501	525	20	7.84	0.04

The absorbance and emission spectra of **FP 2**, folate-FITC, and fluorescein are presented in **Figure 15**. As seen in the emission spectra, **FP 2** shows significant fluorescence quenching, with a residual fluorescence half of that of folate-FITC. This pronounced quenching is an advantageous characteristic of the fluorescent probes for fluorescence-guided surgery. Reduced background fluorescence in surrounding healthy tissues enhances the signal-to-noise ratio, improving the delineation of cancerous tissues during surgical procedures.

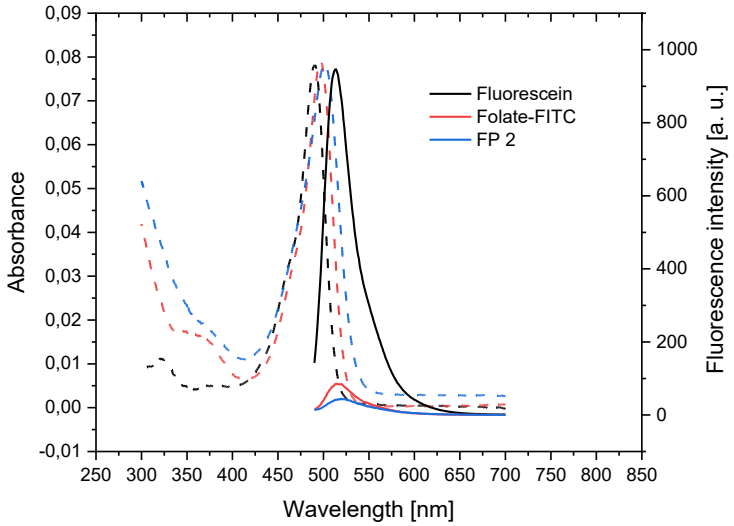

***Figure 15**: Absorbance and emission spectra of 1µM of FP 2, folate-FITC, and fluorescein were measured in PBS (pH = 7.4). Dashed lines represent absorbance spectra, while solid lines correspond to emission spectra at an excitation of 480 nm with a detection voltage of 520 V.*

Additionally, the photobleaching properties of **FP 2** were measured before conducting the cellular experiments.

3.1.3 Photoirradiation experiments of FP 2

Following the spectral characterization, we proceeded to evaluate the photostability of **FP 2**, a critical parameter for its potential application in fluorescence-guided surgery. Photostability is essential for maintaining consistent signal intensity during prolonged imaging sessions, which is often necessary in surgical settings. This property directly impacts the probe's ability to provide reliable and continuous tumor visualization throughout a procedure.

To evaluate photostability, we exposed **FP 2** to 470 nm LED light, simulating typical fluorescence microscopy conditions used in intraoperative fluorescence imaging with fluorescein dye. We compared its photobleaching behavior to that of fluorescein and our reference probe, folate-FITC, **Figure 16**. The goal of these experiments was to quantify the rate of fluorescence decay during continuous light exposure.

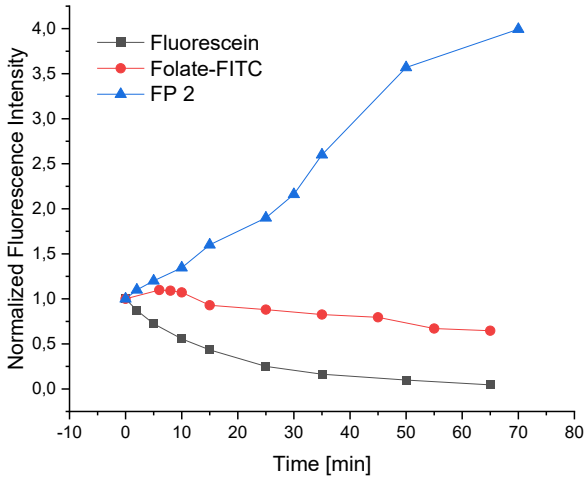

***Figure 16**: Normalized fluorescence intensity of 1µM of fluorescein, folate-FITC, and FP 2 in PBS (pH=7.4) as a function of the irradiation time (λ_{ex}: 480 nm). Fluorescence intensity was normalized and expressed as the ratio I/I_0, where I represents the intensity at each time point and I_0 is the initial intensity. The probes were irradiated with 470 nm LED lamp.*

As shown in **Figure 16**, the fluorescence intensity of both fluorescein and folate-FITC decreased upon light exposure, as expected. In contrast, **FP 2** exhibited an increase in fluorescence intensity when exposed to 470 nm LED light. This phenomenon can be attributed to the photo-induced chemical degradation of **FP 2**, leading to the release of a highly fluorescent fluorescein derivative.

The photo-induced fluorescence enhancement of **FP 2** offers significant potential for application in fluorescence microscopy. When exposed to 470 nm LED light, **FP 2** shows an increase in emission intensity. This enhancement may improve the probe's performance during prolonged in vivo imaging studies.

In a separate part of our study (Chapters 3.1.7 to 3.1.13), we synthesized additional oxime ether fluorescein derivatives and subjected them to photoirradiation. Following this, we performed mass spectrometry and analytical HPLC experiments to identify the resulting photoproducts. The goal of this investigation was to elucidate the specific fluorescein derivatives formed during photoirradiation and to gain a deeper understanding of the photochemical processes contributing to the observed fluorescence enhancement.

3.1.4 Evaluation of cancer cell selectivity of FP 2

To assess the cancer cell selectivity of **FP 2**, we conducted a comprehensive series of cell experiments, comparing its behavior to that of folate-FITC in both cancerous HeLa cells (human cervical carcinoma) and healthy HDFa cells (human dermal fibroblasts).

Our experimental design involved three key conditions: HeLa cells in folic acid-free RPMI medium, HeLa cells in medium with excess folic acid, and HDFa cells in folic acid-free RPMI medium. All cell types were treated with 10 nM of **FP 2** and folate-FITC for 15 minutes at 37°C, conditions optimized for cellular uptake and labeling.

Flow cytometry analysis revealed distinct patterns of cellular labeling across these conditions. In HeLa cells cultured in folic acid-free medium, both **FP 2** and folate-FITC showed significant fluorescence enhancement, indicating selective labeling of these cancer cells. This is clearly illustrated in **Figure 17** (bottom panel, right), where an increase in fluorescence along the x-axis demonstrates successful probe activation.

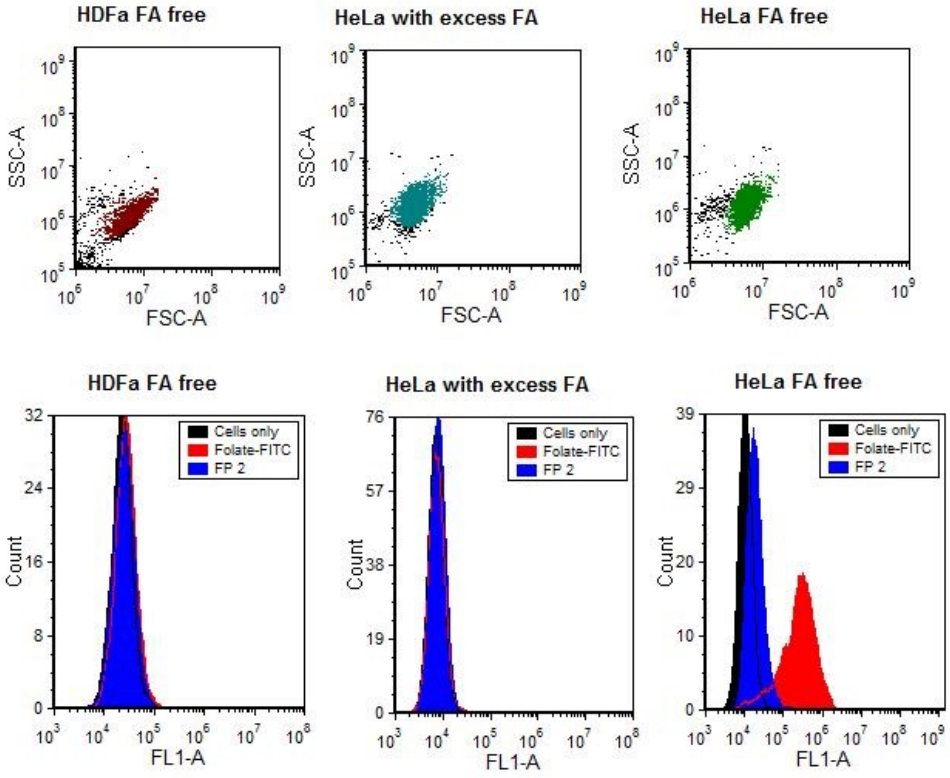

Figure 17: *Flow cytometry analysis of the distribution of HeLa and HDFa cells (top panel) in folic acid-free (FA-free) medium and the medium with an excess of folic acid (FA). The color distribution in the top panel indicates the gate used for the fluorescence measurement. The x-axis represents the forward scatter area (FSC-A), while the y-axis represents the side scatter area (SSC-A). Bottom panel: Representative histograms of flow cytometry analysis of adherent HeLa cells (right and middle) and HDFa cells (left) incubated with 10 nM of probes in RPMI 1640 medium and in a medium with excess of FA at 37°C. After 15 min incubation time, cells were washed twice with PBS (pH=7.4) and detached from the surface using trypsin–EDTA. The measurements were carried out using flow cytometry (excitation: 488 nm, detection: 530/15 nm filter). The horizontal axis represents the fluorescence intensity of probes, and the vertical axis represents the number of events.*

In contrast, when HeLa cells were treated with excess folic acid (FA), no significant fluorescence enhancement was observed (**Figure 17**, bottom panel, middle). This suggests competitive inhibition of probe uptake by excess folic acid, confirming the folate receptor-mediated internalization mechanism. Similarly, in HDFa cells cultured in folic acid-free medium, no significant fluorescence enhancement was detected (**Figure 17**, bottom panel, left), indicating only non-specific binding and activation in healthy cells. These results collectively demonstrate the cancer cell selectivity of **FP 2**, the same as folate-FITC. **FP 2** effectively distinguishes between cancerous and healthy cells, with uptake mediated by folate receptors. The lack of labeling in HeLa

cells treated with excess folic acid further confirms the specificity of the folate-mediated uptake mechanism.

Additionally, the binding and fluorescence enhancement properties of **FP 2** and folate-FITC was evaluated in HeLa cells at various concentrations: 1 nM, 2.5 nM, 5 nM, 10 nM, 25 nM, 50 nM, and 100 nM to determine their saturation concentrations, **Figure 18**.

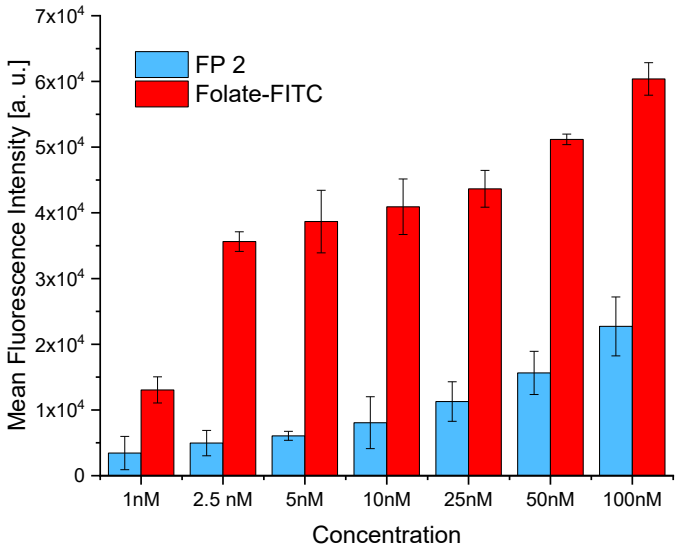

***Figure 18**: Statistical analysis of the mean fluorescence intensities of cells treated with FP 2 and folate-FITC at different concentrations for 15 min at 37°C in RPMI 1640 medium. After incubation time, cells were washed twice with PBS (pH=7.4) and detached using trypsin–EDTA. The measurements were carried out using flow cytometry (excitation: 488 nm, detection: 530/15 nm filter). The fluorescence emissions of the cells were corrected by the value of the background fluorescence of non-stained cells. The error bars correspond to ± standard deviation (SD, n = 3)*

Flow cytometry analysis demonstrated that fluorescent probe **FP 2** effectively binds to cancer cells, leading to increased fluorescence intensity. However, comparing the mean fluorescence intensity of folate-FITC and **FP 2** reveals that the reference compound shows stronger fluorescence in HeLa cells compared to **FP 2**.

At the next part of this study, we conducted a time-dependent analysis to understand how the fluorescence intensity changes over time when HeLa cells are incubated with folate-FITC and **FP 2**.

3.1.5 Time-dependent analysis of fluorescent probe uptake and activation in HeLa cells

In the subsequent phase of our experiments, we investigated the temporal changes in fluorescence intensity of HeLa cells incubated with 10 nM of three different compounds: **FP 2**, folate-FITC, and fluorescein diacetate (FDAc). 10 nM concentration was selected based on the saturation concentration of folate-FITC and **FP 2** in Hela cells observed in **Figure 18** to ensure optimal fluorescence. The chemical structure of **FP 2**, folate-FITC and FDAc are illustrated in **Figure 19**.

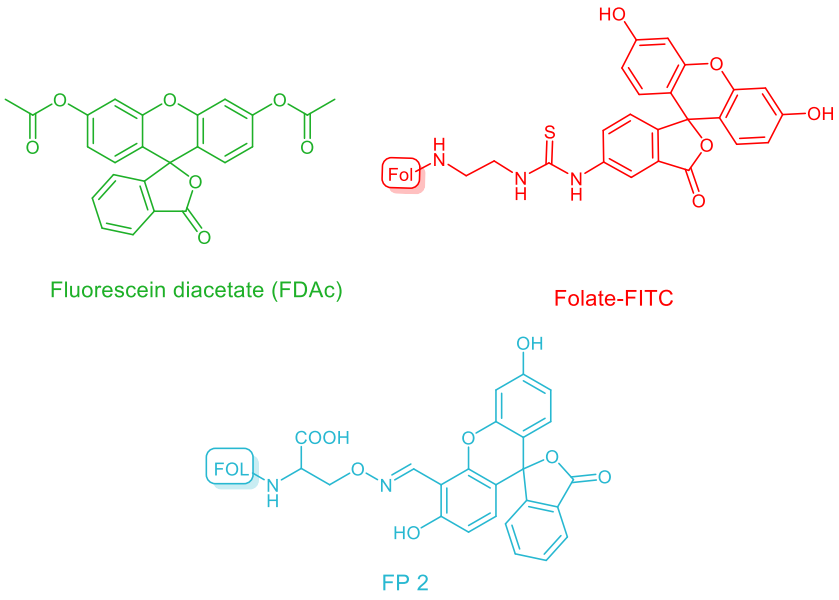

***Figure 19**: Chemical structure of fluorescein diacetate (FDAc), folate-FITC, and FP 2.*

This investigation provided crucial insights into the kinetics of probe internalization and activation within the cellular environment. We measured the enhancement in mean fluorescence intensity within HeLa cells over time using flow cytometry, **Figure 20**.

To establish a reference, we used fluorescein diacetate (FDAc) as a control. This neutral compound is highly membrane permeable and initially non-fluorescent but becomes highly fluorescent upon cleavage by intracellular esterases.

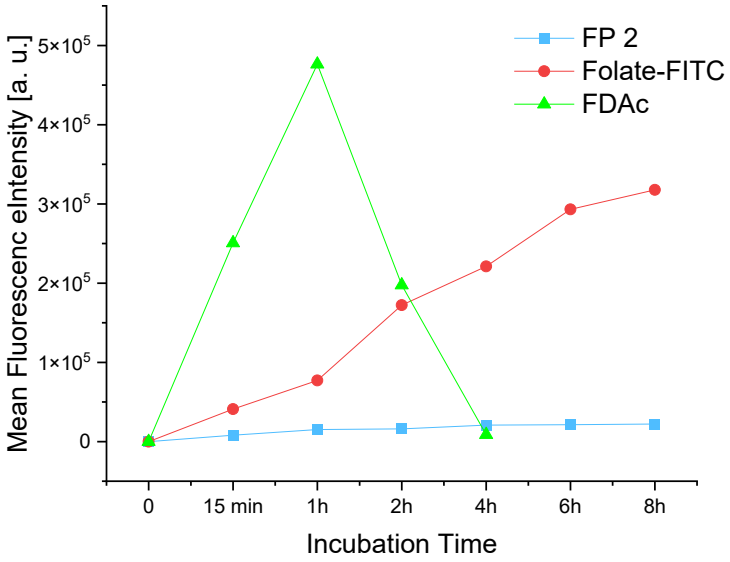

***Figure 20**: Time-dependent changes in fluorescence intensity of HeLa cells incubated with 10 nM of FP 2, folate-FITC, and fluorescein diacetate (FDAc). Following the incubation time, cells were washed twice with PBS (pH=7.4) and detached from the surface using trypsin–EDTA. The measurements were carried out using flow cytometry (excitation: 488 nm, detection: 530/15 nm filter). The fluorescence emissions of the cells were corrected by the value of the background fluorescence of non-stained cells.*

The fluorescence intensity of HeLa cells incubated with fluorescein diacetate (FDAc), our control experiment, shows a rapid increase, reaching its maximum within the first hour of incubation. Importantly, fluorescein diacetate demonstrated the highest fluorescence intensity which serves as a reference point.

In comparison, the fluorescence intensity of HeLa cells incubated with folate-FITC demonstrates a different profile. It reaches its maximum between 6 to 8 hours of incubation time, indicating a more prolonged accumulation of the probe within the cells. The fluorescence intensity of folate-FITC in the cells measured using flow cytometry is slightly lower than that of FDAc.

FP 2 exhibits distinctly different behavior, showing relatively low fluorescence intensity throughout the incubation period compared to both FDAc and folate-FITC. It is evident from the comparison of the curves in **Figure 20** that folate-FITC, shows a significantly higher fluorescence intensity in HeLa cells than **FP 2.**

3.1.6 Factors determining low fluorescence intensity of FP 2 in HeLa cells

Both **FP 2** and folate-FITC are designed to target cancer cells through folate receptor-mediated endocytosis. Upon internalization, these probes are hypothesized to undergo

amide bond cleavage, likely facilitated by enzymatic reactions within lysosomes. Lysosomes contain a variety of proteolytic enzymes, notably cathepsins, which are capable of cleaving the amide bonds.[59-61]

We hypothesized that the lower fluorescence intensity of **FP 2** compared to folate-FITC in HeLa cells is due to the emission characteristics of the cleavage products formed after internalization of the probe in the cell and then amide bond cleavage by proteolytic enzymes. To test this hypothesis, we synthesized and analyzed the predicted cleavage products of both probes (**FP 2** and folate-FITC). **Figure 21** illustrates the proposed cleavage products of these fluorescent probes in cells.

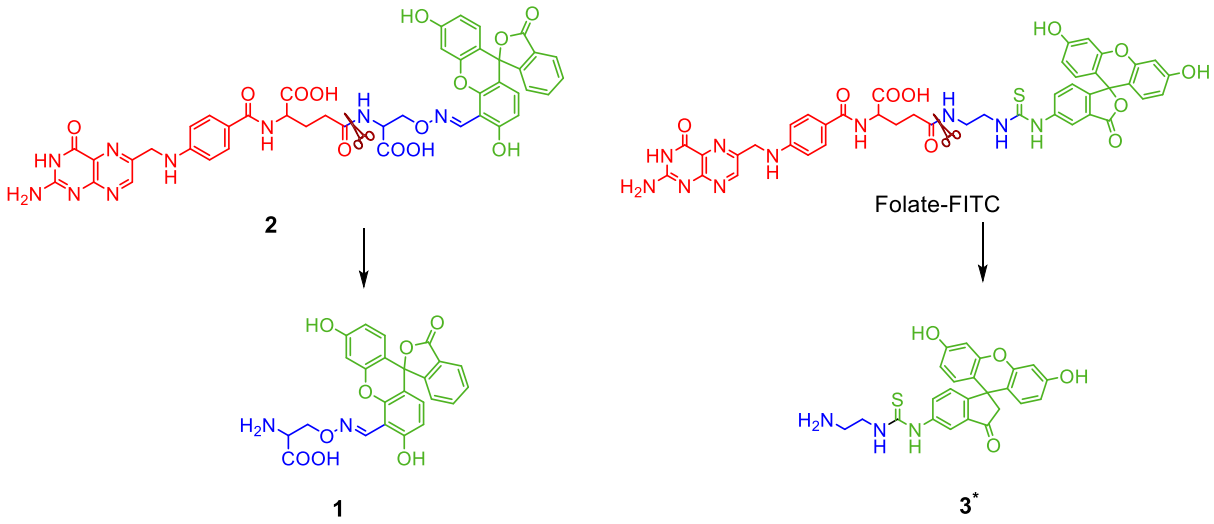

***Figure 21**: Chemical structures of FP 2 and folate-FITC with their hypothesized lysosomal cleavage products*

It was assumed that both **FP 2** and folate-FITC undergo enzymatic cleavage at their amide bonds within the cellular environment, potentially releasing compounds similar to **1** and **3**, respectively. The fluorescence intensity of 1 µM of these putative cleavage products dissolved in PBS (pH=7.4) was measured, **Figure 22**.

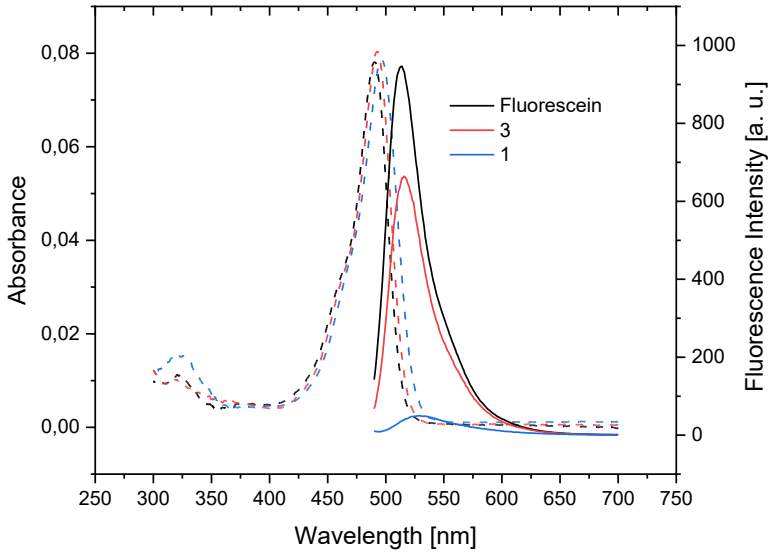

***Figure 22**: Absorbance and emission spectra of 1 µM of fluorescein, **1**, and **3** measured in PBS (pH = 7.4). Dashed lines represent absorbance spectra, while solid lines correspond to emission spectra at an excitation of 480 nm with a detection voltage of 520 V.*

The results, as shown in **Figure 22**, support our hypothesis. The fluorescence measurements of **1** and **3** in solution correlate well with the observed cellular fluorescence patterns of **FP 2** and folate-FITC compared to fluorescein diacetate in the cell experiments, observed in **Figure 20**.

This finding has significant implications for the design of fluorescent probes. Although the oxime bond allows for easy synthesis through a one-pot reaction, it may not be an ideal linker due to its strong fluorescence-quenching effect. This quenching can reduce the fluorescence intensity observed in healthy cells, enhancing the signal-to-noise ratio in targeted imaging applications. However, it also results in a lower overall fluorescence intensity in cancer cells compared to folate-FITC.

3.1.7 Photochemical investigation and characterization of oxime ether fluorescein derivatives under photoirradiation

In this part of our study, we aimed to further investigate the photochemical properties of **FP 2**. For this purpose, we synthesized a series of oxime ether fluorescein derivatives, particularly focusing on the mechanisms responsible for fluorescence enhancement under photoirradiation.

The fluorescein oxime ether derivatives were synthesized through an oxime-click synthesis process between the aldehyde group of fluorescein-monoladehyde and the aminooxy group (-ONH_2) of alkoxyamine, **Figure 23**.

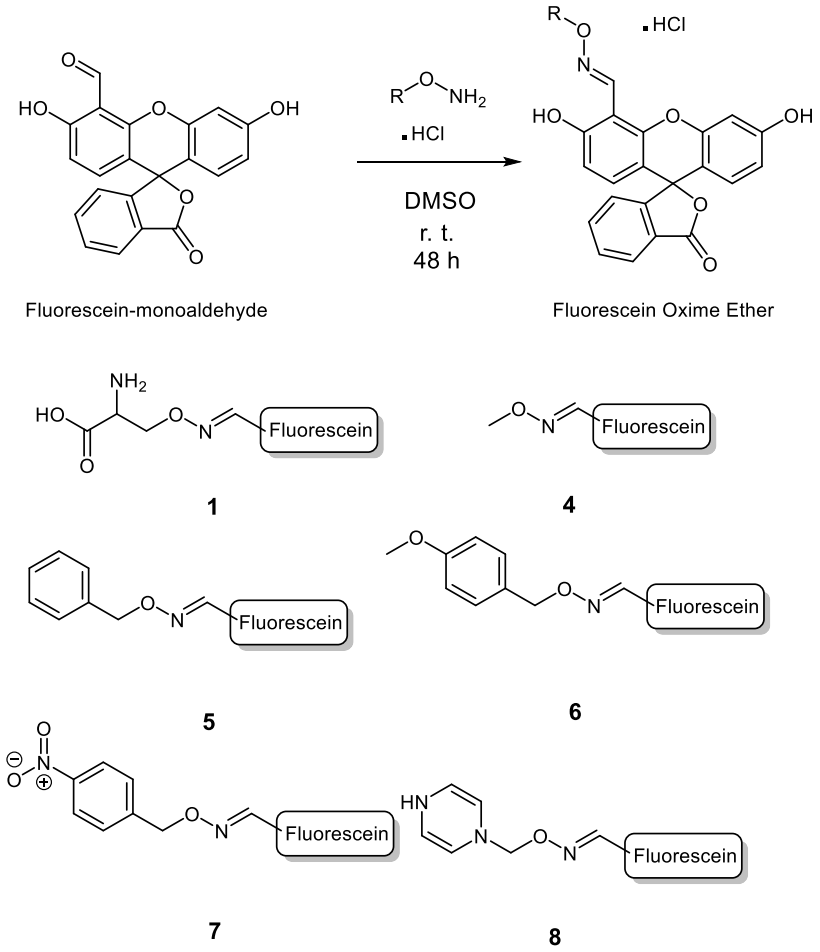

***Figure 23**: Synthesis of fluorescein oxime ether derivatives via an oxime click reaction*

The oxime ligation is particularly attractive since it is a very efficient and chemoselective reaction taking place in aqueous systems under mildly acidic conditions. It is compatible with most of the biomolecule functionalities and water is the only side product formed in this process.[62-64] The extra stability of oximes stems from the α-effect provided by the aminooxy oxygen heteroatom next to the sp^2 nitrogen. The delocalization of the lone pairs of electrons of the heteroatom next to the sp^2 nitrogen makes it less electrophilic. Therefore, the nucleophilic attack by a water molecule is less susceptible. [64, 65]

The reaction between aldehyde and alkoxyamine takes place favourably at a low pH value. **Figure 24** indicates the mechanism of the reaction of an alkoxyamine with an aldehyde to form an oxime ether in the presence of acid.

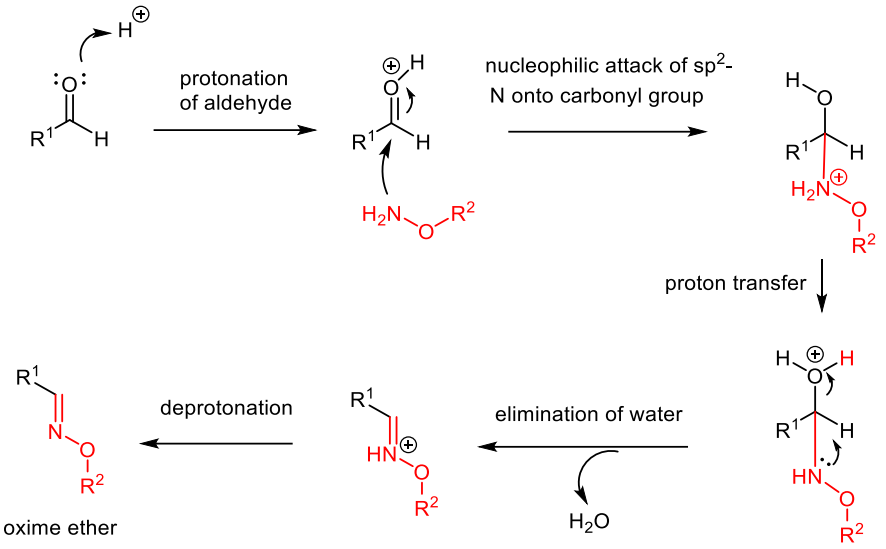

***Figure 24**: The reaction mechanism between aldehyde and alkoxyamine to form oxime ether*[63, 66, 67]

3.1.8 Photophysical characterization

The photophysical properties of the synthesized fluorescein oxime ether derivatives were evaluated by measuring their absorption and emission intensities. All measurements were performed in PBS (pH=7.4) at a concentration of 1 µM. The maximum absorption (λ_{abs}) and emission (λ_{em}) wavelengths were identified, allowing for the calculation of the Stokes shift. **Table 2** summarizes the key photophysical parameters for each derivative.

***Table 2**: Photophysical properties of 1µM of fluorescein, fluorescein monoaldehyde, and fluorescein oxime ether derivatives compounds 1 and 4 - 8 in PBS (pH:7.4) (λ_{ex}: 490 nm).*

Compound	$\lambda_{max\ (Abs)}$[nm]	$\lambda_{max\ (Em)}$[nm]	Stokes shift [nm]	ε [M^{-1} cm^{-1}] 10^4	Quantum yield in PBS (pH=7.4)
Fluorescein	490	515	25	7.90	0.85
Fluorescein-monoaldehyde	486	518	32	7.66	0.65
1	496	528	32	7.64	0.03
4	496	528	32	7.10	0.03
5	496	518	22	7.25	0.04
6	496	518	22	7.15	0.04
7	496	518	22	7.41	0.04
8	496	521	25	7.45	0.04

Fluorescein oxime ether exhibits reduced fluorescence intensity, which might be related to the introduction of the oxime ether group (–C=N–OR). One possible explanation is that this group could affect the conjugated π-electron system, potentially altering intramolecular charge transfer (ICT) dynamics.[68] Alternatively, photoinduced electron transfer (PET) from lone electron pairs on the nitrogen or oxygen atoms could play a role in quenching the fluorescence. This fluorescence quenching effect is evident in **Figure 25** (right), where the fluorescence intensity of fluorescein oxime ether is markedly lower compared to fluorescein and fluorescein-monoaldehyde.

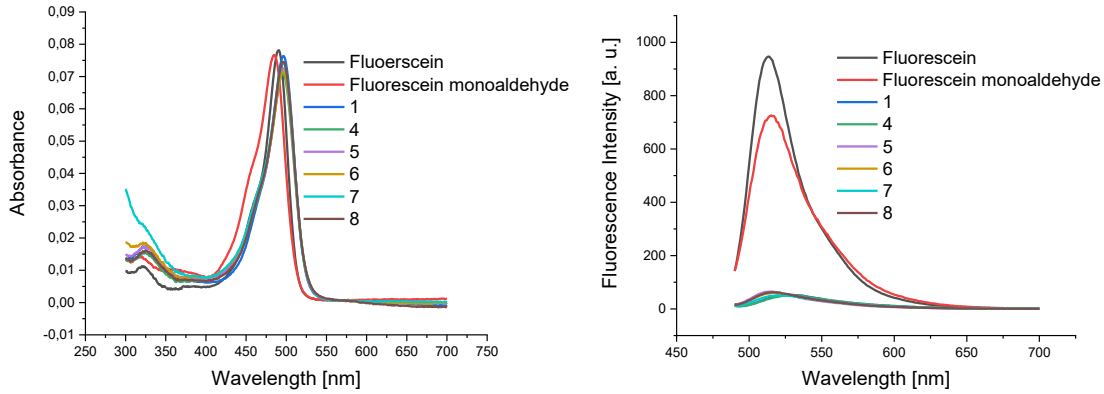

***Figure 25**: Absorbance (left) and emission (right) spectra of 1 μM of fluorescein oxime ether derivatives 1 and 4 - 8 in PBS (pH=7.4), compared to fluorescein and fluorescein monoaldehyde with the excitation wavelength of 480 nm and the detection voltage of 520 V.*

3.1.9 Photostability and light-induced behavior of fluorescein oxime ether derivatives

In this part of our study, we conducted photoirradiation experiments on compounds **1** and **4** – **8** to evaluate the performance of these compounds under light exposure. We prepared 1 μM solutions of each compound in PBS at pH 7.4 and utilized a 96-well plate format for the experiment. The fluorescein and its derivatives were exposed to LED light at seven distinct wavelengths (355, 365, 370, 405, 470, 518, and 593 nm) for a duration of one hour. During this time, we measured the emission intensity as a function of irradiation time.

As illustrated in **Figure 26**, unmodified fluorescein exhibited the expected photobleaching behavior, with a progressive decrease in fluorescence intensity over time under light exposure. This phenomenon is attributed to the photochemical degradation of the fluorescein chromophore.

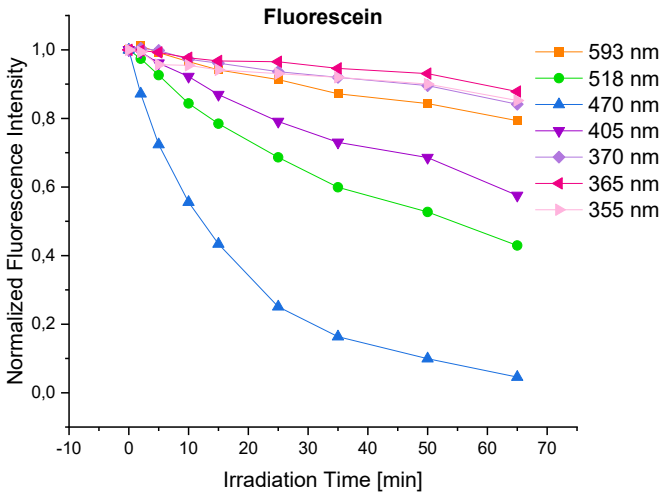

***Figure 26**: Normalized emission intensity of 1μM of fluorescein in PBS (pH=7.4) exposed to LED light at 7 different wavelengths plotted as a function of the irradiation time (λ_{ex}= 490 nm). The normalized fluorescence intensity was calculated with I / I_0, where I represents the intensity at each time point and I_0 is the initial intensity).*

In contrast to the photobleaching observed in unmodified fluorescein, the fluorescein oxime ether derivatives (compounds **1** and **4 - 8**) exhibited a remarkable increase in fluorescence intensity upon light exposure. This unexpected fluorescence enhancement suggests that these derivatives undergo a unique photochemical reaction that potentially amplifies their fluorescent state.

Figure 27, illustrates the fluorescence enhancement of compounds **1** and **4** upon photoirradiation. Notably, the most pronounced intensity increase was observed under irradiation at wavelengths of 470 nm and 518 nm.

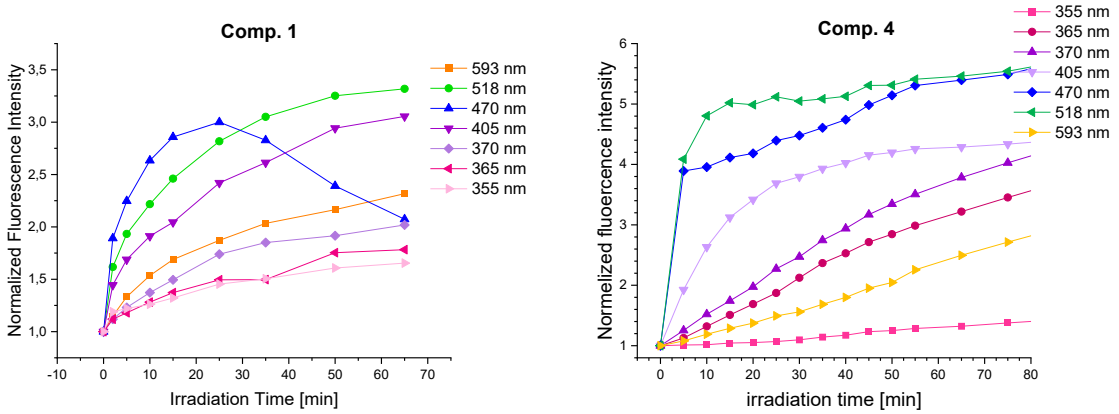

***Figure 27**: Normalized emission intensity of 1μM of 1 and 4 in PBS (pH=7.4) exposed to LED light with 7 different wavelengths plotted as a function of the irradiation time (λ_{ex}= 490 nm). The normalized*

fluorescence intensity was calculated with I / I_0, where I represents the intensity at each time point and I_0 is the initial intensity).

We hypothesize that the unique behavior of compounds **1** and **4** is due to the photocleavage of the oxime bond. This light-induced reaction likely leads to the release of a strongly fluorescent compound. To investigate the unexpected increase in fluorescence intensity upon irradiation, we conducted time-based measurements of fluorescence intensity of irradiated samples. Upon detecting the point of maximal fluorescence increase, we performed analytical HPLC and mass spectrometry analyses to further explore the underlying processes.

During analytical HPLC, we systematically examined the irradiated solutions to detect the appearance of new peaks, potentially indicating the formation of photocleavage products. We also used Electrospray Ionization (ESI) mass spectrometry to determine the molecular masses of these new compounds isolated from the HPLC analysis.

3.1.10 Photoinduced fluorescence enhancement study of compounds 5, 6, and 7

The photoinduced fluorescence enhancement of compounds **5**, **6**, and **7** was investigated using 20 µM solutions of each compound prepared in TEAA buffer (pH=7.2). One group was exposed to 518 nm light, while a control group remained in darkness. Fluorescence intensity was measured for both groups over 5 hours until it reached a stable maximum, after which it began to decrease, **Figure 28**.

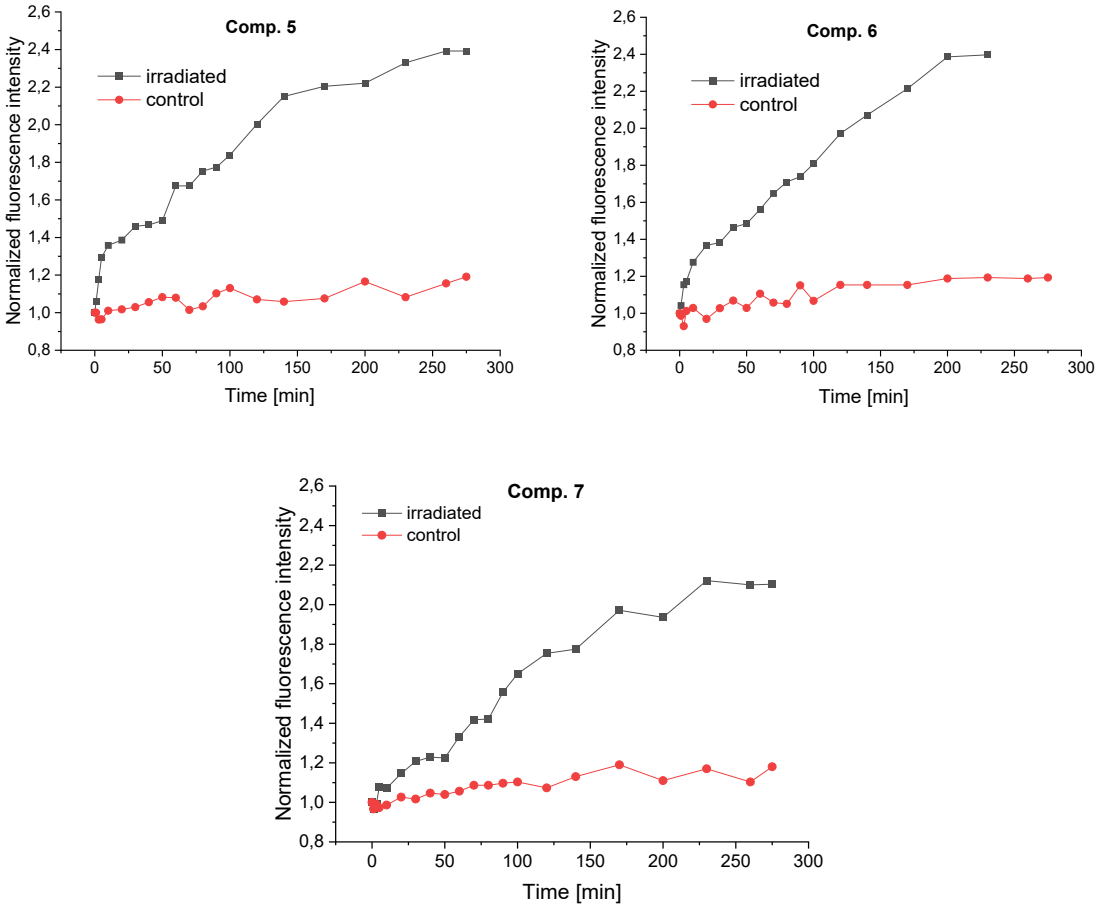

Figure 28: *Light-induced fluorescence enhancement of 5, 6, and 7 over time: 20 µM of samples dissolved in 10 mM triethylammonium acetate (TEAA) buffer (pH 7.4) were irradiated to the light at 518 nm, excited at 490 nm, and measured at 520 V detector voltage. Fluorescence intensity was normalized and expressed as the ratio I/I_0, where I represents the intensity at each time point and I_0 is the initial intensity.*

As illustrated in **Figure 28,** all three fluorescein oxime ether derivatives exhibited a notable increase in fluorescence intensity upon exposure to 518 nm light. The control samples, which were not irradiated, showed no significant change in fluorescence intensity. This contrast between the irradiated and non-irradiated samples confirms that the observed fluorescence enhancement is indeed a light-induced reaction.

3.1.11 Optimizing concentration for ESI and HPLC measurements

In our previous experiments, we measured the fluorescence intensity of fluorescein oxime ether derivatives **5**, **6**, and **7** over irradiation time using a 20 µM concentration in triethylammonium acetate (TEAA) buffer. This concentration was initially chosen to have enough signal intensity in both analytical HPLC and Electrospray Ionization (ESI) mass spectrometry experiments. However, this decision prompted an important

consideration: what is the optimal upper concentration limit to avoid potential aggregation and self-quenching effects?

3.1.12 Determination of critical concentration for optimal fluorescence analysis

To optimize our experiments, we measured the critical concentration of compound **4** in three different buffers: PBS, TEAA, and TEAB. This critical concentration represents the point at which fluorescence enhancement deviates from linearity, indicating the upper limit for the concentration of the samples by the photoirradiation experiments.

Compound **4** and fluorescein were prepared in concentrations starting from 1 µM, increasing in 2 µM steps up to 21 µM, then in 10 µM steps up to 70 µM. For each concentration, the maximum fluorescence intensity was recorded. The data were plotted to identify the point where the fluorescence response deviated from linearity, indicating the onset of saturation, **Figure 29**.

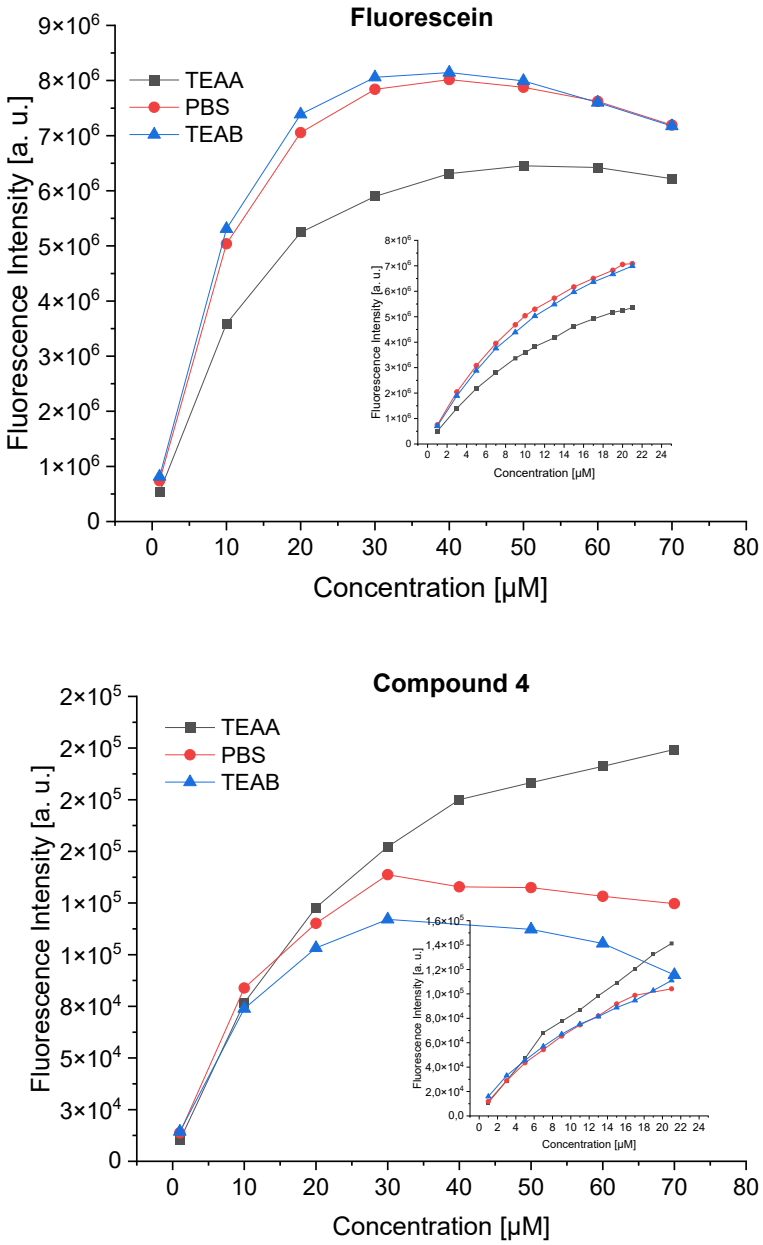

***Figure 29**: Concentration-dependent fluorescence intensity of fluorescein [36] and compound 4 (bottom) in three different buffers (pH 7.4). Measurements were performed in 96-well plates (320 µL/well) using a Perkin Elmer EnSpire plate reader. Left: Concentrations ranging from 1 - 70 µM; Right: Concentrations ranging from 1 - 22 µM. Excitation wavelength: 480 nm. Maximum fluorescence intensity is plotted on the y-axis.*

As it is observed in **Figure 29**, the fluorescence intensity remained linear up to a concentration of approximately 5 - 6 µM for fluorescein and around 20 µM for compound **4**. Within this range, the fluorescence response exhibited an approximately linear increase with concentration, indicating that this range is suitable for reliable and accurate analysis in experiments involving ESI and analytical HPLC.

3.1.13 Investigating the mechanism of photoinduced fluorescence enhancement

Our fluorescein oxime ether derivatives showed significant fluorescence quenching compared to the parent fluorescein molecule, as observed in **Figure 25**. This quenching likely results from either the oxime ether moiety altering internal charge transfer (ICT) or from photoinduced electron transfer (PET) processes.[68-70]

Conversely, light exposure seems to induce a molecular transformation, potentially through conformational changes or partial photocleavage of the oxime ether bond. As suggested in a doctoral thesis conducted within our group, this process results in the release of fluorescein nitrile, whose mass was detected in ESI experiments, thereby explaining the observed fluorescence enhancement. [57] To investigate this observation, we synthesized fluorescein nitrile as a reference compound, following the protocol established by H. Lee et al.[71]

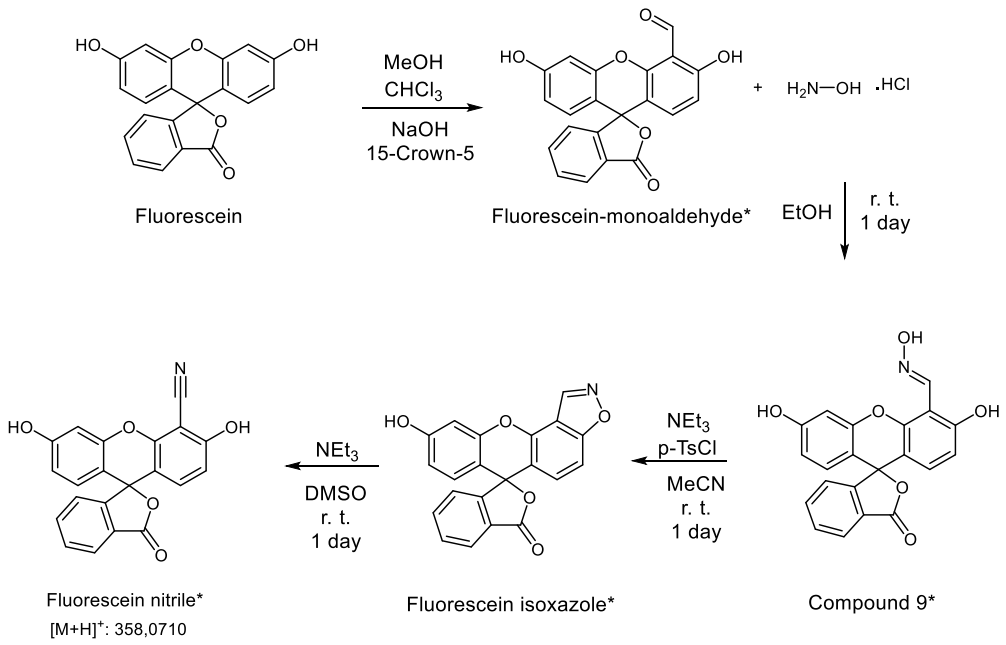

***Figure 30**: Synthesis pathway of fluorescein nitrile*

The synthesis of fluorescein nitrile proceeded through several key steps starting from fluorescein. Initially, fluorescein was converted into fluorescein monoaldehyde by reacting it with sodium hydroxide and chloroform in methanol. Next, the fluorescein monoaldehyde was reacted with hydroxylamine hydrochloride in ethanol to form fluorescein oxime, compound **9**.

In the next step of the synthesis, fluorescein oxime was activated using tosyl chloride (TsCl) in acetonitrile, along with triethylamine as a base. The activation of the oxime led to the formation of an isoxazole intermediate through cyclization.

Finally, the isoxazole intermediate was treated with DMSO and trimethylamine base mixture, promoting its conversion into fluorescein nitrile. The nitrile product was purified and confirmed by NMR spectroscopy and ESI mass spectrometry.

20 µM of compound **6,** was irradiated at 518 nm until maximum fluorescence intensity was achieved. The irradiated sample was then analyzed using electrospray ionization (ESI) mass spectrometry and analytical HPLC. **Figure 31** compares the analytical HPLC chromatograms for three samples: 1) irradiated compound **6**, 2) non-irradiated compound **6**, and 3) fluorescein nitrile. This comparison allows for the assessment of photochemical changes and potential product formation resulting from the irradiation process.

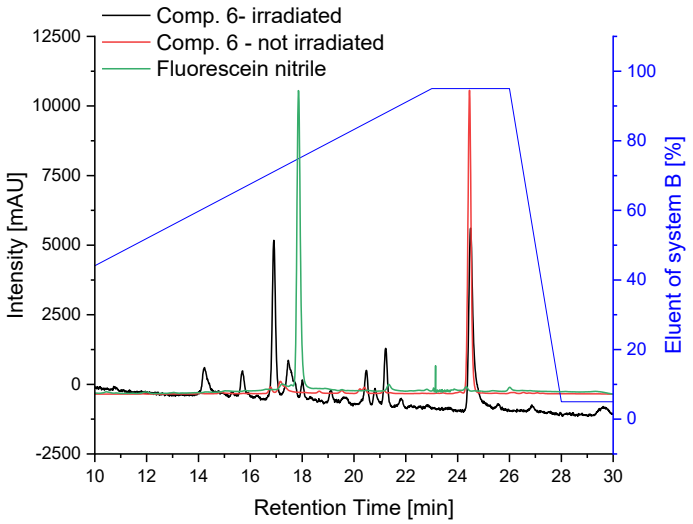

***Figure 31**: Analytical HPLC analysis of 20 µM of 6 in TEAA buffer (pH 7.4) after exposure to 518 nm LED light for 4 hours, compared with non-irradiated sample and the hypothesized photocleavage product, fluorescein nitrile.*

Analysis of this chromatogram reveals several key observations:

1. The main peak in both irradiated and non-irradiated samples correspond to the intact fluorescein oxime ether, compound **6**. This peak remains dominant even after 4 hours' irradiation, indicating that the majority of the compound does not undergo photocleavage or significant structural changes.

2. Notably, we observe a very small peak corresponding to the retention time of fluorescein nitrile, suggesting that nitrile is not the major product of the irradiated compound **6**.
3. We observe the appearance of several small new peaks in the chromatogram of the irradiated sample. These minor peaks likely represent photoproducts formed during irradiation, but their exact nature requires further investigation.

To identify these unknown peaks, we initially attempted to collect them from analytical HPLC and perform ESI mass spectrometry. However, due to the low concentration of the collected fractions we were unable to obtain reliable results from these diluted a-HPLC fractions. To overcome this challenge, we instead performed ESI mass spectrometry on the irradiated samples before running analytical HPLC experiments.

Both positive and negative ESI modes were employed. Notably, the positive ion mode produced reliable results, and the negative mode did not yield comparable data. ESI-MS analysis in positive mode of the irradiated compounds revealed three predominant peaks at m/z 358.07, 377.07, and 399.05 in the majority of the mass spectra obtained.

The peak at m/z 358.07 may correspond to fluorescein nitrile or fluorescein isoxasol. The species observed at m/z 399.05 likely represents the sodium adduct of the compound detected at m/z 377.07. We hypothesize that the species at m/z 377.07 could be a carboxylic acid derivative of the fluorescein core structure.

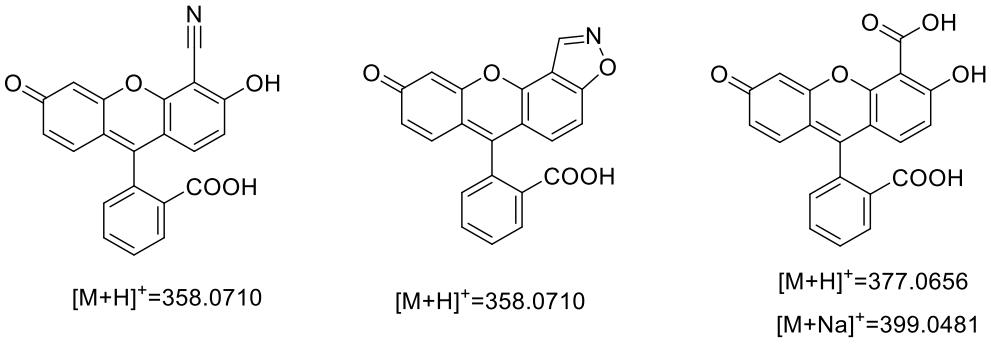

***Figure 32**: Proposed structures corresponding to the observed exact masses in ESI-MS experiments.*

Lushun Wang et al. explained the mechanism of the formation of carbonyl from oxime upon irradiation.[68] Upon exposure to visible light, the oxime group undergoes a transformation, leading to the formation of bi-radical intermediates, **Figure 33**. These radicals are formed when the light energy excites the oxime group, making it highly reactive. These reactive intermediates undergo a [2+2] cycloaddition with molecular

oxygen (O_2), forming a transient four-membered ring. This unstable ring quickly dissociates, causing the cleavage of the oxime group and the restoration of the carbonyl group at the fluorophore. The reformation of the carbonyl group reinstates the internal charge transfer (ICT) process, thereby reactivating the fluorophore's fluorescence.

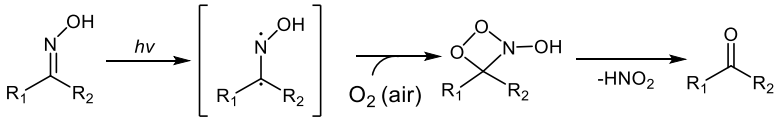

***Figure 33**: Proposed photoactivation mechanism of oxime-caged fluorophores.*[68]

To explain the m/z 377.1 peak in our ESI experiments, we propose that the oxime group in **6** is also transformed into a highly reactive intermediate upon exposure to visible light, consistent with the mechanism suggested by Wang et al. [68] However, the possibility of forming a carboxylic acid upon irradiation of fluorescein oxime ether derivatives remains unexplained and needs further investigation.

The emission spectra of photoirradiated fluorescein oxime ether derivatives as represented by compound **1** in **Figure 34**, reveal a noticeable blue shift, along with an increase in fluorescence intensity for photirradiated samples.

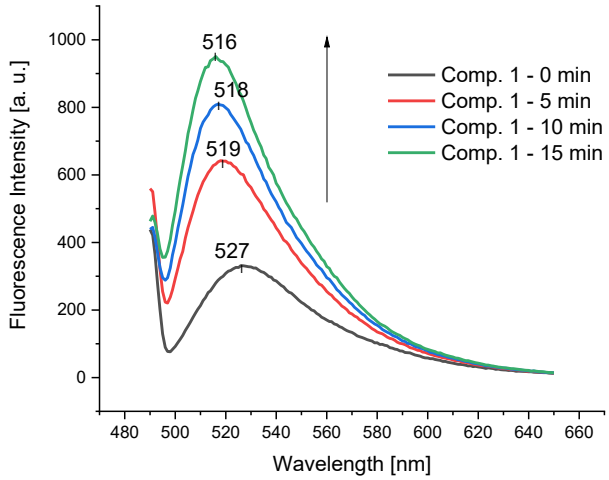

***Figure 34**: Emission spectra of 1 µM photoirradiated comp. 1 in PBS (pH=7.4), showing a time-dependent blue shift and increased fluorescence intensity following exposure to LED light at 470 nm.*

As shown in **Table 2**, coupling the oxime to fluorescein initially results in a red shift of the maximum emission wavelength. However, upon irradiation, the oxime moiety is

likely cleaved, releasing other fluorescein derivatives. This causes a blue shift in the maximum emission wavelength.

3.2 Development of fluorescent probes with a cleavable disulfide linker

In the previous section, the synthesis of **FP 2**, which incorporated an oxime bond between folate and fluorescein, was discussed. While this design allowed for straightforward synthesis, the oxime mioety caused substantial fluorescence quenching, limiting the probe's efficacy. To overcome this issue, a shift was made toward using a disulfide linker. This linker is cleavable in the intracellular environment, particularly in cancer cells where glutathione is overexpressed. Upon cleavage, the disulfide bond releases fluorescein derivatives, significantly enhancing the fluorescence intensity in target cells.

3.2.1 Design and synthesis of disulfide linker fluorescent probes

To investigate the effect of the cleavable disulfide linker, folate-conjugated fluorescent probes, **FP 10** - **FP 15** were synthesized, each incorporating the disulfide linker and fluorophores, including fluorescein isothiocyanate (FITC), 5(6)-carboxyfluorescein, and 5(6)-Carboxytetramethylrhodamine (TAMRA). In addition to these, two control probes were synthesized, which lacked the disulfide bond but maintained similar linker lengths. These control probes were used to specifically evaluate the effect of disulfide cleavage on fluorescence activation within cells. The chemical structure of **FP 10** - **FP 15** is given in **Figure 35**.

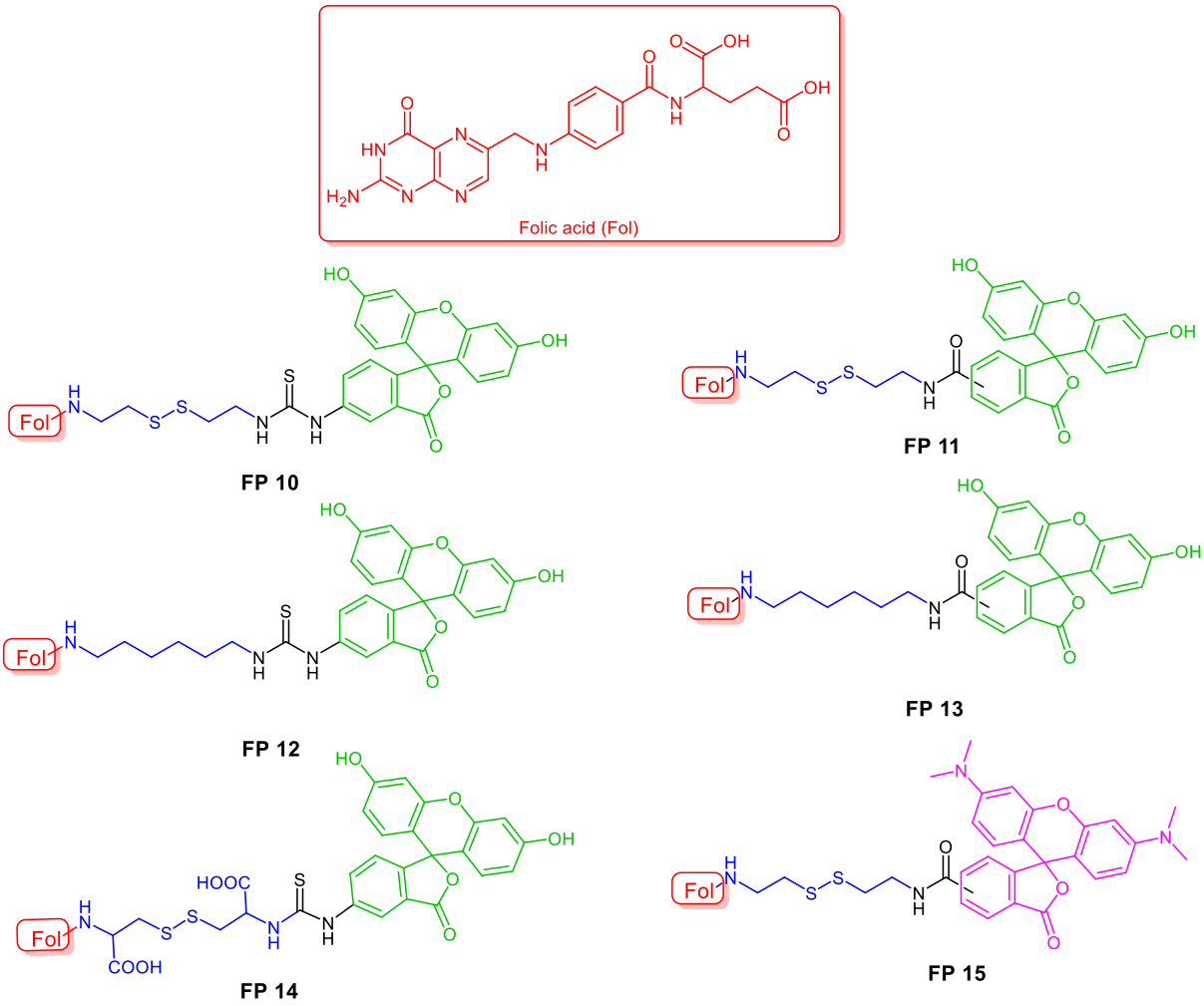

***Figure 35**: Chemical structure of the synthesized fluorescent probes (**FP 10** – **FP 15**)*

Notably, **FP 14** was designed with a linker containing two carboxylic acid groups. This modification was introduced to evaluate how the increased negative charge influences the probe's cellular uptake and its fluorescence properties in cancer cells.

The synthesis of **FP 10** - **15** involved a multi-step process to create folate-linker-fluorophore conjugates. The initial step focused on the amide coupling reaction between the carboxylic acid group of folic acid and the amine terminus of various linkers. This coupling was facilitated using O-(Benzotriazol-1-yl)-N,N,N′,N′-tetramethyluronium tetrafluoroborate (TBTU) as the coupling reagent and N,N-Diisopropylethylamine (DIPEA) as the base. The linkers used in this synthesis were initially protected at one N-terminus with a tert-butyloxycarbonyl (Boc) group to ensure selective coupling at the desired amine. Notably, for the synthesis of **FP 12**, the carboxylic acid of the linker was protected with a tert-butyl group, providing selectivity in the coupling reactions.

Following the coupling reaction, the protection groups were removed using trifluoroacetic acid (TFA) or 4M HCl / dioxane, revealing the free amine group on the linker essential for subsequent reactions.

The next phase of the synthesis involved the attachment of different fluorophores to the folate-linker conjugates. For fluorescein isothiocyanate (FITC), the coupling was straightforward, requiring only DIPEA as a base due to the high reactivity of the isothiocyanate group towards primary amines. In contrast, the coupling of carboxyfluorescein required an amide coupling reaction using TBTU and DIPEA, mirroring the conditions used in the initial step of coupling folic acid to the linker.

To expand the spectral range of our probes, we also incorporated tetramethylrhodamine (TAMRA), which was coupled using similar conditions to carboxyfluorescein. The inclusion of TAMRA allowed us to observe fluorophore characteristics with a red-shifted emission spectrum, broadening the potential applications of our probes.

The purification of all synthesized probes was successfully achieved using RP-HPLC. To enhance the solubility of the crude products for HPLC purification, they were dissolved in a DMSO: acetonitrile: water mixture in a ratio of 1:2:2. The inclusion of DMSO was crucial for improving the solubility of the crude products. However, the separation of isomers proved to be challenging. As shown in **Figure 36** (left column), **FP 10**, **FP 12**, and **FP 14** exhibit two isomers: γ and α. The chemical structure of **FP 11**, **FP 13**, and **FP 15** contains 5- and 6-isomers of carboxyfluorescein. When combined with the γ and α isomers of the product, this results in a complex mixture comprising four distinct isomers for each probe: the α-isomer with 5-carboxyfluorescein, the α-isomer with 6-carboxyfluorescein, the γ-isomer with 5-carboxyfluorescein, and the γ-isomer with 6-carboxyfluorescein, **Figure 36** (right column).

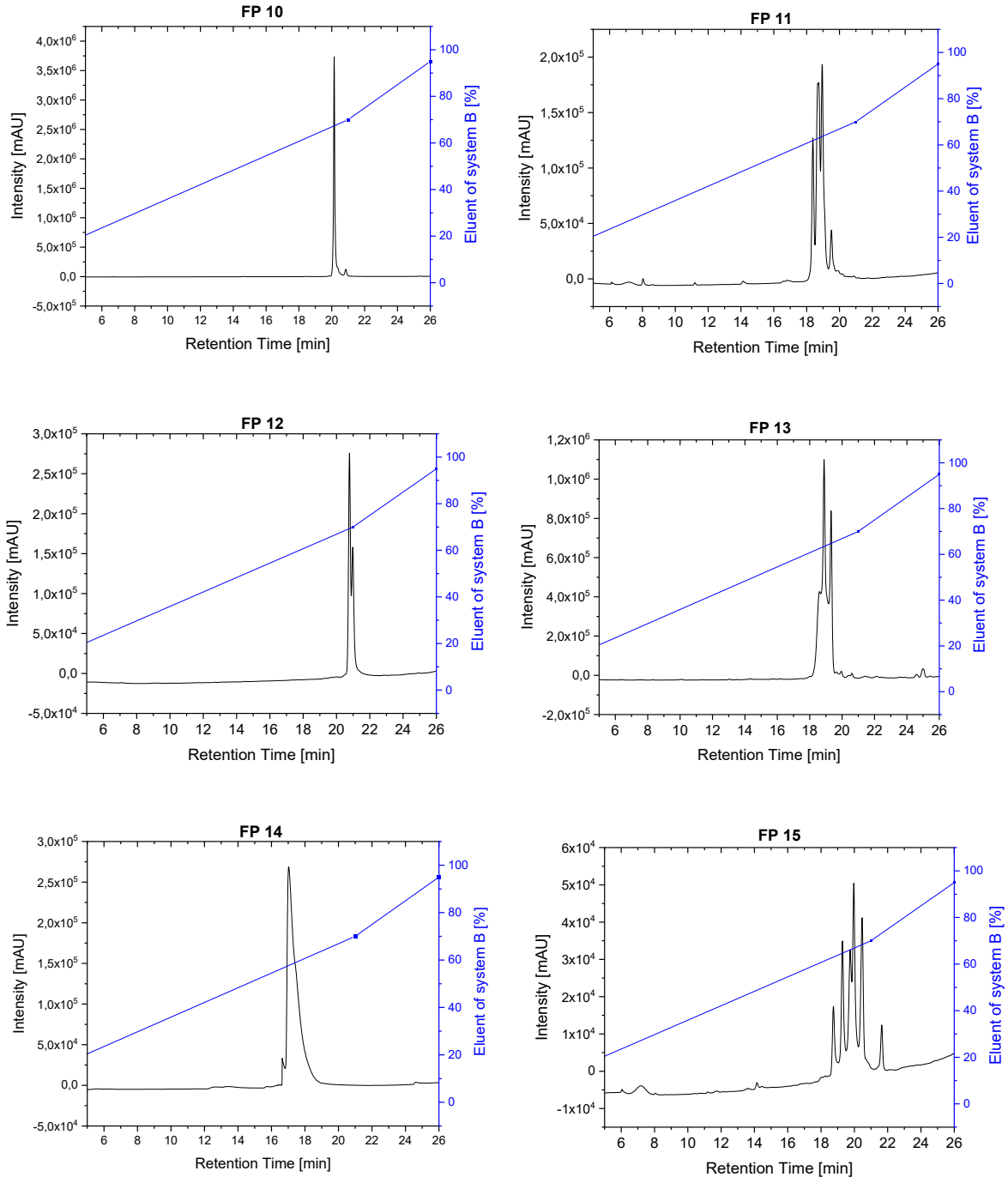

***Figure 36**: Analytical HPLC Chromatograms of FP 10 – FP 15. FP 10 and FP 14 contain the γ isomer. FP 12 exhibits two isomers: γ and α. FP 11, FP 13, and FP 15, incorporating 5(6)-carboxyfluorescein as the fluorophore, display four distinct isomers in the purified product.*

The products were purified and analysed using RP-HPLC and ESI-MS to determine the probes' purities and molecular weights. Additionally, ^{1}H and ^{13}C-NMR, and correlation spectroscopies (COSY, HSQC, HMBC) confirmed the structures of the probes.

Following the successful purification and characterization of **FP 10** – **FP 15**, we proceeded to investigate their photophysical properties to evaluate their suitability as fluorescent probes.

3.2.2 Photophysical properties of synthesized FP 10 – FP 15

The photophysical properties of folate-conjugated fluorescent probes, **FP 10** – **FP 15**, were evaluated by measuring their absorbance and fluorescence emission spectra. All measurements were performed in PBS (pH=7.4) at a concentration of 1 µM. The maximum absorption (λ_{abs}) and emission (λ_{em}) wavelengths were identified, allowing for the calculation of the Stokes shift. **Table 3** summarizes the key photophysical parameters for each derivative. Quantum yields were determined using the comparative method, employing fluorescein as a reference standard (φ_R = 0.85 in PBS).[58]

***Table 3**: Photophysical properties of 1 µM concentrations of FP 10 - 15, folate-FITC, and fluorescein were assessed in PBS (pH 7.4). FP 10 - 14, fluorescein, and folate-FITC were excited at 480 nm, while FP 15 was excited at 540 nm. The detector voltage was set to 520 V.*

Compound	$\lambda_{max\ (Abs)}$[nm]	$\lambda_{max\ (Em)}$[nm]	Stokes shift [nm]	ε [M^{-1} cm^{-1}] 10^4	Quantum yield in PBS (pH=7.4)
Fluorescein	490	515	25	7.90	0.85
Folate-FITC	496	516	20	7.84	0.08
FP 10	496	517	21	6.84	0.10
FP 11	498	518	20	7.36	0.20
FP 12	496	516	20	6.61	0.10
FP 13	496	516	20	7.36	0.22
FP 14	496	516	20	6.56	0.11
FP 15	556	578	22	6.32	0.08

The absorbance and emission spectra of **FP 10** – **FP 15** and folate-FITC are observed in **Figure 37**.

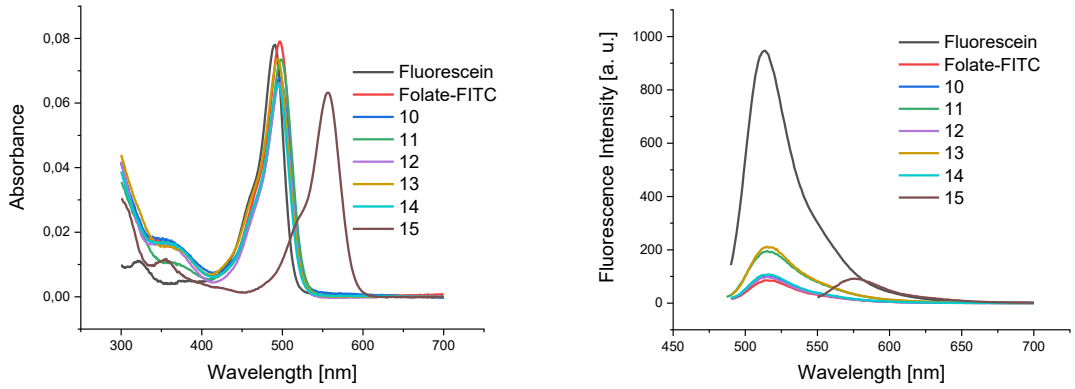

***Figure 37**: Absorbance and emission spectra of FP 10 – FP 15, fluorescein, and folate-FITC in PBS buffer, pH=7. FP 10 - FP 14, fluorescein, and folate-FITC were excited at 480 nm, while FP 15 was excited at 540 nm. The detector voltage was set to 520 V.*

Figure 37 (right) shows that the emission intensities of **FP 10**, **FP 12**, and **FP 14** are notably lower than those of **FP 11** and **FP 13**. To assess the potential influence of the functional group directly attached to fluorescein on fluorescence intensity, we first compared the fluorescence intensity of readily available 5(6)-carboxyfluorescein, and fluorescein isothiocyanate (FITC), **Figure 38**.

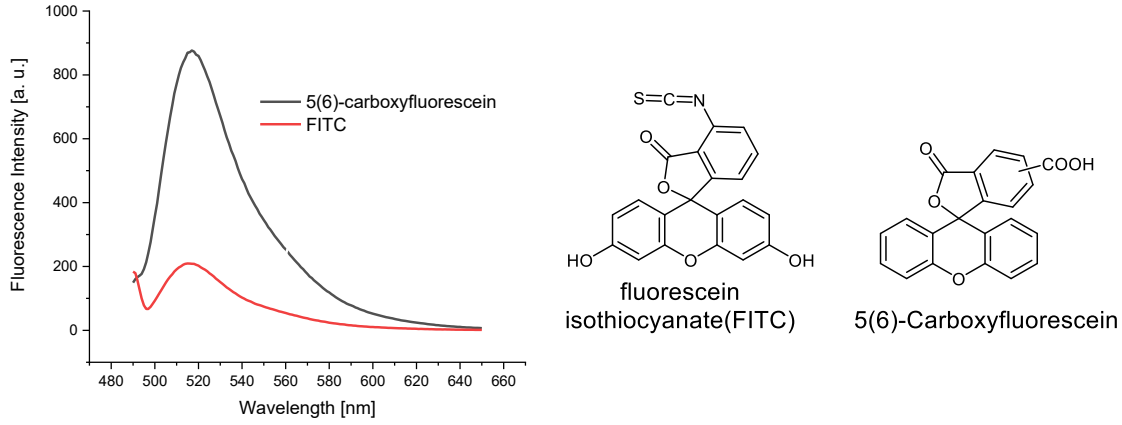

***Figure 38**: Emission spectra and the chemical structure of fluorophores. Emission spectra of 1 µM solutions of 5(6)-carboxyfluorescein, and fluorescein isothiocyanate (FITC) in PBS buffer (pH 7.4). Excitation wavelengths: 490 nm.*

As it is observed in **Figure 38**, the fluorescence intensity of 5(6)-carboxyfluorescein is significantly stronger than that of FITC, prompting us to investigate further. We have therefore performed a refined analysis and compared the fluorescence of fluorescein

derivatives **16** and **17** that lack the folate moiety. The emission of carboxy substituted **17** is indeed somewhat higher compared with the thiourea substituted **16**, **Figure 39**.

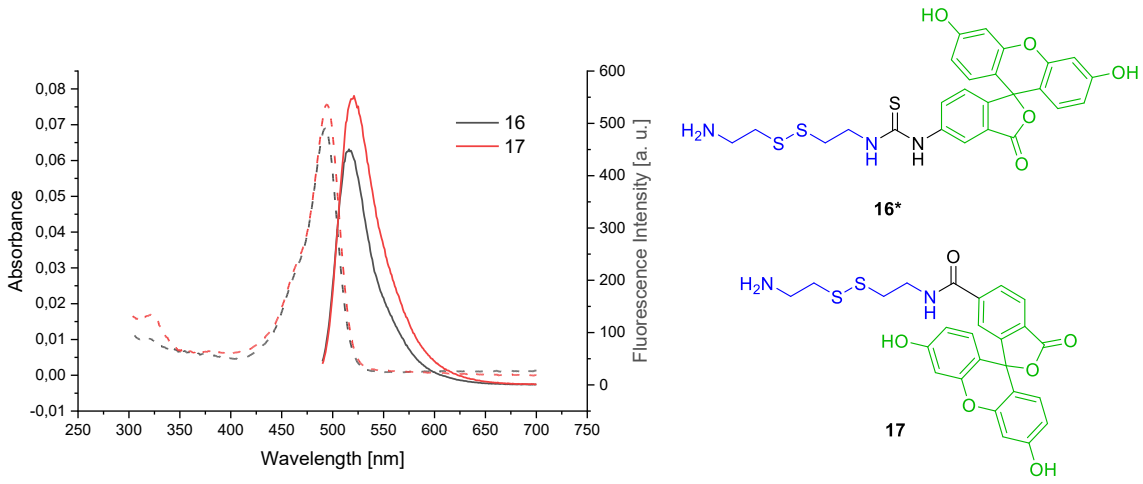

***Figure 39**: Right: Chemical structure of 16 and 17, left: Absorbance (dashed lines) and emission spectra (solid line) of 1 µM solutions of compounds 16 and 17, recorded in PBS at pH 7.4. The excitation wavelength was set to 480 nm, with a detector voltage of 520.*

The lower fluorescence quantum yield of folate-FITC compared to **FP 10**, **FP 12,** and **FP 14,** observed in **Figure 37**, indicates that the quenching effect decreases as the length of the linker between folic acid and the fluorophore increases. This observation shows an inverse relationship between linker length and the quenching effect of folic acid on the fluorophore.

3.2.3 Photostability experiments of FP 10 – FP 15

To evaluate the long-term stability and performance of synthesized probes containing a disulfide linker for fluorescence imaging applications, we conducted photostability experiments using 470 nm LED light. These tests were designed to assess the probes' resistance to photobleaching when exposed to prolonged excitation light, which closely mimics the conditions encountered during fluorescence microscopy. Since these probes can potentially be used in intraoperative fluorescence imaging, their ability to resist photobleaching is especially important.

FP 10, **FP 11**, **FP 14**, and **FP 15** were prepared at a concentration of 1 µM in a PBS solution and exposed to 470 nm LED light. The fluorescence intensity was measured at regular time intervals, and the normalized emission intensity (I/I_0) was plotted against the irradiation time.

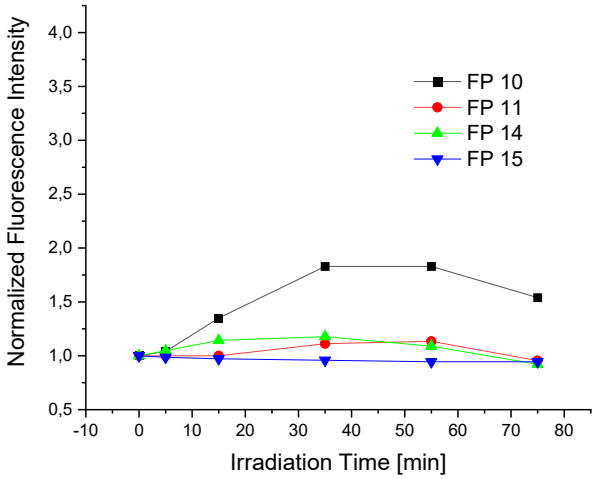

***Figure 40**: Normalized fluorescence intensity of 1µM of FP 10, FP 11, FP 14, and FP 15 in PBS (pH=7.4) as a function of the irradiation time. The normalized intensity was calculated with I / I_0. The excitation wavelength was set to 480 nm. The probes were irradiated to the light of a 470 nm LED lamp.*

As shown in **Figure 40**, the emission intensity remained relatively stable after 80 min irradiation time. Since the probe's emission was already partially quenched, the conventional photobleaching process may be less pronounced, resulting in the observed stability of fluorescence intensity over time.

FP 12 and **FP 13,** which have the same linker length but lack the disulfide component were excluded from the photobleaching experiments. The purpose of their synthesis was to investigate the impact of disulfide on the fluorescence intensity in cancer cells.

3.2.4 Glutathione-mediated fluorescence enhancement of disulfide-linked probes

To investigate the effect of glutathione (GSH) on the synthesized fluorescent probes containing disulfide linkers, initial experiments were performed before progressing to In Vitro studies with cells. This approach aimed to mimic the intracellular environment of cancer cells, where GSH is typically overexpressed. In HeLa cells, GSH concentrations range from 7 to 10 mM, significantly higher than in healthy cells. It is known that elevated levels of GSH can reduce disulfide bonds, leading to the release of the folate moiety and resulting in fluorescence enhancement, which can be detected as an increase in fluorescence intensity.[74, 75]

For this purpose, we performed experiments in cuvettes using 1 µM of **FP 10**, **FP 11**, and **FP 15** dissolved in PBS. The probes were treated with 1 mM concentrations of

GSH, and fluorescence measurements were recorded over time. As shown in **Figure 41**, we observed a marked increase in fluorescence intensity under the treatment of our probes with GSH.

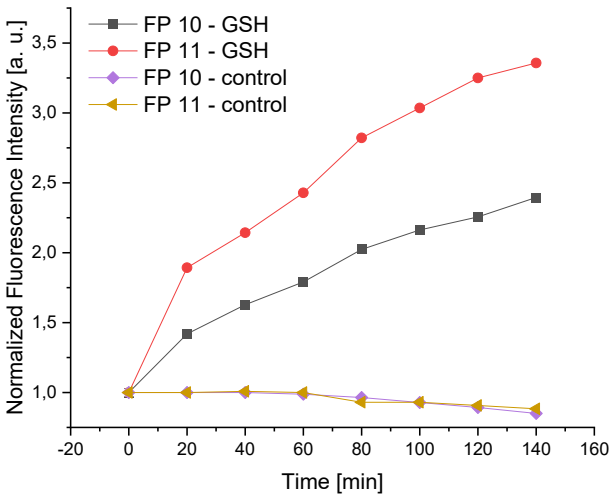

***Figure 41**: Time-dependent fluorescence enhancement of 1 µM of FP 10, FP 11, and FP 14 in PBS (pH= 7.4), in the presence of 1 mM glutathione (λex: 490 nm). Fluorescence intensity was normalized and expressed as the ratio I / I_0, where I represents the intensity at each time point and I_0 is the initial intensity.*

In the next phase of our experiments, we conducted cell assays to evaluate the behavior of synthesized **FP 10** – **FP 15** in both cancerous and healthy cells.

3.2.5 Evaluation of cancer cell selectivity of FP 10 – FP 15

To investigate the cancer cell selectivity of **FP 10** – **FP 15**, we conducted a series of cell experiments, comparing their behavior with that of folate-FITC in both cancerous HeLa cells (human cervical carcinoma) and non-cancerous HDFa cells (human dermal fibroblasts).

The experimental setup mirrored that used for **FP 2**, consisting of three key conditions: HeLa cells in folic acid-free RPMI medium, HeLa cells in medium supplemented with excess folic acid, and HDFa cells in folic acid-free medium. In each case, the cells were treated with 10 nM of probe for 15 minutes at 37°C, conditions optimized for maximum cellular uptake and labeling efficiency.

Flow cytometry analysis revealed distinct fluorescence patterns from cellular labeling with **FP 10** – **FP 14**, enabling clear differentiation between cancerous and non-cancerous cells. In HDFa cells maintained in folic acid (FA)-free medium, no significant

fluorescence enhancement was observed in **Figure 42** (left). Similarly, HeLa cells treated with an excess of folic acid showed no notable increase in fluorescence, **Figure 42** (middle). In contrast, HeLa cells cultured in FA-free medium exhibited substantial fluorescence enhancement, indicating selective uptake by cancer cells, **Figure 42** (right). The fluorescence increase along the x-axis demonstrates this selective internalization and activation, indicating successful probe entry in cancer cells.

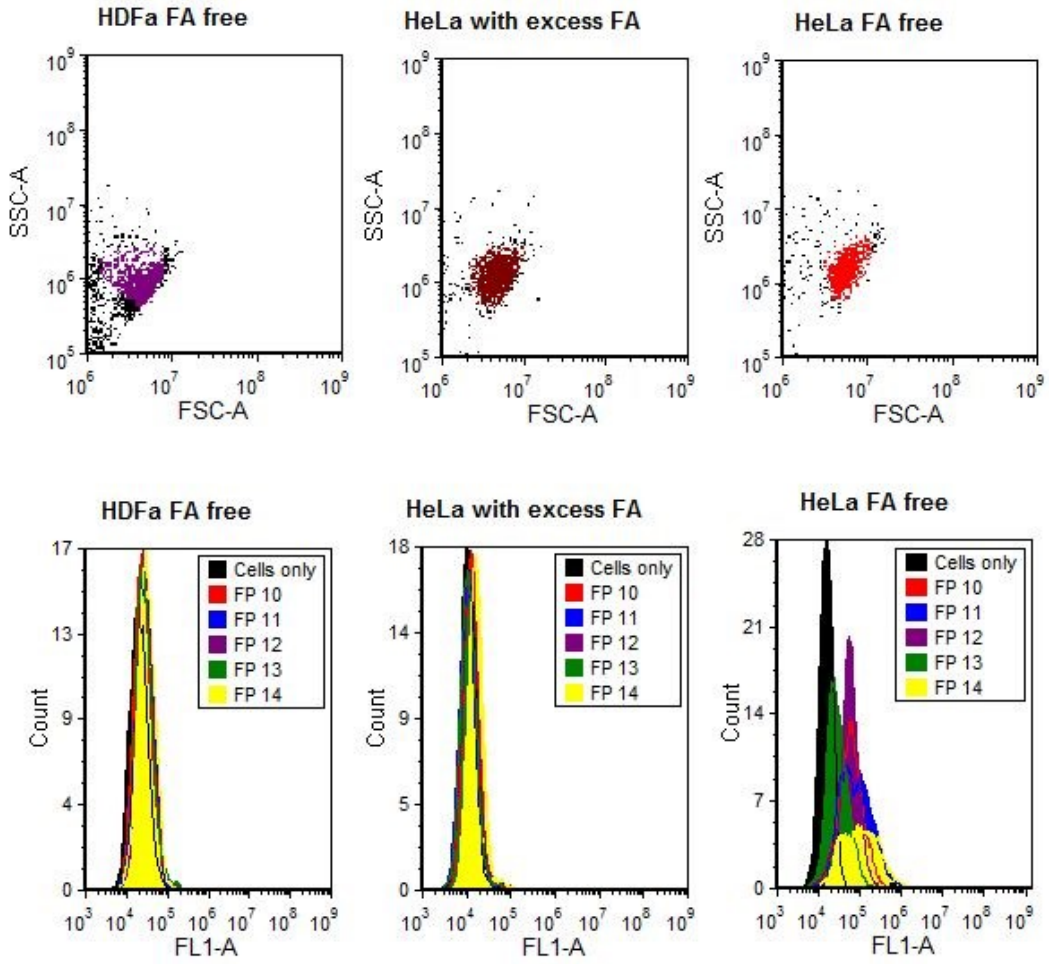

***Figure 42**: Flow cytometry analysis of the distribution of HeLa and HDFa cells (top panel) in Folic acid-free (FA-free) medium and the medium with an excess of folic acid (FA). The color distribution in the top panel indicates the gate used for the fluorescence measurement. The x-axis represents the forward scatter area (FSC-A), while the y-axis represents the side scatter area (SSC-A). Bottom panel: Representative histograms of flow cytometry analysis of adherent HeLa cells (right and middle) and HDFa cells (left) incubated with 10 nM of probes in RPMI 1640 medium and in a medium with an excess of FA at 37°C. After 15 min incubation time, cells were washed twice with PBS (pH=7.4) and detached from the surface using trypsin–EDTA. The measurements were carried out using flow cytometry (excitation: 488 nm, detection: 530/15 nm filter). The horizontal axis represents the fluorescence intensity of probes, and the vertical axis represents the number of events.*

Cell experiments with **FP 15** were performed by treating HeLa cells in a folic acid-free medium. **FP 15** has an absorption maximum of 556 nm and an emission peak of 578 nm due to the TAMRA dye**.** However, the flow cytometer available in our lab was equipped with excitation wavelengths of 488 nm and 640 nm. Although TAMRA can be excited by the 488 nm laser, it is done so with reduced efficiency compared to the dye's optimal excitation wavelength (540 nm). This suboptimal excitation likely contributed to the lack of significant fluorescence enhancement that was observed.

Additionally, we evaluated the binding and fluorescence enhancement properties of **FP 10** – **FP 14** and folate-FITC in HeLa cells at various concentrations: 1 nM, 2.5 nM, 5 nM, 10 nM, 25 nM, 30 nM, and 50 nM to determine their saturation concentrations.

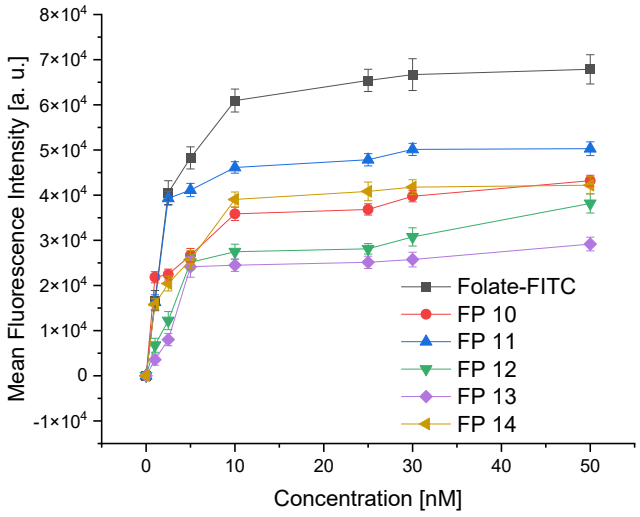

***Figure 43**: Mean fluorescence intensity of HeLa cells incubated with FP 10 - 14 at different concentrations. Cells were treated with fluorescent probes for 15 min at 37°C in RPMI 1640 medium. After incubation time, cells were washed twice with PBS (pH=7.4) and detached using trypsin–EDTA. The measurements were carried out using flow cytometry (excitation: 488 nm, detection: 530/15 nm filter). The mean fluorescence intensity of the cells was corrected by the value of the background fluorescence of non-stained cells. The error bars correspond to ± standard deviation (SD, n = 3)*

As shown in **Figure 43**, folate-FITC exhibits higher cell labeling compared to **FP 10** – **FP 14** when analyzed by flow cytometry. Notably, the higher labeling efficiency of **FP 10** and **FP 11**, which contain disulfide linkers, compared to **FP 12** and **FP 13**, which lack these linkers, suggests efficient internalization and cleavage within HeLa cells. This suggests that the overexpression of glutathione in these cells facilitates the reduction of disulfide bonds, leading to the release of the fluorophore and subsequent

fluorescence enhancement. This observation aligns with findings in Chapter 3.3.3, **Figure 52**, where the rapid binding and internalization of folate-FITC and **FP 19 - 21** are discussed.

FP 14, designed with two carboxylic acid groups in the linker to potentially enhance cellular uptake through increased negative polarity, did not show a significant difference in fluorescence compared to **FP 10** in HeLa cells. This suggests that the additional carboxylic acid groups did not substantially impact cellular internalization or fluorescence intensity.

As previously noted, the disulfide linkers in **FP 10**, **FP 11**, and **FP 14** may undergo cleavage within cells, facilitated by glutathione reduction. We hypothesize that the lower fluorescence intensity observed in HeLa cells treated with **FP 10**, compared to **FP 11**, is due to differences in the fluorescence intensity of the cleavage reduction product within the cells. As shown in **Figure 39**, the emission intensities of compounds **16** and **17**, which lack the folate moiety, were measured. The emission of the carboxy-substituted **17** was slightly higher than that of **16**. This feature may contribute to the slightly higher cellular fluorescence of **FP 11** compared with **FP 12**, assuming that this fluorescence originates from intracellular probe cleavage.

Further, we synthesized **FP18**, which maintains the same linker as folate-FITC but incorporates carboxyfluorescein in place of FITC, **Figure 44**. The cell labeling efficiency of **FP 18** to that of folate-FITC was compared to assess whether the presence of carboxyfluorescein in the fluorescent probe enhances fluorescence intensity within the cell.

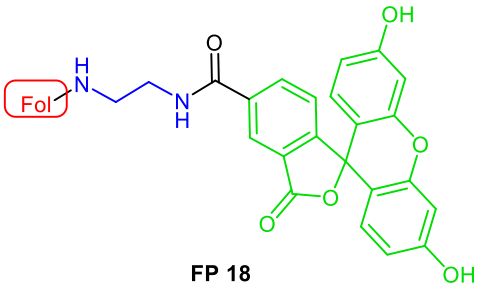

FP 18

***Figure 44**: Chemical structure of FP 18*

For the synthesis of **FP 18**, we used 5-carboxyfluorescein, rather than 5(6)-carboxyfluorescein, to avoid the complexity arising from different isomers in the product. The 5-carboxyfluorescein was coupled to the γ isomer of folic acid, linked to

ethylenediamine, similar as in folate-FITC. Purification of **FP 18** was conducted using RP - HPLC, the analytical HPLC result of **FP 18** is presented in **Figure 45**.

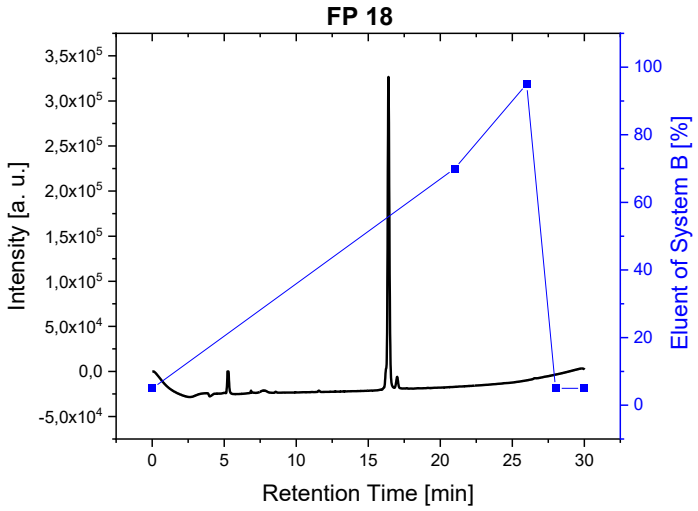

***Figure 45**: Analytical HPLC chromatograms of FP 18 with separated γ isomer (t_R=16.4).*

The emission and absorbance spectra of 1 µM of **FP 18**, compared to fluorescein and folate-FITC, are shown in **Figure 46**. The fluorescence spectrum of **FP 18** reveals the quenching effect upon coupling of folate to the fluorescein, like that observed with folate-FITC.

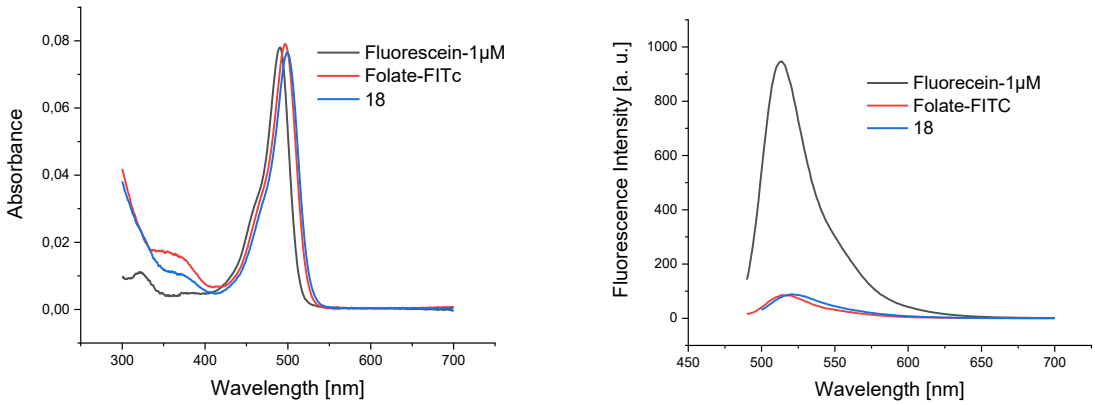

***Figure 46**: Absorbance (left) and emission (right) spectra of 1 µM solutions of FP 18, folate-FITC, and fluorescein, recorded in PBS at pH 7.4. The excitation wavelength was set to 480 nm, with a detector voltage of 520 V.*

In the next phase of our study, we assessed the binding and fluorescence enhancement properties of folate-FITC and **FP 18** in HeLa cells across a range of concentrations: 1 nM, 2.5 nM, 5 nM, 10 nM, 25 nM, 30 nM, and 50 nM

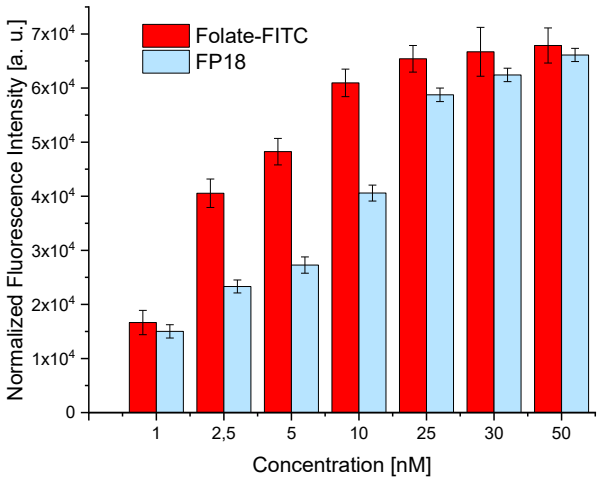

***Figure 47**: Statistical analysis of the mean fluorescence intensities of cells treated with FP 18 and folate-FITC at different concentrations for 15 min at 37°C in RPMI 1640 medium. After incubation time, cells were washed twice with PBS (pH=7.4) and detached using trypsin–EDTA. The measurements were carried out using flow cytometry (excitation: 488 nm, detection: 530/15 nm filter). The fluorescence emissions of the cells were corrected by the value of the background fluorescence of non-stained cells. The error bars correspond to ± standard deviation (SD, n = 3)*

As illustrated in **Figure 47**, at a probe concentration of 50 nM, the labelled cells exhibit comparable fluorescence intensity across both probes. However, Folate-FITC achieves fluorescence saturation at a lower concentration (approximately 10 nM), indicating more efficient cell surface binding and/or internalization, whereas **FP 18** showed a more gradual increase, approaching saturation at higher concentrations (around 25 to 30 nM). These findings suggest that folate-FITC has a stronger binding affinity and/or is taken up more efficiently by cells, whereas **FP 18** exhibits lower binding affinity and slower cellular uptake at comparable concentrations.

3.2.6 Temporal analysis of fluorescence intensity in HeLa cells

We investigated the temporal changes in fluorescence intensity of HeLa cells incubated with 10 nM concentrations of **FP 10** - **FP 14**, **FP 18**, folate-FITC, and fluorescein diacetate (FDAc). This study provided valuable insights into the kinetics of probe internalization and activation within the cellular environment. The increase in

mean fluorescence intensity over time was quantitatively assessed using flow cytometry, as shown in **Figure 48**.

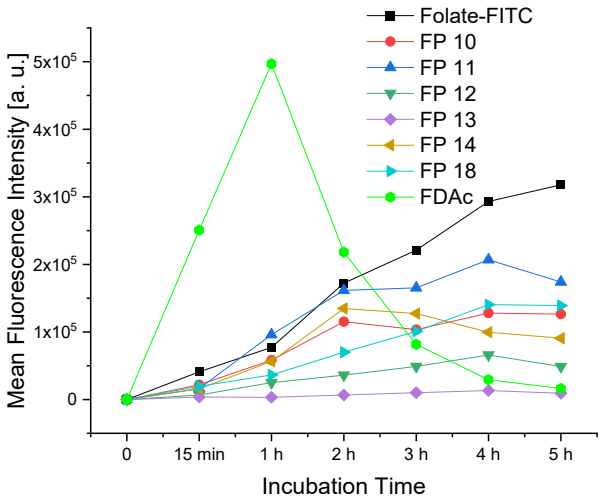

***Figure 48**: Time-dependent changes in fluorescence intensity of HeLa cells incubated with 10 nM of FP 10 – FP 14, FP 18, folate-FITC, and Fluorescein diacetate (FDAc). Following the incubation time, cells were washed twice with PBS (pH=7.4) and detached from the surface using trypsin–EDTA. The measurements were carried out using flow cytometry (excitation: 488 nm, detection: 530/15 nm filter).*

The fluorescence intensity of various probes incubated with HeLa cells changes over time, showing distinct patterns. In our control experiment, HeLa cells incubated with fluorescein diacetate (FDAc) showed a rapid increase in fluorescence intensity, peaking within the first hour. Importantly, fluorescein diacetate demonstrated the highest fluorescence intensity which serves as a reference point.

Folate-FITC indicated a steady increase in fluorescence intensity over the 5-hour incubation period, indicating consistent and prolonged interaction or uptake by the cells. **FP 10 - 14**, and **FP 18** displayed significantly lower fluorescence intensity throughout the incubation period compared to folate-FITC. **FP 10**, **FP 11**, and **FP 14** showed moderate increases during the first 1 - 2 hours, likely due to the reduction of the disulfide linker and subsequent release of dye within the cells. **FP 12** and **FP 13**, which lack the disulfide linker, exhibited the lowest fluorescence intensity with minimal changes over time. The absence of the disulfide linker in these probes appears to hinder the efficient intracellular release of the fluorophore resulting in significantly reduced fluorescence intensity.

Although **FP 18** and folate-FITC have the same linker, folate-FITC exhibited significantly higher cell labeling efficiency. Folate-FITC's superior labeling suggests it has a higher affinity for folate receptors, leading to more effective and specific cell labeling.

3.3 Fluorescent probe with very short linkers

3.3.1 Design and synthesis of fluorescent probes with very short linkers

In the field of folate-targeted fluorescent probes, numerous studies focus on the impact of varying the fluorophore or the structure of the linker on probe properties. [76, 77] The effect of very short-linker conjugated folic acid on a fluorophore has been less well explored. In this part of our study, we tried to elucidate the properties of fluorescent probes with minimized linker length, their fluorescent brightness, and cellular labeling efficacy compared to the commercially available folate-FITC. To design our fluorescent probes with minimized linker length, we employed folic acid as a cancer cell-selective ligand coupled to 5- and 6-aminofluorescein as the fluorescent dye, **Figure 49**.

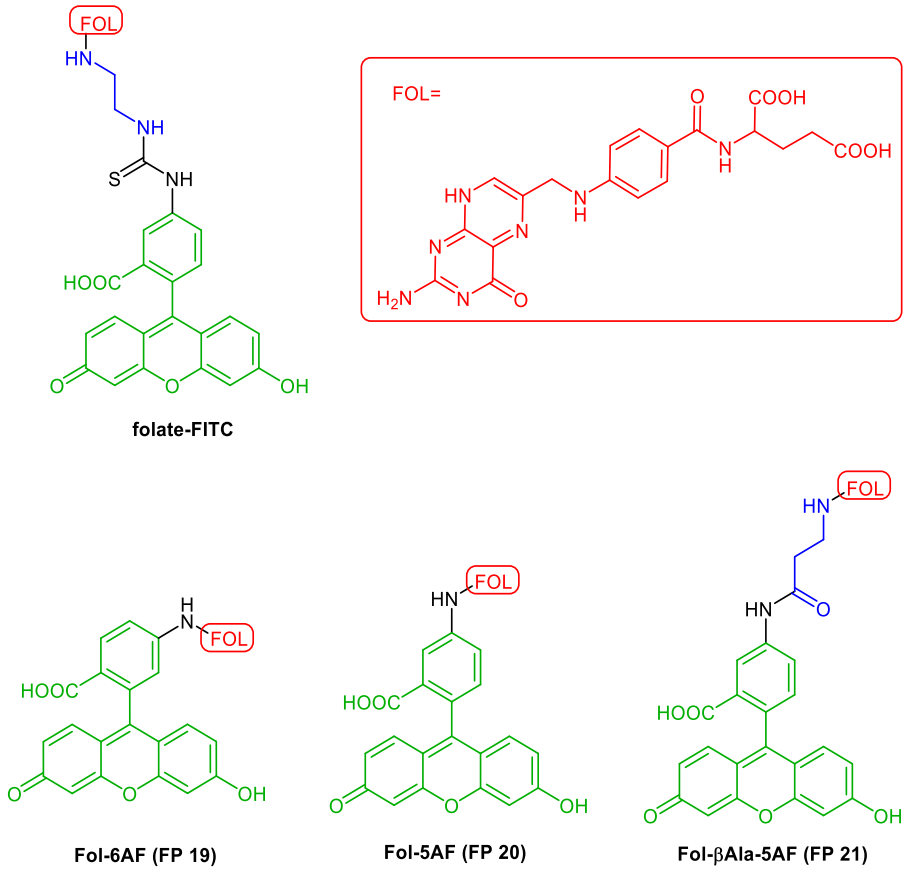

***Figure 49**: Chemical structure of the synthesized fluorescent probes with minimized linker length.*

In the design of most folate-conjugated fluorescent probes, the synthesis typically involves multiple steps, which can be time-consuming and complex. [77, 78] However, our fluorescent probes stand out due to their straightforward synthesis process. The chemical structure of our synthesized fluorescent probes is illustrated in **Figure 49**. The synthesis of folate-FITC was carried out in a three-step process: first, the amide coupling reaction of folic acid with the N-protected ethylenediamine; second, the deprotection of the amine group; and finally, the reaction of fluorescein isothiocyanate (FITC) with the free amine group to form a thiourea linkage. Fol-6AF (**19**) and Fol-5AF (**20**) were synthesized through a one-step synthetic route of the amide coupling reaction between the carboxylic acid of folic acid and the amine of commercially available 6- or 5-aminofluorescein, respectively.

For the synthesis of **FP 20**, we used TBTU (as the amide coupling reagent) and DIPEA as the base. We initially used DMTMM ((4-(4,6-dimethoxy-1,3,5-triazin-2-yl)-4-methyl-morpholinium chloride)) as a reagent for the synthesis of **FP 19**. We attempted the amide coupling of folic acid to 6-aminofluorescein using other reagents such as TBTU, DCC (Dicyclohexylcarbodiimide) with DMAP (4-(Dimethylamino)pyridine), Oxyma Pure with DIC (N,N′-Diisopropylcarbodiimide), and PyBOP (benzotriazol-1-yloxytripyrrolidinophosphonium hexafluorophosphate). However, these attempts were unsuccessful. The reaction only succeeded with DMTMM as the coupling reagent.

Additionally, we developed another probe, Fol-βAla-5AF (**FP 21**), incorporating a short beta-alanine linker, also synthesized via an amide coupling reaction. The structure of **21** was designed to realize the differences in photophysical properties and cancer cell labeling efficacy when a short linker, like in folate-FITC, is introduced to the structure of Fol-5AF (**20**).

The products were purified and analysed using RP-HPLC and ESI-MS to determine the probes' purities and molecular weights. Additionally, ^{1}H and ^{13}C-NMR, correlation spectroscopies (COSY, HSQC, HMBC), and analytical HPLC confirmed the structures of the probes.

Furthermore, we attempted to synthesize Fol-βAla-6AF. The reaction product was purified using HPLC and analyzed using ESI mass spectrometry, followed by measurement of its photophysical properties. The absorption spectrum of this compound indicated that it was not our desired product, although the mass

spectrometry analysis showed the expected exact mass. We hypothesize that an intramolecular cyclization might have occurred.

3.3.2 Photophysical properties of FP 19 – FP 21 and folate-FITC

The photophysical properties of **FP 19** – **FP 21** were evaluated by measuring their absorption and emission intensities. These measurements were conducted in two distinct solvents: phosphate-buffered saline (PBS) and human blood plasma (BP), both maintained at a pH of 7.4. This dual-solvent approach enabled the assessment of the probes' behavior in a standard buffer and biologically relevant media, providing insights into their performance under conditions that mimic physiological environments. The comparative absorption and emission spectra are illustrated in **Figure 50**.

As shown in **Figure 50, B**, the stability of all four fluorescent probes in human blood plasma is confirmed, indicating their potential reliability and effectiveness in biological applications.

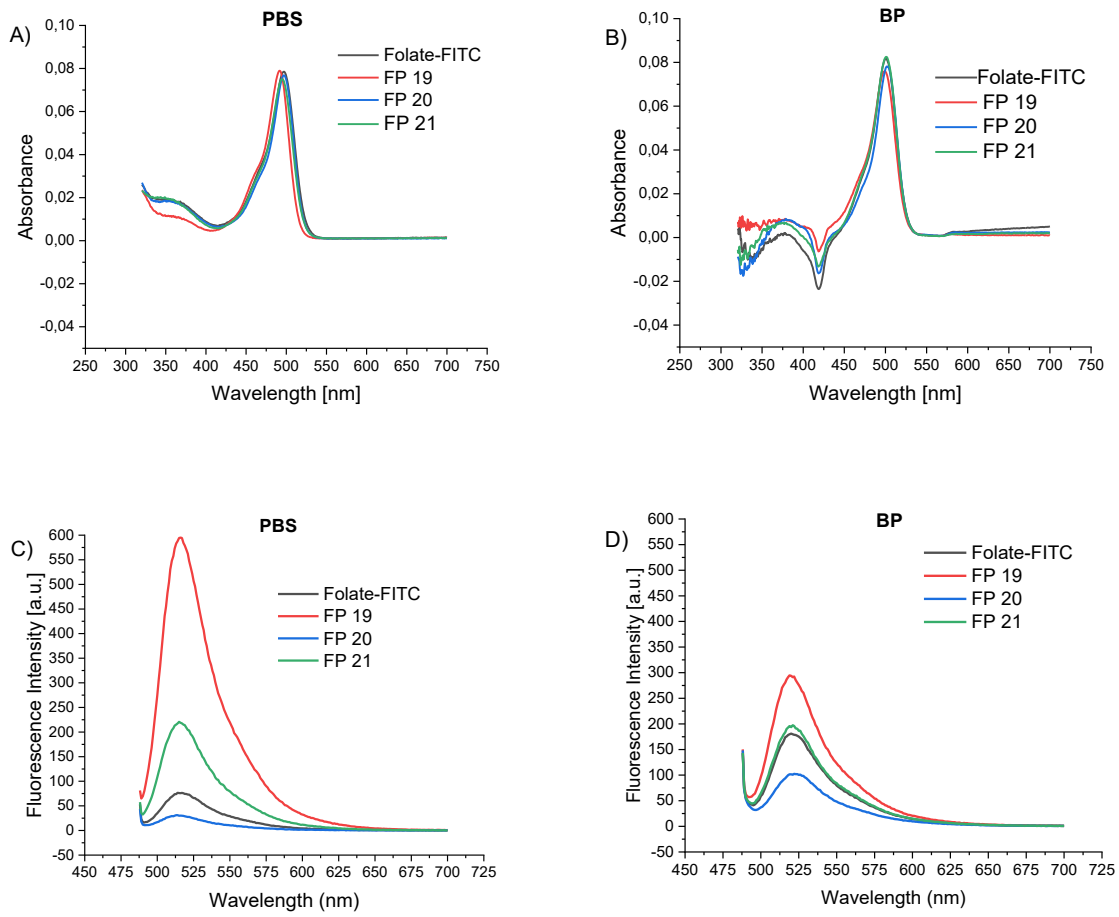

***Figure 50**: Absorption spectra of 1μM solution of FP 19 – 21 and folate-FITC in A) PBS (pH=7.4) and B) in human blood plasma (BP) (pH=7.4). C) Emission spectra of 1μM of fluorescent probes in PBS,*

and D) human blood plasma (BP). The excitation wavelength was set to 480 nm, with a detector voltage of 520 V.

Table 4 summarizes the key photophysical parameters of **FP 19** - **FP 21** compared to folate-FITC and fluorescein. Quantum yields were determined using the comparative method, employing fluorescein as a reference standard (φR = 0.85 in PBS).[58]

***Table 4**: Photophysical properties of 1 μM concentrations of FP 19 - 21, folate-FITC, and fluorescein were assessed in PBS (pH:7.4). The excitation wavelength was set to 480 nm, with a detector voltage of 520 V.*

Compound	$\lambda_{max\ (Abs)}$[nm]	$\lambda_{max\ (Em)}$[nm]	Stokes shift [nm]	ε [M^{-1} cm^{-1}] 10^4	Quantum yield in PBS (pH=7.4)
Fluorescein	490	515	25	7.90	0.85
Folate-FITC	496	516	20	7.84	0.08
FP 19	492	516	24	7.87	0.59
FP 20	496	516	20	7.63	0.03
FP 21	494	516	22	7.45	0.21

In PBS, Fol-5AF (**FP 20**) showed significant emission quenching due to the proximity of the folic acid to the fluorophore, resulting in low fluorescence intensity with a quantum yield of only 0.03, representing approximately 37.5% of the quantum yield of folate-FITC. The proximity of folic acid to the fluorophore in this isomer likely leads to increased quenching and, consequently, resulting in a markedly reduced fluorescence intensity.

Fol-βAla-5AF (**FP 21**), which incorporates a β-alanine linker between folic acid and fluorescein, had a quantum yield of 0.21, about 7 times higher than Fol-5AF (**FP 20**). The increased distance between the folic acid (quenching moiety) and the fluorophore due to the beta-alanine linker reduces the quenching effect of folic acid on fluorophore.

The optical characteristics of Fol-6AF (**FP 19**) showed a significant difference in the fluorescence intensity of this probe compared to Fol-5AF (**FP 20**). This significant difference can be attributed to the spatial configuration of the molecule and electronic environment of the fluorophore. The 6-aminofluorescein isomer likely places the folic acid in a position that reduces the efficiency of the quenching mechanism, thereby minimizing the quenching effect on the fluorophore.

In blood plasma, the fluorescence brightness of fluorescent probes is modulated possibly by interaction with proteins or other plasma components. Remarkably, the much stronger quenching of **FP 20** compared with folate-FITC is maintained in plasma, the residual fluorescence of the latter is about twice as high. This is an encouraging result that promises a lower background fluorescence of the extracellular fluid in imaging application, **Figure 50, D**.

3.3.3 Cell Experiments

To determine the selectivity of the probes we conducted cell experiments in both HeLa (human cervical carcinoma) and HDFa (healthy human dermal fibroblasts) cells. The distributions of HeLa and HDFa cells used in our experiments are illustrated in **Figure 51,** top panel. We chose HeLa cells as the representative cell line due to their high expression levels of the folate receptors (FRα), compared to healthy cells. The cells were cultured in folic acid-free, RPMI 1640 media, for six passages. The scatter plots showing the distribution of HeLa and HDFa cells are presented in **Figure 51,** bottom panel.

To determine whether our new probes exhibit selectivity to cancer cells, both HeLa cells and HDFa were treated with 10 nM of probes for 30 min at 37°C, based on optimal incubation conditions for the cells. Flow cytometry measurements revealed selective labeling of the cancer cells, as shown in **Figure 51**, (right). In this figure, an increase in fluorescence on the x-axis is apparent. In contrast, **Figure 51** (left) shows the HDFa cells, where there is no enhancement in fluorescence, indicating no labeling occurred in these cells.

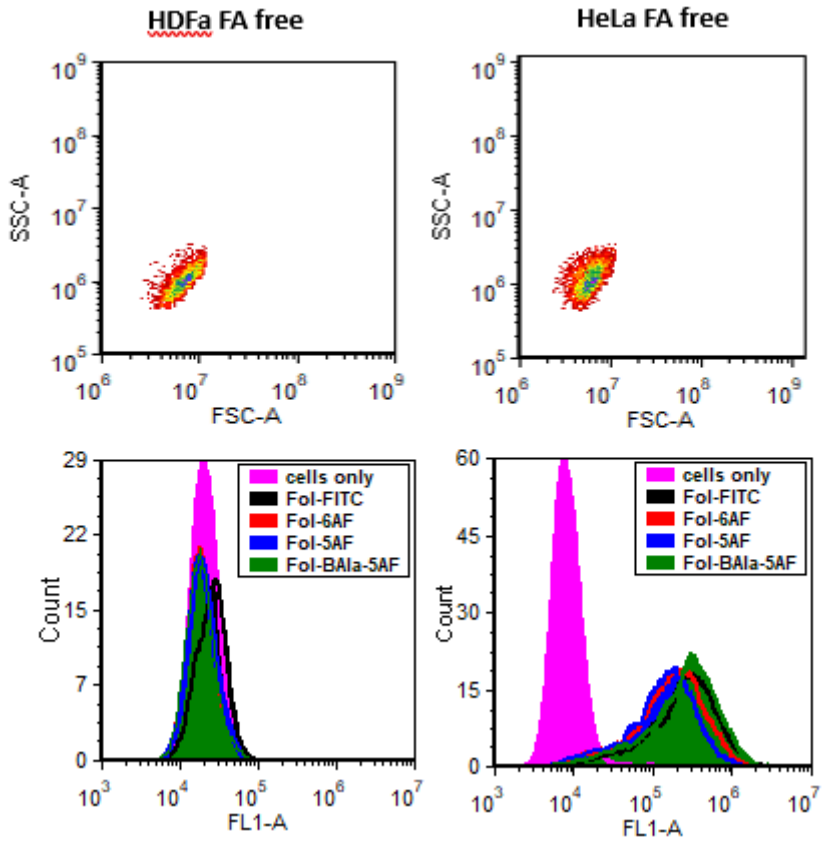

***Figure 51**: Flow cytometry analysis of the distribution of HeLa and HDFa cells (top panel) in Folic acid-free (FA-free) medium. The color distribution in the top panel indicates the gate used for the fluorescence measurement. The x-axis represents the forward scatter area (FSC-A), while the y-axis represents the side scatter area (SSC-A). Bottom panel: Representative histograms of flow cytometry analysis of adherent HeLa cells (right) and HDFa cells (left) incubated with 10 nM of probes in RPMI 1640 medium at 37°C. After 15 min incubation time, cells were washed twice with PBS (pH=7.4) and detached from the surface using trypsin–EDTA. The measurements were carried out using flow cytometry (excitation: 488 nm, detection: 530/15 nm filter). The horizontal axis represents the fluorescence intensity of probes, and the vertical axis represents the number of events.*

Additionally, we evaluated the binding and fluorescence enhancement properties of synthesized fluorescent probes in HeLa cells at various concentrations: 1 nM, 2.5 nM, 5 nM, 10 nM, 25 nM, 50 nM, and 100 nM to determine their saturation concentrations and compared these results with folate-FITC, **Figure 52**. To determine the amount of unspecific binding of the fluorescent probes, we simultaneously incubated HeLa cells with probes in the presence of an excess of folic acid (ex. Fol). In all cases, binding was almost completely inhibited by the excess of folic acid, which indicates an extremely low amount of non-specific binding, **Figure 52**, left.

The flow cytometry analysis demonstrated that all probes effectively bind to cancer cells, leading to enhanced fluorescence. All probes have a saturation concentration in

the low nanomolar range, comparable to folate-FITC. This high affinity means that only a small amount of our probes is needed to bind to folate receptors. This characteristic offers several advantages, especially in intraoperative fluorescence imaging. Using probes that perform optimally at lower concentrations can result in brighter fluorescence signals, facilitating better visualization of cancerous tissues during surgery. Another interesting feature is the different fluorescence intensity, folate-FITC > 19 > 20, 21, of the cells upon probe saturation at relatively short incubation times. This is apparently a consequence of different fluorescent intensities of the folate receptor-bound probes, assuming that receptor binding masks the quenching effect of the folate moiety and restores the fluorescence of the quenched-free probes.

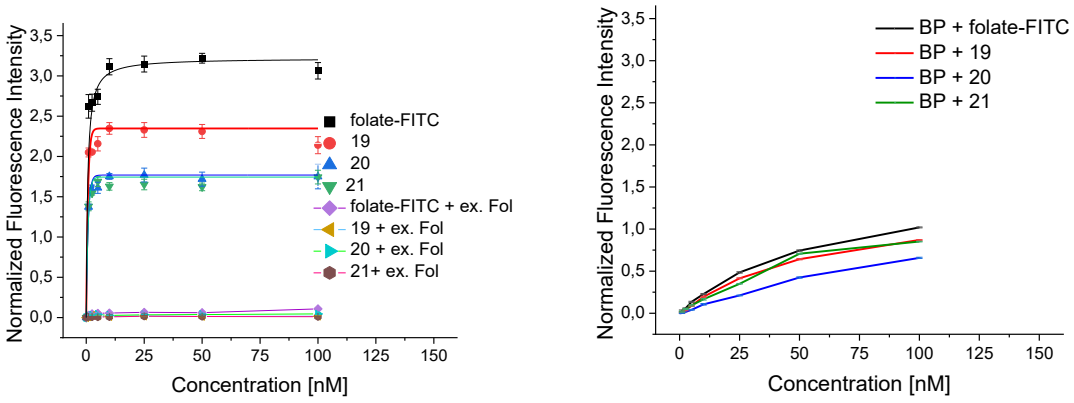

.

***Figure 52**. Fluorescence intensity of HeLa cells incubated with fluorescent probes at different concentrations. Left: Cells were labeled with fluorescent probes for 30 min at 37°C in RPMI 1640 medium in the absence (black, red, blue, and green) and the presence (purple, orange, turquoise, and maroon) of an excess of folic acid (ex. Fol), and right: in 1 mL of blood plasma (BP). After incubation time, cells were washed twice with PBS (pH=7.4) and detached using trypsin–EDTA. The measurements were carried out using flow cytometry (excitation: 488 nm, detection: 530/15 nm filter). The fluorescence emissions of the cells were corrected by the value of the background fluorescence of non-stained cells. The error bars correspond to ± standard deviation (SD, n = 3)*

To further evaluate the binding efficacy of probes in a more physiologically relevant environment, HeLa cells cultured in RPMI 1640 medium were incubated with 10 nM of each probe in 1 mL blood plasma serum solution (BP) for 30 minutes at 37°C, **Figure 52**, right. The fluorescence intensity of the cells was then measured using flow cytometry at various probe concentrations. The results indicated that the fluorescence of HeLa cells began to increase at probe concentrations of 25 - 50 nM. This shift in the concentration required for fluorescence enhancement, compared to the 1 - 2 nM

observed in a folic acid-free medium, is attributed to the presence of folic acid in human blood plasma. This folic acid competes with the probes for binding to folate receptors, thereby blocking these receptors at lower probe concentrations. At higher concentrations, however, the probes can outcompete the plasma folic acid, allowing folate-conjugated probes to bind to the folate receptors and resulting in the observed fluorescence enhancement.

3.3.4 Live cell imaging

After conducting flow cytometry experiments to measure the fluorescence of HeLa cells incubated with probes, we progressed to live cell imaging using confocal microscopy. Adherent HeLa and HDFa cells were incubated with 10 nM of each probe in a live cell imaging solution buffered with HEPES at pH 7.4 for 15 minutes. The cells were incubated with Hoechst for 5 minutes. Confocal microscopy images were then captured, as shown in **Figure 53**. Typically, cells are washed before imaging to remove any free fluorescent probe in the medium, but we omitted this step to better mimic intraoperative fluorescence imaging conditions. This approach provides a more accurate representation of real intraoperative imaging conditions.

In HeLa cells, all probes are internalized within the cells, indicating successful uptake of the probes by the cancer cells. This internalization and the resulting fluorescence signal confirm that the probes are effectively targeting the folate receptors on the HeLa cells. The strong intracellular fluorescence observed in confocal images suggests that the probes are actively transported into the cells. This is crucial for effective imaging, as internalized probes can provide a more stable and robust fluorescence signal compared to surface-bound probes, which might be more susceptible to environmental quenching or removal.

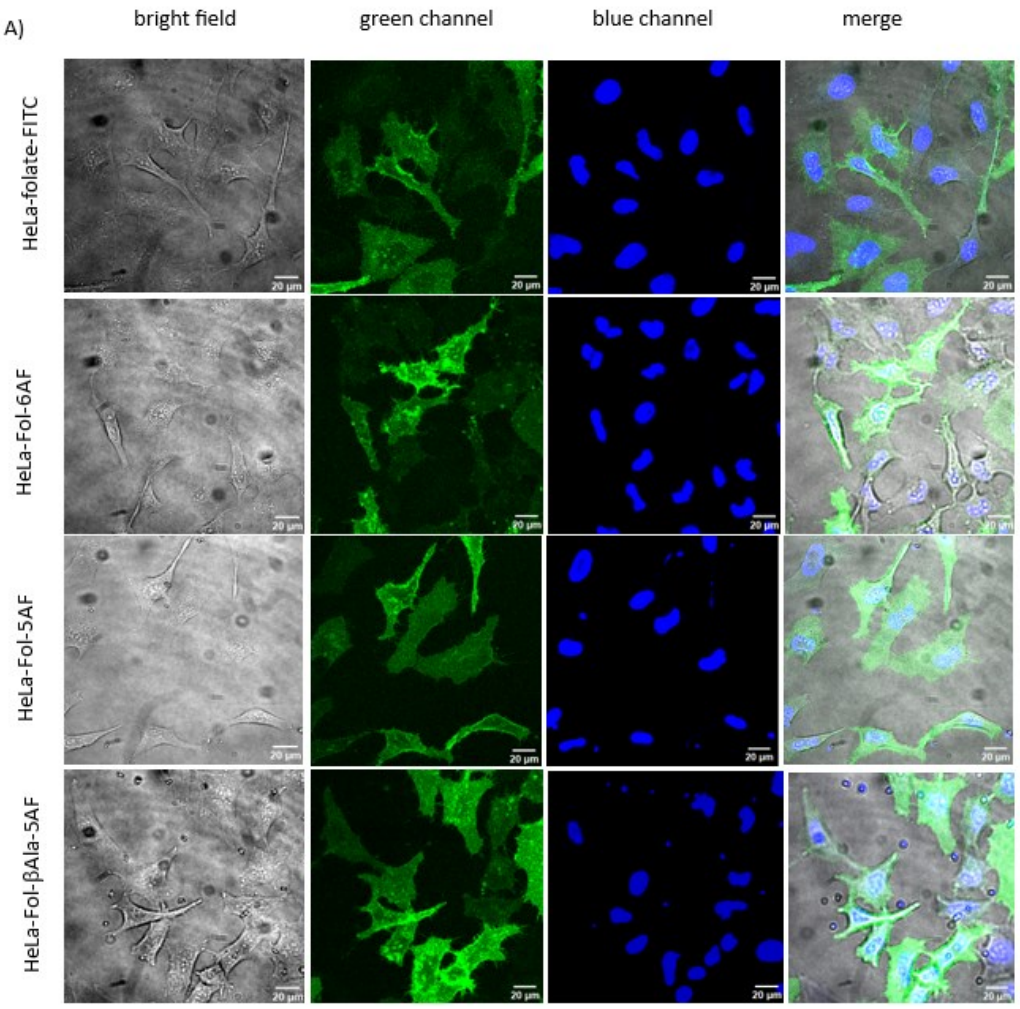
A)
bright field
green channel
blue channel
merge
HeLa-folate-FITC
HeLa-Fol-6AF
HeLa-Fol-5AF
HeLa-Fol-βAla-5AF
20 µm

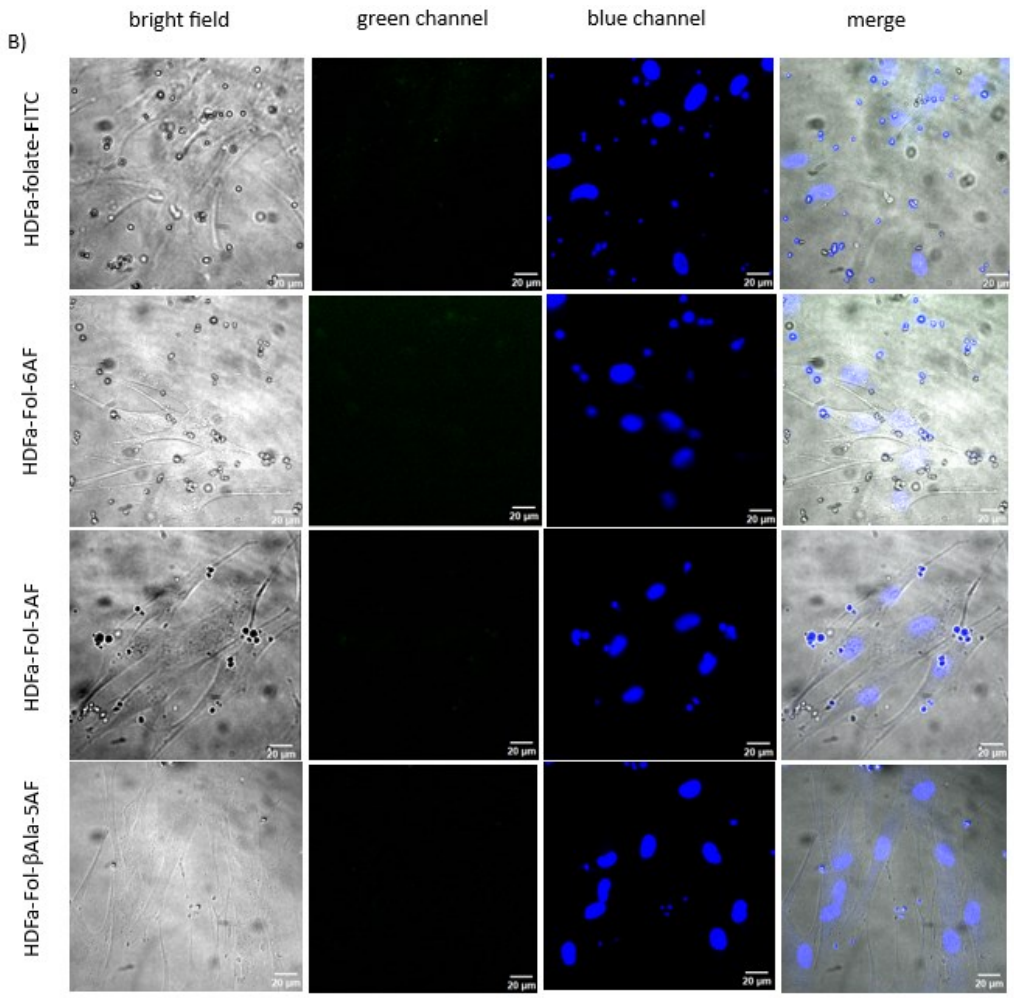

***Figure 53**: Confocal fluorescence microscopy images of live A) HeLa cells and B) HDFa cells treated with fluorescent probes. Cells were incubated with probes (10 nM, 15 min, 37°C), subsequently stained with Hoechst 33342 (nuclei stain) and were imaged by confocal microscopy. Scale bar = 20 µm. Filters: Hoechst (λex/em = 403/440 nm), fluorescein (λex/em = 487/515 nm). The 15-minute incubation time was selected to align with standard cell staining protocols and to ensure experimental practicality.*

The comparison of these data with HDFa cells, which exhibited extremely low fluorescence, further highlights the specificity of the probes for cancer cells. The minimal fluorescence observed in HDFa cells indicates that healthy cells have a weak uptake of the probes. The extremely low fluorescence in HDFa cells ensures a clear contrast between cancerous and non-cancerous cells. This high specificity and low background fluorescence are advantageous for intraoperative tumor resection, allowing surgeons to delineate tumor margins and minimize damage to surrounding healthy tissue more accurately.

4. Summary

This study focused on the synthesis and evaluation of a series of folate-conjugated fluorescent probes designed to specifically target cancer cells overexpressing folate receptors while minimizing background fluorescence in healthy tissues.

Three types of probes were synthesized: (1) **FP 2**, containing an O-aminoserine linker, coupled to fluorescein via an oxime-click reaction; (2) **FP 10** – **FP 15**, incorporating a disulfide linker designed to release fluorescein upon reduction by glutathione, which is overexpressed in cancer cells; and (3) **FP 19** – **FP 21**, where folic acid was directly coupled to aminofluorescein, enabling the evaluation of fluorescent probes with very short linkers in terms of cellular uptake and fluorescence behavior. All probes were synthesized using established amide coupling reactions and purified via reverse-phase HPLC.

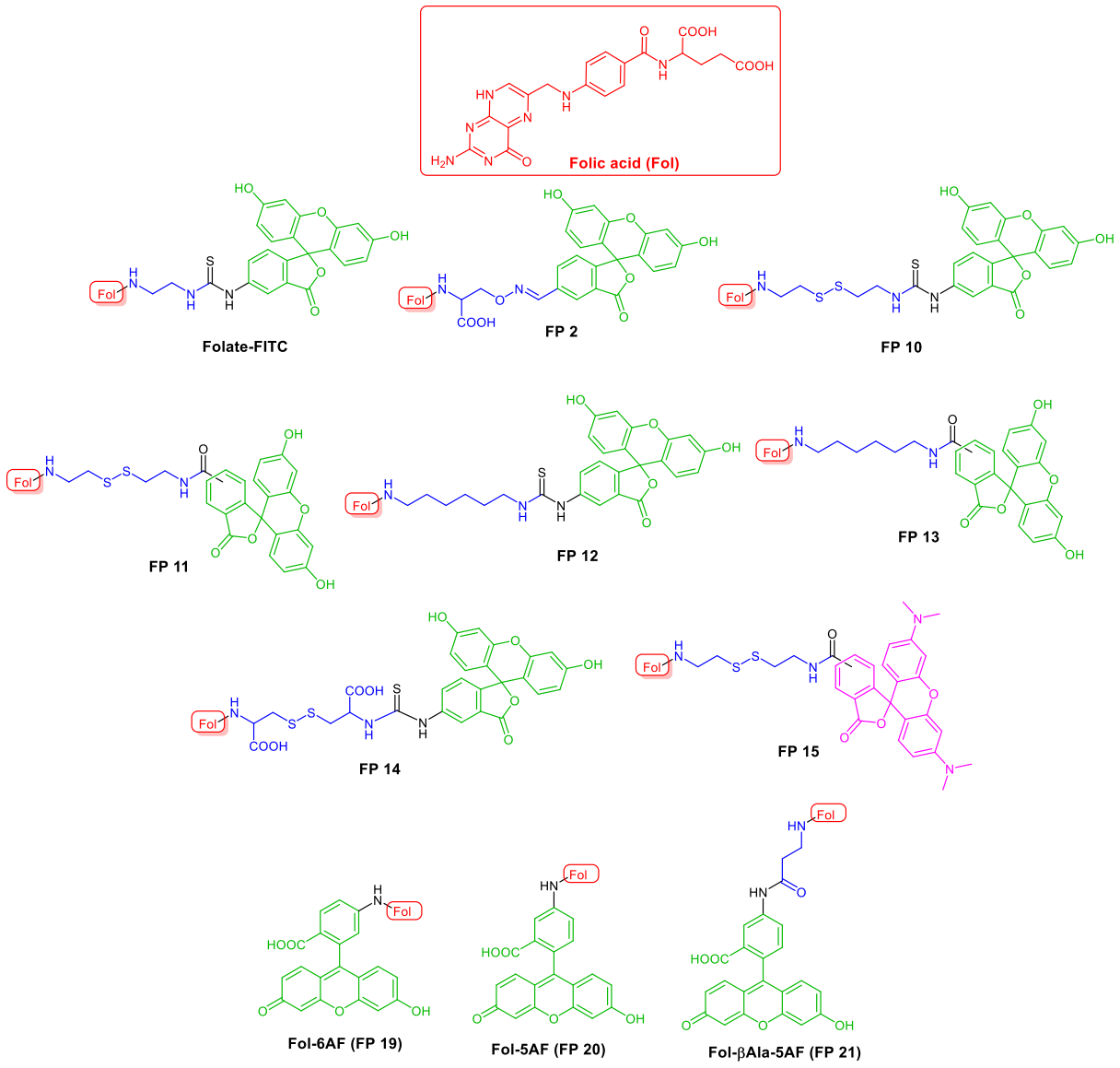

The primary objective was to develop probes that outperform folate-FITC, which is currently in phase 2 clinical trials for FDA approval. Photophysical measurements revealed that Fol-5AF (**FP 20**) and **FP 2** exhibited fluorescence quantum yields 3- and 2-fold lower than folate-FITC, respectively. This reduced fluorescence yield could reduce the signal-to-noise ratio, making it easier to distinguish cancerous tissues from healthy ones.

Photostability of the probes was also investigated. Notably, 1 μM of **FP 2** dissolved in PBS exhibited a fourfold increase in fluorescence intensity after 70 minutes of exposure to 470 nm LED light. **FP2** initially has low fluorescence due to quenching by the oxime moiety, likely caused by altered internal charge transfer (ICT) or photoinduced electron transfer (PET), as observed in **Figure 25**. Upon photoirradiation, the oxime moiety is cleaved, releasing a fluorescent moiety with higher emission intensity. In contrast, other probes (**FP 10**, **FP 11**, **FP14**, and **FP 15**) showed the expected reduction in fluorescence after irradiation. **FP2** combines photoinduced fluorescence turn-on with high cancer cell selectivity, and application to cellular imaging would be an interesting extension of the present study due to its potential for contrast enhancement and to overcome photobleaching.

Cancer specificity was tested using HeLa and non-cancerous cells, as well as HeLa cells with excess folic acid. All probes selectively enhanced fluorescence in HeLa cells, confirming their cancer specificity, while showing no fluorescence enhancement in non-cancerous cells and HeLa cells incubated with excess folic acid.

The properties of **FP 10** and **FP 11** (with disulfide linkers) were compared with **FP 12** and **FP 13**, which lacked disulfide linkers. Flow cytometry revealed that **FP 10** and **11** showed higher fluorescence intensity in HeLa cells compared to **FP 12** and **FP 13**. This result supports the hypothesis that our synthesized folate-conjugated fluorescent probes are not only bound to folate receptors on the cell membrane but are also internalized into the cells. Inside the cell, the disulfide bond is reduced by glutathione (overexpressed in cancer cells), removing the folic acid (the quenching component) and releasing the fluorescein dye, leading to enhanced fluorescence compared to probes without disulfide linkers, which remain less fluorescent.

The study also examined the saturation concentrations of the probes. **FP 19** – **FP 21** exhibited saturation concentrations comparable to folate-FITC. In blood plasma, the saturation concentration for HeLa cells incubated with folate-FITC and **FP 19** – **FP 21**

increased to 90 - 100 nM, likely due to the presence of folic acid in the plasma, which binds the folate receptors and necessitated higher probe concentrations for binding. According to the WHO, the concentration of folic acid in blood plasma typically falls within the normal range of 14 – 46 nM. [79]

Confocal microscopy provided deeper insights into the performance of the probes. The fluorescence intensity of HeLa and non-cancerous HDFa cells, treated with 10 nM of **FP 19** - **FP 21** and folate-FITC, was analyzed. **FP 19** – **FP 21** exhibited cancer-specific labeling similar to folate-FITC. A comparison of the confocal images of HeLa and HDFa cells confirmed that the probes are cancer-specific due to the overexpression of folate receptors on cancer cells, leading to their internalization and activation potentially through a bioenzymatic process within the cells. The observed fluorescence in HeLa cells suggests that the probes were successfully internalized, the quenching moiety was cleaved and the fluorescein component responsible for fluorescence was released.

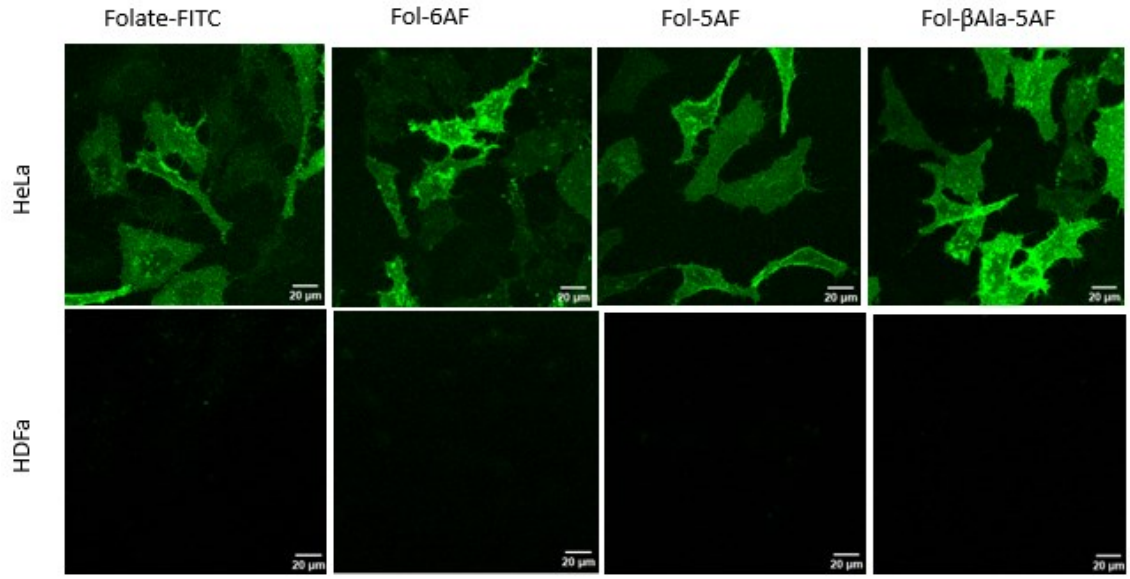

In conclusion, the newly synthesized folate-conjugated fluorescent probes, particularly **FP 19** - **FP 21**, show significant promise for cancer-specific imaging. Their high labeling efficiencies along with low nonspecific fluorescence in human plasma and non-cancerous cells suggest they could be highly effective for fluorescence-guided surgery. Further optimization, including in vivo testing, is required to fully assess their potential for use in cancer cell imaging applications.

5. Instruments, Chemicals, and Analytical Techniques

5.1 General Remarks

Air- and moisture sensitive substances were handled under a dry, inert argon atmosphere using standard Schlenk-techniques and flame-dried glassware. Anhydrous solvents were obtained commercially or dried using standard techniques and stored under argon over molecular sieves.

Temperature-sensitive compounds were stored at 4 °C or -20 °C. Stock solutions were prepared in DMSO and stored at -85 °C in the dark.

Atom numbers for NMR assignments are not always based on IUPAC nomenclature.

5.2 Chemicals

Chemicals used for syntheses were obtained from Sigma-Aldrich, TCI, Thermo Scientific, BLDpharm, Merck, Fischer Scientific, Alfa Aesar, and Carl Roth or bought at the central store of the chemical institutes at Heidelberg University. Commercial reactants and solvents were obtained at 97% purity or better and used without further purification.

5.3 Thin-Layer and Flash Chromatography

TLCs were performed on Polygram Sil G/UV254 or Alugram RP18 W/UV245 plates (Macherey-Nagel). Spots were visualized by UV light or ninhydrine staining. For flash chromatography, silica gel (40 - 63 μm, 60 A pore size, Sigma-Aldrich) was used. R_f-values were determined in the solvent system used for flash chromatography unless otherwise specified.

5.4 Nuclear Magnetic Resonance Spectra

Nuclear magnetic resonance spectra were recorded using Bruker Avance III 600 or Bruker Avance Neo 700 spectrometers. Deuterated solvents were obtained from Deutero or Sigma-Aldrich. Chemical shifts δ are given in ppm and coupling constants J in Hz. Spectra were calibrated using the residual ^{1}H or ^{13}C signals of the deuterated solvents. Measurements were performed at 298 K unless otherwise specified. The following abbreviations were used to describe the multiplicities of the signals: s (singlet), d (doublet), t (triplet), q (quartet), m (multiplet), and br. (broad). Signals were assigned using COSY, HSQC, and HMBC spectra.

5.5 Mass Spectrometry

Mass spectra were recorded on a Bruker ApexQe hybrid 9.4 T FT-ICR (HR-ESI). The symbol M in mass signal assignments refers to the molecule shown in the corresponding drawing without the counter ions depicted therein.

5.6 Preparative and Analytical HPLC

Preparative HPLC purifications were performed on Shimadzu HPLC systems at 20 °C. Crude products were filtered using a syringe filter (Mini-sart RC 4, 0.2 µm, RC-membrane, PP-housing) from Sartorius prior to HPLC-purification.

Preparative HPLCs for all derivatives were performed on a Shimadzu HPLC system with LC-20AD pumps, SPD-20A UV-detector, CBM-20A controller, SIL-10AP autosampler, FCV-20AH2 valve unit. The C18 columns which served as stationary phases are named in line with the synthetic protocols. H_2O with 0.1 % TFA as system A and 80% MeCN, 20% H_2O with 0.1 % TFA as system B, were used as eluents. Products were collected manually and identified by MALDI-TOF and ESI mass spectrometry.

Analytical HPLCs for all derivatives were performed on a Shimadzu HPLC system with LC-20AD pumps, SPD-M20A diode-array detector, DGU-14A degasser, and a CTO-10ASvp column oven.

For the analytical HPLCs, we used a detector wavelength of 254 nm to ensure better observation of product purity.

5.7 UV/Vis Spectroscopic Analysis and Fluorescence Measurements

UV/Vis spectra were recorded on Shimadzu UV-2600 in 1 mL PMMA cuvettes (Sigma-Aldrich) at 20 °C. Stock solutions of the samples for the determination of molar extinction coefficients were prepared from samples in DMSO or DMSO-d_6 with isopropanol or DCM as standard using NMR-spectroscopy to determine the concentration of these stock solutions. Stock solutions were diluted in PBS to measure at least four different concentrations in the range of 1.2 µM to 0.6 µM. The molar extinction coefficients at the absorption maximum λ_{max} (Abs) were obtained using Beer's law at 1.2 µM to 0.6 µM dilution.

Fluorescence measurements were performed on a Varian Cary Eclipse spectrophotometer. The emission scan setup included an excitation wavelength of 480 nm, an emission range from 490 nm to 700 nm, and slit widths of 5 nm. The scan rate

was set to medium. The Y-axis limits are set from 0 to 1000. The PMT detector voltage was manually set to 520 V. After preparing the 4 different concentrations of samples, measurements were taken in 1 mL PMMA cuvettes. These settings were consistently applied across all measurements. The emission spectra observed in the Photophysical Properties section were measured at least 10 times with different concentrations of fluorescent probes, each following the identical procedure. The results were uniformly consistent, demonstrating the reliability and reproducibility of the results.

6. Cell Experiments

6.1 Cell Lines and Media

Human cervical cancer cells (HeLa acc57) were obtained from the DSMZ and cultivated in EMEM (Lonza BE12-125F) supplemented with 10% FCS (Biochrom), 1% penicillin/streptomycin (sigma), and 1% L-glutamine (Gibco). the cells were cultivated in RPMI 1640 without folic acid (see below) for 6 passages.

Adult human dermal fibroblasts (HDFa) were obtained from Life Technologies and cultivated in DMEM without phenol red (Lonza BE12-917F) with 10% FCS, 1% penicillin/streptomycin, and 1% L-glutamine.

The cells were cultivated in RPMI 1640 without folic acid for 4 - 6 passages.

RPMI 1640 without Folic Acid

.

Volume	Ingredient	Stock concentration	Final concentration
402.5 mL	Sterile water		
50 mL	RPMI 1640 with phenol red; without folic acid (Sigma-Aldrich R1145)	10x	1x
25 mL	FCS		5 %
12.5 mL	$NaHCO_3$ (stock solution)	80 g/l	2 g/l
5 mL	L-glutamine	100x	2 mM (1 %)
5 mL	Streptomycin/penicillin	100x	100 µg/mL (1 %)

6.2 Cell Culture

Adherent cells were grown in 50 ml or 250 ml cultivation vessels (CellStar) as monolayers. Exponentially growing cultures were maintained at 37 °C in a humidified

atmosphere with 5% CO_2 and passaged twice weekly using 0.05%/0.02% (w/v) Trypsin/EDTA solution (Sigma).

6.3 Preparation and Flow Cytometry Analysis of Fluorescent Probes-General

Fluorescent probes were prepared in different concentrations in PBS or human blood plasma (The Blood Bank of IKTZ Heidelberg, Interdisciplinary Clinical Transfusion Center Heidelberg). After removal of the growth medium, cells were washed with PBS (2x 1 mL) and incubated with the different probes for 30 minutes at 37 °C. Subsequently, the cells were washed with PBS (2x 1 mL), detached from the well-plate with trypsin/EDTA, suspended in PBS, and subjected to analysis by flow cytometry.

Flow cytometry experiments were performed on a C6 cytometer (Accuri). Adherent cells were seeded in 24-well plates (CellStar) 24 hours before the measurement.

All flow-cytometry measurements were performed in triplicates on live cells and included 2000-5000 events in the gated area chosen as the area of the cells using a blank sample.

Fluorescence excitation was at 488 nm, emission was detected using a 530 ± 30 nm filter. The mean fluorescence intensity of this channel (FL-1A) was plotted after subtraction of the blank value (unlabeled cells).

6.4 Confocal Microscopy

The confocal fluorescence microscopy images discussed in the live cell imaging were obtained using the methods described here. Cells were seeded in 8-well glass slides (ibidi GmbH; 20 000 cells per well) 24 hours before the experiment. After carefully removing the growth medium and washing with PBS (2 x 200 μL), Cells were incubated with 10 nM of probes, and subsequently stained with Hoechst 33342 (nuclei stain) for 15 minutes at 37 °C. The 15-minute incubation time was selected to align with standard cell staining protocols and to ensure experimental practicality.

Without washing the incubated probes, images were recorded using A1plus software in Galvano mode. Channel 1 (DAPI) was set with a 403 nm laser and a 425-475 nm emission range, with the HV (high voltage) at 115. Channel 2 (FITC) was set with a 487 nm laser and an emission range of 500-550 nm, with the HV at 118. We used a Nikon Plan Apo IR 60x NA 1.27 WI (WD 0.18 - 0.16mm, FOV 0.21 x 0.21mm) objective. These settings were consistently applied across all measurements to ensure uniformity and accuracy of the imaging.

All literature-known compounds are labelled with a star *.

7. Synthetic Procedure

7.1 Synthesis of Fol-eda * (Folic acid coupled on ethylendiamine):

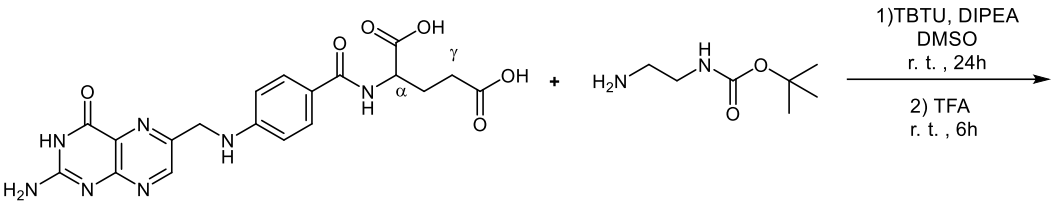

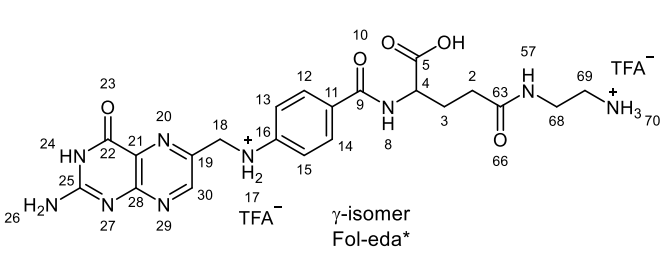

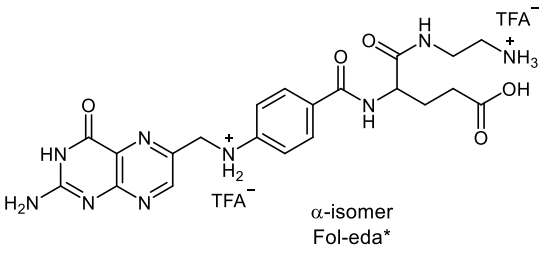

The synthesis of Fol-eda was carried out following the procedure reported by Krämer et al. with slight modifications. [80]

Folic acid dihydrate (510.0 mg, 1.00 eq) was dissolved in 15 mL DMSO and 5 mL DMF. DIPEA (242 µL, 179.5 mg, 1.30 eq) and TBTU (411.6 mg, 1.20 eq) were then added, and the solution was stirred for 20 minutes. N-Boc-ethylenediamine (188.3 mg, 1.10 eq) was dissolved in 1 mL of DMF and subsequently added to the mixture. The reaction was stirred at room temperature overnight. The reaction mixture was precipitated using 250 mL of cold diethyl ether and centrifuged. The supernatant was discarded, and the residue was treated with 5 mL of TFA. This solution was stirred for 6 hours at room temperature and the solid was precipitated again using 200 mL of ethyl acetate and centrifuged. The crude product was lyophilized and then purified using preparative RP-HPLC, 5 cm-Latek ProSep C18 (5µm, 250 mm x 20mm), H_2O with 0.1% TFA (system A) / 80% MeCN-20% H_2O and 0.1 % TFA (system B), 80 mL/min. After lyophilisation, the desired product was obtained as an orange amorphous powder. The separation of isomers yielded in γ- modified Fol-eda (82.8 mg, 10.9%) α- modified Fol-eda (101.8, 13.4%) mg, and mixed α and γ isomers (74.0 mg, 9.7%).

The identification of α and γ isomers of Fol-eda was accomplished through analysis of the HMBC NMR spectrum. The spectral data were compared to those reported by

Krämer et al [80], which provide a comprehensive description of isomeric differentiation for such derivatives. Our observed NMR data align closely with those presented in the referenced study, confirming the assignment of our product as the γ isomer.

7.1.1 HMBC NMR of γ-Fol-eda*

Coupling was observed between H-4 and the carbon signal at 174.3 ppm, which also coupled to H-3. As this signal showed no additional couplings, it was assigned to the COOH group. Another coupling was detected between H-68, H-69 and NH-57 with the carbon signal at 172.9 ppm, which also couples to H-2. This indicates that the 172.9 ppm signal corresponds to the amide carbonyl next to H-2.

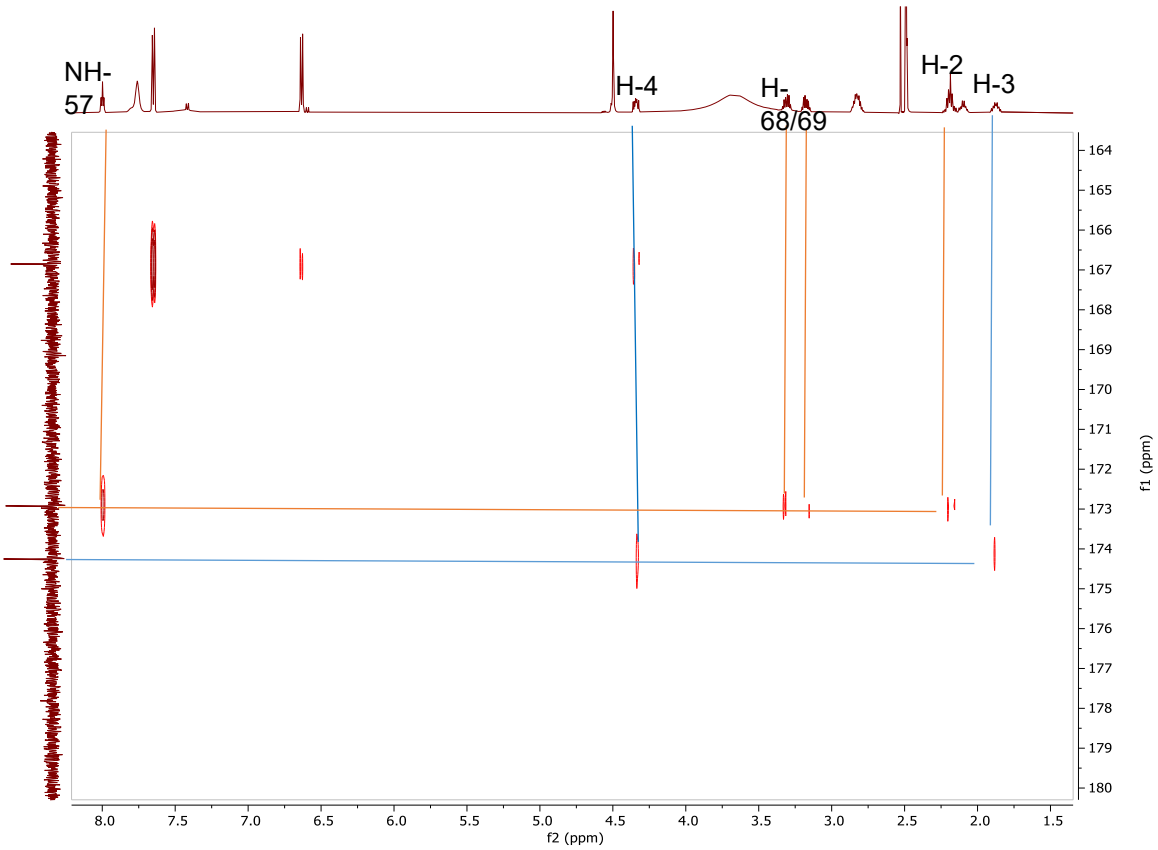

***Figure 54**: HMBC NMR spectra of γ isomer of Fol-eda in DMSO- d_6*

^{1}H NMR of γ isomer of Fol-eda (600 MHz, DMSO) δ 8.66 (s, 1H, H-30), 8.10 (d, *J* = 7.4 Hz, 1H, H-8), 8.07 (t, *J* = 5.8 Hz, 1H, H-57), 7.76 (br, 2H, H-70), 7.68 (d, *J* = 8.8 Hz, 2H, H-12/14), 6.68 – 6.60 (d, *J* = 8.9 Hz, 2H, H-13/15), 4.51 (s, 2H, H-18), 4.34 – 4.28 (m, 1H, H-4), 3.35 – 3.24 (m, *J* = 7.5, 6.9 Hz, 2H, H-68), 2.89 – 2.83 (m, 2H, H-69), 2.34 – 2.18 (m, 2H, H-2), 2.07 – 1.98 (m, 1H, H-3), 1.94 – 1.83 (m, 1H, H-3). **^{13}C NMR** (151 MHz, DMSO-d_6) δ 26.8 (1C, CH_2, C-3), 32.2 (1C, CH_2, C-2), 36.8 (1C, CH_2, C-68), 39.2 (1C, CH_2, C-69) 46.3 (1C, CH_2, C-18), 52.1 (1C, CH, C-4), 111.67(2C, CH,

C-13/15), 116.2, 118.1, 121.6, 128.4, 129.5 (2C, CH, C-12/14), 148.8 (1C, CH, C-30), 149.8, 151.3, 154.0, 159.4, 161.1, 166.8, 172.9 (1C, CO, C-63), 174.3 (1C, CO, C-5). **MS** (HR-ESI$^+$):m/z = 484.2062 [M+H] $^+$, calculated for $C_{21}H_{26}N_9O_5^+$: 484.2051. **Analytical HPLC**: Nucleosil C18 (5 µm, 4.6 mm x 25 mm), H_2O with 0.1% TFA (system A) / 80% MeCN-20% H_2O and 0.1 % TFA (system B), 1 mL/min, 0.02 min - 5% eluent of system B, 21 min - 40% eluent of system B, (γ-isomer: t_R = 14.8 min, α- isomer: t_R = 15.0 min)

7.2 Synthesis of Folate-FITC*:

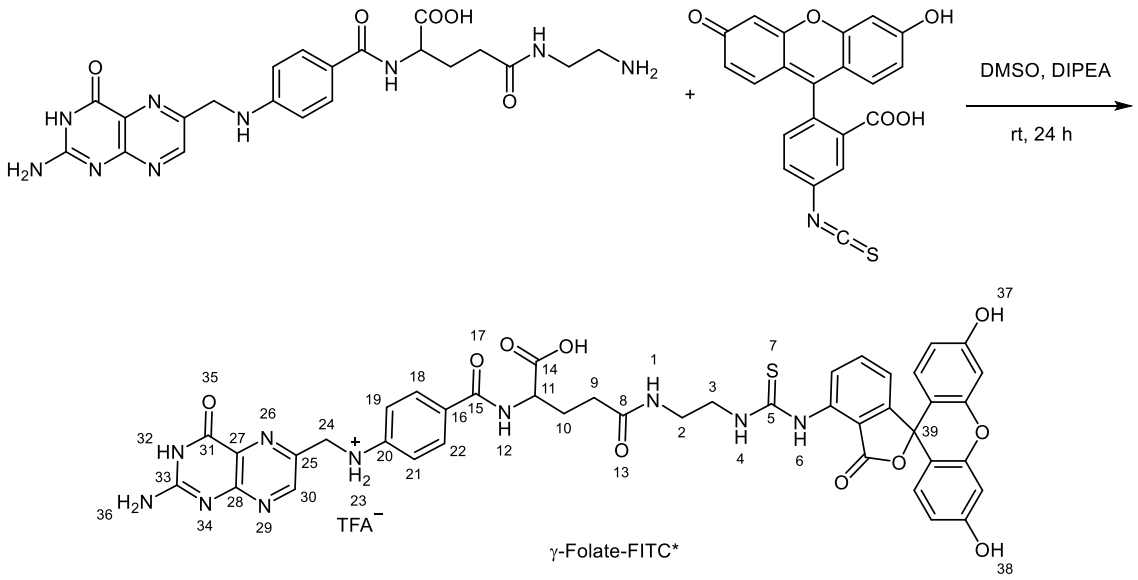

The synthesis of folate-FITC was conducted following the protocol described in the doctoral dissertation of Karin Dootz titled "Folatrezeptor-vermittelte, selektive Markierung von Krebszellen [57]

Fol-eda γ isomer (35 mg, 1.00 eq) was dissolved in 3 mL anhydrous DMSO. To this solution, fluorescein isothiocyanate isomer I (19.3 mg, 1.00 eq) and DIPEA (12.7 mg, 17 µL, 2.00 eq) were added. The reaction mixture was stirred overnight in the dark under an argon atmosphere. After completion of the reaction, the crude product was precipitated using an excess of diethyl ether. The residue was then dried under a vacuum and subsequently washed with acetone to purify the final product. The desired product was obtained as a yellow amorphous powder (20.5 mg, 48%). **^{1}H NMR** (600 MHz, DMSO) δ 11.50 (br, 1H), 10.23 (br, 2H), 10.11 (br, 1H), 8.62 (s, 1H, H-30), 8.21 (s, 1H), 8.19 (d, *J* = 7.9 Hz, 1H, H-12), 8.13 (br, 1H), 8.02 (s, 1H), 7.71 (br, 1H), 7.63 (d, *J* = 8.4 Hz, 2H, H-18/22), 7.14 (d, *J* = 8.2 Hz, 1H), 6.91 (t, *J* = 6.1 Hz, 1H), 6.66 (d, *J* = 2.3 Hz, 2H), 6.62 (d, *J* = 8.5 Hz, 2H, H-19/21), 6.58 (d, *J* = 8.7 Hz, 2H), 6.54 (dd, *J*

= 8.6, 2.4 Hz, 2H), 4.47 (d, *J* = 6.1 Hz, 2H, H-24), 4.30 – 4.25 (m, 1H), 3.55 (2H, H-3) this peak is observed in HSQC NMR, it is overlapped with water peak of the DMSO-d_6 solvent, 3.30 – 3.22 (m, 2H, H-2), 2.24 – 2.16 (m, 2H, H-9), 2.10 – 1.99 (m, 1H, H-10), 1.95 – 1.88 (m, 1H).**^{13}C NMR** (151 MHz, DMSO-d_6) δ 27.0 (1C, CH_2, C-10), 32.4 (1C, CH_2, C-9), 38.2 (1C, CH_2, C-2), 43.9 (1C, CH_2, C-3), 46.3 (1C, CH_2, C-24), 52.6 (1C, CH_2, C-11), 83.6 (1C, C_q, C-39), 102.7, 110.1, 111.7, 113.0, 113.0, 117.3, 121.7, 124.5, 127.0, 128.3, 129.4, 129.5, 141.6, 147.7, 148.8, 149.0, 149.2 (CH, C-30), 149.9, 151.2, 152.3, 152.3, 152.4, 154.2, 156.1, 156.9, 159.9, 161.5, 167.0, 169.1, 169.5, 172. 8 (1C, CO, C-8), 174.4 (1C, CO, C-14), 174.9, 181.2, 191.6 (1C, CS, C-5). **MS** (HR-ESI$^-$):m/z = 871.2268 [M-H] $^-$, calculated for $C_{42}H_{35}N_{10}O_{10}S^-$: 871.2264. **Analytical HPLC**: Nucleosil C18 (5 µm, 4.6 mm x 25 mm), H_2O with 0.1% TFA (system A) / 80% MeCN-20% H_2O and 0.1 % TFA (system B), 1 mL/min, 0.02 min - 5% eluent of system B, 21 min - 70% eluent of system B, t_R = 17.4 min. **UV/Vis** (PBS): $\lambda_{max\ (Abs)}$ [nm] (ε [$M^{-1}cm^{-1}$]) = 496 (79000); **Fluorescence** (PBS): λ_{ex} [nm] = 480, $\lambda_{max\ (em)}$ [nm] = 515.

7.3 Synthesis of fluorescein-monoaldehyde*

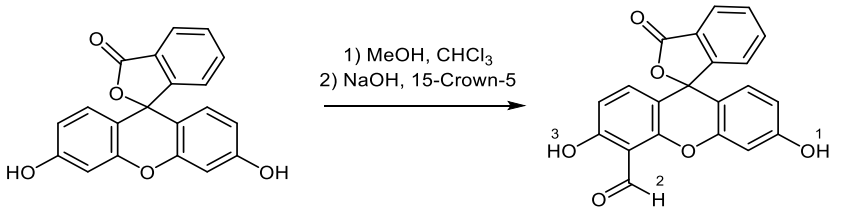

Fluorescein-monoaldehyde*

The synthesis of fluorescein-monoaldehyde was carried out following the procedure reported by Brandl et al. with slight modifications. [81]

In a 100 mL flask, fluorescein (2.5 g, 7.52 mmol, 1.0 eq.), 6 mL MeOH and 9 mL chloroform (112.80 mmol, 1.0 eq.) were added. After stirring for 10 min, 15 crown-5 (150 µl, 752 µmol, 0.1 eq.) and 50 % NaOH (9.62 g, 120.32 mmol, 15 eq.) were added to this mixture. The reaction stirred at 55°C for 48 h. After cooling, the reaction mixture was poured on stirred ice-cold 2 N HCl. The crude product precipitated quickly. The solid was filtered off and washed with ice-cold water. The wet brownish solid was frozen and lyophilized. The product was purified using column chromatography on silica gel (0% to 50% EtOAc in petroleum ether) to yield the product (orange solid, 310 mg, 11.4 % yield). **^{1}H NMR** (400 MHz, DMSO-d_6) δ 11.90 (s, 1H, H-2), 10.65 (s, 1H, H-1/3), 10.28 (s, 1H, H-1/3), 8.03 (d, *J* = 7.7 Hz, 1H), 7.82 (t, *J* = 7.5, 1H), 7.78 – 7.72 (m, 1H), 7.33 (d, *J* = 7.7 Hz, 1H), 6.97 (d, *J* = 9.0 Hz, 1H), 6.86 (d, *J* = 1.9 Hz, 1H),

6.72 (d, *J* = 8.9 Hz, 1H), 6.66 – 6.59 (m, 2H). **MS** (ESI^-):m/z =359.0466 $[M-H]^-$, calculated for $C_{21}H_{11}O_6^-$: 359.0561. **Analytical HPLC**: Nucleosil C18 (5 µm, 4.6 mm x 25 mm), H_2O with 0.1% TFA (system A) / 80% MeCN-20% H_2O and 0.1 % TFA (system B), 1 mL/min, 0.02 min - 5% eluent of system B, 23 min - 95% eluent of system B, t_R = 19.4 min

7.4 Synthesis of Compound 1

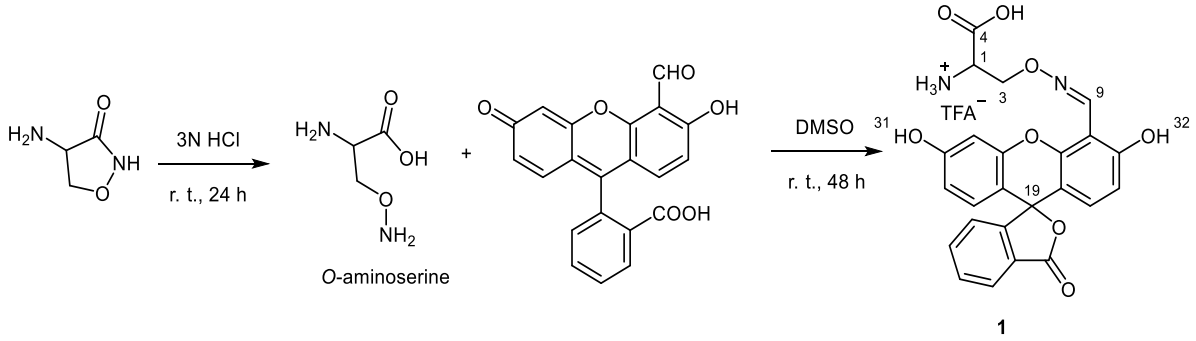

1

D-Cycloserine (20 mg, 196 µmol, 1 eq.) was dissolved in 2 mL 3N HCl/H_2O. This mixture was stirred for 24 hours at room temperature. The mass spectroscopy monitoring of the reaction indicated the formation of the O-aminoserine. This crude product was added to fluorescein-monoaldehyde (34.50 mg, 96 µmol, 0.5 eq.) dissolved in 2 mL DMSO. The reaction mixture was stirred for 48 h at room temperature in the dark. The desired product was purified using preparative RP-HPLC (Marcherey-Nagel C18 5 µm, 250 mm x 20 mm). For this purpose, the reaction mixture was solved in 6 mL H_2O/MeCN (1:1). This solution was filtered through a syringe filter (Mini-sart RC 4, 0.2 µm). For the preparative RP-HPLC, system A of HPLC eluent contained H_2O with 0.1 % TFA and system B contained 80% acetonitrile with 20 % HPLC H_2O and 0.1 % TFA. After lyophilisation, the desired product was obtained as an orange amorphous powder 14.0 mg, 32%. **^{1}H NMR** (600 MHz, DMSO-d_6) δ 10.29 (s, 2H, H-32/31), 8.82 (d, *J* = 1.8 Hz, 1H, H-9), 8.65 – 8.26 (br, 2H, NH_2), 8.01 (d, *J* = 7.7 Hz, 1H), 7.81 (t, *J* = 7.5, 1H), 7.73 (t, *J* = 7.5 Hz, 1H), 7.28 (dd, *J* = 7.7, 3.3 Hz, 1H), 6.80 (d, *J* = 2.3 Hz, 1H), 6.75 – 6.65 (m, 2H), 6.62 –6.56 (m, 2H), 4.67 – 4.57 (m, 2H, H-3), 4.35 (t, *J* = 4.0 Hz, 1H, H-1). **^{13}C NMR** (151 MHz, DMSO-d_6) δ, 52.9 (1C, CH_2, C-3), 72.27 (1C, CH, C-1), 82.9, 158.9 (1C, C, C-19), 103.0, 104.9, 109.9, 110.5, 113.2, 113.7, 124.5, 125.2, 126.5, 129.4, 130.7, 131.4, 136.2, 147.3, 149.9, 151.7, 151.7, 152.7, 158.9 (1C, CH=N, C-9), 160.1, 169.1, 169.3 (1C, CO, C-4). **MS** (ESI^+):m/z = 463.1039 $[M+H]^+$, calculated for $C_{24}H_{19}N_2O_8^+$: 463.1136. **UV/Vis** (PBS): $\lambda_{max\ (Abs)}$ [nm] (ε [$M^{-1}cm^{-1}$]) = 496 (79000); **Fluorescence** (PBS): λ_{Ex} [nm] = 525. **Analytical HPLC**:

Nucleosil C18 (5 µm, 4.6 mm x 25 mm), H_2O with 0.1% TFA (system A) / 80% MeCN-20% H_2O and 0.1 % TFA (system B), 1 mL/min, 0.02 min - 5% eluent of system B, 21 min - 70% eluent of system B, t_R = 18.2 min.

7.5 Synthesis of FP 2

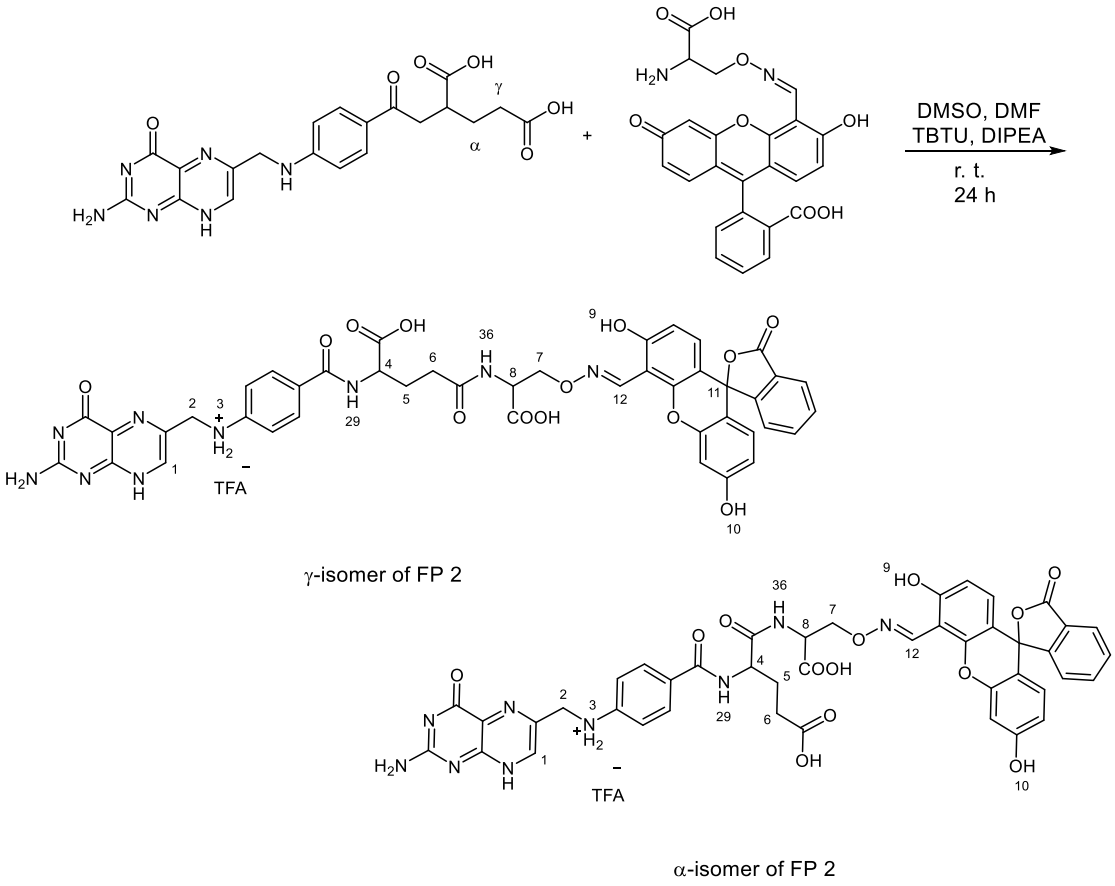

Folic acid dihydrate (12.8 mg, 27 µmol, 1.0 eq.) was dissolved in 2 mL anhydrous DMSO and 0.5 mL DMF under an inert atmosphere. DIPEA (11 µL, 62 µmol, 2.3 eq.) and TBTU (8.7 mg, 27 µmol, 1.0 eq.) were added to this mixture. After stirring for 30 min, compound 1 (13.7 mg, 29.7 µmol, 1.1 eq.) solved in 1 mL DMSO was added to the mixture and the reaction was stirred overnight at room temperature. The reaction mixture was poured into 100 mL cold diethyl ether and the yellow precipitation was centrifuged. The product was purified using preparative RP-HPLC (Marcherey-Nagel C18 5 µm, 250 mm x 20 mm). System A of HPLC eluent contained H_2O with 0.1 % TFA and system B contained 80% acetonitrile with 20 % H_2O and 0.1 % TFA. After lyophilization, the desired product with γ- and α-modified of FP 2 fluorescein was obtained as a yellow amorphous powder (9.1 mg, 38%). **^{1}H NMR** (600 MHz, DMSO-d_6) δ 10.44 (s, 1H, H-9/10), 10.21 (s, 1H, H-9/10), 8.87 – 8.81 (m, 1H, H-12), 8.72 – 8.66 (m, 1H, H-1), 8.47 – 8.37 (m, 1H, H-3/36), 8.29 – 8.11 (m, 1H, H-29), 8.06 – 7.99

(m, 1H, H-3/36), 7.83 – 7.77 (m, 1H), 7.76 – 7.70 (m, 1H), 7.70 – 7.62 (m, 2H), 7.33 – 7.26 (m, 1H), 6.84 (d, *J* = 2.4 Hz, 1H), 6.69 (d, *J* = 2.8 Hz, 2H), 6.64 (d, *J* = 8.5 Hz, 2H), 6.61 – 6.56 (m, 2H), 4.71 – 4.63 (m, 1H, H-7), 4.59 – 4.51 (m, 1H, H-8), 4.50 – 4.47 (m, 2H, H-2), 4.46 – 4.42 (m, 1H, H-8), 4.37 – 4.29 (m, 1H, H-4), 2.39 – 2.28 (m, 2H, H-6), 2.11 – 2.01 (m, 1H, H-5), 1.98 – 1.86 (m, 1H, H-5). **^{13}C NMR** (151 MHz, DMSO-d_6) δ 27.9, 30.8, 52.3, 52.6, 54.8, 73.6, 82.4, 103.1, 104.9, 109.7, 110.5, 111.6, 113.2, 113.6, 115.3, 117.3, 121.9, 124.5, 125.2, 126.5, 128.4, 129.4, 129.5, 129.5, 130.7, 131.2, 136.2, 148.7, 149.8, 151.1, 151.7, 153.6, 156.1, 158.9, 160.0, 160.7, 166.8, 169.1, 171.3, 171.8, 174.3, 174.7 (1C, CO, next to C-4), 191.7. **MS** (ESI$^-$):m/z = 884.2440 [M-H]$^-$, calculated for $C_{43}H_{34}N_9O_{13}^-$: 884.2282. **Analytical HPLC**: Nucleosil C18 (5 µm, 4.6 mm x 25 mm), H_2O with 0.1% TFA (system A) / 80% MeCN-20% H_2O and 0.1 % TFA (system B), 1 mL/min, 0.02 min - 5% eluent of system B, 21 min - 70% eluent of system B, t_R = 18.6 min. **UV/Vis** (PBS): $\lambda_{max\ (Abs)}$ [nm] (ε [$M^{-1}cm^{-1}$]) = 501 (78400); Fluorescence (PBS): λ_{ex} [nm] = 480, $\lambda_{max\ (Em)}$ [nm] = 521.

7.6 Synthesis of compound 3*

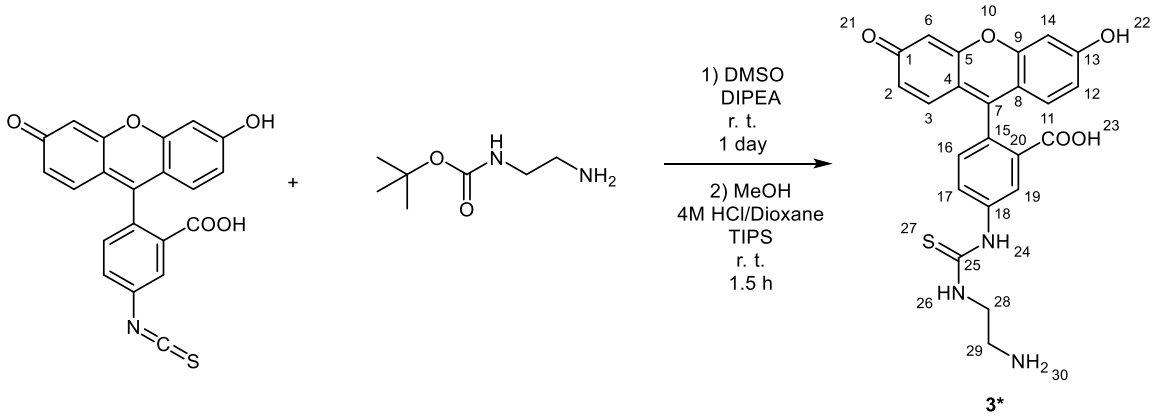

Compound **3** is a literature-known substance previously reported in the literature. [82-84] However, the synthetic method described here has not been previously documented.

Fluorescein isothiocyanate isomer I (48.6 mg; 124.8 µmol 1.00 eq.) was dissolved in 4 mL anhydrous DMSO. Subsequently, N-Boc-ethylenediamine (20.0 mg, 124.8 µmol, 1.00 eq.) dissolved in 1 mL of DMSO, and DIPEA (44 µL; 249.7 µmol, 2.00 eq.) were added to the mixture. The mixture was stirred at room temperature overnight in the dark. After completion of the reaction monitored by HPLC and ESI, the reaction mixture was precipitated using ice-cold diethyl ether. The Boc-protected product was purified using preparative RP-HPLC (Marcherey-Nagel C18 5 µm, 250 mm x 20 mm). This product was dissolved in 2 mL methanol. To this mixture was added 1 mL of 4 M HCl

solution in dioxane and triisopropylsilane (32.0 µL,1.7 eq.). The mixture was stirred at room temperature for 90 minutes. Then the solvent was evaporated and the desired product **3** was achieved as a yellow solid (37.7 mg, 67.3%). **^{1}H NMR** (600 MHz, DMSO) δ 10.66 (s, 1H, NH-24/OH-22), 10.19 (s, 1H, NH-24/OH-22), 8.54 (s, 1H, H-26), 8.29 (d, *J* = 4.9 Hz, 1H), 8.03 (s, 2H, H-30), 7.80 (s, 1H), 7.21 (d, *J* = 8.3 Hz, 1H), 6.71 (d, *J* = 2.9 Hz, 2H), 6.62 (d, *J* = 8.4 Hz, 2H), 6.60 – 6.56 (m, 2H), 3.79 (q, *J* = 6.3 Hz, 2H, H-28), 3.06 (q, *J* = 6.3 Hz, 2H, H-29). **MS** (ESI$^+$):m/z = 450.0819 [M+H] $^+$, calculated for $C_{23}H_{20}N_3O_5S^+$: 450.1118. **Analytical HPLC**: Nucleosil C18 (5 µm, 4.6 mm x 25 mm), H_2O with 0.1% TFA (system A) / 80% MeCN-20% H_2O and 0.1 % TFA (system B), 1 mL/min, 0.02 min - 5% eluent of system B, 21 min - 70% eluent of system B, t_R = 15.2 min. **UV/Vis** (PBS): $\lambda_{max\ (Abs)}$ [nm] (ε [$M^{-1}cm^{-1}$]) = 493 (70000); **Fluorescence** (PBS): λ_{Ex} [nm] = 480, $\lambda_{max\ (Em)}$ [nm] = 515.

7.7 Synthesis of fluorescein-oxime ether derivatives

General Procedure (GP) 1
Alkoxyamine (1.00 eq.) and fluorescein-monoaldehyde (1.00 eq.) were dissolved in 0.5 mL DMSO-d_6. The reaction mixture was stirred at room temperature for 2 days in the dark.

7.7.1 Compound 4: Oxime ligation with O-ethylhydroxylamine hydrochloride

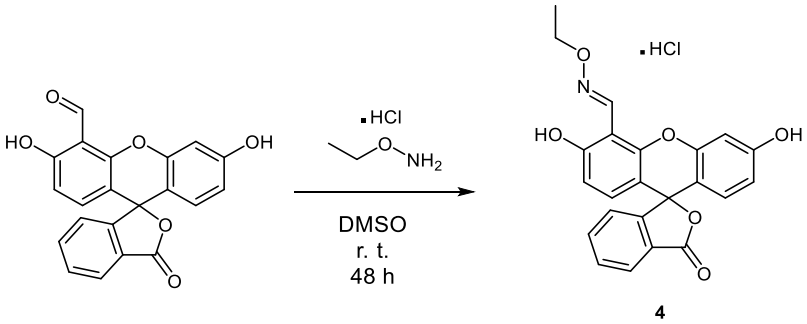

4

Following General Procedure 1 (GP1), O-ethylhydroxylamine hydrochloride (2.00 mg, 1.00 eq) and fluorescein aldehyde (7.43 mg, 1.00 eq) were dissolved in DMSO-d_6. The yellow solution containing the fluorescein-oxime ether product was used without further purification. **^{1}H NMR** (600 MHz, DMSO-d_6) δ 8.85 (s, 1H, imide-H), 8.01 (d, *J* = 7.7 Hz, 1H), 7.81 (td, *J* = 7.4, 1.1 Hz, 1H), 7.73 (t, *J* = 7.5 Hz, 1H), 7.29 (d, *J* = 7.7 Hz, 1H), 6.85 (d, *J* = 2.3 Hz, 1H), 6.72 (d, *J* = 8.8 Hz, 1H), 6.66 (d, *J* = 8.9 Hz, 1H), 6.62 – 6.54 (m, 2H), 4.28 (q, *J* = 7.1 Hz, 2H), 1.33 (t, *J* = 7.0 Hz, 3H). **MS** (ESI$^+$):m/z = 426.0962 [M+Na], calculated for $C_{23}H_{17}NNaO_6$: 426.0954. **Analytical HPLC**: Nucleosil C18 (5 µm, 4.6 mm x 25 mm), H_2O with 0.1% TFA (system A) / 80% MeCN-20% H_2O and 0.1

% TFA (system B), 1 mL/min, 0.02 min - 5% eluent of system B, 23 min - 95% eluent of system B, t_R = 22.4 min.

7.7.2 Compound 5: Oxime ligation with O-benzylhydroxylamine hydrochloride

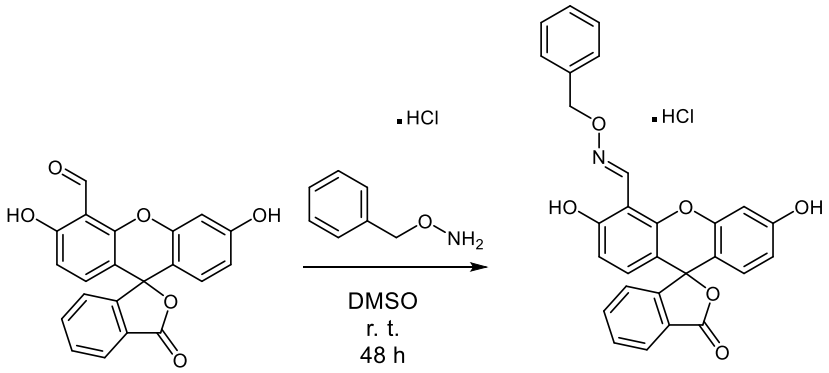

5

Following General Procedure 1 (GP1), O-benzylhydroxylamine hydrochloride (2.00 mg, 1.00 eq) and fluorescein aldehyde (4.51 mg, 1.00 eq) were dissolved in DMSO-d_6. The resulting yellow solution containing the fluorescein-oxime ether product was used without further purification. **^{1}H NMR** (600 MHz, DMSO-d_6) δ 8.91 (s, 1H, imide-H), 8.00 (d, *J* = 7.8 Hz, 1H), 7.80 (td, *J* = 7.5, 1.2 Hz, 1H), 7.72 (td, *J* = 7.5, 1.0 Hz, 1H), 7.55 – 7.47 (m, 2H), 7.42 (t, *J* = 7.5 Hz, 2H), 7.37 (d, *J* = 7.4 Hz, 1H), 7.28 (d, *J* = 7.7 Hz, 1H), 6.83 (d, *J* = 2.3 Hz, 1H), 6.71 – 6.63 (m, 2H), 6.62 – 6.52 (m, 2H), 5.29 (s, 2H). **^{13}C NMR** (151 MHz, DMSO-d_6) δ 76.5, 103.1, 105.0, 109.7, 110.5, 113.2, 113.7, 124.5, 125.2, 126.4, 128.6, 128.8, 128.9, 129.0, 129.1, 129.3, 130.7, 131.0, 136.2, 137.5, 146.3, 149.8, 151.7, 152.7, 159.0, 160.0, 169.1. **MS** (ESI$^+$):m/z = 488.1145 [M+Na], calculated for $C_{28}H_{19}NNaO_6$: 488.1110. **Analytical HPLC**: Nucleosil C18 (5 µm, 4.6 mm x 25 mm), H_2O with 0.1% TFA (system A) / 80% MeCN-20% H_2O and 0.1 % TFA (system B), 1 mL/min, 0.02 min - 5% eluent of system B, 23 min - 95% eluent of system B, t_R = 24.4 min.

7.7.3 Compound 6: Oxime ligation with O-(4-methoxybenzyl)hydroxylamine hydrochloride

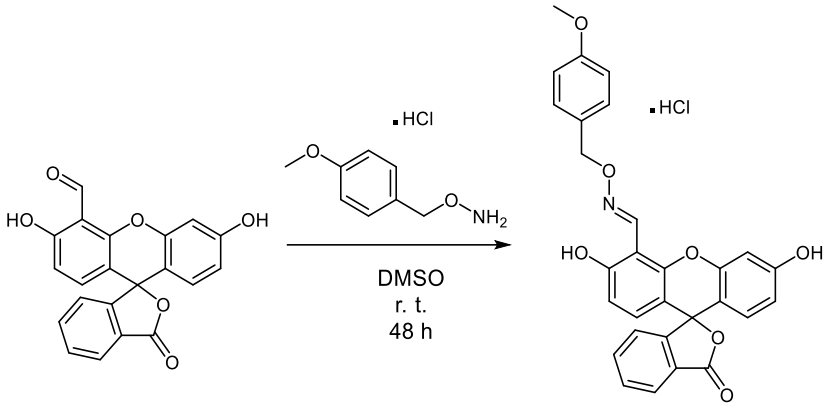

6

Following GP1, O-(4-methoxybenzyl)hydroxylamine hydrochloride (2.00 mg, 1.00 eq) and fluorescein aldehyde (3.80, 1.00 eq) were dissolved in DMSO-d_6. The resulting yellow solution containing the fluorescein-oxime ether product was used without further purification. **^{1}H NMR** (600 MHz, DMSO-d_6) δ 8.87 (s, 1H, imide-H), 8.00 (d, *J* = 7.7 Hz, 1H), 7.80 (td, *J* = 7.5, 1.2 Hz, 1H), 7.72 (td, *J* = 7.5, 0.9 Hz, 1H), 7.42 (d, *J* = 8.6 Hz, 1jjH), 7.35 (d, *J* = 8.7 Hz, 1H), 7.27 (d, *J* = 7.7 Hz, 1H), 7.00 – 6.95 (m, 2H), 6.83 (d, *J* = 2.3 Hz, 1H), 6.71 – 6.63 (m, 2H), 6.61 – 6.52 (m, 2H), 5.20 (s, 1H), 4.92 (s, 1H), 3.76 (d, *J* = 3.7 Hz, 3H). **^{13}C NMR** (151 MHz, DMSO-d_6) δ 55.6, 76.2, 103.1, 105.0, 109.6, 110.5, 113.2, 113.7, 114.3, 114.5, 124.5, 125.2, 126.4, 129.3, 130.7, 130.9, 131.0, 131.7, 136.2, 146.1, 149.7, 151.7, 152.7, 159.0, 159.7, 160.1, 169.1. **MS** (ESI$^+$):m/z = 518.1246 [M+Na], calculated for $C_{29}H_{21}NNaO_7$: 518.1216. **Analytical HPLC**: Nucleosil C18 (5 µm, 4.6 mm x 25 mm), H_2O with 0.1% TFA (system A) / 80% MeCN-20% H_2O and 0.1 % TFA (system B), 1 mL/min, 0.02 min - 5% eluent of system B, 23 min - 95% eluent of system B, t_R = 24.4 min.

7.7.4 Compound 7: Oxime ligation with O-(4-nitrobenzyl)hydroxylamine hydrochloride

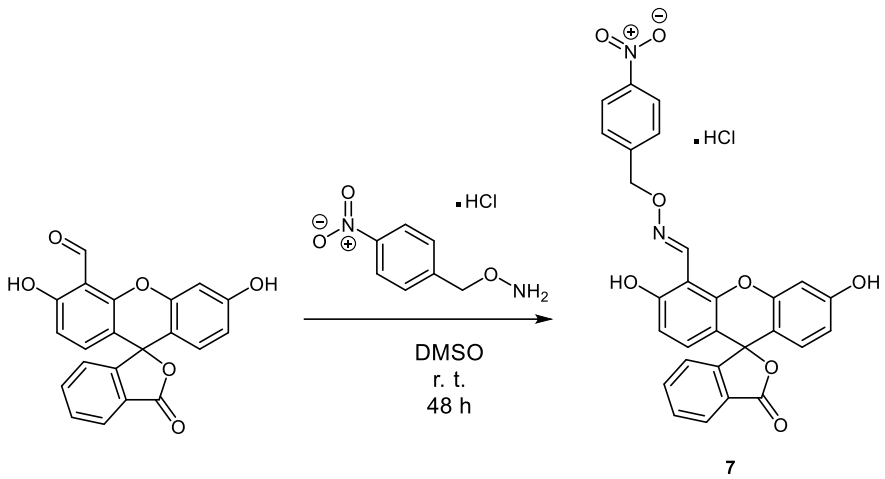

Following GP1, O-(4-nitrobenzyl)hydroxylamine hydrochloride (2.00 mg, 1.00 eq) and fluorescein aldehyde (3.52, 1.00 eq). were dissolved in DMSO-d_6. The resulting yellow solution containing the fluorescein-oxime ether product was used without further purification. **^{1}H NMR** (600 MHz, DMSO-d_6) δ 8.91 (s, 1H), 8.29 (d, *J* = 1.3 Hz, 1H), 8.27 (d, *J* = 1.4 Hz, 1H), 7.99 (d, *J* = 7.7 Hz, 1H), 7.80 (td, *J* = 7.5, 1.1 Hz, 1H), 7.75 (d, *J* = 8.7 Hz, 2H), 7.72 (t, *J* = 7.5 Hz, 1H), 7.69 (d, *J* = 8.7 Hz, 1H), 7.26 (d, *J* = 7.7 Hz, 1H), 6.70 (d, *J* = 2.3 Hz, 1H), 6.67 (d, *J* = 8.1 Hz, 1H), 6.58 (dd, *J* = 8.7, 2.3 Hz, 1H), 6.55 (d, *J* = 8.7 Hz, 1H), 5.44 (s, 1H), 5.13 (s, 1H). **^{13}C NMR** (151 MHz, DMSO-d_6) δ 74.7, 74.9, 103.1, 105.1, 109.7, 110.5, 113.1, 113.6, 124.1, 124.2, 124.5, 125.2, 126.5, 129.3, 129.5, 130.3, 130.7, 131.2, 136.2, 145.9, 146.6, 147.6, 149.9, 151.7, 160.1, 169.1. **MS** (ESI$^+$):m/z = 511.1138 [M+H] $^+$, calculated for $C_{28}H_{19}N_2O_8^+$: 511.1136. **Analytical HPLC**: Nucleosil C18 (5 µm, 4.6 mm x 25 mm), H_2O with 0.1% TFA (system A) / 80% MeCN-20% H_2O and 0.1 % TFA (system B), 1 mL/min, 0.02 min - 5% eluent of system B, 23 min - 95% eluent of system B, t_R = 23.9 min.

7.7.5 Compound 8: Oxime ligation with O-(2-(pyrazin-1(4H)-yl)ethyl)hydroxylamine hydrochloride

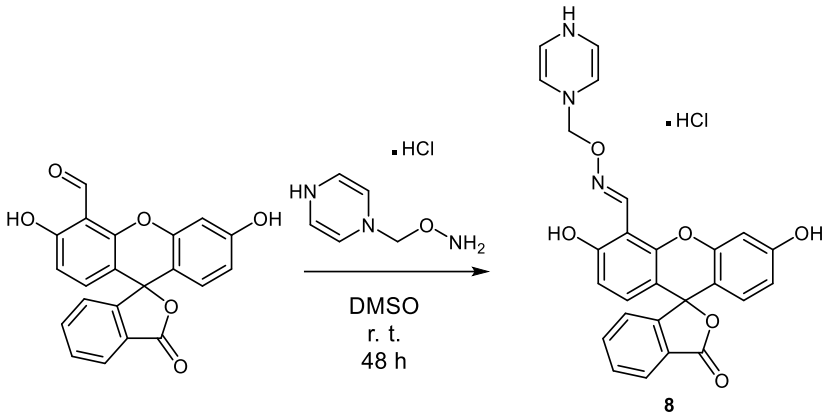

8

Following GP1, O-(2-(pyrazin-1(4H)-yl)ethyl)hydroxylamine hydrochloride (2.00 mg, 1.00 eq) and fluorescein aldehyde (4.06, 1.00 eq) were dissolved in DMSO-d_6. The resulting yellow solution containing the fluorescein-oxime ether product was used without further purification. **^{1}H NMR** (600 MHz, DMSO-d_6) δ 8.81 (s, 1H), 8.01 (d, *J* = 7.7 Hz, 1H), 7.86 (t, *J* = 1.7 Hz, 1H), 7.82 (td, *J* = 7.5, 1.1 Hz, 1H), 7.79 (t, *J* = 1.7 Hz, 1H), 7.74 (dd, *J* = 7.6, 0.9 Hz, 1H), 7.74 – 7.69 (m, 2H), 7.29 – 7.25 (m, 2H), 6.84 (d, *J* = 2.4 Hz, 1H), 6.72 (d, *J* = 8.8 Hz, 1H), 6.68 (d, *J* = 8.9 Hz, 1H), 6.63 – 6.58 (m, 1H), 6.57 (d, *J* = 8.7 Hz, 1H), 4.63 (s, 2H). **MS** (ESI$^+$):m/z = 470.1883 [M+H] $^+$, calculated for $C_{26}H_{20}N_3O_6^+$: 470.1347.

7.8 Synthesis of Compound 9*

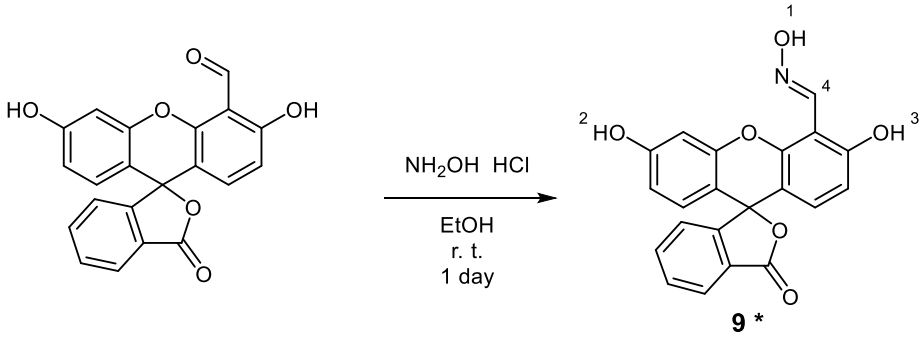

9 *

This is a literature-known compound that was synthesized according to the procedure by Lee et al.[71]

Fluorescein monoaldehyde (68.00 mg, 188.72 µmol, 1.00 eq.) and hydroxylammonium chloride (19.67 mg, 283.08 µmol, 1.50 eq.) were dissolved in 3.00 mL of ethanol in a 10 mL flask under argon. The reaction mixture was stirred overnight at room temperature, turning the solution reddish. The solvent was then removed under

reduced pressure using a rotary evaporator, and the crude product was purified by column chromatography (silica gel, PE/EtOAc, 1:1). The desired product was isolated as a reddish solid (39 mg, 103.9 µmol, 55%). R_f (PE/EtOAc, 1:1) = 0.5. **^{1}H-NMR** (400 MHz, DMSO-d_6): δ = 11.94 (s, 1H, H-1), 11.12 (s, 1H, H-2/3), 10.20 (s, 1H, H-2/3), 8.86 (s, 1H, H-4), 8.02 (d, *J* = 7.5 Hz, 1H), 7.80 (td, *J* = 7.5 Hz, *J* = 1.3 Hz, 1H), 7.73 (td, *J* = 7.5 Hz, *J* = 1.1 Hz, 1H), 7.31 (d, *J* = 7.6 Hz, 1H), 6.86 (d, *J* = 2.1 Hz, 1H), 6.73 – 6.63 (m, 2H), 6.61 – 6.59 (m, 2H). **MS** (ESI$^+$): m/z = 376.0692 [M+H]$^+$, calculated for $C_{21}H_{14}NO_6^+$: 376.0816.

7.9 Synthesis of fluorescein isoxazole*

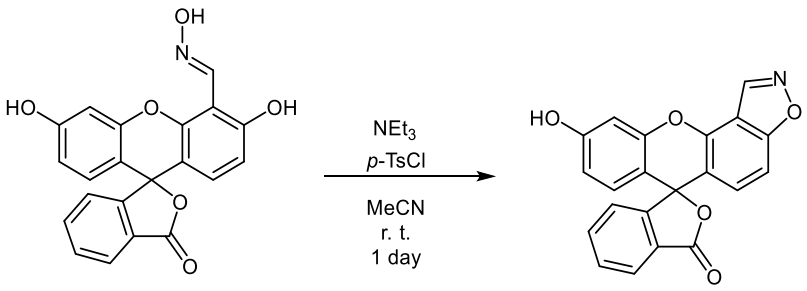

This is a literature-known compound that was synthesized according to the procedure by Lee et al.[71]

Fluorescein oxim (37.00 mg, 98.58 µmol, 1.00 eq.) was dissolved in 1.5 mL of acetonitrile in a 10 mL flask. Triethylamine (15.11 µL, 108.44 µmol, 1.10 eq.) and p-tosyl chloride (28.19 mg, 147.87 µmol, 1.50 eq.) were added. The reaction mixture was stirred overnight at room temperature. After removal of the solvent, the crude yellow product was purified via column chromatography (silica gel, PE/EtOAc 1:1), yielding a yellow solid (25 mg, 69.97 µmol, 71%). **R_f** (PE/EtOAc, 1:1) = 0.5 **^{1}H-NMR** (400 MHz, DMSO-d_6): δ = 10.32 (s, 1H, OH), 9.64 (s, 1H, imine H), 8.05 (d, ^3J = 7.4 Hz, 1H), 7.85 – 7.71 (m, 2H), 7.52 (dd, *J* = 8.8, 1.1 Hz, 1H), 7.32 (d, *J* = 7.7 Hz, 1H), 7.04 (d, *J* = 8.8 Hz, 1H), 6.84 (d, *J* = 2.0 Hz, 1H), 6.72 – 6.63 (m, 2H). **MS** (ESI$^+$): m/z = 380.0516 [M+Na]$^+$, calculated for $C_{21}H_{11}NNaO_5$: 380.0535.

7.10 Synthesis of Fluorescein nitrile*

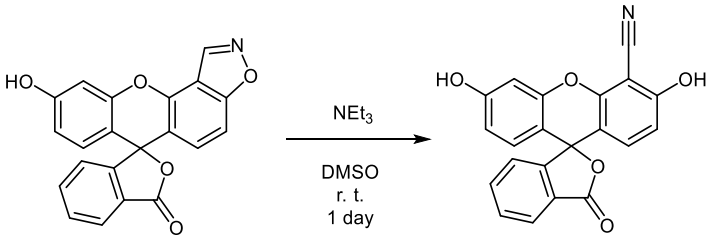

Fluorescein nitrile*

This is a literature-known compound that was synthesized according to the procedure by Lee et al. with slide modification. [71]

Fluorescein isoxazole (14.40 mg, 40.30 µmol, 1.00 eq.) was dissolved in DMSO (0.5 mL), followed by the addition of triethylamine (7.30 µL, 52.39 µmol, 1.30 eq.). The reaction mixture was stirred overnight at room temperature under dark conditions. After completion of the reaction, the solvent was removed under reduced pressure. The crude product was extracted with ethyl acetate. The organic layers were combined and dried over anhydrous Na_2SO_4. The residue was purified by column chromatography using MeOH/CH_2Cl_2 (1:20). The product was obtained as a reddish solid (7 mg, 19.6 µmol, 49% yield).**^{1}H NMR** (600 MHz, DMSO-d_6) δ 11.90 (s, 1H, OH), 10.32 (s, 1H, OH), 8.02 (d, *J* = 7.7 Hz, 1H), 7.80 (td, *J* = 7.5, 1.2 Hz, 1H), 7.73 (td, *J* = 7.5, 1.0 Hz, 1H), 7.34 (d, *J* = 7.7 Hz, 1H), 6.90 (d, *J* = 8.9 Hz, 1H), 6.76 (d, *J* = 8.9 Hz, 1H), 6.73 (d, *J* = 2.1 Hz, 1H), 6.64 – 6.59 (m, 2H). **MS** (ESI$^+$): m/z = 358.1058 [M+H]$^+$, calculated for $C_{21}H_{12}NO_5^+$: 358.0710. **Analytical HPLC**: Nucleosil C18 (5 µm, 4.6 mm x 25 mm), H_2O with 0.1% TFA (system A) / 80% MeCN-20% H_2O and 0.1 % TFA (system B), 1 mL/min, 0.02 min - 5% eluent of system B, 23 min - 95% eluent of system B, t_R = 17.8 min.

7.11 Synthesis of N-Boc-cystamine

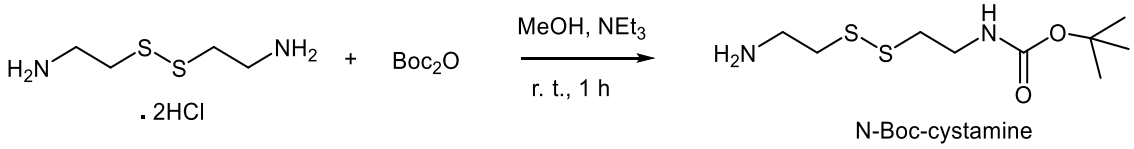

N-Boc-cystamine

This is a known compound which was synthesized following a procedure by Nie Yu et al. [85]

In a 250 mL flask, cystamine dihydrochloride (8.0 g, 35.5 mmol, 1.0 eq) was dissolved in 100 mL of methanol and cooled to 0°C. Triethylamine (15 mL, 107 mmol, 3.0 eq) was then added, and the mixture was stirred for 30 min. Boc anhydride (7.75 g, 35.5 mmol, 1.0 eq) was added dropwise over 5 minutes, and the reaction mixture was stirred at room temperature for 1 hour. The solvent was evaporated, and the crude product was dissolved in 1N NaOH and extracted with diethyl ether (3 × 50 mL) and DCM (2 × 50 mL) The organic layers were combined and dried over $MgSO_4$. The solvent was evaporated under reduced pressure, and the residue was purified by column

chromatography on silica gel using a DCM - MeOH - NEt_3. (9: 1: 0.1) elution system. The product was obtained as a colorless oil (2.8 g, 31.2% yield). R_f: 0.5 using DCM: MeOH: NEt3. (9: 1: 0.1) as solvent. 1H NMR (600 MHz, DMSO-d_6) δ 7.00 (t, *J = 5.8* Hz, 1H), 3.24 – 3.17 (m, 2H), 2.79 (t, *J = 6.2* Hz, 2H), 2.77 – 2.70 (m, 4H), 1.38 (s, 9H). MS (ESI^+): $[M+Na]^+$ calculated for $C_9H_{20}N_2NaO_2S_2^+$: 275.0846, found: 275.1390.

7.12 Synthesis of Fol-cystamine*:

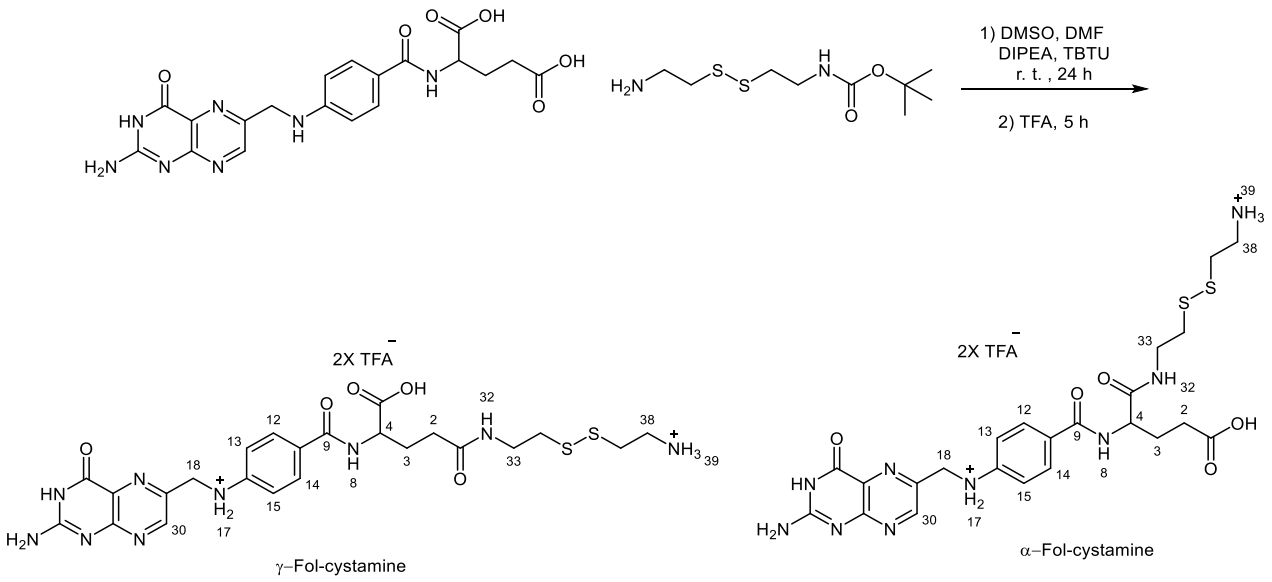

This is a known compound and the synthesis was carried out following the procedure reported by Jun Li et al. with slight modifications. [86]

Folic acid dihydrate (477.0 mg, 1.0 µmol, 1.0 eq.) was dissolved in 20 mL anhydrous DMSO and 5 mL DMF under an inert atmosphere. DIPEA (227 µL, 1.3 µmol, 1.3 eq.) and TBTU (352.87 mg, 1.1 µmol, 1.1 eq.) were added to this mixture. After stirring for 30 min, N-Boc-cystamine (277.6 mg, 1.1 µmol, 1.1 eq.) was added to the mixture and the reaction was stirred overnight at room temperature. The reaction mixture was poured into 250 mL of cold diethyl ether, resulting in a yellow residue collected by centrifugation, and the supernatant was discarded. 5 mL of trifluoroacetic acid (TFA) was added to the crude product, and the mixture was stirred for 5 hours. The solid was then precipitated again by adding 200 mL of ethyl acetate, followed by centrifugation. The product was purified using preparative RP-HPLC (Marcherey-Nagel C18, 5 µm, 250 mm x 20 mm). System A of HPLC eluent contained H_2O with 0.1 % TFA and system B contained 80% acetonitrile with 20 % H_2O and 0.1 % TFA. After lyophilization, the desired product was obtained as an orange amorphous powder with

γ-modified of Fol-cystamine (40.6 mg, 5.3%), α-modified (19.2 mg, 2.5%), and the mixture of both isomers (169.7 mg, 22%).

The identities of α and γ isomers were performed using HMBC NMR.

7.12.1 HMBC NMR of γ-Fol-cystamine:

Coupling was observed between H-4 and the carbon signal at 174.5 ppm, which also coupled to H-2 and H-3. As this signal showed no additional couplings, it was assigned to the COOH group. Another coupling was detected between H-33 and NH-32 with the carbon signal at 172.4 ppm, which also couples to H-2. This indicates that the 172.4 ppm signal corresponds to the amide carbonyl next to H-2.

7.12.2 HMBC NMR of α-Fol-cystamine:

Coupling was detected between NH-32, H-33 and H-4 to the amide carbonyl at 172.4 ppm. Additionally, H-2 and H-3 showed coupling to COOH carbon next to H-2 at 174.5 ppm.

7.12.3 ^{1}H-NMR of γ-Fol-cystamine

^{1}H NMR (600 MHz, DMSO-d_6) δ 8.67 (s, 1H, H-30), 8.21 (d, *J* = 7.6 Hz, 1H, H-8), 8.11 – 8.04 (m, 1H, H-32), 7.93 (br, 2H, H-39), 7.66 (d, *J* = 8.6 Hz, 2H, H-12/14), 6.65 (d, *J* = 8.8 Hz, 2H, H-13/15), 4.51 (s, 2H, H-18), 4.32 – 4.27 (m, 1H, H-4), 3.43 – 3.27 (m, 2H, H-33), 3.14 – 3.07 (m, 2H, H-38), 2.91 (t, *J* = 2.2 Hz, 2H), 2.76 (t, *J* = 6.8 Hz, 2H), 2.23 – 2.16 (m, 2H, H-2), 2.10 – 2.03 (m, 1H, H-3), 1.94 – 1.86 (m, 1H, H-3).

7.12.4 ^{1}H-NMR of α-Fol-cystamine

^{1}H NMR (600 MHz, DMSO-d_6) δ 8.66 (s, 1H, 27), 8.13 – 8.04 (m, 1H, H-32), 8.02 (d, *J* = 7.8 Hz, 1H, H-8), 7.91 (br, 2H, H-39), 7.67 (d, *J* = 8.7 Hz, 2H, H-12/14), 6.64 (d, *J* = 8.7 Hz, 2H, H-13/15), 4.51 (s, 2H, 18), 4.37 – 4.31 (m, 1H, H-4), 3.44 – 3.28 (m, 2H, H-33), 3.14 – 3.07 (m, 2H, H-38), 2.91 (t, *J* = 7.0 Hz, 2H), 2.80 (t, *J* = 6.9 Hz, 2H), 2.30 – 2.24 (m, 2H, H-2), 2.04 – 1.95 (m, 1H, H-3), 1.90 – 1.82 (m, 1H, H-3).

7.12.5 ^{13}C NMR of γ-Fol-cystamine

^{13}C NMR (151 MHz, DMSO-d_6) δ 26.9 (1C, CH_2, C-3), 32.4 (1C, CH_2, C-2), 34.6, 37.3, 38.2 (1C, CH_2, C-38), 38.4 (1C, CH_2, C-33), 46.3 (1C, CH_2, C-18), 52.5 (1C, CH, C-4), 111.6 (2C, CH, C13/15), 121.8, 128.4, 129.4 (2C, CH, C-12/14), 148.9, 149.5 (1C, CH,

C-30), 151.2, 154.1, 158.7, 159.0, 166.8, 172.2 (1C, CONH next to C-2) , 174.3 (1C, COOH next to C-4) .

7.12.6 ^{13}C NMR of α-Fol-cystamine

^{13}C NMR (151 MHz, DMSO-d_6) δ 27.3 (1C, CH_2, C-3), 31.0 (1C, CH_2, C-2), 34.6, 37.3, 38.3 (1C, CH_2, C-38), 38.4 (1C, CH_2, C-33), 46.3 (1C, CH_2, C-18), 53.3 (1C, CH, C-4), 111.6 (2C, CH, C13/15), 121.7, 128.4, 129.6 (2C, CH, C-12/14), 148.9, 149.5 (1C, CH, C-30), 151.2, 154.1, 158.7, 158.9, 166.8, 172.4 (1C, CONH next to C-4), 174.5 (1C, COOH next to C-2)

MS (ESI$^+$):m/z = 576.2569 [M+H] $^+$, calculated for $C_{23}H_{30}N_9O_5S_2^+$: 576.1806. **Analytical HPLC** of α and γ isomers of Fol-cystamine: Nucleosil C18 (5 µm, 4.6 mm x 25 mm), H2O with 0.1% TFA (system A) / 80% MeCN-20% H_2O and 0.1 % TFA (system B), 1 mL/min, 0.02 min - 5% eluent of system B, 21 min - 48% eluent of system B, (γ-isomer: t_R = 15.3 min, α- isomer: t_R = 15.6 min)

7.13 Synthesis of FP 10

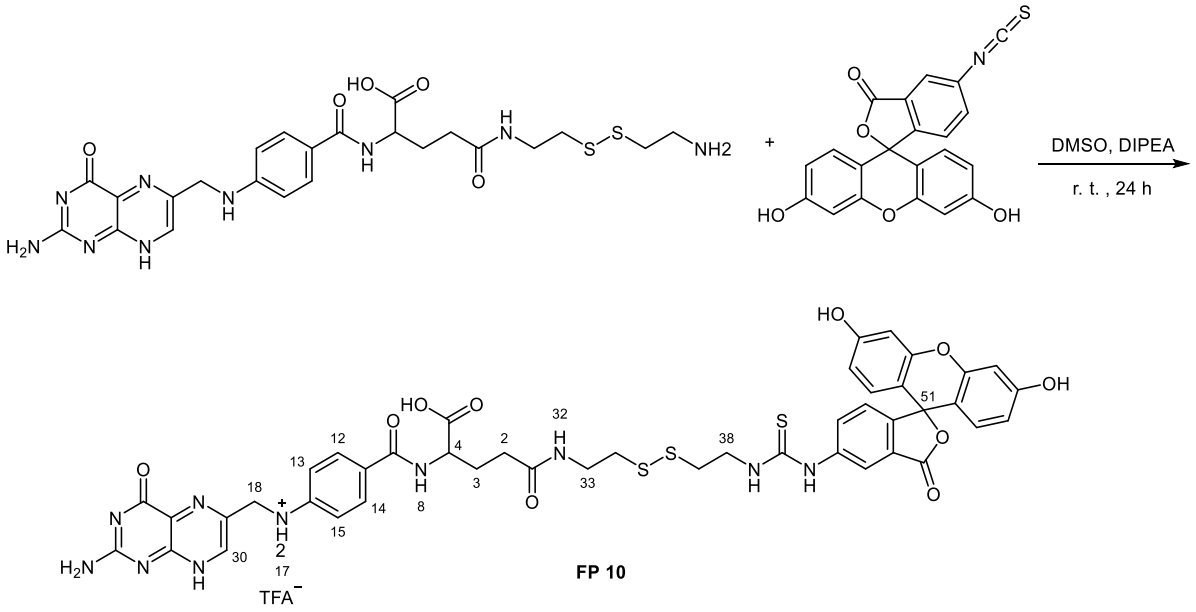

Fluorescein isothiocynate isomer I (17.0 mg, 1.0 eq, 43.4 µmol) was dissolved in 2 mL anhydrous DMSO. To this solution were added γ-Fol-cytamine (25.0 mg, 1.0 eq, 43.4 µmol) and DIPEA (11.2 mg, 15 µL, 2.0 eq). The reaction mixture was stirred overnight in the dark under an argon atmosphere. After completion of the reaction, the crude product was precipitated using an excess of diethyl ether. The product was purified using preparative RP-HPLC (Marcherey-Nagel C18, 5 µm, 250 mm x 20 mm), H_2O with 0.1% TFA (system A) / 80% MeCN-20% H_2O and 0.1 % TFA (system B), 80

mL/min. After lyophilisation, the desired product was obtained as an orange amorphous powder (15.5 mg, 34.5%). **^{1}H NMR** (600 MHz, DMSO-d_6) δ 8.64 (d, *J* = 2.5 Hz, 1H, H-30), 8.31 (s, 1H), 8.11 (t, *J* = 6.1 Hz, 1H), 8.04 (d, *J* = 6.8 Hz, 1H), 7.79 (d, *J* = 8.4 Hz, 1H), 7.64 (d, *J* = 8.2 Hz, 2H, H-12/14), 7.18 (d, *J* = 8.2 Hz, 1H), 6.97 – 6.91 (m, 1H, H-17), 6.68 (d, *J* = 2.3 Hz, 1H), 6.64 (d, *J* = 8.9 Hz, 2H, H-13/15), 6.61 (d, *J* = 8.7 Hz, 2H), 6.58 (d, *J* = 2.3 Hz, 2H), 4.48 (d, *J* = 6.0 Hz, 1H, H-18), 4.29 – 4.22 (m, 1H, H-4), 3.82 – 3.79 (m, 2H), 3.37 – 3.31 (m, 2H), 3.02 – 2.92 (m, 2H), 2.84 – 2.77 (m, 2H), 2.25 – 2.17 (m, 1H, H-2), 2.10 – 2.02 (m, 1H, H-3), 1.95 – 1.89 (m, 1H, H-3). **^{13}C NMR** (151 MHz, DMSO-d_6) δ 27.5 (1C, CH_2, C-3), 32.5 (1C, CH_2, C-2), 35.8, 36.8, 38.3, 43.5, 46.4 (1C, CH_2, C-18), 53.4 (1C, CH, C-4), 83.6 (1C, C_q, C-51), 102.7, 110.2, 111.7 (2C, CH, C13/15), 113.1, 116.8, 124.7, 127.0, 128.4, 129.3, 129.5 (2C, CH, C12/14), 139.0, 141.8, 147.5 (1C, CH, C-30), 148.9, 149.0, 151.2, 152.3, 154.3, 158.3, 158.5, 160.0, 166.5 (1C, CO next to C12/14), 168.4, 169.0, 172.4, 175.0 (1C, COOH next to C4). Signals that were not visible in the ^{13}C NMR were identified through correlation-based analysis in the 2D HMBC NMR spectrum. **MS** (ESI$^-$):m/z = 963.2040 [M-H]$^-$, calculated for $C_{44}H_{39}N_{10}O_{10}S_3^-$: 963.2018. **Analytical HPLC** of γ isomers of probe 10: Nucleosil C18 (5 µm, 4.6 mm x 25 mm), H_2O with 0.1% TFA (system A) / 80% MeCN-20% H_2O and 0.1 % TFA (system B), 1 mL/min, 0.02 min - 5% eluent of system B, 21 min - 70% eluent of system B, (t_R = 20.1 min). **UV/Vis** (PBS): $\lambda_{max\ (Abs)}$ [nm] (ε [$M^{-1}cm^{-1}$]) = 496 (68400); **Fluorescence** (PBS): λ_{ex} [nm] = 480, $\lambda_{max\ (em)}$ [nm] = 517.

7.14 Synthesis of FP 11

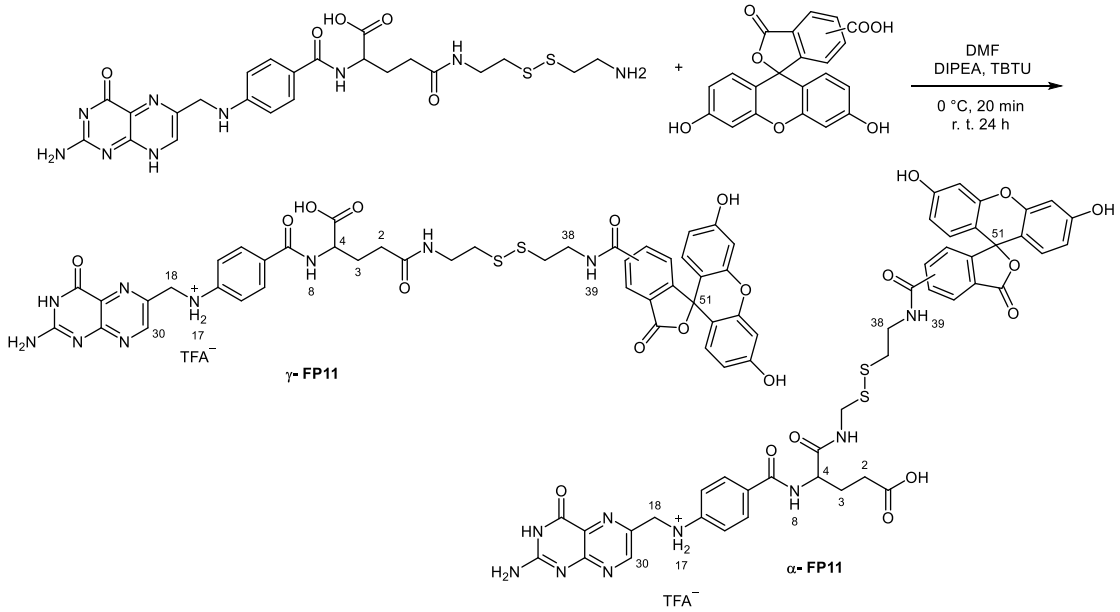

5(6)-carboxyfluorescein (16.3 mg, 43.4 µmol, 1.0 eq) was dissolved in 2 mL anhydrous DMF under an argon atmosphere at 0°C. DIPEA (11.2 mg, 15 µL, 86.8 µmol, 2.0 eq) and TBTU (16.7 mg, 52.1 µmol, 1.2 eq) were added to the reaction, and the reaction mixture was stirred at 0°C for 20 min. Subsequently, a solution of α/γ-Fol-cystamine, (25.0 mg, 43.4 µmol, 1.0 eq) in anhydrous DMF (1 mL) was added dropwise to the reaction mixture. The reaction was stirred overnight at room temperature in the dark. The resulting reaction mixture was quenched by pouring into cold diisopropyl ether, leading to precipitation. The solid crude product was collected by centrifugation. The crude product was purified by preparative RP-HPLC (Marcherey-Nagel C18, 5 µm, 250 mm x 20 mm), H_2O with 0.1% TFA (system A) / 80% MeCN-20% H_2O and 0.1 % TFA (system B), 80 mL/min. After lyophilisation, the desired product was obtained as an orange amorphous powder with 4 isomers, 2 from α and γ isomers of folic acid and 2 from the 5 and 6 carboxyfluorescein (10.5 mg, 25.8%). **^{1}H NMR** (600 MHz, DMSO-d_6) δ 10.18 (s, 2H), 9.05 – 9.02 (t, 0.5H, NH-39, α/γ isomer) & 8.91 – 8.85 (t, 0.5H, NH-39, α/γ isomer), 8.66 (d, *J* = 2.7 Hz, 1H), 8.47 (s, 1H), 8.25 (d, *J* = 8.2 Hz, 1H), 8.17 (d, *J* = 8.1 Hz, 1H), 8.09 (d, *J* = 8.5 Hz, 1H), 8.02 – 7.96 (m, 1H), 7.67 (d, *J* = 8.8 Hz, 2H), 7.39 (d, *J* = 8.0 Hz, 1H), 6.71 – 6.68 (m, 2H), 6.66 – 6.62 (m, 2H), 6.59 (d, *J* = 8.6 Hz, 2H), 6.58 – 6.53 (m, 4H), 4.50 (s, 2H, 18), 4.38 – 4.32 (m, 0.5H, H-4, α/γ isomer), 4.31 – 4.25 (m, 0.5H, H-4, α/γ isomer), 3.49 (d, *J* = 6.3 Hz, 2H), 3.38 – 3.25 (m, 2H), 2.96 – 2.92 (m, 1H), 2.85 – 2.79 (m, 2H), 2.28 – 2.17 (m, 2H, H-2), 2.09 – 1.96 (m, 1H, H-3), 1.94 – 1.82 (m, 1H, H-3). The ratio of α- to γ-isomers, as determined by proton NMR analysis, is 1:1. **^{13}C NMR** (151 MHz, DMSO-d_6) δ 27.0 (1C, CH_2, C-3), 31.1 (1C, CH_2, C-2), 37.3, 38.5, 39.0, 41.1, 46.4 (1C, CH_2, C-18), 52.6 (1C, CH, C-4), 83.4 (1C, C_q, C-51), 102.7, 106.4, 109.5, 109.6, 111.5, 113.2, 122.3, 123.8, 124.9, 125.8, 128.4, 129.6, 135.2, 148.1,149.2, 152.3, 158.0, 160.1, 165.0, 166.6, 172.1, 173.3,174.8. The carbon signals were identified through COSY and HMBC NMR experiments. **MS** (ESI^-):m/z = 932.2201 $[M-H]^-$, calculated for $C_{44}H_{38}N_9O_{11}S_2^-$: 932.2138. **Analytical HPLC** of probe 11 as a mixture of all its 4 isomers: Nucleosil C18 (5 µm, 4.6 mm x 25 mm), H_2O with 0.1% TFA (system A) / 80% MeCN-20% H_2O and 0.1 % TFA (system B), 1 mL/min, 0.02 min - 5% eluent of system B, 21 min - 70% eluent of system B, (t_R =18.3 min for the first isomer, 18.6 min for the second isomer, 18.8 min for the third isomer, and 18.9 min for the fourth isomer). **UV/Vis** (PBS): $\lambda_{max\ (Abs)}$ [nm] (ε [$M^{-1}cm^{-1}$]) = 498 (73600); **Fluorescence** (PBS): λ_{ex} [nm] = 480, $\lambda_{max\ (em)}$ [nm] = 518.

7.15 Synthesis of N-(6-Aminohexyl) folic acid*

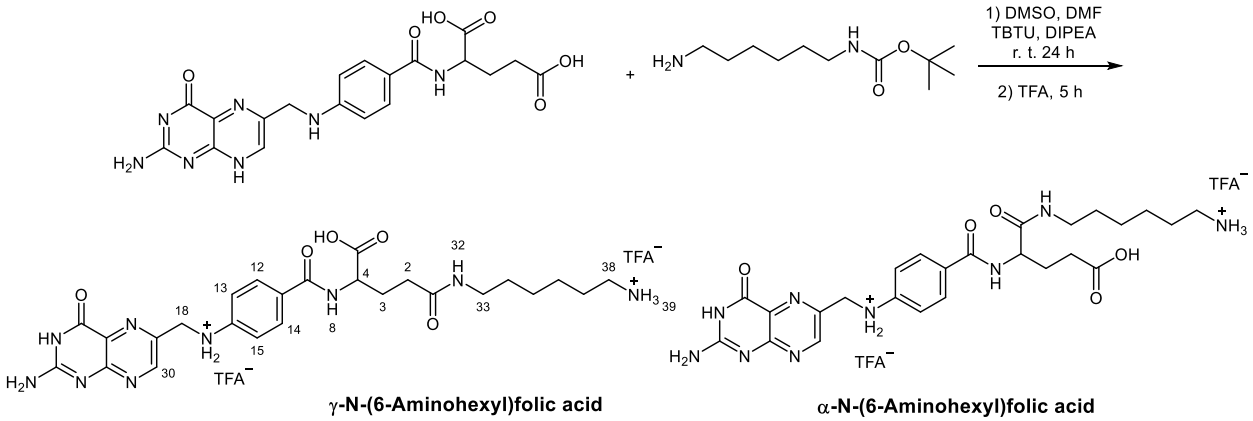

This is a known compound, and the synthesis was carried out following the procedure reported by Bulgakova et al. with slight modifications. [87]

Folic acid dihydrate (400.0 mg, 837.8 µmol, 1.0 eq.) was dissolved in 20 mL anhydrous DMSO and 5 mL DMF under an inert atmosphere. DIPEA (190 µL, 1.1 µmol, 1.3 eq.) and TBTU (296.0 mg, 921.6 µmol, 1.1 eq.) were added to this mixture. After stirring for 30 min, N-Boc-hexandiamine (199.4 mg, 921.6 µmol, 1.1 eq.) was added to the mixture and the reaction was stirred overnight at room temperature. The reaction mixture was poured into 250 mL of cold diethyl ether, resulting in a yellow precipitate, which was collected by centrifugation, and the supernatant was discarded. To the crude product, 5 mL of trifluoroacetic acid (TFA) were added, and the mixture was stirred for 5 hours. The solid was then precipitated again by adding 200 mL of ethyl acetate, followed by centrifugation. The product was purified using preparative RP-HPLC (Marcherey-Nagel C18, 5 µm, 250 mm x 20 mm). System A of HPLC eluent contained H_2O with 0.1 % TFA and system B contained 80% acetonitrile with 20 % H_2O and 0.1 % TFA. After lyophilization, the desired product was obtained as an orange amorphous powder with γ-modified of N-(6-Aminohexyl)folic acid (8.0 mg, 1.3%), α-modified (12.0 mg, 2.0%), and the mixture of both isomers (40.0 mg, 6.5%). **^{1}H NMR** (600 MHz, DMSO-d_6) δ 8.65 (d, *J* = 3.3 Hz, 1H, H-30), 8.21 (d, *J* = 7.5 Hz, 0.6H, NH-8, α/γ isomer), 7.96 (d, *J* = 7.9 Hz, 0.4H, NH-8, α/γ isomer), 7.83 (p, *J* = 5.7 Hz, 1H, H-32), 7.70 (s, 2H, H-39), 7.66 (dd, *J* = 8.8, 3.2 Hz, 2H, H12/14), 6.64 (dd, *J* = 8.8, 3.5 Hz, 2H, H-13/15), 4.49 (s, 2H, H-18), 4.37 – 4.24 (m, 1H, H-4), 3.09 – 2.96 (m, 2H, H-38), 2.81 – 2.72 (m, 2H), 2.34 – 2.23 (m, 1H, H-2, α/γ isomer), 2.21 – 2.15 (m, 1H, H-2, α/γ isomer), 2.16 – 2.01 (m, 1H, H-3), 2.01 – 1.82 (m, 1H, H-3), 1.53 – 1.45 (m, 2H), 1.42 – 1.31 (m, 2H), 1.31 – 1.19 (m, 4H). **^{13}C NMR** (151 MHz, DMSO-d_6) δ 25.9, 26.2, 27.0, 27.4

(1C, CH_2, C-3), 29.3, 31.0 & 32.5 (1C, CH_2, C-2, α/γ isomer), 38.8 (1C, CH_2, C-33), 39.2 (1C, CH_2, C-38), 46.4 (1C, CH_2, C-18), 52.7 (1C, CH, C-4, α/γ isomer), 53.3 (1C, C_q, C-4, α/γ isomer), 111.6 (2C, CH, C13/15), 116.6, 118.6, 121.8, 128.4, 129.5 (2C, CH, C12/14), 149.1 (1C, CH, C-30), 151.2, 154.3, 158.8, 166.7 (1C, amide C, next to C12/14), 171.8 & 171.9 (1C, amide C, next to C-33, α/γ isomer), 172.0 (1C, amide C, next to C-33, α/γ isomer), 174.3 (1C, COOH next to C-4, γ isomer), 174.6 (1C, COOH next to C-2, α isomer). **MS** (ESI^+):m/z = 540.2840 $[M+H]^+$, calculated for $C_{25}H_{34}N_9O_5^+$: 540.2677 **Analytical HPLC** of γ isomers of N-(6-Aminohexyl)folic acid : Nucleosil C18 (5 µm, 4.6 mm x 25 mm), H_2O with 0.1% TFA (system A) / 80% MeCN-20% H_2O and 0.1 % TFA (system B), 1 mL/min, 0.02 min - 5% eluent of system B, 21 min - 70% eluent of system B, (t_R =12.8 min for the first isomer, 13.0 min for the second isomer).

7.16 Synthesis of FP 12

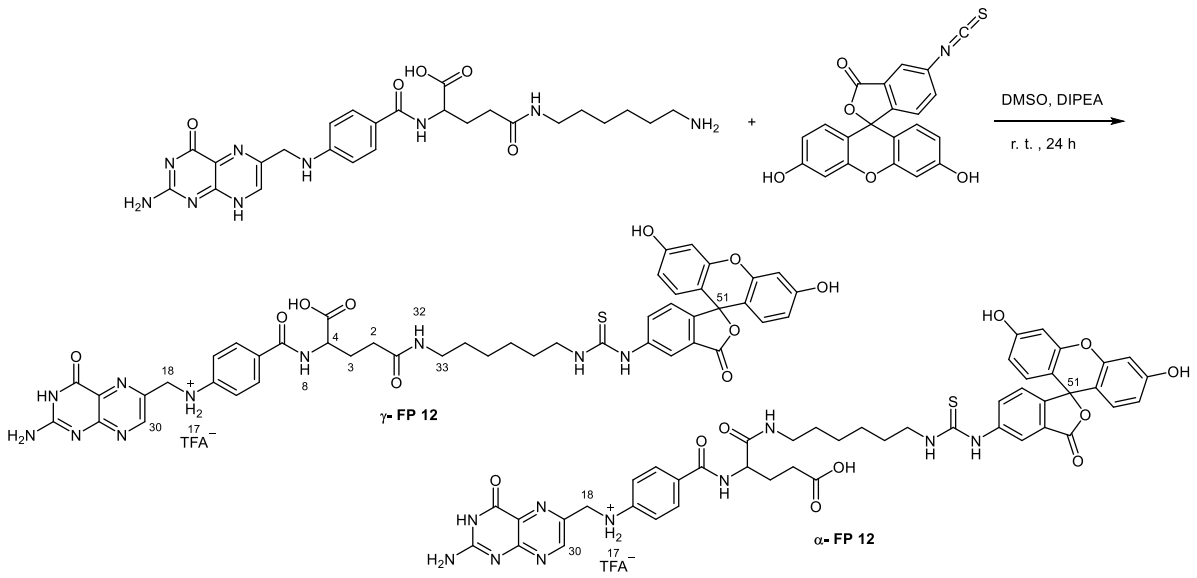

Fluorescein isothiocynate isomer I (14.4 mg, 37.0 µmol, 1.0 eq) was dissolved in 2 mL anhydrous DMSO. To this mixture were added α/γ-N-(6-Aminohexyl)folic acid (20.0 mg, 37.0 µmol, 1.0 eq) and DIPEA (9.6 mg, 13.0 µL, 74.1 µmol, 2.0 eq). The reaction mixture was stirred overnight in the dark under an argon atmosphere. After completion of the reaction, the crude product was precipitated using an excess of diethyl ether. The product was purified using preparative RP-HPLC (Marcherey-Nagel C18, 5 µm, 250 mm x 20 mm), H_2O with 0.1% TFA (system A) / 80% MeCN-20% H_2O and 0.1 % TFA (system B), 80 mL/min. After lyophilisation, the desired product as a mixture of α/γ isomers was obtained as an orange amorphous powder (4.2 mg, 10.8%). **^{1}H NMR** (600 MHz, DMSO-d_6) δ 10.15 (s, 2H), 10.00 – 9.88 (m, 1H), 8.65 (d, J = 2.1 Hz, 1H, H-30),

8.25 (s, 1H), 8.20 – 8.16 (m, 0.6H, NH-8, α/γ isomer), 7.96 – 7.93 (m, 0.4H, NH-8, α/γ isomer), 7.87 – 7.82 (m, 1H, NH-32), 7.77 – 7.72 (m, 1H), 7.66 (dd, *J* = 8.7, 5.1 Hz, 2H), 7.18 (d, *J* = 8.3 Hz, 1H), 6.94 (t, *J* = 6.2 Hz, 1H, NH-17), 6.68 (d, *J* = 2.3 Hz, 2H), 6.64 (dd, *J* = 8.8, 3.4 Hz, 2H), 6.61 (d, *J* = 8.7 Hz, 2H), 6.57 (dd, *J* = 8.6, 2.3 Hz, 2H), 4.48 (d, *J* = 6.1 Hz, 2H, H-18), 4.37 – 4.23 (m, 1H, H-4), 3.51 – 3.48 (m, 2H), 3.11 – 2.98 (m, 2H, H-33), 2.28 – 2.23 (m, 1H, H-2, α/γ isomer), 2.20 – 2.15 (m, 1H, H-2, α/γ isomer), 2.08 – 1.94 (m, 1H, H-3), 1.94 – 1.81 (m, 1H, H-3), 1.57 – 1.53 (m, 2H), 1.44 – 1.36 (m, 2H), 1.31 – 1.28 (m, 4H). **^{13}C NMR** (151 MHz, DMSO-*d*$_6$) δ 26.7, 27.6 (1C, CH_2, C-3), 28.8, 29.4, 29.5, 31.4 & 32.4 (1C, CH, C-2, α/γ isomer), 38.9 (1C, CH_2, C-33), 44.2, 46.4 (1C, CH_2, C-18), 52.8 (1C, CH, C-4), 83.5 (1C, C_q, C-51), 102.7, 110.2, 111.6, 113.0, 121.9, 128.6, 129.4, 142.3, 149.2, 151.4, 152.3, 154.3, 159.9, 167.0, 169.0, 172.0, 174.9. Due to the low concentration of the compound in the NMR tube, not all carbon peaks are visible. The listed carbon signals were identified using COSY, HSQC, and 1D carbon NMR spectra. **MS** (ESI^-):m/z = 927.1439 $[M-H]^-$, calculated for $C_{46}H_{43}N_{10}O_{10}S^-$: 927.2890. **Analytical HPLC** of probe 12: Nucleosil C18 (5 µm, 4.6 mm x 25 mm), H_2O with 0.1% TFA (system A) / 80% MeCN-20% H_2O and 0.1 % TFA (system B), 1 mL/min, 0.02 min - 5% eluent of system B, 21 min - 70% eluent of system B, (t_R =20.7 min for the first isomer, and 20.9 min for the second isomer). **UV/Vis** (PBS): $\lambda_{max\ (Abs)}$ [nm] (ε [$M^{-1}cm^{-1}$]) = 496 (66100); **Fluorescence** (PBS): λ_{ex} [nm] = 480, $\lambda_{max\ (em)}$ [nm] = 516.

7.17 Synthesis of FP 13

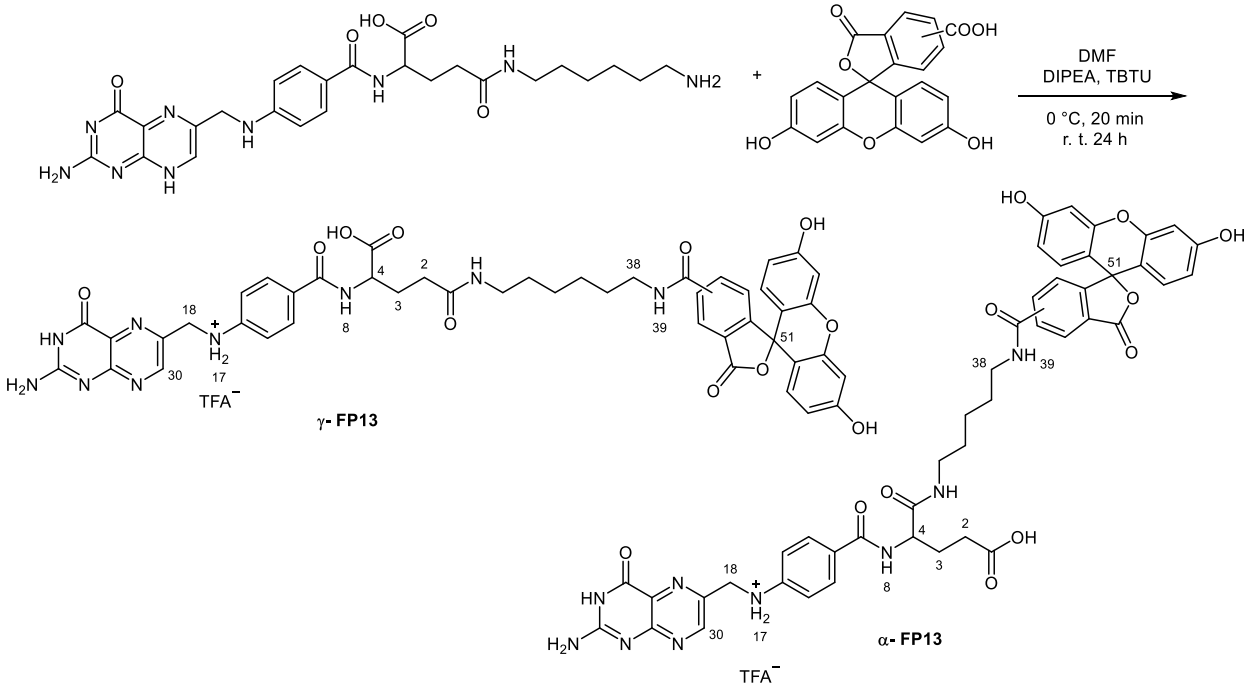

5(6)-carboxyfluorescein (17.4 mg, 46.3 µmol, 1.0 eq) was dissolved in 3 mL anhydrous DMF under an argon atmosphere at 0°C. DIPEA (29.8 mg, 40 µL, 92.6 µmol, 2.0 eq) and TBTU (7.2 mg, 55.6 µoml, 1.2 eq) were added to the reaction, and the reaction mixture was stirred at 0°C for 20 min. Subsequently, a solution of α/γ-N-(6-Aminohexyl)folic acid , (25.0 mg, 46.3 µmol, 1.0 eq) in anhydrous DMF (1 mL) was added dropwise to the reaction mixture. The reaction was stirred overnight at room temperature in the dark. The resulting reaction mixture was quenched by pouring into cold diisopropyl ether, leading to precipitation. The solid crude product was collected by centrifugation. The crude product was purified by preparative RP-HPLC (Marcherey-Nagel C18, 5 µm, 250 mm x 20 mm), H_2O with 0.1% TFA (system A) / 80% MeCN-20% H_2O and 0.1 % TFA (system B), 80 mL/min. After lyophilisation, the desired product was obtained as a purple amorphous powder with 4 isomers, 2 from α and γ isomers of folic acid and 2 from the 5 and 6 carboxyfluorescein (7.6 mg, 16.2%). **MS** (ESI^-):m/z = 896.3040 $[M-H]^-$, calculated for $C_{46}H_{42}N_9O_{11}^-$: 896.3009. **Analytical HPLC** of probe 13: Nucleosil C18 (5 µm, 4.6 mm x 25 mm), H_2O with 0.1% TFA (system A) / 80% MeCN-20% H_2O and 0.1 % TFA (system B), 1 mL/min, 0.02 min - 5% eluent of system B, 21 min - 70% eluent of system B, (t_R =18.9 & 19.3 min). **UV/Vis** (PBS): $\lambda_{max\ (Abs)}$ [nm] (ε [$M^{-1}cm^{-1}$]) = 496 (73600); **Fluorescence** (PBS): λ_{ex} [nm] = 480, $\lambda_{max\ (em)}$ [nm] = 516.

7.18 Synthesis of N-Boc-Cystine di-t-But

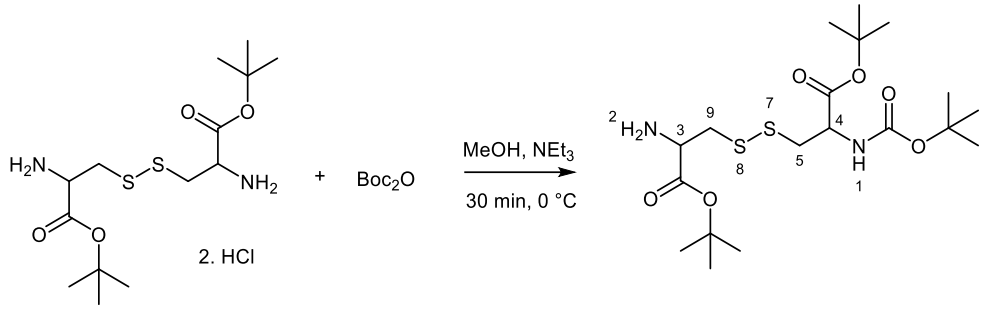

This compound was synthesized following a procedure by Nie Yu et al. [85]

L-Cystine di-t-But (500.0 mg, 1.2 mmol, 1.0 eq) was dissolved in 7 mL of methanol (MeOH) and cooled to 0 °C. Triethylamine (328 µL, 2.4 mmol, 2.0 eq) and di-tert-butyl dicarbonate (Boc_2O, 256.5 mg, 1.2 mmol, 1.0 eq) were added to the reaction mixture. The solution was stirred at 0 °C for 30 minutes, and the progress of the reaction was monitored by TLC. Upon completion, the solvent was evaporated under reduced pressure, and the residue was diluted with ethyl acetate. The organic phase was

washed sequentially with saturated sodium bicarbonate solution (50 mL) and brine (50 mL) to remove ionic impurities. The washed organic layer was dried over magnesium sulfate, filtered, and concentrated under reduced pressure. The crude product was then purified by column chromatography on silica gel using a EtOAc: PE: NEt_3. (2: 1: 0.1) elution system to yield the desired product as a colourless solid (368.0 mg, 52%). **R_f**: 0.6 using EtOAc: PE: NEt_3. (2: 1: 0.1) as solvent. **^{1}H NMR** (600 MHz, DMSO-d_6) δ 7.29 (d, *J* = 8.2 Hz, 1H, NH-1), 4.15 – 4.07 (m, 1H, H-3), 3.47 (t, *J* = 6.3 Hz, 1H), 3.06 (dd, *J* = 13.6, 4.6 Hz, 1H), 2.99 (dd, *J* = 13.1, 5.9 Hz, 1H), 2.95 – 2.84 (m, 2H), 1.42 (s, 9H, CH_3), 1.41 (s, 9H, CH_3), 1.39 (s, 9H, CH_3). **MS** (ESI^+):m/z = 453.2038 $[M+H]^+$, calculated for $C_{19}H_{37}N_2O_6S_2^+$: 453.2088**.**

7. 19 Synthesis of Fol-cystine

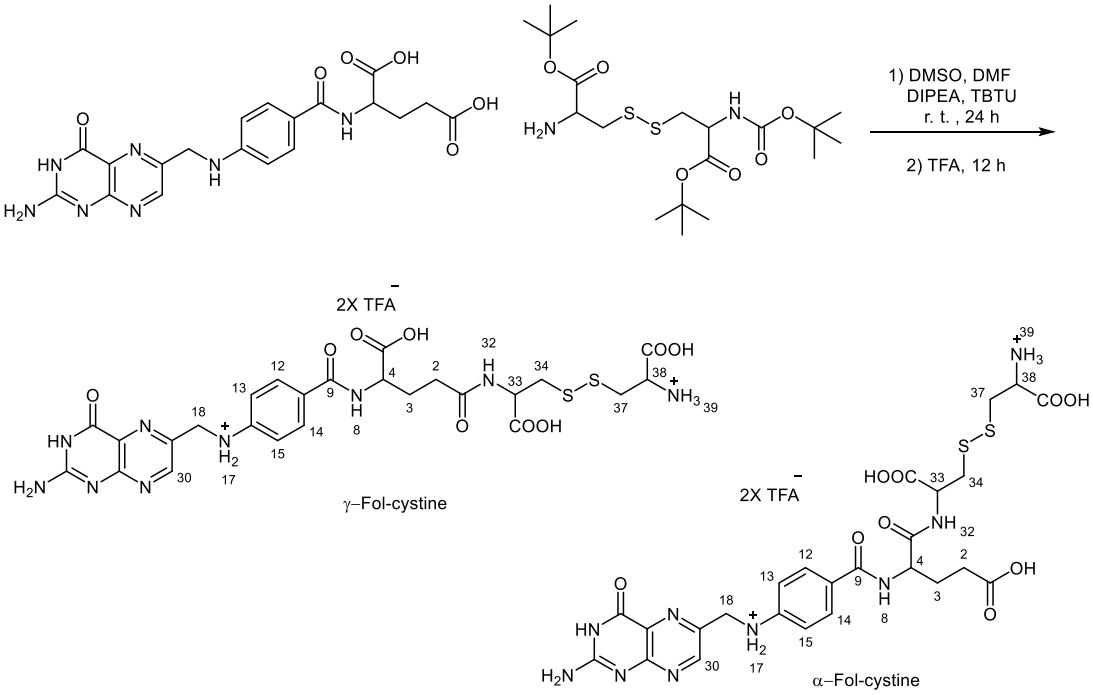

Folic acid dihydrate (477.5 mg, 1.0 µmol, 1.0 eq.) was dissolved in 20 mL anhydrous DMSO and 5 mL DMF under an inert atmosphere. DIPEA (349 µL, 2.0 µmol, 2.0 eq.) and TBTU (417.5 mg, 1.3 µmol, 1.3 eq.) were added to this mixture. After stirring for 30 min, N-Boc-Cystine di-tBut (498.0 mg, 1.1 µmol, 1.1 eq.) was added to the mixture and the reaction was stirred overnight at room temperature. The reaction mixture was poured into 250 mL of cold diethyl ether, resulting in a yellow precipitate, which was collected by centrifugation, and the supernatant was discarded. To the crude product, 5 mL of trifluoroacetic acid (TFA) were added, and the mixture was stirred for 12 hours. The solid was then precipitated again by adding 200 mL of ethyl acetate, followed by centrifugation. The product was purified using preparative RP-HPLC (Marcherey-

Nagel C18, 5 µm, 250 mm x 20 mm). System A of HPLC eluent contained H_2O with 0.1 % TFA and system B contained 80% acetonitrile with 20 % H_2O and 0.1 % TFA. After lyophilization, the desired product was obtained as an orange amorphous powder with γ-modified of Fol-cystine (32.6 mg, 3.8%), α-modified (24.0 mg, 3.0%), and the mixture of both isomers (56.0 mg, 6.5%). **^{1}H NMR** of γ-modified of Fol-cystine (400 MHz, DMSO-*d*$_6$) δ 8.64 (s, 1H, H-30), 8.39 – 8.25 (m, 1H, NH-32), 8.25 – 8.18 (m, 1H, NH-8), 7.66 (d, 2H, H-12/14), 7.11 (br, 2H, NH_2-39), 6.99-6.87 (m, 1H, NH-17), 6.64 (d, *J* = 8.5 Hz, 2H, H-13/15), 4.57 – 4.50 (m, 1H, H-33), 4.48 (s, 2H, H-18,) 4.35-4.24 (m, 1H, H-4), 3.97-3.87 (m,1H, H-38), 3.34 (dd, *J* = 14.3, 4.0 Hz, 1H,H-37), 3.29 – 3.24 (m, 1H, H-34), 3.03 (dd, *J* = 14.4, 7.7 Hz, 1H, H-37), 2.87 (dd, *J* = 13.6, 9.1 Hz, 1H, H-34), 2.35 – 2.15 (m, 2H, H-2), 2.10-1.98 (m, 1H, H-3), 1.97-1.83 (m, 1H, H-3).**^{13}C NMR** (101 MHz, DMSO-*d*6) δ = 27.0 (1C, CH_2, C-3), 32.3 (1C, CH_2, C-2), 39.7 (1C, CH_2, C-37/34), 39.9 (1C, CH_2, C-34/37), 46.4 (1C, CH2, C-18), 51.8 (1C, CH, C-33), 52.3 (1C, CH, C-38), 52.8 (1C, CH-C4), 111.7 (2C, CH, C-13/15), 121.5, 128.2, 128.5, 129.5 (2C, CH, C-12/14), 149.0 (1C, CH, C-30), 151.2, 154.3, 156.6, 167.0, 174.3. The listed ^{13}C peaks are derived from CH coupling data obtained through HMBC and COSY NMR experiments. **MS** (ESI^+):m/z = 664.1779 $[M+H]^+$, calculated for $C_{25}H_{30}N_9O_9S_2^+$: 664.1602 **Analytical HPLC** of γ isomers of Fol-cystine: Nucleosil C18 (5 µm, 4.6 mm x 25 mm), H_2O with 0.1% TFA (system A) / 80% MeCN-20% H_2O and 0.1 % TFA (system B), 1 mL/min, 0.02 min - 5% eluent of system B, 22 min - 50% eluent of system B, (t_R =11.7 min for γ-isomer, and 11.9 min for the α isomer).

7.20 Synthesis of FP 14

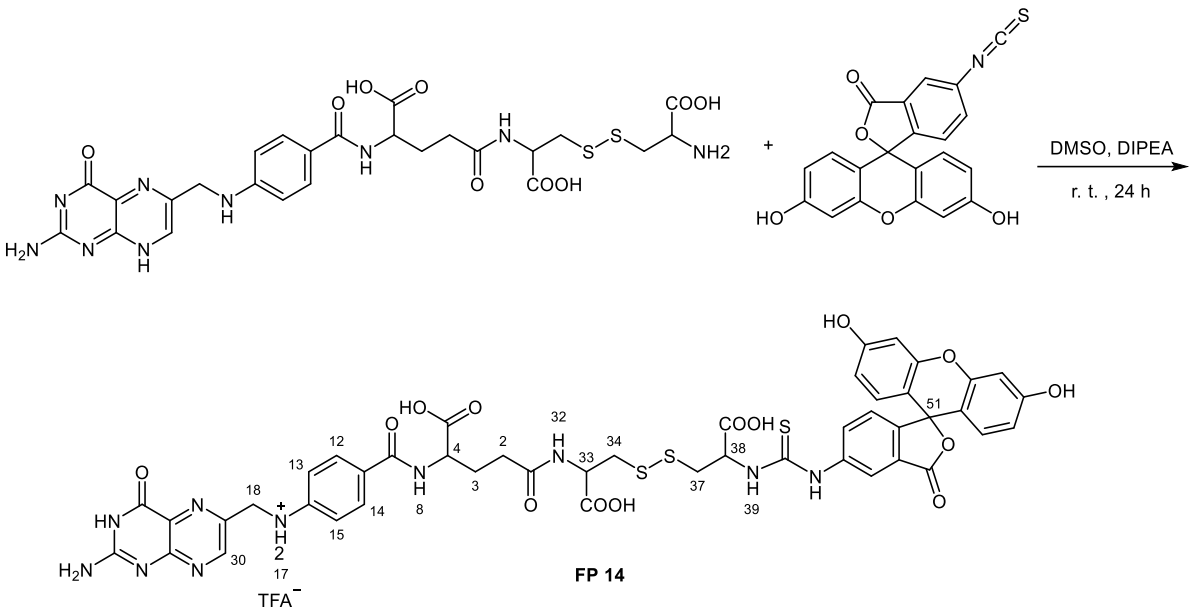

Fluorescein isothiocynate isomer I (17.6 mg, 1.0 eq, 45.2 µmol) was dissolved in 2 mL anhydrous DMSO. To this solution were added γ-Fol-cytine (30.0 mg, 1.0 eq, 45.2 µmol) and DIPEA (11.7 mg, 16 µL, 90.4 µmol, 2.0 eq). The reaction mixture was stirred overnight in the dark under an argon atmosphere. After completion of the reaction, the crude product was precipitated using an excess of diethyl ether. The product was purified using preparative RP-HPLC (Marcherey-Nagel C18, 5 µm, 250 mm x 20 mm), H_2O with 0.1% TFA (system A) / 80% MeCN-20% H_2O and 0.1 % TFA (system B), 80 mL/min. After lyophilisation, the desired product was obtained as an orange amorphous powder (15.5 mg, 30.0%). **^{1}H NMR** (600 MHz, DMSO-d_6) δ 10.30 (s, 1H), 10.19 (s, 1H), 10.13 (s, 2H), 8.66 (s, 1H, H-30), 8.39-8.36 (m, 1H, NH-39), 8.36-8.34 (m, 1H), 8.34 – 8.29 (m, 1H, NH-32), 8.22 – 8.17 (m, 1H, NH-8), 7.80-7.75 (m, 1H), 7.74 – 7.69 (m, 1H), 7.66 (d, *J* = 6.4 Hz, 2H, H-12/14), 7.20 (dd, *J* = 8.2, 1.9 Hz, 1H), 6.71 - 6.69 (m, 1H), 6.68 (d, *J* = 2.3 Hz, 2H), 6.64 (d, 2H, *J*= 8.6 *Hz*, H-13/15), 6.62 – 6.60 (m, 2H), 6.58 – 6.57 (m, 1H), 6.56 – 6.55 (m, 1H), 5.28 - 5.22 (m, 1H, H-38),4.53 - 4.50 (m, 1H, H-33), 4.50 (s, 2H, H-18), 4.34 – 4.27 (m, 1H, H-4), 3.36-3.32 (m, 1H, H-37), 3.26 - 3.23 (m, 1H, H-37), 3.19-3.14 (m, 1H, H-34), 2.97-2.91 (m, 1H, H-34), 2.29-2.24 (m, 2H, H-2), 2.08-2.02 (m, 1H, H-3), 1.94-1.88 (m, 1H,H-3). **^{13}C NMR** (151 MHz, DMSO-d_6) δ 27.1 (1C, CH_2, C-3), 32.8 (1C, CH_2, C-2), 39.9 (1C, CH_2, C-37/34), 40.2 (1C, CH_2, C-37/34), 46.3 (1C, CH_2, C-18), 51.5 (1C, CH, C-33), 53.0 (1C, CH, C-4), 56.5 (1C, CH, C-38), 83.6 (1C, C_q, C-51), 103.0, 109.8, 111.7 (2C, CH, C13/15),

113.4, 117.2, 121.6, 124.9, 127.3, 129.3, 129.7 (2C, CH, C12/14), 149.0, 150.8, 152.4, 155.7, 159.8, 166.6, 169.2. The listed ^{13}C peaks are derived from ^{1}H - ^{13}C coupling data obtained through HMBC and COSY NMR experiments. **MS** (ESI^-):m/z = 1051.1621 $[M-H]^-$, calculated for $C_{46}H_{39}N_{10}O_{14}S_3^-$: 1051.1815. Analytical HPLC of **FP 14**, Nucleosil C18 (5 µm, 4.6 mm x 25 mm), H_2O with 0.1% TFA (system A) / 80% MeCN-20% H_2O and 0.1 % TFA (system B), 1 mL/min, 0.02 min - 5% eluent of system B, 21 min - 70% eluent of system B (t_R =17.1 min). **UV/Vis** (PBS): $\lambda_{max\ (Abs)}$ [nm] (ε [$M^{-1}cm^{-1}$]) = 496 (65600); **Fluorescence** (PBS): λ_{ex} [nm] = 480, $\lambda_{max\ (em)}$ [nm] = 516.

7.21 Synthesis of FP 15

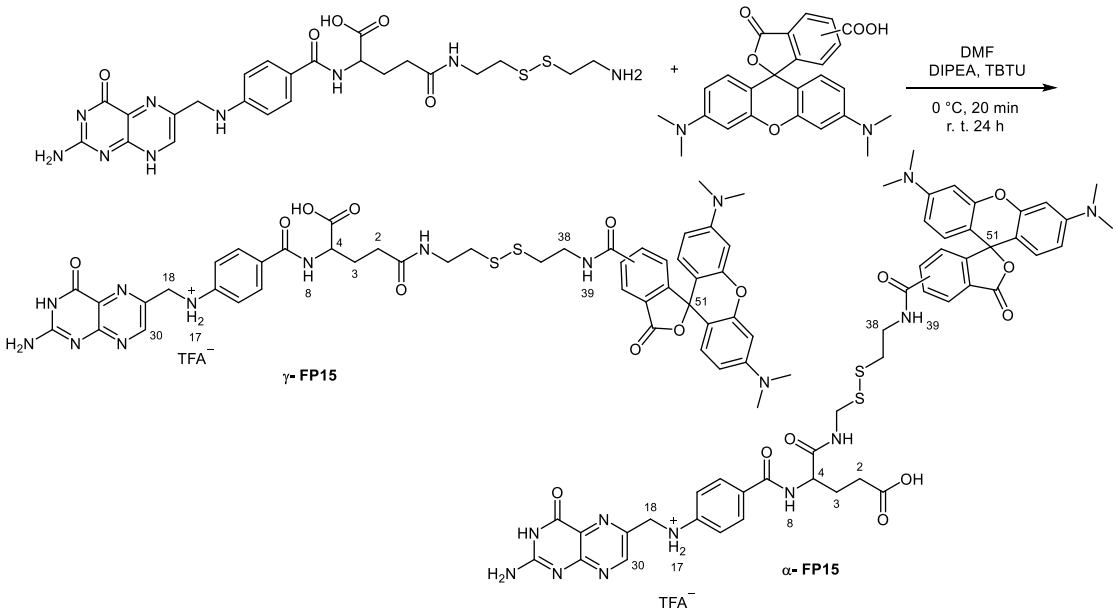

5(6)-TAMRA (28.7 mg, 66.6 µmol,1.1 eq) was dissolved in 1 mL anhydrous DMF under an argon atmosphere at 0°C. DIPEA (15.7mg, 21.1 µL, 121.2 µmol, 2.0 eq) and TBTU (23.3 mg, 72.7 µoml, 1.2 eq) were added to the reaction, and the reaction mixture was stirred at 0°C for 20 min. Subsequently, a solution of α/γ-Fol-cystamine, (35.0 mg, 60.6 µmol, 1.0 eq) in anhydrous DMF (1 mL) was added dropwise to the reaction mixture. The reaction was stirred overnight at room temperature in the dark. The resulting reaction mixture was quenched by pouring into cold diisopropyl ether, leading to precipitation. The solid crude product was collected by centrifugation. The crude product was purified by preparative RP-HPLC (Marcherey-Nagel C18, 5 µm, 250 mm x 20 mm), H_2O with 0.1% TFA (system A) / 80% MeCN-20% H_2O and 0.1 % TFA (system B), 80 mL/min. After lyophilisation, the desired product was obtained as an orange amorphous powder with 4 isomers, 2 from α and γ isomers of folic acid and 2 from the 5 and 6 carboxyfluorescein (4.3 mg, 7.2%). **MS** (ESI^-):m/z = 986.3186 $[M-H]^-$

, calculated for $C_{48}H_{48}N_{11}O_9S_2^-$: 986.3083. **Analytical HPLC** of probe 15 as a mixture of all isomers: Nucleosil C18 (5 µm, 4.6 mm x 25 mm), H_2O with 0.1% TFA (system A) / 80% MeCN-20% H_2O and 0.1 % TFA (system B), 1 mL/min, 0.02 min - 5% eluent of system B, 21 min - 70% eluent of system B, (t_R =19.3 min for the first isomer, 19.7 min for the second isomer, 19.9 min for the third isomer, and 20.3 min for the fourth isomer). **UV/Vis** (PBS): $\lambda_{max\ (Abs)}$ [nm] (ε [$M^{-1}cm^{-1}$]) = 556 (63200); **Fluorescence** (PBS): λ_{ex} [nm] = 540, $\lambda_{max\ (em)}$ [nm] = 578. Obtaining clear and interpretable ^1H and ^{13}C NMR spectra for the compound was challenging, likely due to the low sample concentration and signal overlaps caused by the presence of four isomers of α- and γ-forms of Fol-cystamnie and the 5- and 6-carboxyfluorescein, limiting the inclusion of detailed NMR data in this study.

7.22 Synthesis of compound 16*

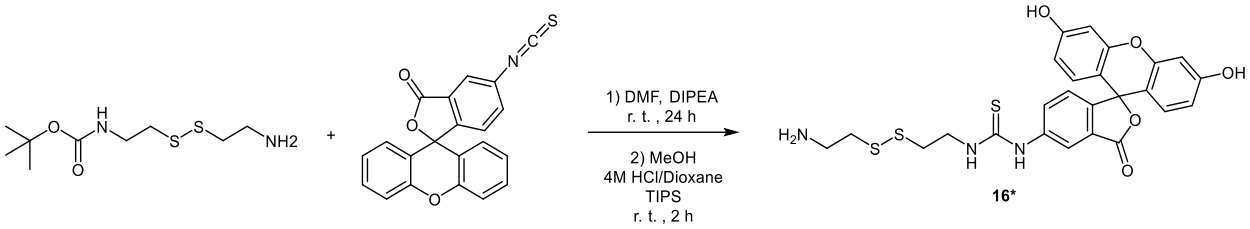

This is a known compound, and the synthesis was carried out following the procedure reported by Tatsuo Maruyama et al. with slight modifications. [88]

N-Boc-cystamine (20.0 mg; 79.2 µmol 1.00 eq.) was dissolved in 2 mL anhydrous DMF. Subsequently, Fluorescein isothiocyanate isomer I (28.3 mg, 79.2 µmol, 1.00 eq.), and DIPEA (28 µL; 158.5 µmol, 2.00 eq.) were added to the reaction mixture. The reaction was stirred at room temperature overnight in the dark. After completion of the reaction monitored by ESI, the solvent was evaporated. The Boc-protected product was purified by column chromatography on silica gel using a DCM: MeOH: NEt_3. (1: 1: 0.1) elution system. This product was dissolved in 2 mL methanol. To this mixture was added 1 mL of 4 M HCl solution in dioxane and triisopropylsilane (22.0 µL,1.7 eq.). The mixture was stirred at room temperature for 2 h. Then the solvent was evaporated and the desired product was achieved as a yellow solid (15.0 mg, 34.9). **^{1}H NMR** (600 MHz, DMSO-d_6) δ 10.23 (s, 1H), 8.40 (t, *J* = 5.6 Hz, 1H), 8.23 (s, 1H), 7.89 (br, 2H), 7.73 (d, *J* = 8.3 Hz, 1H), 7.21 (d, *J* = 8.3 Hz, 1H), 6.69 (d, *J* = 2.3 Hz, 2H), 6.61 (d, *J* = 8.7 Hz, 2H), 6.57 (dd, *J* = 8.7, 2.3 Hz, 2H), 3.86 (d, *J* = 6.5 Hz, 2H), 3.19 – 3.10 (m, 2H), 3.02 (t, *J* = 6.9 Hz, 2H), 2.96 (t, *J* = 7.0 Hz, 2H). **MS** (ESI^+):m/z = 542.1159 $[M+H]^+$,

calculated for $C_{25}H_{24}N_3O_5S^+$: 542.0873. **UV/Vis** (PBS): $\lambda_{max\ (Abs)}$ [nm] (ε [$M^{-1}cm^{-1}$]) = 493 (68900); **Fluorescence** (PBS): λ_{ex} [nm] = 480, $\lambda_{max\ (em)}$ [nm] = 516.

7.23 Synthesis of compound 17

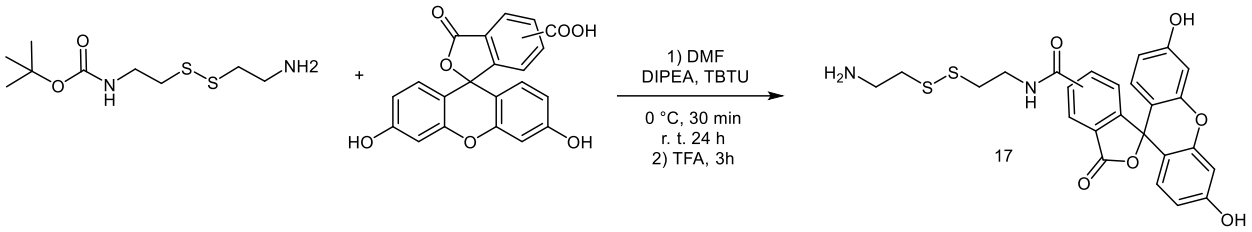

5(6)-carboxyfluorescein (15.0 mg, 39.9 µmol, 1.0 eq) was dissolved in 1 mL anhydrous DMF under an argon atmosphere at 0°C. DIPEA (10.3 mg, 14.0 µL, 79.7 µmol, 2.0 eq) and TBTU (14.1 mg, 43.8 µoml, 1.1 eq) were added to the reaction, and the reaction mixture was stirred at 0°C for 30 min. Subsequently, a solution of N-Boc-cystamine (20.0 mg, 79.7 µmol, 1.0 eq) in anhydrous DMF (1 mL) was added dropwise to the reaction mixture. The reaction was stirred overnight at room temperature at the dark. The solvent was evaporated, and the Boc-protected product was purified by column chromatography on silica gel using a DCM - MeOH - NEt_3. (4: 1: 0.1) elution system. Then the solvent was evaporated, and the desired product was achieved as a yellow solid (12.6 mg, 62.0%). **^{1}H NMR** (600 MHz, DMSO-d_6) δ 10.22 (s, 1H), 9.06 (t, *J* = 5.6 Hz, 1H), 8.91 (t, *J* = 5.6 Hz, 0.4H), 8.46 (s, 1H), 8.25 (dd, *J* = 8.0, 1.6 Hz, 1H), 8.17 (dd, *J* = 8.1, 1.4 Hz, 0.4H), 8.10 (d, *J* = 8.1 Hz, 0.4H), 7.91 (br, 2H), 7.67 (s, 0.4H), 7.41 (d, *J* = 8.0 Hz, 1H), 6.70 (d, *J* = 2.3 Hz, 2H), 6.61 – 6.58 (m, 2H), 6.58 – 6.53 (m, 2H), 3.68 – 3.61 (m, 2H), 3.17 – 3.05 (m, 2H), 3.00 – 2.93 (m, 2H), 2.93 – 2.89 (m, 2H). Additional peaks observed in the proton NMR spectrum, with lower integral values relative to the main peaks, are attributed to the presence of the 5- and 6-isomers of carboxyfluorescein, which exhibit distinct chemical shifts due to differences in their molecular environments. **MS** (ESI^+):m/z = 511.1754 $[M+H]^+$, calculated for $C_{25}H_{23}N_2O_6S_2^+$: 511.0992. **UV/Vis** (PBS): $\lambda_{max\ (Abs)}$ [nm] (ε [$M^{-1}cm^{-1}$]) = 495 (75000); **Fluorescence** (PBS): λ_{ex} [nm] = 480, $\lambda_{max\ (em)}$ [nm] = 519.

7.24 Synthesis of FP 18

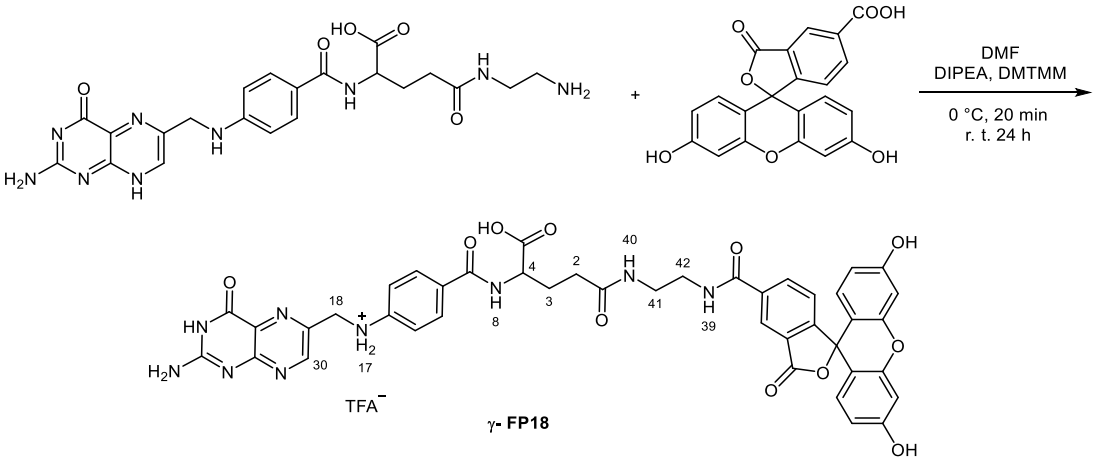

5-carboxyfluorescein (10.0 mg, 26.6 µmol, 1.0 eq) was dissolved in 2 mL anhydrous DMF under an argon atmosphere at 0°C. DIPEA (6.9 mg, 10 µL, 53.1 µmol, 2.0 eq) and DMTMM (8.8 mg, 31.9 µmol, 1.2 eq) were added to the reaction, and the reaction mixture was stirred at 0°C for 20 min. Subsequently, a solution of γ isomer of Fol-eda , (14.1 mg, 29.2 µmol, 1.1 eq) in anhydrous DMF (1 mL) was added dropwise to the reaction mixture. The reaction was stirred overnight at room temperature in the dark. The resulting reaction mixture was quenched by pouring into cold diisopropyl ether, leading to precipitation. The solid crude product was collected by centrifugation. The crude product was purified by preparative RP-HPLC (Marcherey-Nagel C18, 5 µm, 250 mm x 20 mm), H_2O with 0.1% TFA (system A) / 80% MeCN-20% H_2O and 0.1 % TFA (system B), 80 mL/min. After lyophilisation, the desired product was obtained as an orange amorphous powder (3.6 mg, 14.4%). **^{1}H NMR** (700 MHz, DMSO-d_6) δ 10.16 (s, 2H), 8.85 (t, *J* = 5.6 Hz, 1H, H-39), 8.65 (s, 1H, H-30), 8.45 (d, *J* = 1.8 Hz, 1H), 8.24 – 8.23 (m, 1H), 8.23 – 8.22 (m, 1H, NH-8), 8.01 (t, *J* = 5.9 Hz, 1H, NH-40), 7.66 (dd, *J* = 9.1, 2.4 Hz, 2H), 7.36 (d, *J* = 8.0 Hz, 1H), 6.92 (br, 1H, NH-17), 6.69 (d, *J* = 2.2 Hz, 2H), 6.66 – 6.62 (m, 2H), 6.59 – 6.53 (m, 4H), 4.48 (s, 2H), 4.37 – 4.27 (m, 2H), 4.2–4.4 (overlapped with the isopropanol signal, used as the reference for determining the product concentration in the NMR tube), 3.35 (overlapped by the water signal of DMSO-d_6, H-42, confirmed by 2D COSY NMR), 3.25 (overlapped by the water signal of DMSO-d_6, H-41; confirmed by 2D COSY NMR), 2.27–2.20 (m, 2H, H-2), 2.08 (d, J = 2.2 Hz, 1H, H-3), 1.97–1.89 (m, 1H, H-3). **MS** (ESI$^-$):m/z = 840.2418 [M-H]$^-$, calculated for: $C_{42}H_{34}N_9O_{11}^-$: 840.2383. **Analytical HPLC** of FP 18: Nucleosil C18 (5 µm, 4.6 mm x 25 mm), H_2O with 0.1% TFA (system A) / 80% MeCN-20% H_2O and 0.1 % TFA (system B), 1 mL/min, 0.02 min - 5% eluent of system B, 21 min - 70% eluent

of system B, (t_R =16.4 min). **UV/Vis** (PBS): $\lambda_{max\ (Abs)}$ [nm] (ε [$M^{-1}cm^{-1}$]) = 498 (75600); **Fluorescence** (PBS): λ_{ex} [nm] = 480, $\lambda_{max\ (em)}$ [nm] = 521.

7.25 Synthesis of FoI-6AF (FP 19):

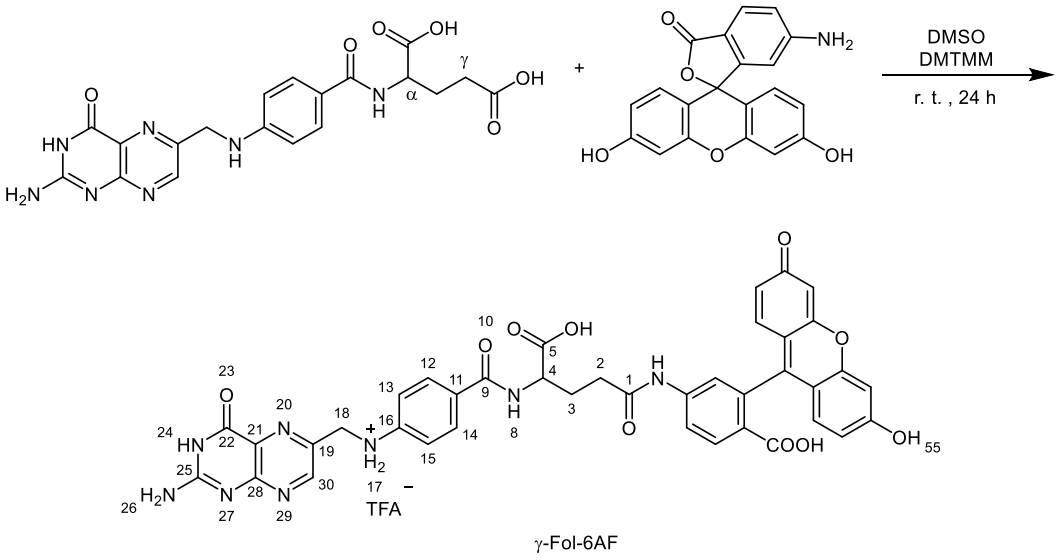

γ-FoI-6AF

Folic acid dihydrate (30.0 mg, 1.0 eq.) was completely dissolved in anhydrous DMSO (5 mL). Then 6-aminofluorescein (24.0 mg, 1.1 eq.) and DMTMM (19.1 mg, 1.1 eq.) were added and stirred at room temperature overnight. The solution was poured into cold Et_2O (80 mL), and the solid material was collected by centrifugation. It was then washed with acetone and dried in vacuo. The crude product was purified by RP HPLC Cosmosil 5C_{18}-MS-II (5µm, 250 mm x 20mm), H_2O with 0.1% TFA (system A) / 80% MeCN-20% H_2O and 0.1 % TFA (system B), 15 mL/min. After lyophilization, the desired product with the predominance of the γ-modified FoI-6AF was obtained as an orange amorphous powder (13.2 mg, 25%). The characterization of the γ and α isomers was achieved using HMBC coupling. The ratio of the γ to α isomers was determined by integrating the proton signal of H-4 in the ^1H NMR spectrum. The multiplet signal observed at 4.34–4.39 ppm corresponds to H-4 with the integral of 1 proton. The sum of the integral of the peaks in the range of 4.45–4.55 ppm gives an integral of 2.09 protons, which after subtracting the contribution of the 2 protons from the H-18, revealed a γ-to-α isomer ratio of 10:1 for FoI-6AF.

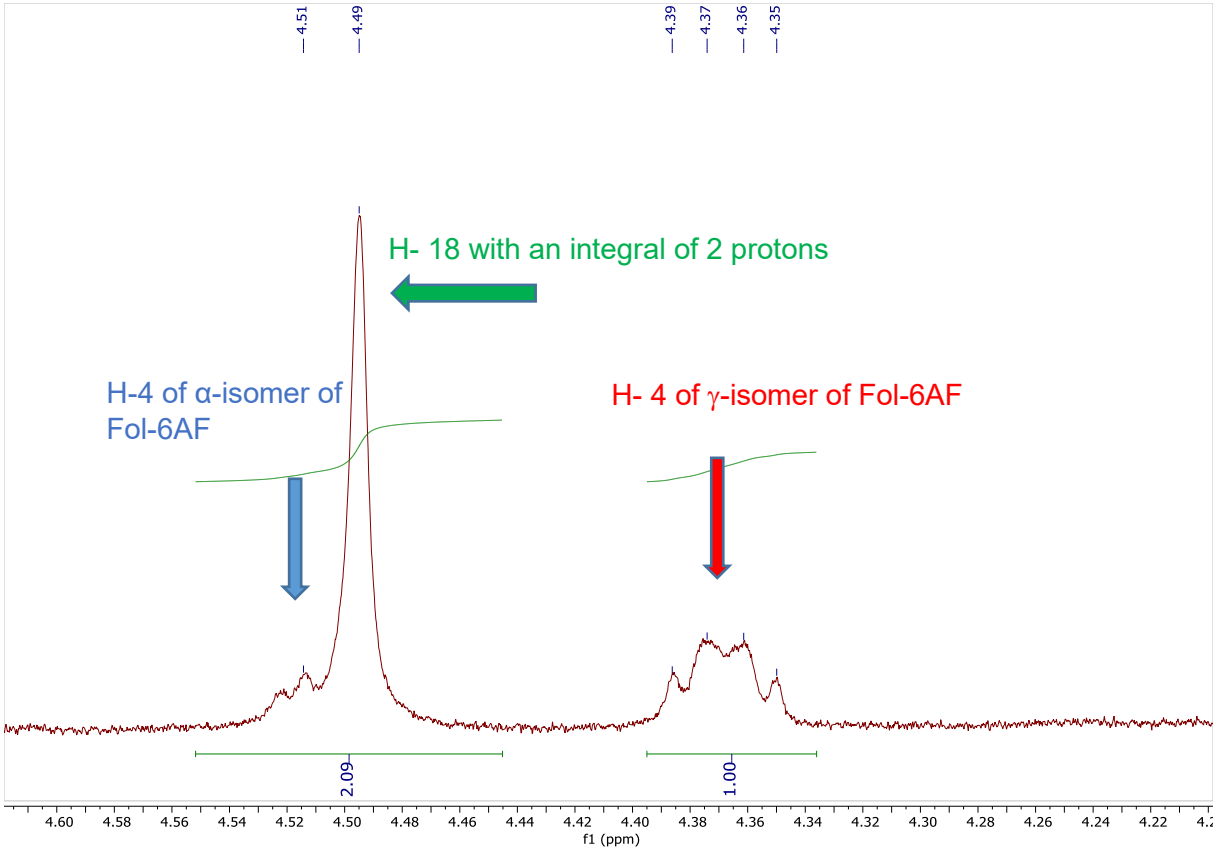

^{1}H NMR of Fol-6AF with the predominant γ isomer (600 MHz, DMSO-d_6) δ 10.82 (s, 1H), 8.66 (s, 1H, H-30), 8.15 (d, *J* = 7.0 Hz, 1H, H-8), 7.92 (d, *J* = 8.4 Hz, 1H), 7.78 (dd, *J* = 8.6, 1.8 Hz, 1H), 7.62 (d, *J* = 8.4 Hz, 2H), 7.54 (d, *J* = 1.7 Hz, 1H), 6.67 (d, *J* = 2.4 Hz, 1H), 6.66 (d, *J* = 2.4 Hz, 1H), 6.63 (dd, *J* = 10.8, 2.4 Hz, 2H), 6.62 – 6.57 (m, 2H), 6.59 – 6.52 (m, 3H), 4.49 (s, 1H, H-18), 4.34- 4.39 (m, 1H, H-4), 2.37 – 2.22 (m, 1H, H-2), 2.02 – 1.93 (m, 1H, H-3), 1.94 – 1.89 (m, 1H, H-3). **^{13}C NMR** (151 MHz, DMSO-d_6) δ 27.0 (1C, CH_2, C-3), 31.3 (1C, CH_2, C-2), 46.5 (1C, CH_2, C-18), 54.9 (1C, CH_2, C-4), 102.9, 106.3, 110.3, 110.3, 111.4, 111.9, 113.3, 113.5, 121.1, 121.5, 121.7, 126.4, 126.7, 128.6, 129.7, 129.8, 129.8, 129.9, 146.1, 149.1, 150.4, 151.5, 152.3, 152.5, 154.0, 155.1, 158.9, 159.1, 159.9, 160.2, 161.3, 167.4, 169.1, 172.6 (1C, CO, C-1), 174.7 (1C, CO, C-4). **MS** (HR-ESI^{+}):m/z = 771.2178 [M+H] $^{+}$, calculated for $C_{39}H_{31}N_8O_{10}^{+}$: 771.2158. **Analytical HPLC**: Nucleosil C18 (5 µm, 4.6 mm x 25 mm), H_2O with 0.1% TFA (system A) / 80% MeCN-20% H_2O and 0.1 % TFA (system B), 1 mL/min, 0.02 min - 5% eluent of system B, 21 min - 70% eluent of system B, t_R = 17.9 min. **UV/Vis** (PBS): $\lambda_{max\ (Abs)}$ [nm] (ε [$M^{-1}cm^{-1}$]) = 492 (79000); **Fluorescence** (PBS): λ_{ex} [nm] = 480, $\lambda_{max\ (em)}$ [nm] = 515.

7.26 Synthesis of FoI-5AF (FP 20):

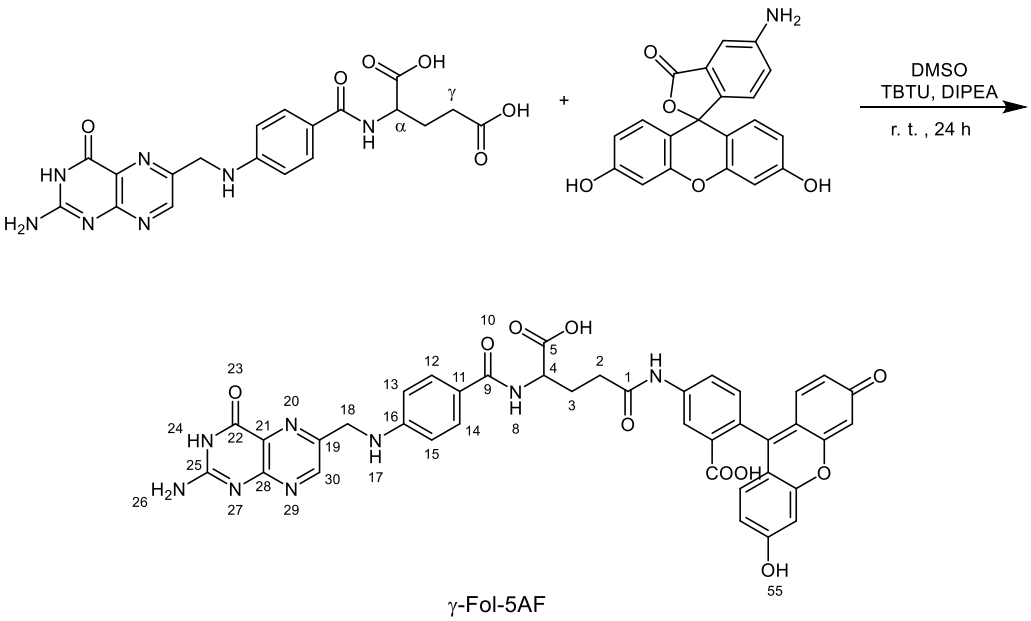

γ-FoI-5AF

Folic acid dihydrate (125.0 mg, 1.0 eq.) was completely dissolved in anhydrous DMSO (15 mL). Then TBTU (168.1 mg, 2.0 eq.) and anhydrous DIPEA (91 µL, 67.7 mg, 2.0 eq.) were added and the mixture was stirred at room temperature for 10 minutes. Subsequently, 5-aminofluorescein (100.0 mg, 1.1 eq.) was added, and stirring was continued overnight. The solution was poured into cold Et_2O (200 mL), and the solid material was collected by centrifugation. Then it was washed with acetone and dried in vacuo. The crude product was purified by RP HPLC Cosmosil $5C_{18}$-MS-II (5µm, 250 mm x 20mm), 10 mM ammonium acetate buffer (pH=7.0)/MeCN, 15 mL/min. After lyophilization, the desired product with the predominance of the γ-modified FoI-5AF was obtained as an orange amorphous powder (53 mg, 22%). The characterization of the γ and α isomers was achieved using HMBC coupling. The ratio of the γ to α isomers was determined by integrating the proton signal of H-4 in the ^{1}H NMR spectrum. The multiplet signal observed at 4.31–4.34 ppm corresponds to H-4 with the integral of 1. The sum of the integral of the peaks in the range of 4.43–4.51 ppm gives an integral of 2.11, which after subtracting the contribution of the 2 protons from the H-18, revealed a γ-to-α isomer ratio of 10:1 for FoI-5AF.

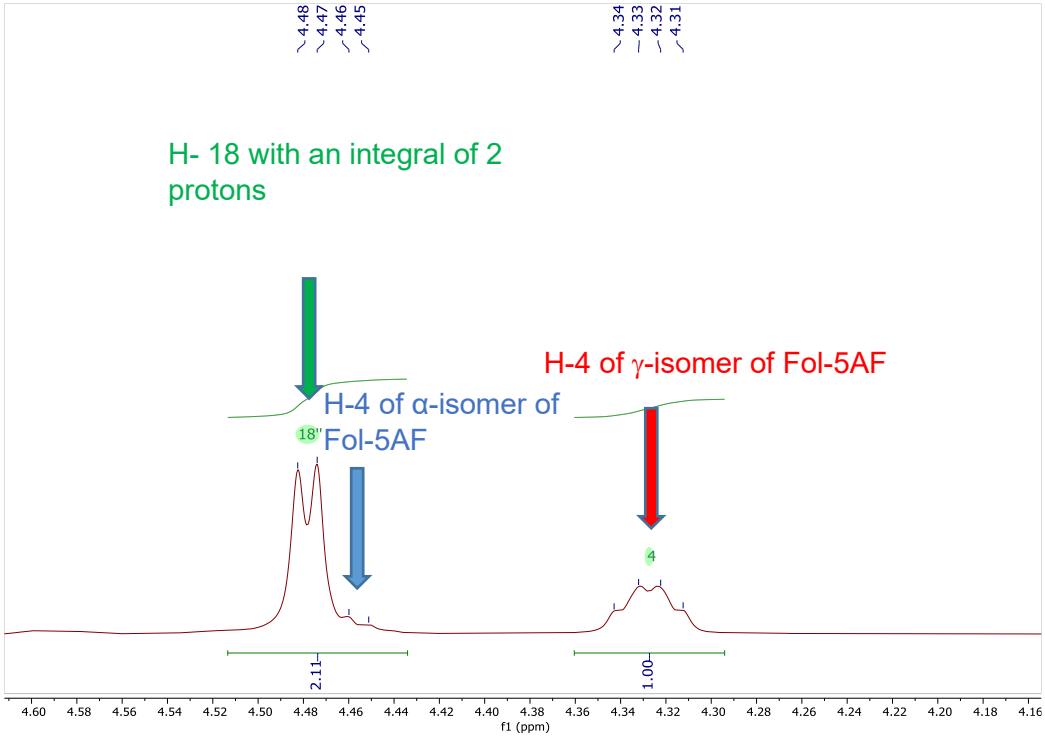

^{1}H NMR of Fol-5AF with the predominant γ isomer (700 MHz, DMSO-d_6) δ 10.50 (s, 1H), 8.63 (s, 1H, H-30), 8.30 (s, 1H), 8.04 (s, 1H, H-8), 7.79 (dd, *J* = 8.4, 1.9 Hz, 1H), 7.66 (d, *J* = 8.3 Hz, 2H, H-12/14), 7.17 (d, *J* = 8.3 Hz, 1H), 6.92 (t, *J* = 6.2 Hz, 1H, H-17), 6.67-6.63 (m, 4H), 6.57 (dd, *J* = 8.7, 2.1 Hz, 2H, H-13/15), 6.54 (dd, *J* = 8.7, 2.3 Hz, 2H), 4.48 (d, *J* = 6.0 Hz, 2H, H-18), 4.36 – 4.30 (m, 1H, H-4), 2.49 – 2.46 (m, 1H, H-2), 2.24 – 2.15 (m, 1H, H-3), 2.05 – 1.97 (m, 1H, H-3). **^{13}C NMR** (176 MHz, DMSO-d_6) δ 27.5 (1C, CH_2, C-3), 33.7 (1C, CH_2, C-2), 46.4 (1C, CH_2, C-18), 52.9 (1C, CH_2, C-4), 102.6, 110.2, 111.7, 113.1, 113.80, 122.0, 124.8, 126.7, 127.4, 128.4, 129.3, 129.6, 141.3, 147.1, 148.9, 149.0 (1C, CH, C-30), 151.2, 152.4, 154.5, 156.7 (visible in HSQC), 159.9, 166.5, 169.1, 171.9 (1C, CO, C-1), 172.6, 172.9, 174.6 (1C, CO, C-5). **MS** (HR-ESI$^-$):m/z = 769.2073 $[M-H]^-$, calculated for $C_{39}H_{29}N_8O_{10}^-$: 769.2012. **Analytical HPLC**: Nucleosil C18 (5 µm, 4.6 mm x 25 mm), H_2O with 0.1% TFA (system A) / 80% MeCN-20% H_2O and 0.1 % TFA (system B), 1 mL/min, 0.02 min - 5% eluent of system B, 21 min - 70% eluent of system B, t_R = 17.1 min **UV/Vis** (PBS): $\lambda_{max\ (Abs)}$ [nm] (ε [$M^{-1}cm^{-1}$]) = 496 (79000); **Fluorescence** (PBS): λ_{ex} [nm] = 480, $\lambda_{max\ (em)}$ [nm] = 515.

7.27 Synthesis of βAla-5AF:

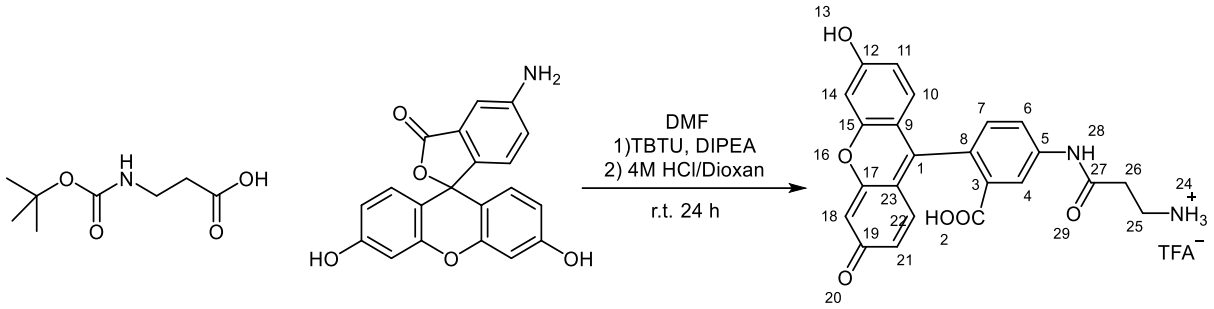

N-Boc-β-Alanine (25.0 mg, 1.1 eq.) was completely dissolved in anhydrous DMF (2 mL). Then TBTU (42.4 mg, 1.2 eq.) and anhydrous DIPEA (23 µL, 17.1 mg, 1.2 eq.) were added and the mixture was stirred at room temperature for 10 minutes. Subsequently, 5-aminofluorescein (41.7 mg, 1.0 eq.) in DMSO (2 mL) was added, and stirring was continued overnight. The solution was poured into cold diisopropyl ether (100 mL) and the solid material was collected by centrifugation. It was then redissolved in 4M HCl/Dioxane (2mL) and stirred at room temperature for 6 hours. The solvent was dried in a vacuum. The crude product was purified by RP HPLC Cosmosil 5C18-MS-II (5µm, 250 mm x 20mm), H_2O with 0.1% TFA (system A) / 80% MeCN-20% H_2O and 0.1 % TFA (system B), 15 mL/min. After lyophilization, the desired product was obtained as an orange amorphous powder (15 mg, 24%). **^{1}H NMR** (600 MHz, Methanol-d_4) δ 8.41 (d, *J* = 2.0 Hz, 1H), 7.83 (dd, *J* = 8.3, 2.0 Hz, 1H), 7.17 (d, *J* = 8.3 Hz, 1H), 6.69 (d, *J* = 2.4 Hz, 2H), 6.62 (d, *J* = 8.7 Hz, 2H), 6.55 (dd, *J* = 8.7, 2.4 Hz, 2H), 3.31 (t, *J* = 1.7 Hz, 2H), 2.88 (t, *J* = 6.2 Hz, 2H). **^{13}C NMR** (151 MHz, Methanol-d_4) δ 32.4, 39.0, 102.1, 110.2, 112.4, 114. 8, 116.2, 124. 6, 126.4, 127.8, 128.8, 140.2, 152.9, 160.1, 169.5, 169. 8. **MS** (HR-ESI$^+$):m/z = 419.1265 [M+H] $^+$, calculated for $C_{23}H_{19}N_2O_6^+$: 419.1238. **Analytical HPLC**: Nucleosil C18 (5 µm, 4.6 mm x 25 mm), H_2O with 0.1% TFA (system A) / 80% MeCN-20% H_2O and 0.1 % TFA (system B), 1 mL/min, 0.02 min - 5% eluent of system B, 21 min - 70% eluent of system B, t_R = 15.9 min

7.28 Synthesis of Fol-βAla-5AF (FP 21):

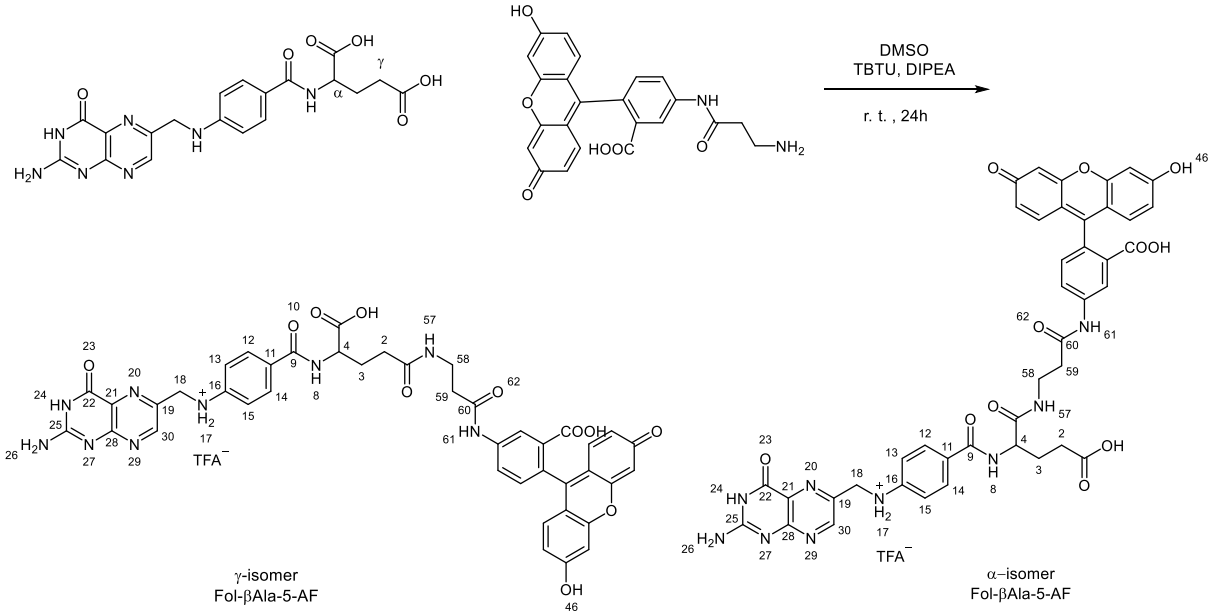

Folic acid dihydrate (22.8 mg, 2.0 eq.) was completely dissolved in anhydrous DMSO (2 mL). Then TBTU (15.3 mg, 2.0 eq.) and anhydrous DIPEA (9 µL, 6.2 mg, 2.0 eq.) were added and stirred at room temperature for 10 minutes. Subsequently, βAla-5AF (10.0 mg, 1.0 eq.) dissolved in 3 mL DMSO was added, and stirring was continued overnight. The solution was poured into cold Et_2O (200 mL) and the solid was collected by centrifugation. It was then washed with acetone and dried in a vacuum. The crude product was purified by RP HPLC Cosmosil 5C18-MS-II (5µm, 250 mm x 20mm), H_2O with 0.1 % TFA / MeCN with 0.1 % TFA, 15 mL/min. After lyophilization, the desired product with γ- and α-modified of Fol-βAla-5AF was obtained as an orange amorphous powder (6.2 mg, 27%).

The ratio of γ to α isomers in the purified product was determined using proton NMR spectroscopy, specifically by analyzing the relative integrals of the H-4 proton signals for each isomer. The multiplet signal of H-4 from the predominant gamma isomer, appearing between 4.27 and 4.32 ppm, was set as the reference with an integral of 1.00. The total integral of this peak and its corresponding α isomer signal (4.32 to 4.38 ppm) was 1.42, indicating an isomeric ratio of 10:4 (γ: α). An impurity was observed near the H-18 signal. The extent of this impurity in the final product was estimated to be approximately 10%. This estimation was made by comparing the integral of the two

H-18 protons at 4.52 ppm with the total integral of the adjacent peak, which included both the H-18 signal and the impurity.

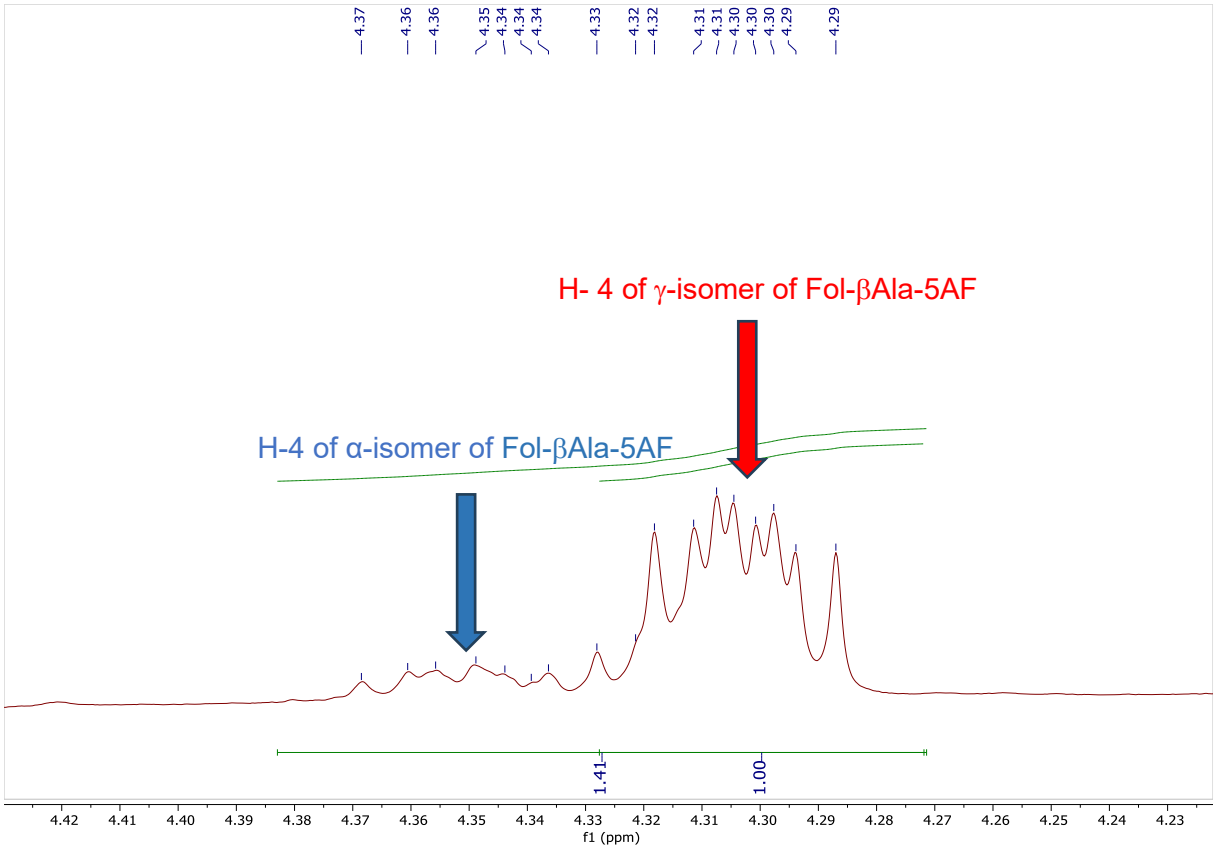

^{1}H NMR (700 MHz, DMSO-d_6) δ 10.44 (s, 1H, H-46), 8.68 (s, 1H, H-30), 8.33 (d, *J* = 2.0 Hz, 1H), 8.24 (d, *J* = 7.6 Hz, 1H, H-8), 8.03 (t, 1H, H-57), 7.81 (d, *J* = 2.0 Hz, 1H, H-61), 7.67 (d, *J* = 8.9 Hz, 2H, H-12, H-14), 7.45 (d, *J* = 8.8 Hz, 1H), 7.20 (d, *J* = 7.8 Hz, 1H), 6.68 (d, *J* = 2.3 Hz, 2H) 6.65 (s, 1H), 6.59 (d, *J* = 8.6 Hz, 2H, H-13/15), 6.56 (d, *J* = 2.5 Hz, 2H), 4.52 (d, 2H, H-18), 4.33 – 4.27 (m, 1H, H-4), 3.37 (m, 2H, H-58), 3.18 – 3.12 (m, 2H, H-59), 2.26 – 2.16 (m, 2H, H-2), 2.12 – 2.03 (m, 1H, H-3), 1.97 – 1.89 (m, 1H, H-3). **^{13}C NMR** (176 MHz, DMSO-d_6) δ 27.0 (1C, CH_2, C-3), 32.4 (1C, CH_2, C-2), 35.55 (1C, CH_2, C-59), 36.9 (1C, CH_2, C-58), 46.3 (1C, CH_2, C-4, α or γ isomer), 52.6 (1C, CH_2, C-4, α or γ isomer), 56.5 (1C, CH_2, C-18), 102.6, 110.0, 110.1, 111.7, 113.1, 113.5, 114.0, 121.8, 124.8, 126.9, 127.3, 128.4, 129.4 (2C, CH, C-12, C14), 129.5, 129.6, 132.6, 141.1, 147.1, 148.8, 149.01 (1C, CH, C-30), 150.1, 151.1, 152.4 (2C, CH, C-13, C15), 153.7, 156.0, 159.9, 160.9, 166.9 (1C, CO next to C-9), 169.1, 169.5, 170.6, 172.7 (1C, CO next to C-2, γ isomer)., 174.3 (1C, CO next to C-4, γ isomer). **MS** (HR-ESI$^-$):m/z = 842.2559 [M+H] $^+$, calculated for $C_{42}H_{36}N_9O_{11}^+$:

842.2529. **Analytical HPLC**: Nucleosil C18 (5 µm, 4.6 mm x 25 mm), H_2O with 0.1% TFA (system A) / 80% MeCN-20% H_2O and 0.1 % TFA (system B), 1 mL/min, 0.02 min - 5% eluent of system B, 21 min - 70% eluent of system B, t_R = 16.6 min. **UV/Vis** (PBS): $\lambda_{max\ (Abs)}$ [nm] (ε [$M^{-1}cm^{-1}$]) = 496 (79000); **Fluorescence** (PBS): λ_{ex} [nm] = 480, $\lambda_{max\ (em)}$ [nm] = 515.

8. List of Molecules

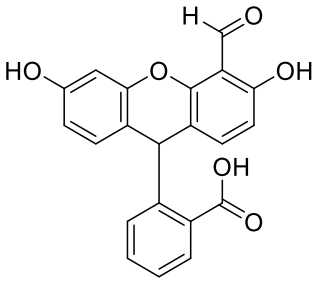

Fluorescein-monoaldehyde *

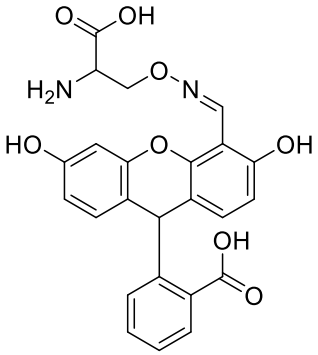

1

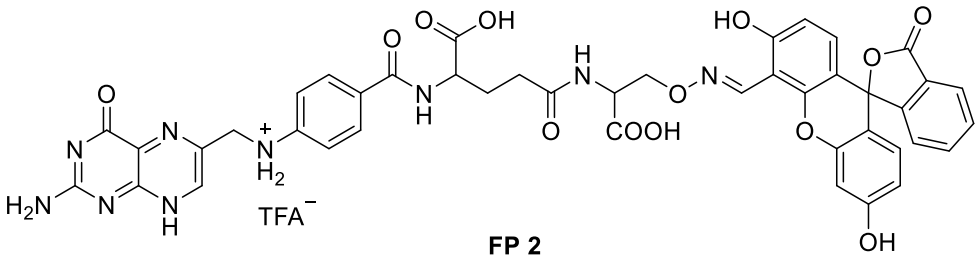

FP 2

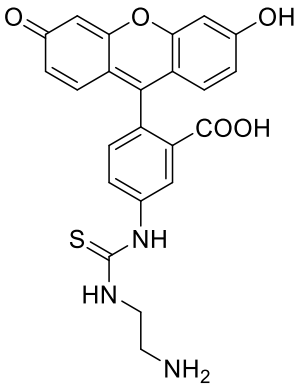

3*

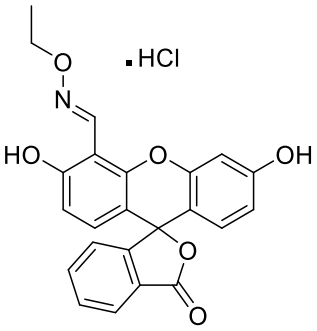

4

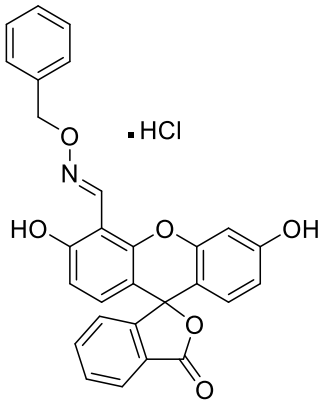

5

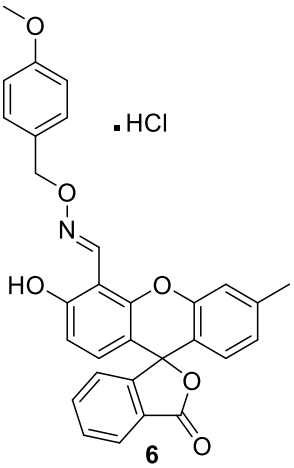

6

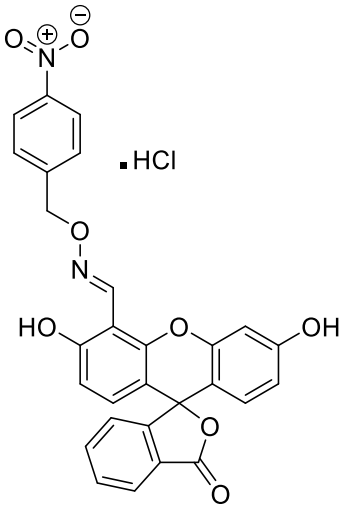

7

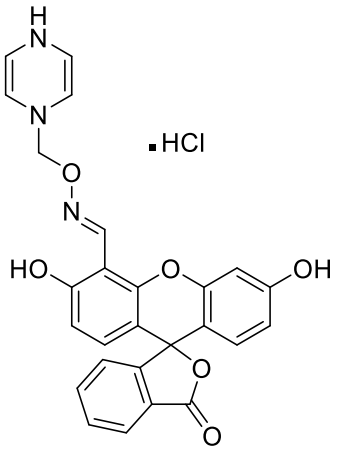

8

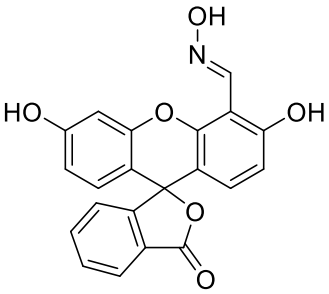

9*

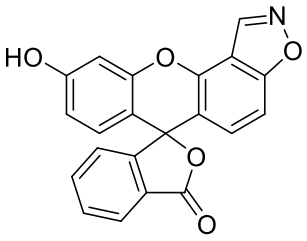

Fluorescein isoxazole*

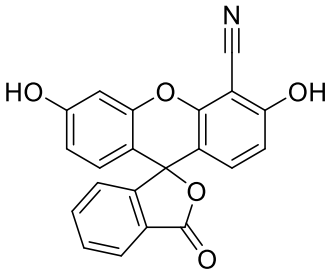

Fluorescein nitrile*

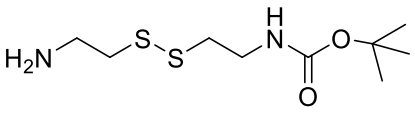

N-Boc-cystamine*

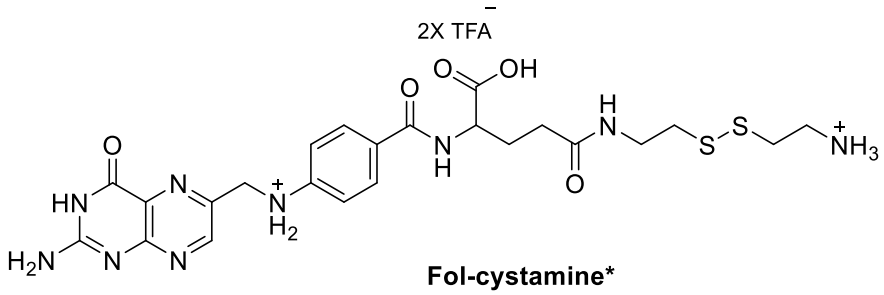

Fol-cystamine*

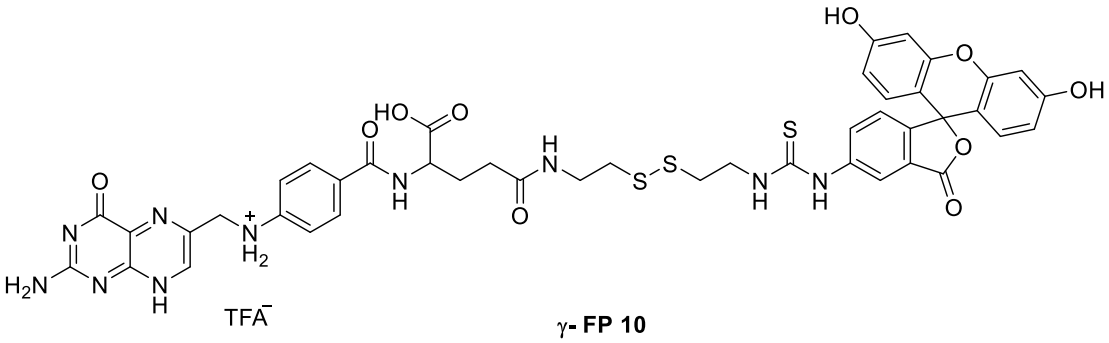

γ- FP 10

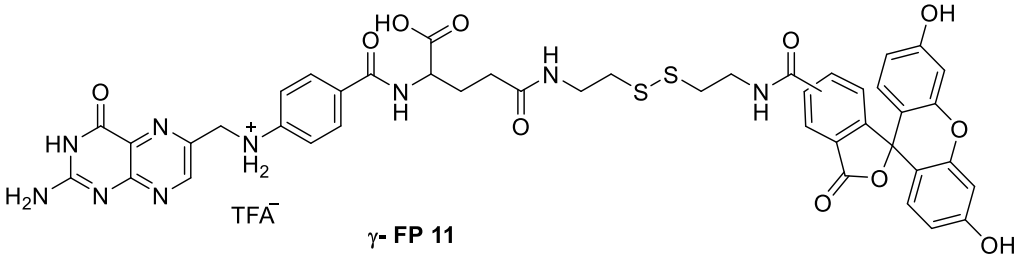

γ- FP 11

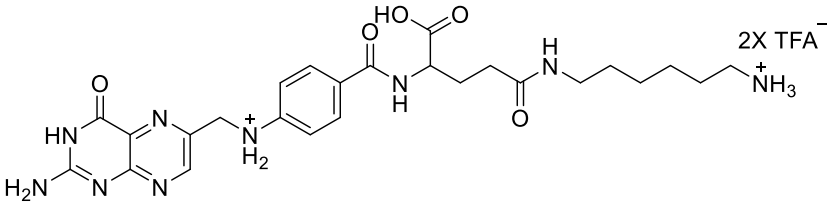

γ-N-(6-Aminohexyl)folic acid

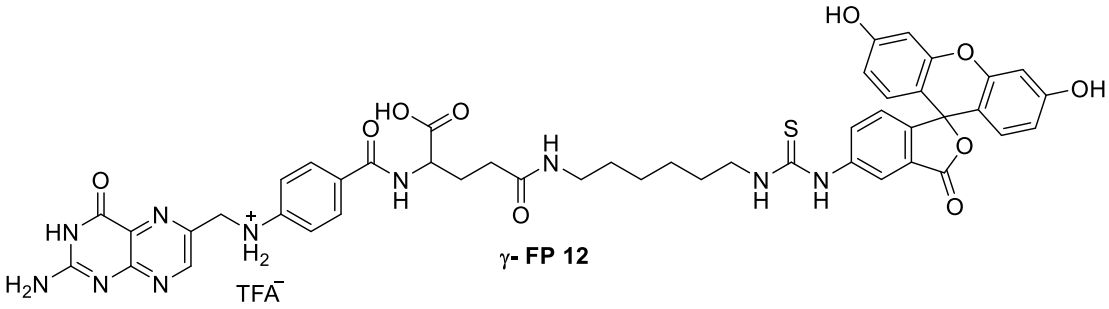

γ- FP 12

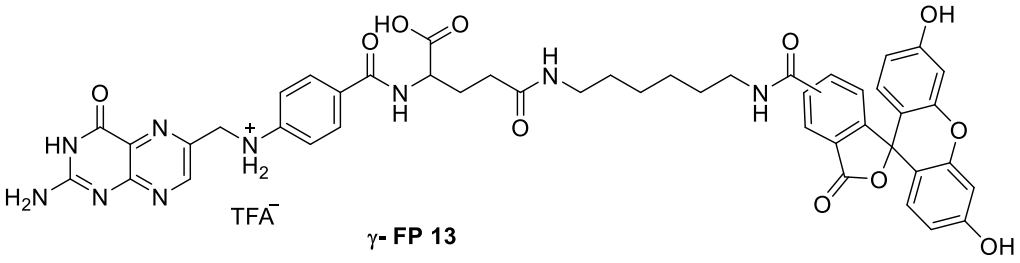

γ- FP 13

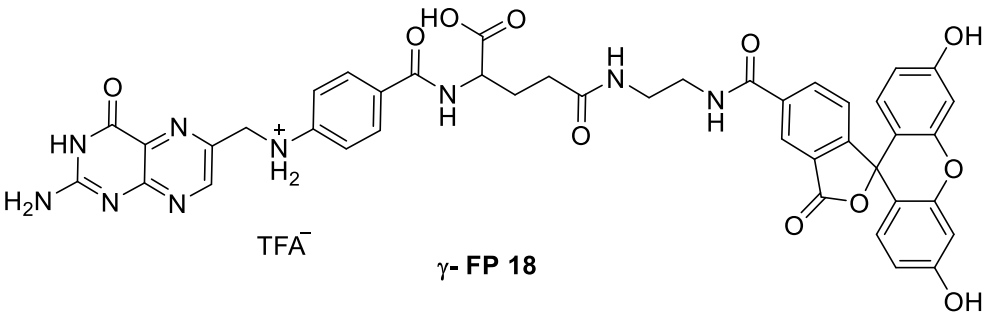

γ- FP 18

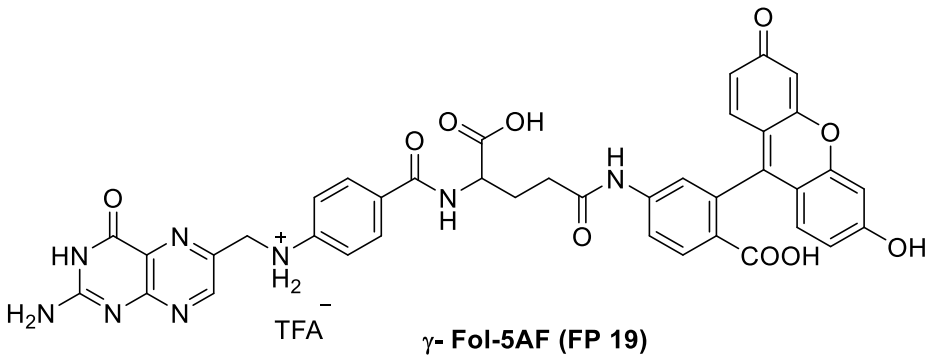

γ- Fol-5AF (FP 19)

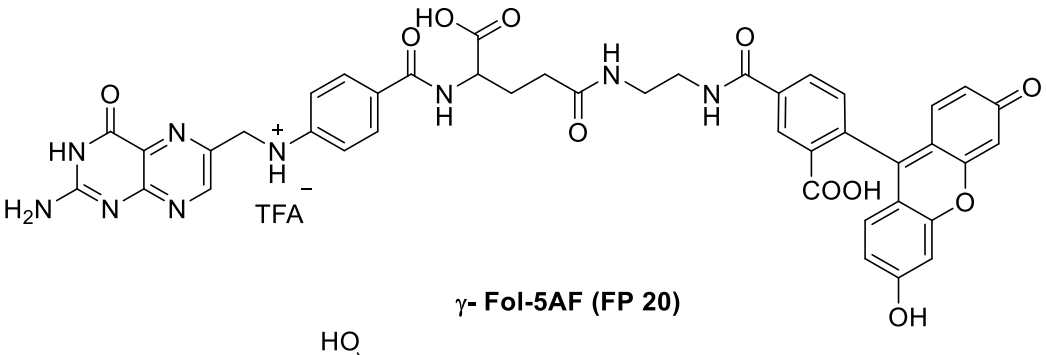

γ- Fol-5AF (FP 20)

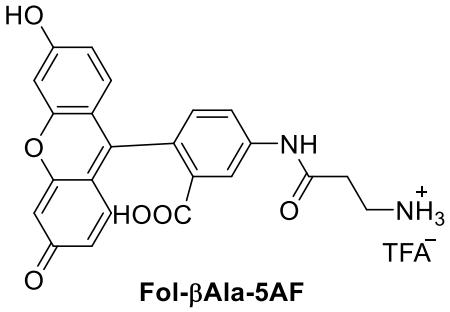

Fol-βAla-5AF

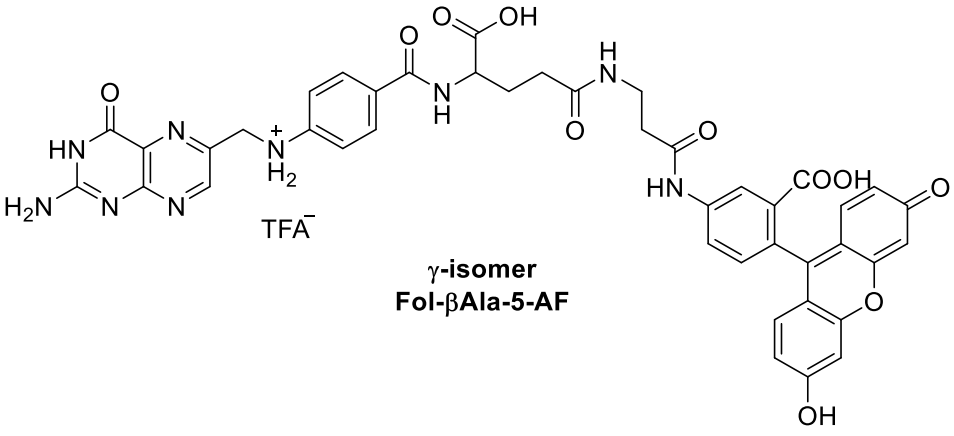

γ-isomer
Fol-βAla-5-AF

9. Spectra

8.1 Fol-eda*

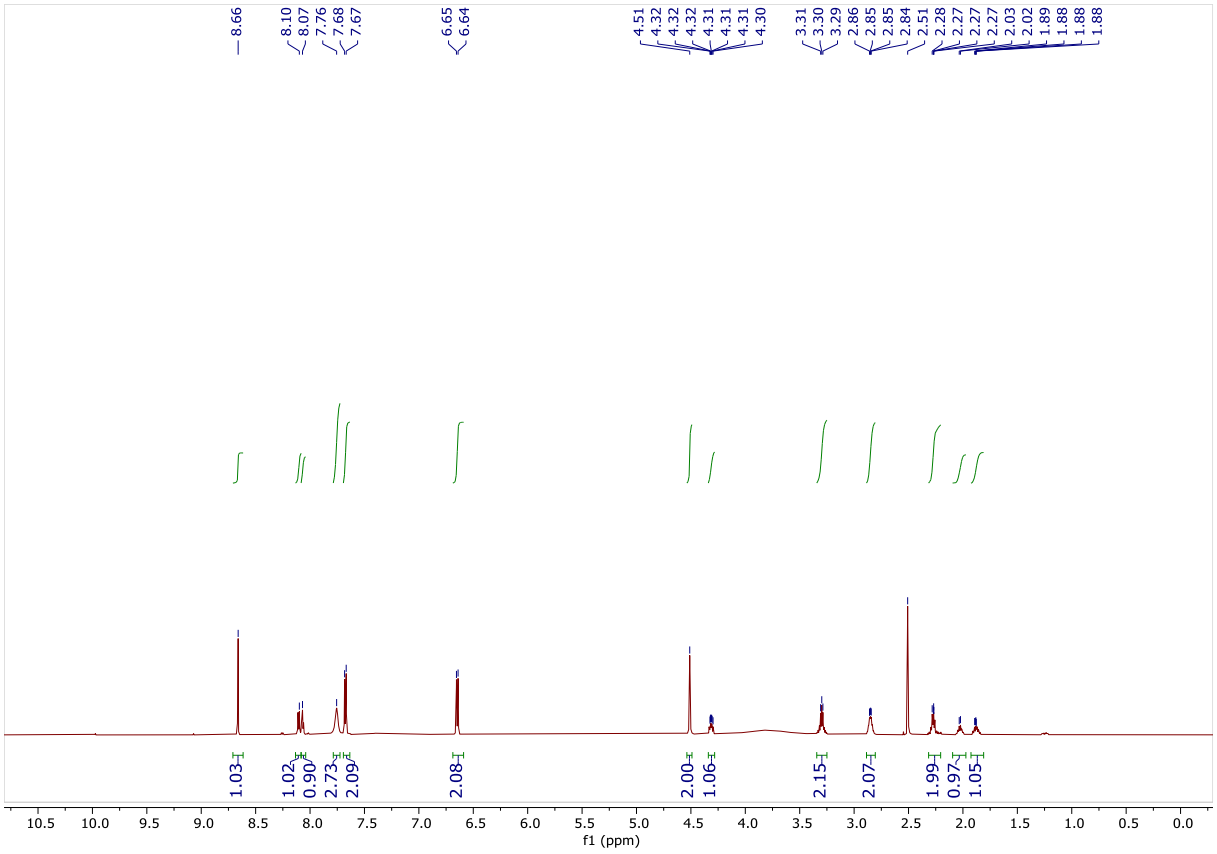

***Figure 55**: [1]H-NMR of γ isomer of Fol-eda, 600 MHz, DMSO-d_6*

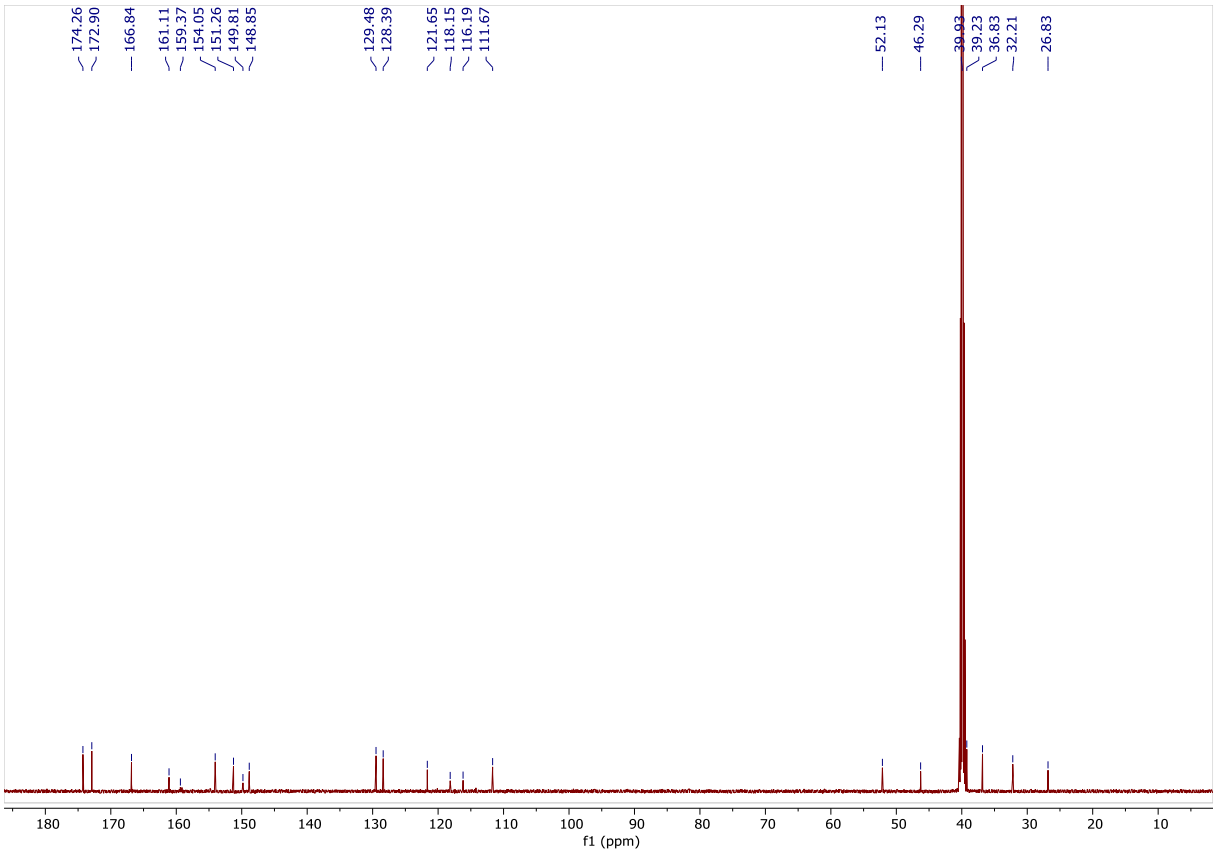

***Figure 56**: ^{13}C-NMR of γ isomer of Fol-eda, 151 MHz, DMSO-d_6*

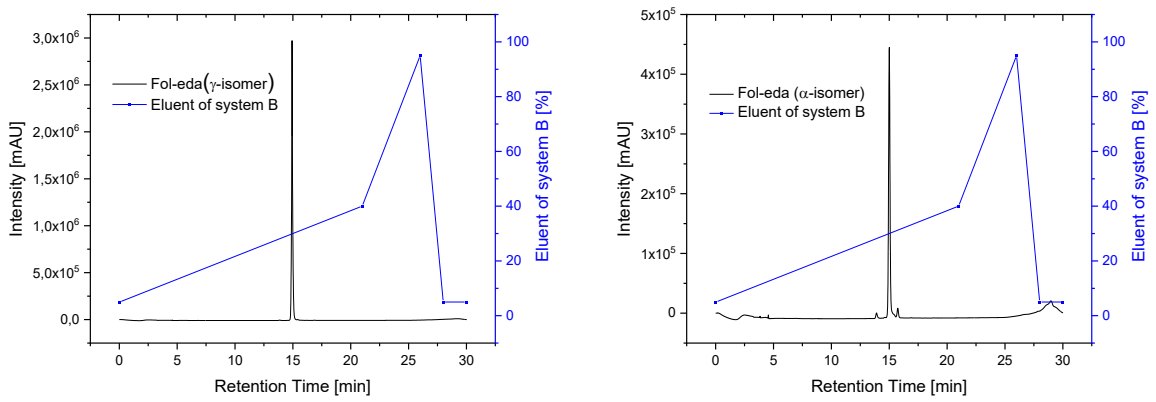

***Figure 57**: Analytical HPLC of Fol-eda, Nucleosil C18 (5 µm, 4.6 mm x 25 mm), H_2O with 0.1% TFA (system A) / 80% MeCN-20% H_2O and 0.1 % TFA (system B), 1 mL/min, 0.02 min - 5% eluent of system B, 21 min - 40% eluent of system B, (γ-isomer: t_R = 14.8min, α- isomer: t_R = 15.0 min)*

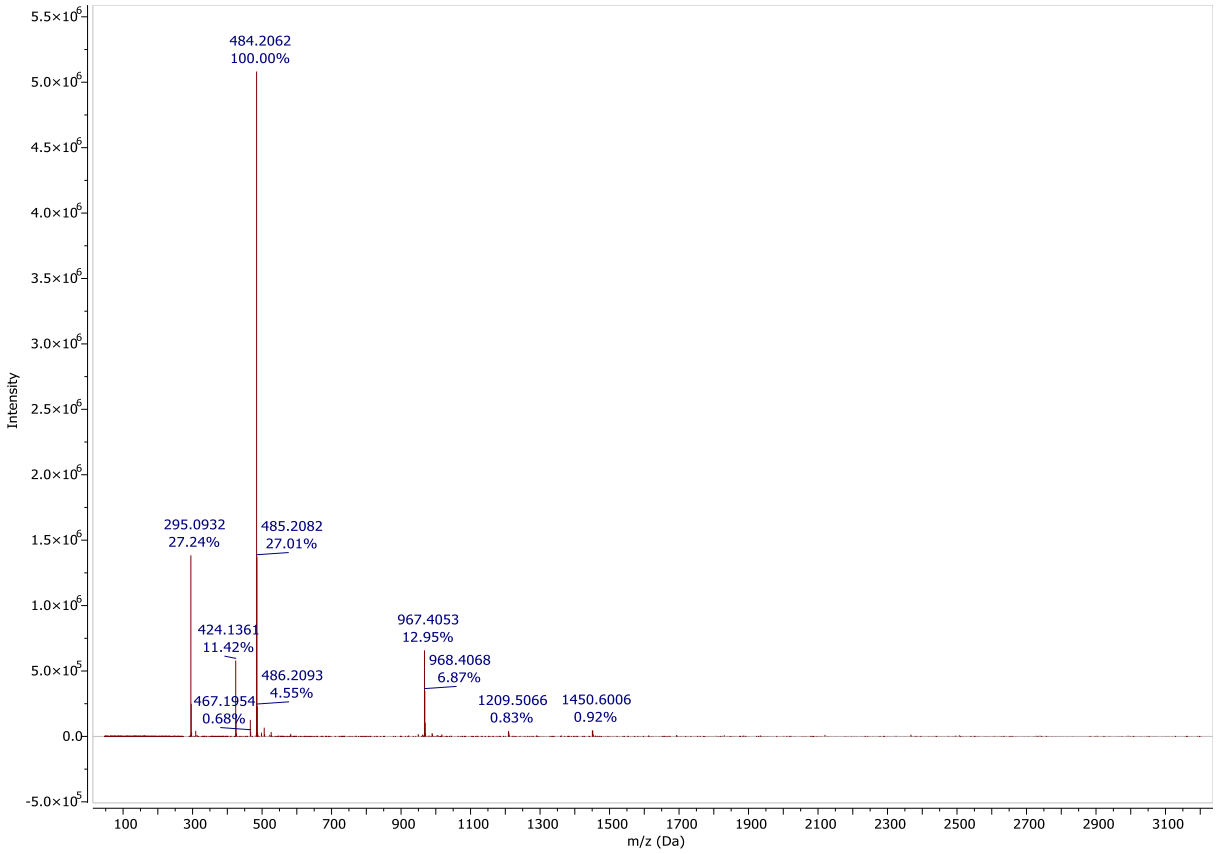

***Figure 58**: HR-ESI MS of Fol-eda, positive mode*

8.2 Folate-FITC*

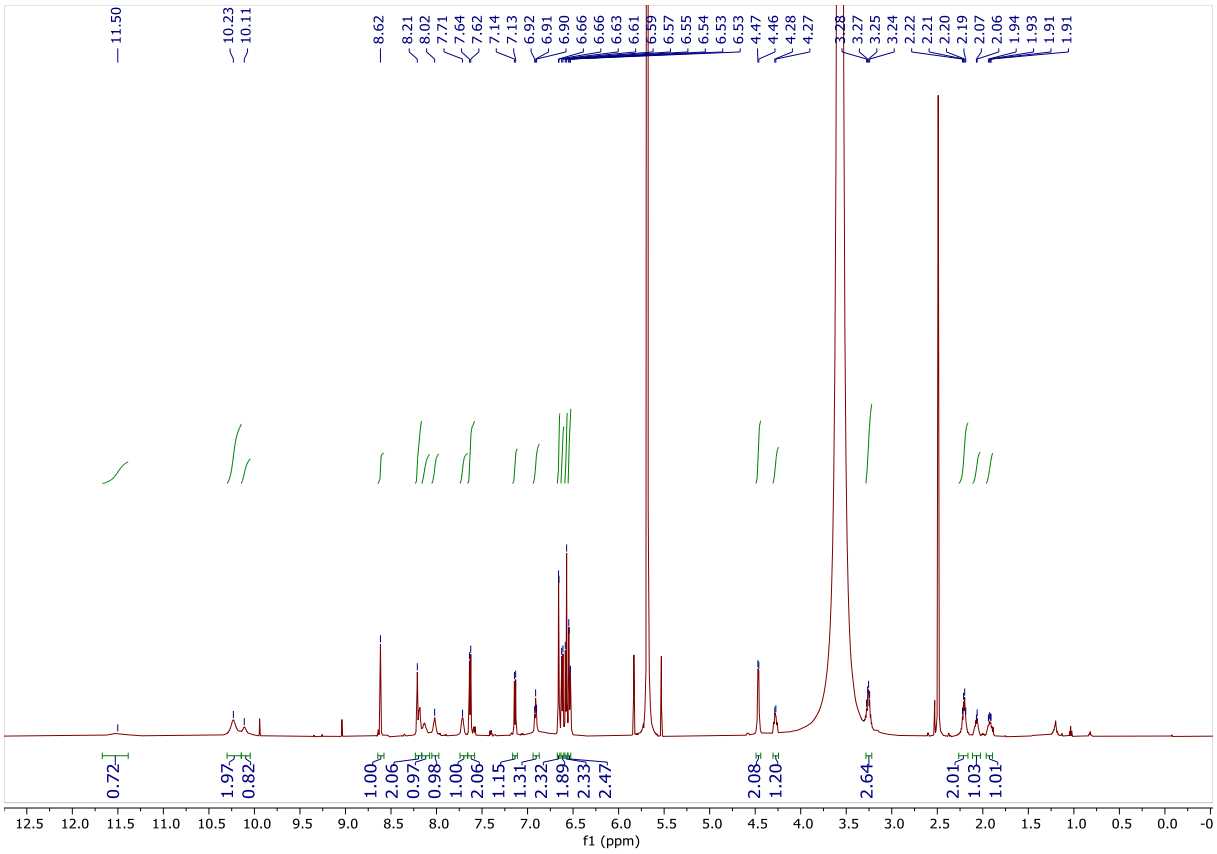

***Figure 59**: [1]H-NMR of folate-FITC, 600 MHz, DMSO-d_6, the peak at 2.49 ppm corresponds to the DMSO-d_6 solvent. The peak at 3.57 ppm is attributed to the water peak present in DMSO. The hydrogen signal of the CH_2 group in the ethylene linker overlaps with the water peak of DMSO which is identified at 3.3 ppm in the [1]H NMR of Fol-eda Fig. S1. Additionally, the peak observed at 5.68 ppm is associated with dichloromethane (DCM), which is used as a reference for determining the concentration of folate-FITC in the NMR tube.*

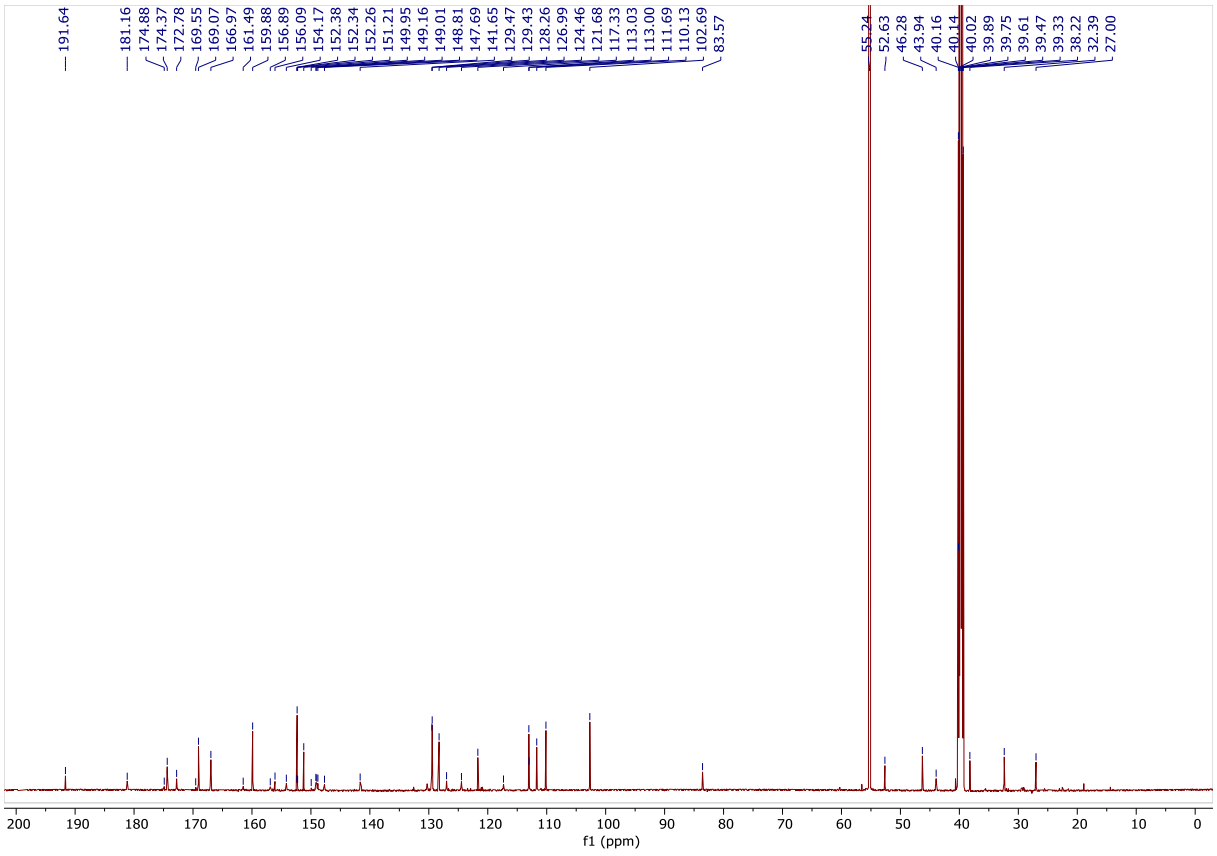

***Figure 60**: [13]C- NMR of folate-FITC, 151 MHz, DMSO-d_6*

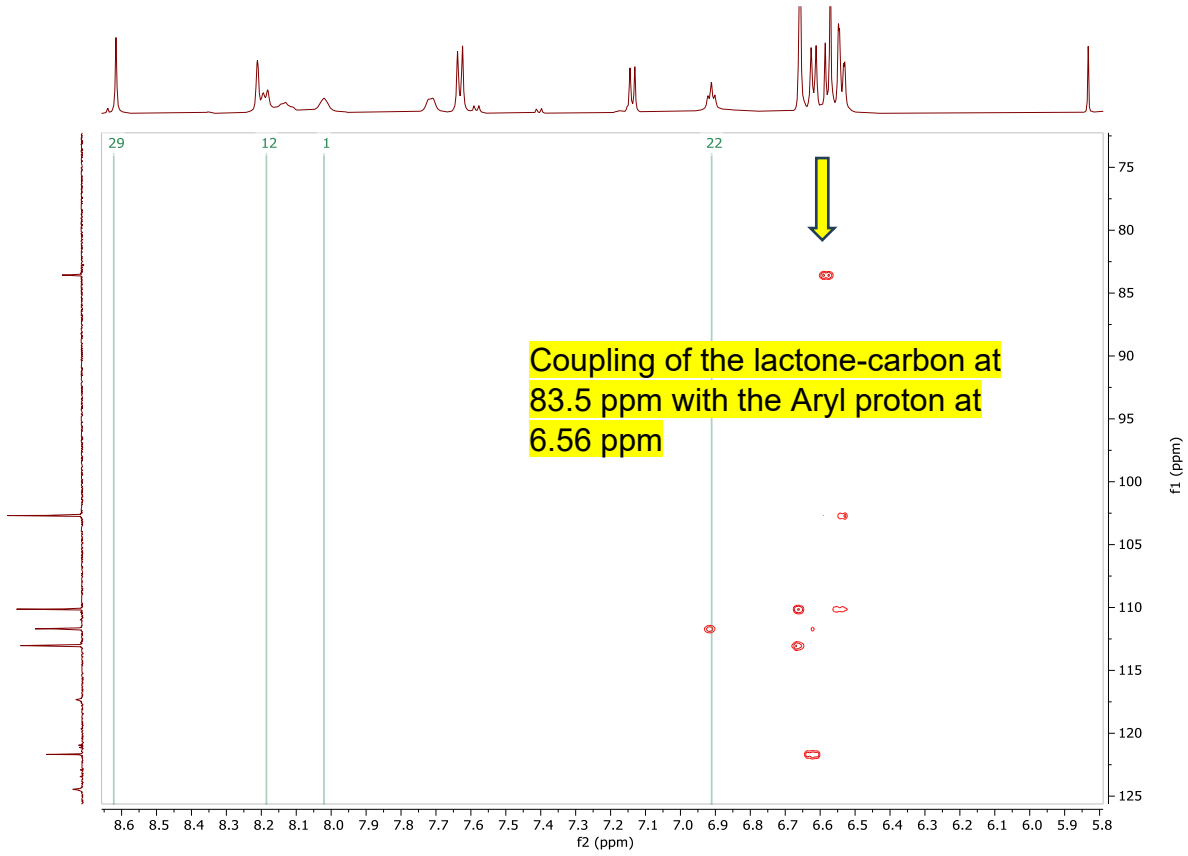

***Figure 61**: HMBC NMR of Folate-FITC in DMSO-d_6*

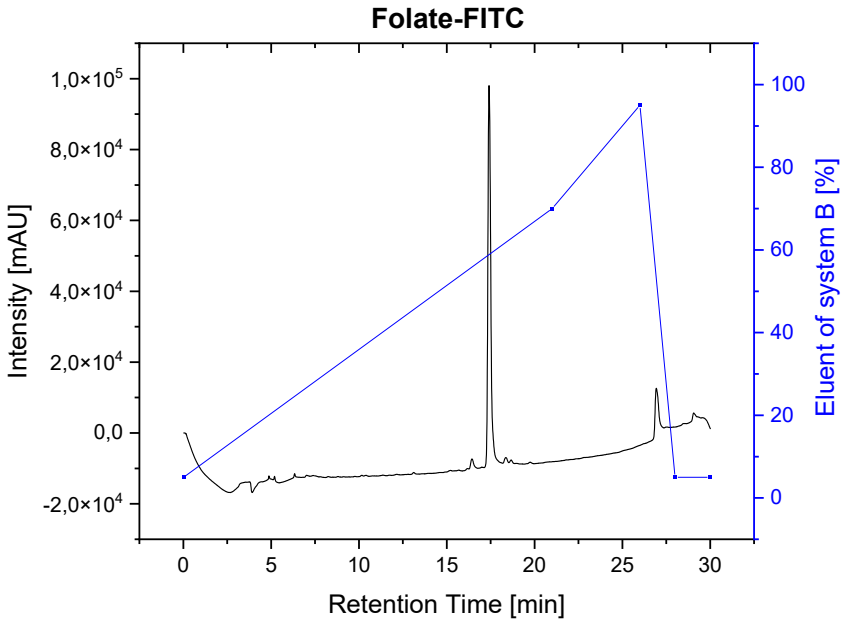

***Figure 62**: Analytical HPLC of folate-FITC, Nucleosil C18 (5 µm, 4.6 mm x 25 mm), H_2O with 0.1% TFA (system A) / 80% MeCN-20% H_2O and 0.1 % TFA (system B), 1 mL/min, 0.02 min - 5% eluent of system B, 21 min - 70% eluent of system B, t_R = 17.4 min.*

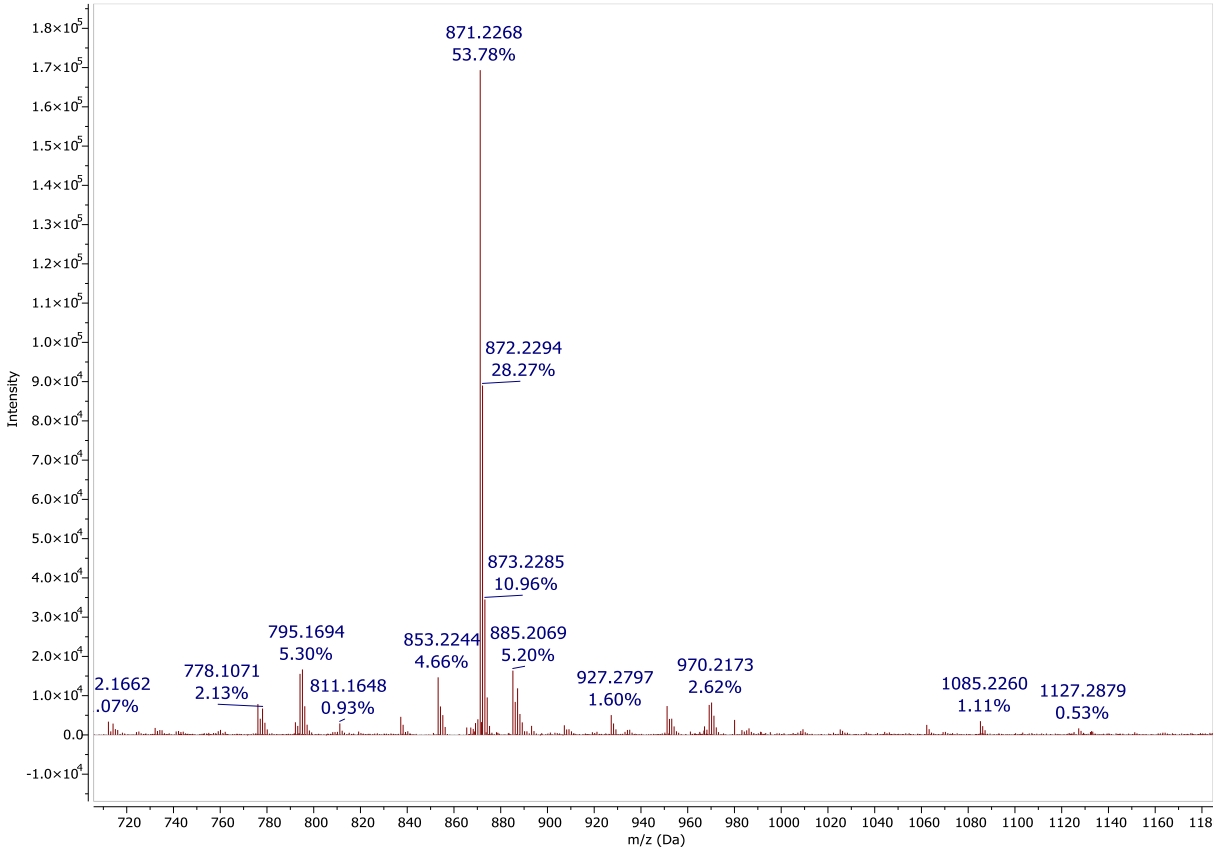

***Figure 63**: HR-ESI MS of folate-FITC, negative mode*

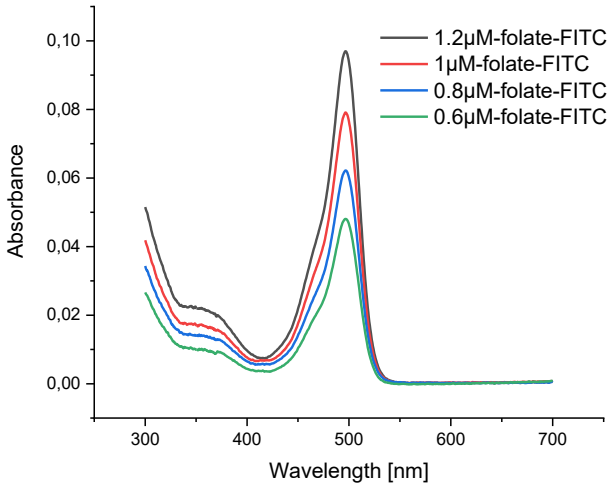

***Figure 64**: Absorption spectra of folate-FITC in 4 different concentrations, PBS (pH=7.4)*

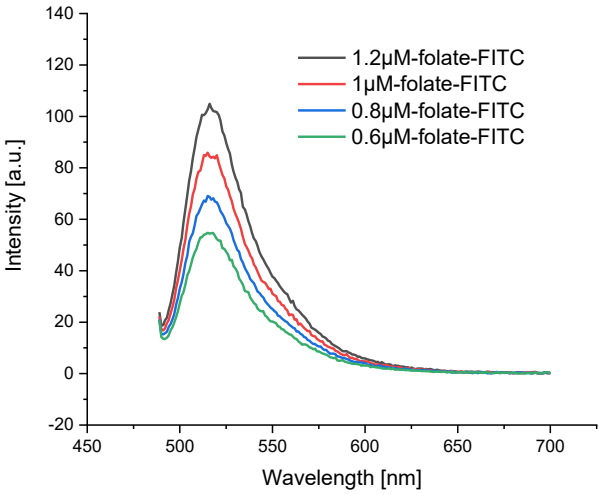

***Figure 65**: Fluorescence emission spectra of folate-FITC in 4 different concentrations, PBS (pH=7.4), Excitation wavelength: 480 nm*

8.3 Fluorescein-monoaldehyde*

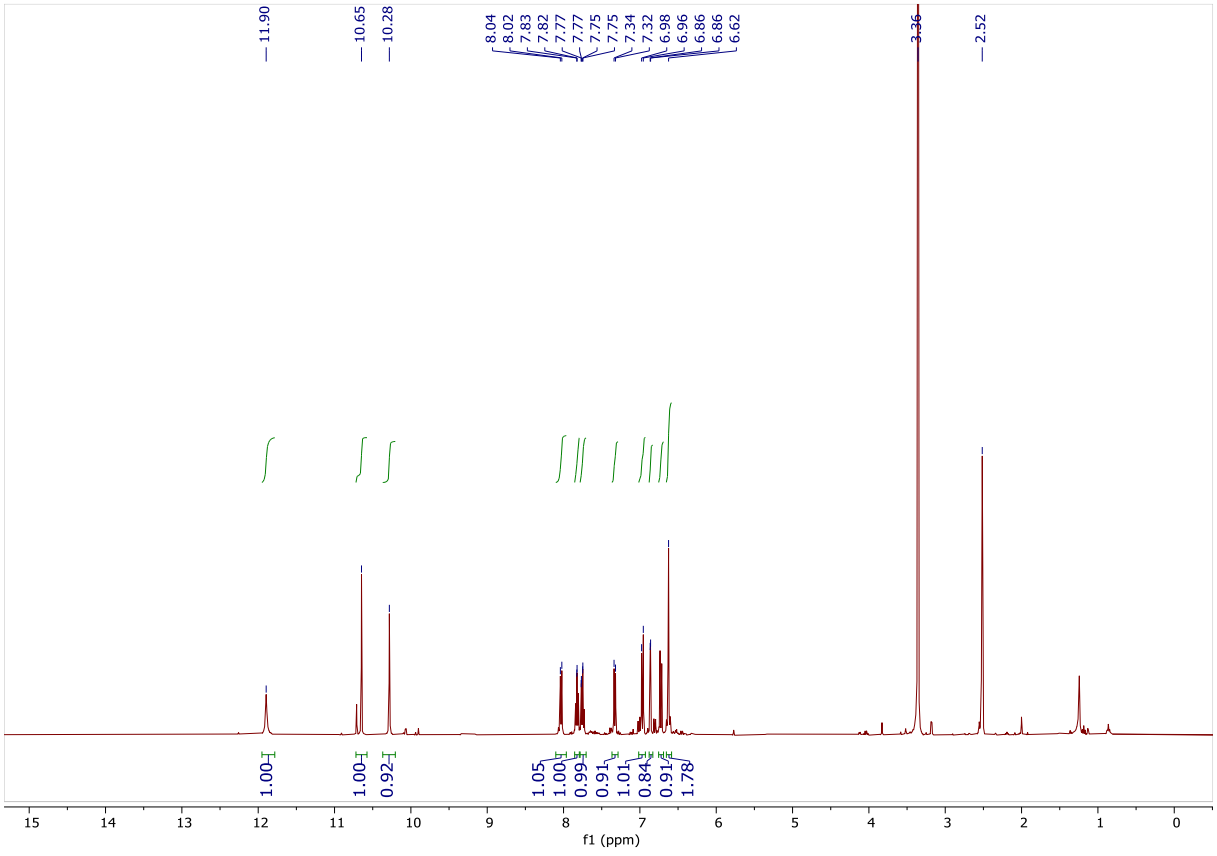

***Figure 66**: ^{1}H- NMR of Fluorescein-monoaldehyde, 400 MHz, DMSO-d_6*

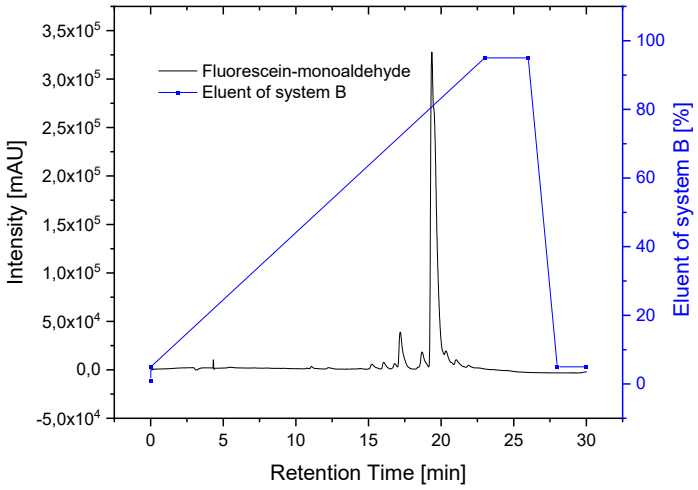

***Figure 67**: Analytical HPLC of Fluorescein-monoaldehyde, Nucleosil C18 (5 µm, 4.6 mm x 25 mm), H_2O with 0.1% TFA (system A) / 80% MeCN-20% H_2O and 0.1 % TFA (system B), 1 mL/min, 0.02 min - 5% eluent of system B, 23 min - 95% eluent of system B, (t_R = 19.4 min)*

8.4 Compound 1

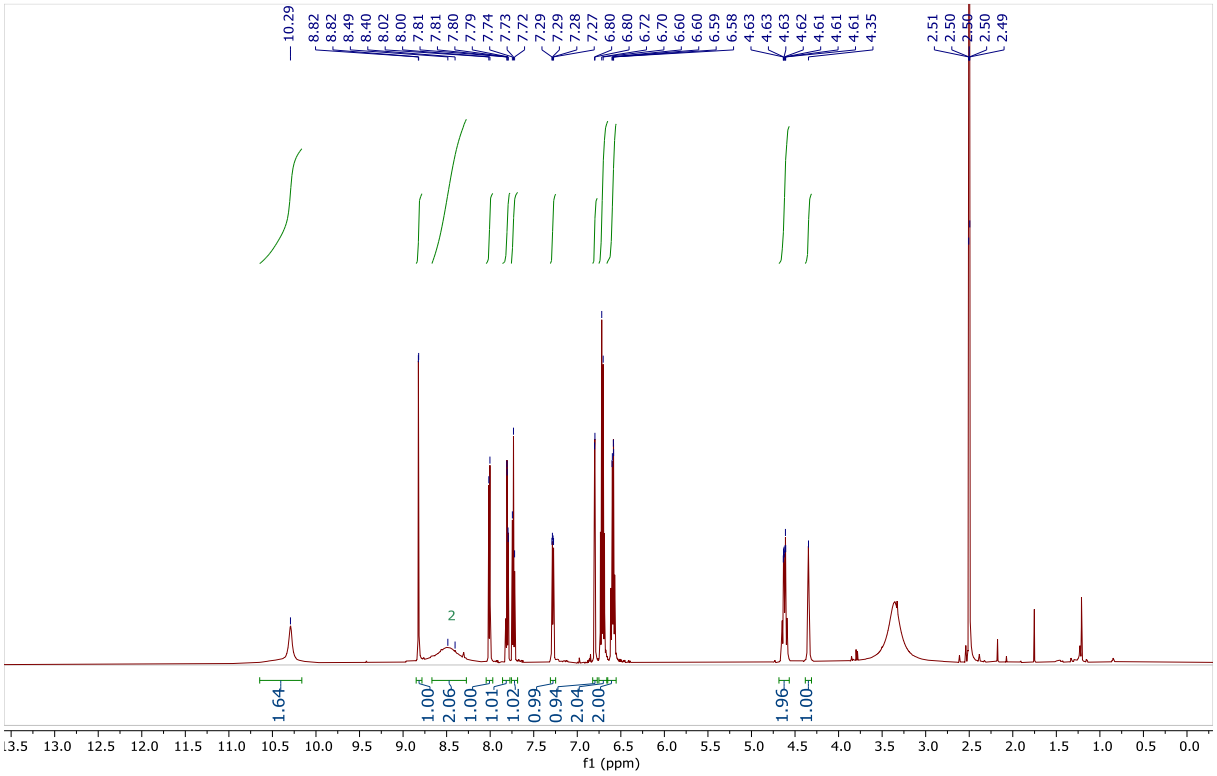

***Figure 68**: ^1H - NMR of 1, 600 MHz, DMSO-d_6*

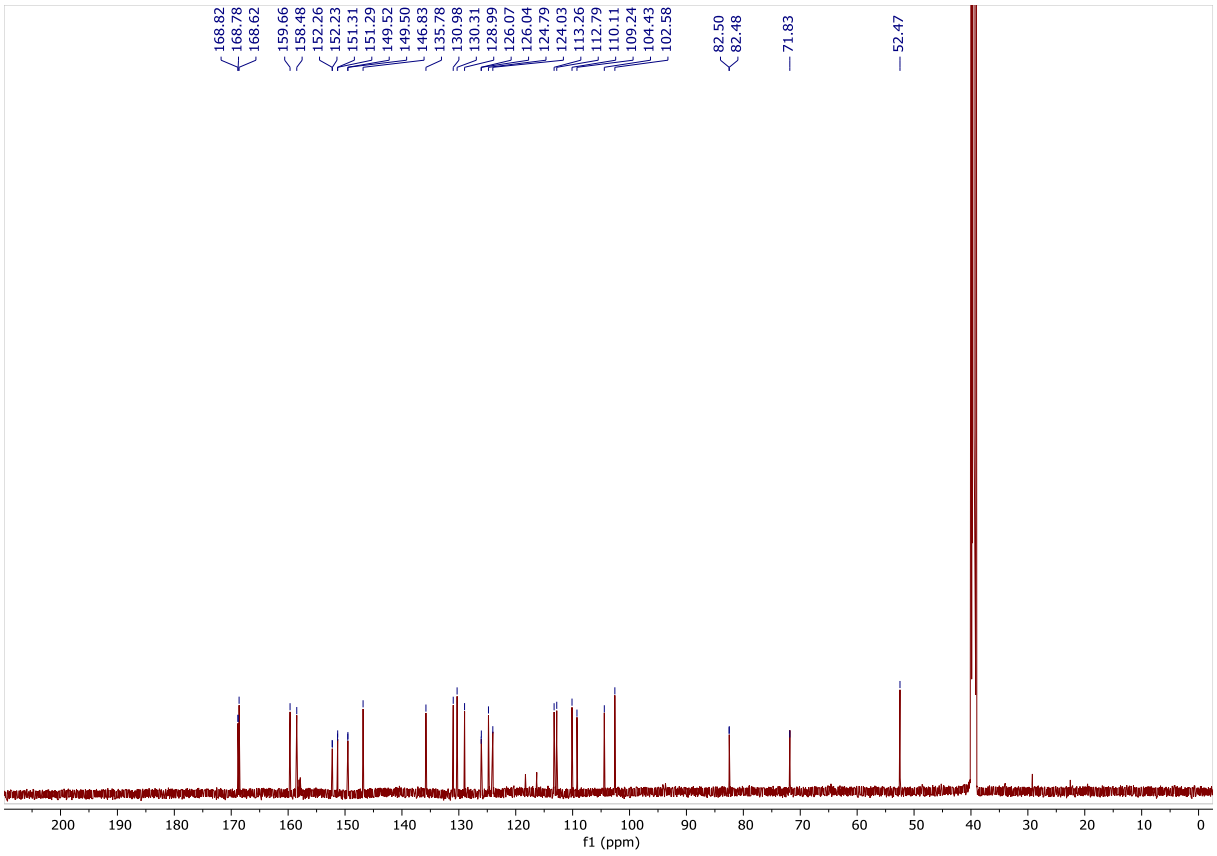

***Figure 69**: ^{13}C NMR of 1, 151 MHz, DMSO-d_6*

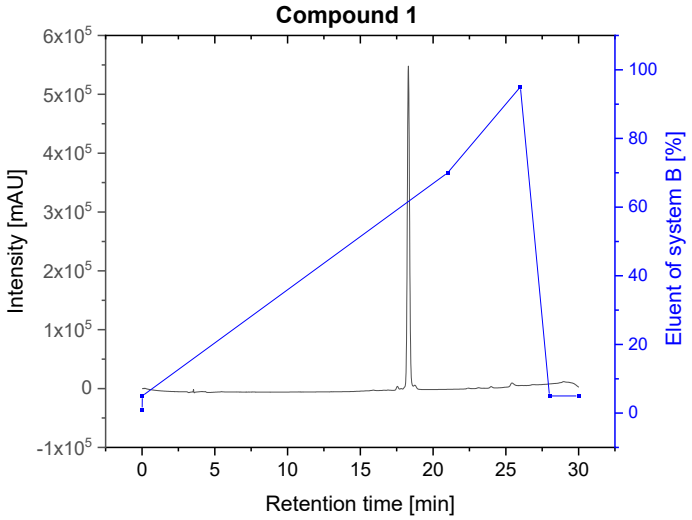

***Figure 70**: Analytical HPLC of 1, Nucleosil C18 (5 µm, 4.6 mm x 25 mm), H_2O with 0.1% TFA (system A) / 80% MeCN-20% H_2O and 0.1 % TFA (system B), 1 mL/min, 0.02 min - 5% eluent of system B, 21 min - 70% eluent of system B, (t_R = 18.2 min)*

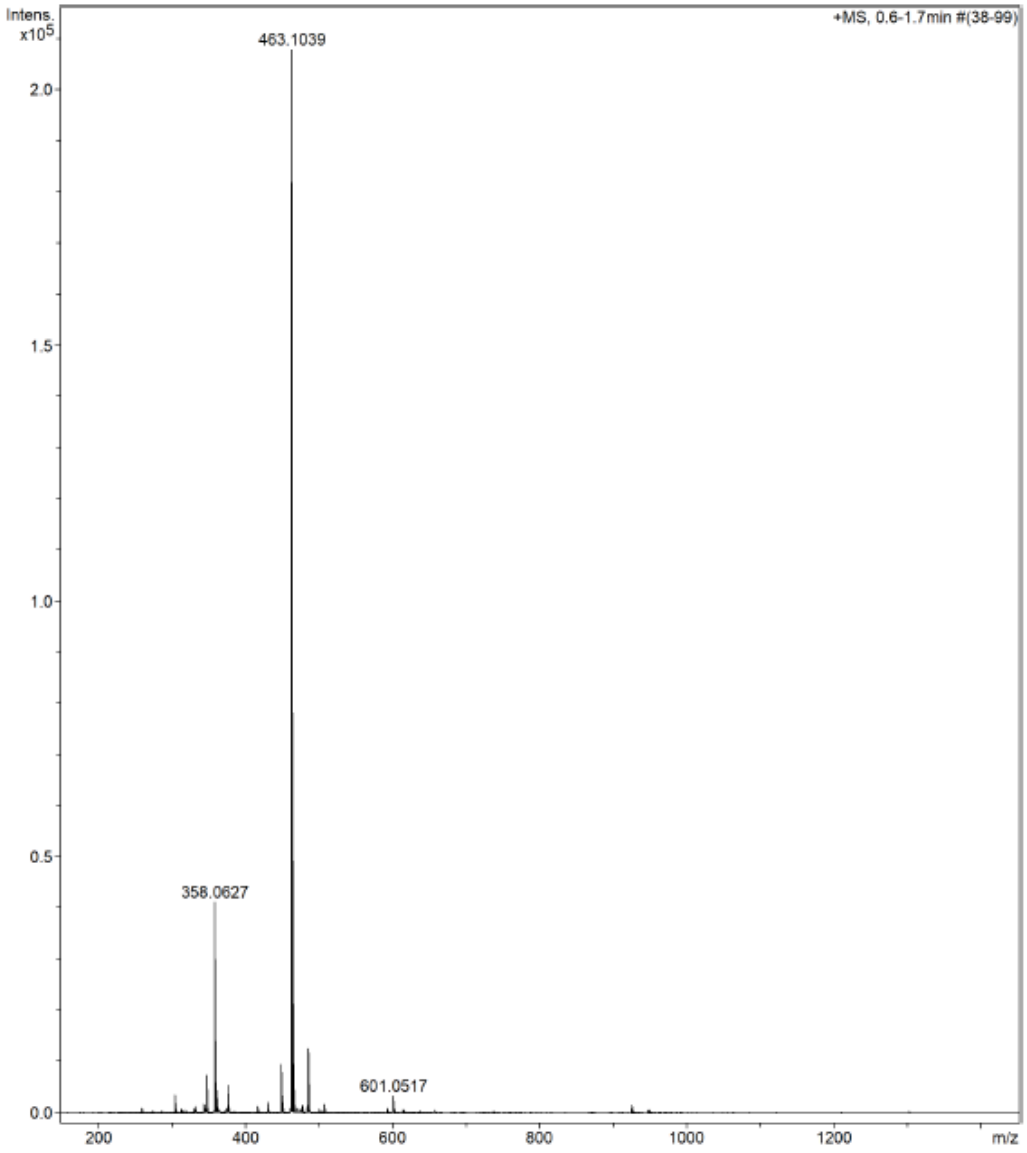

***Figure 71**: ESI-MS of 1, positive mode*

8.5 FP 2

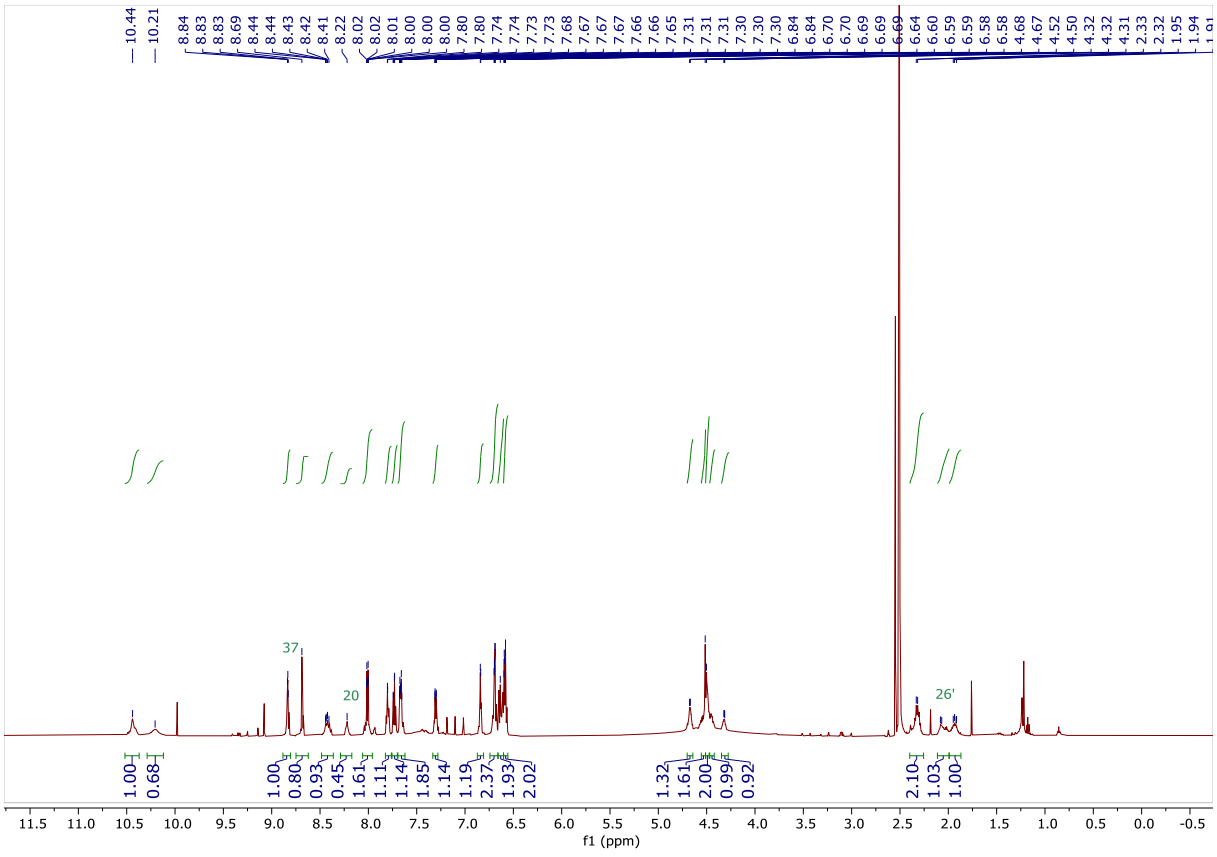

***Figure 72**: [1]H NMR of FP 2, 600 MHz, in DMSO-d_6*

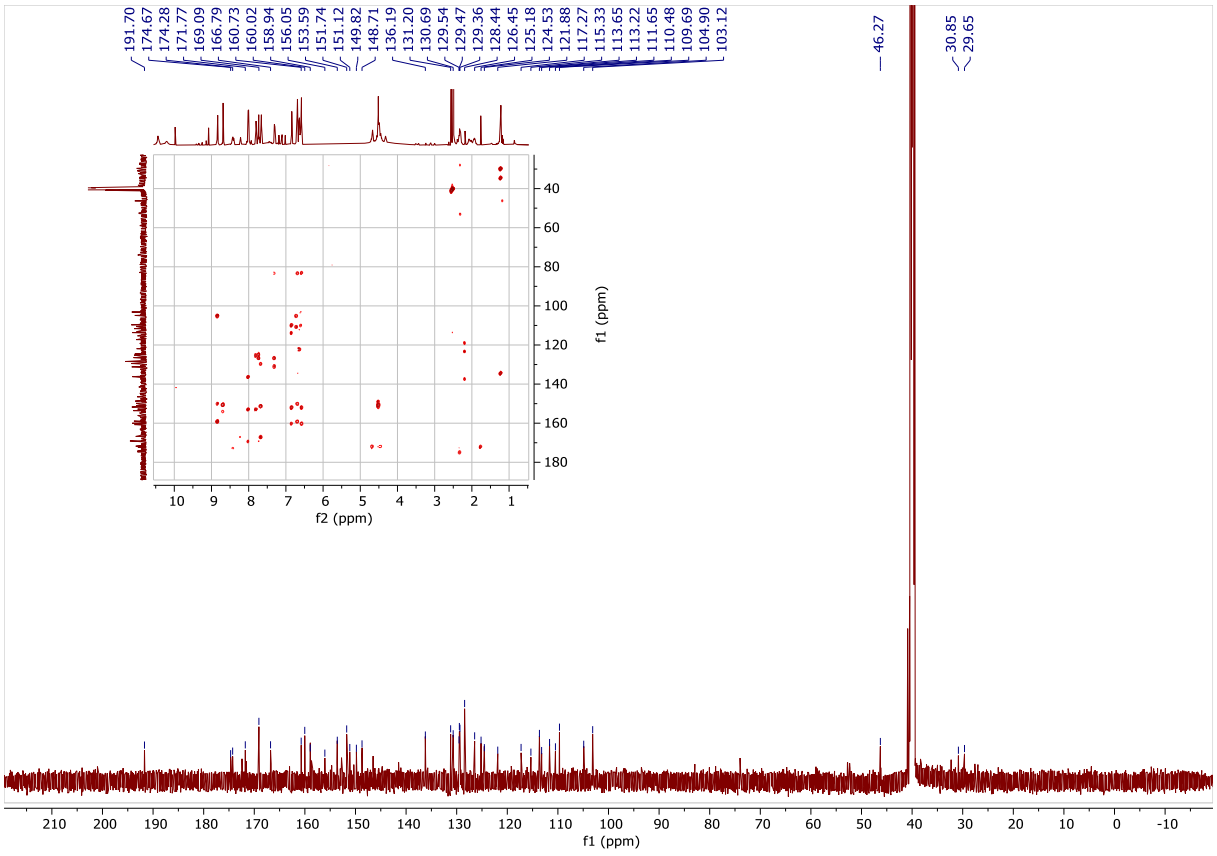

***Figure 73**: ^{13}C-NMR of FP 2, 151MHz, DMSO-d_6, with a 2D HMBC spectrum inset showing proton-carbon correlations.*

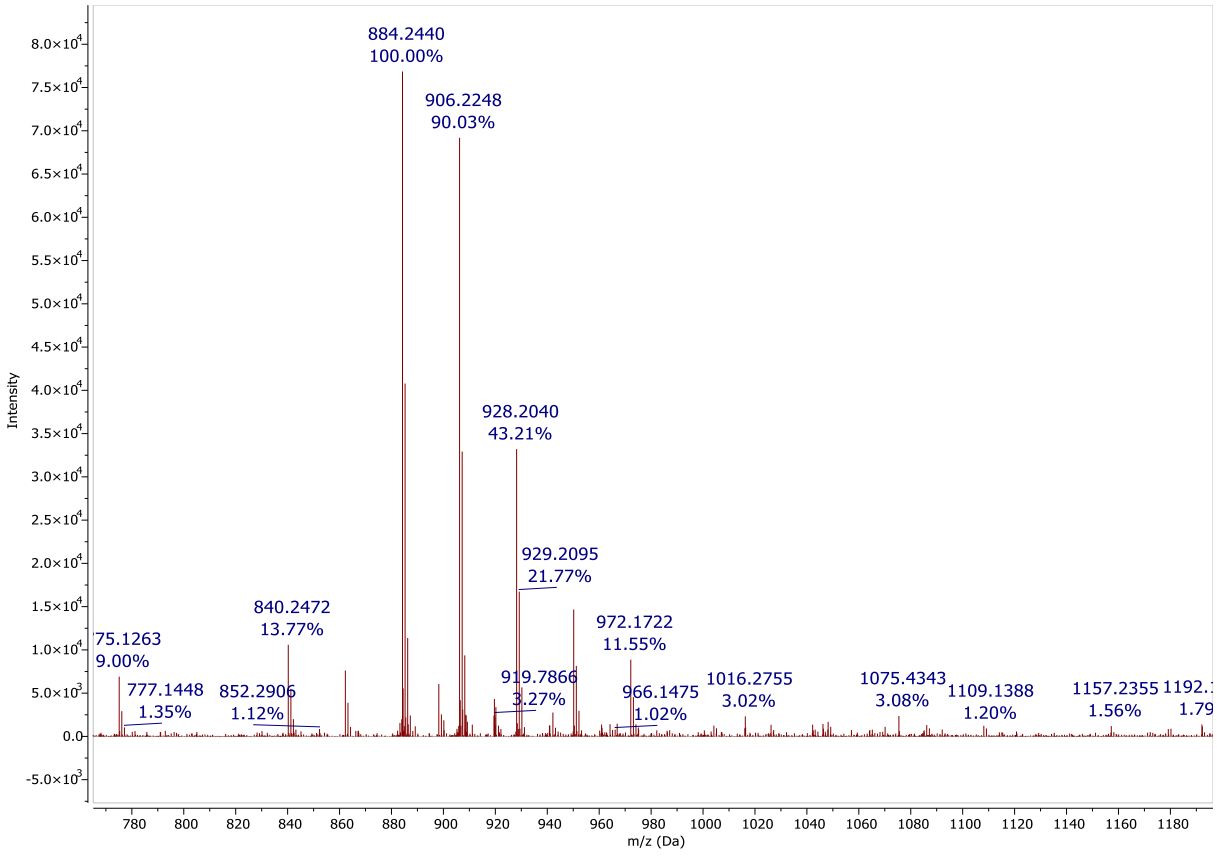

***Figure 74**: ESI MS of FP 2, negative mode*

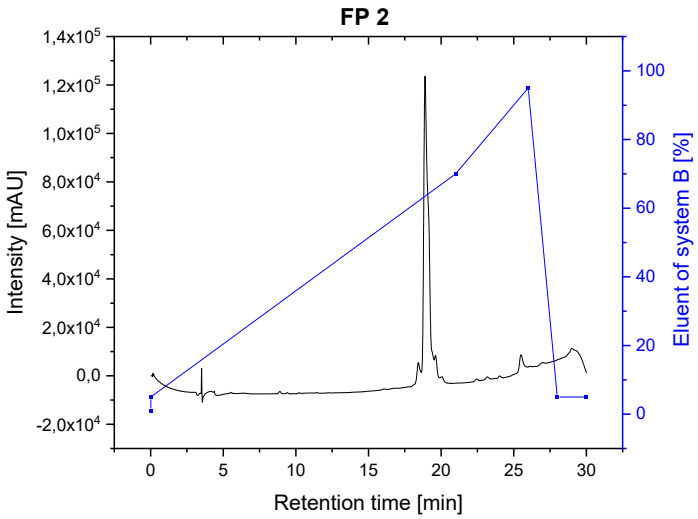

***Figure 75**: Analytical HPLC of FP 2, Nucleosil C18 (5 µm, 4.6 mm x 25 mm), H_2O with 0.1% TFA (system A) / 80% MeCN-20% H_2O and 0.1 % TFA (system B), 1 mL/min, 0.02 min - 5% eluent of system B, 21 min - 70% eluent of system B, (t_R = 18.6 min)*

8.6 Compound 3*

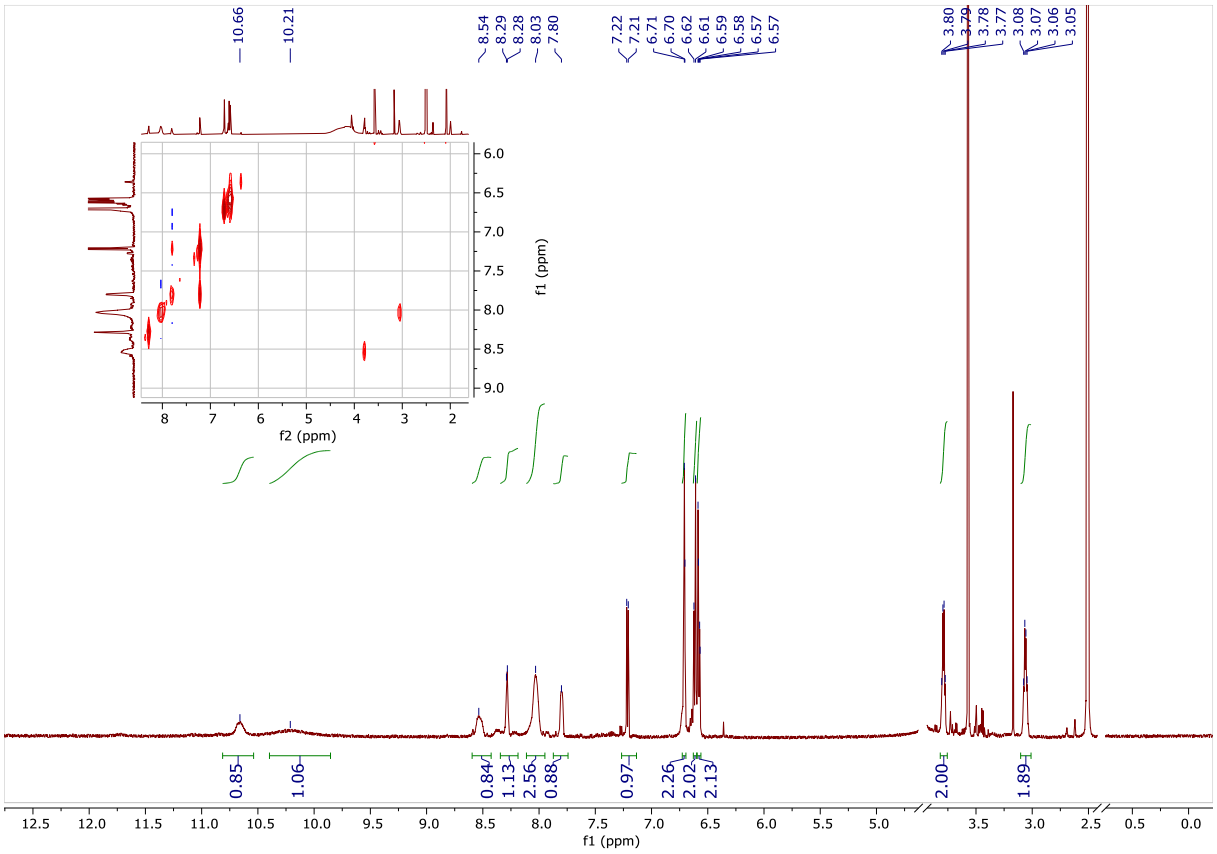

***Figure 76**: [1]H-NMRspectrum of 3, 600 MHz in DMSO-d_6. The inset highlights the coupling interactions between the amine hydrogens of ethylenediamine and the methylene hydrogens of the ethylene group.*

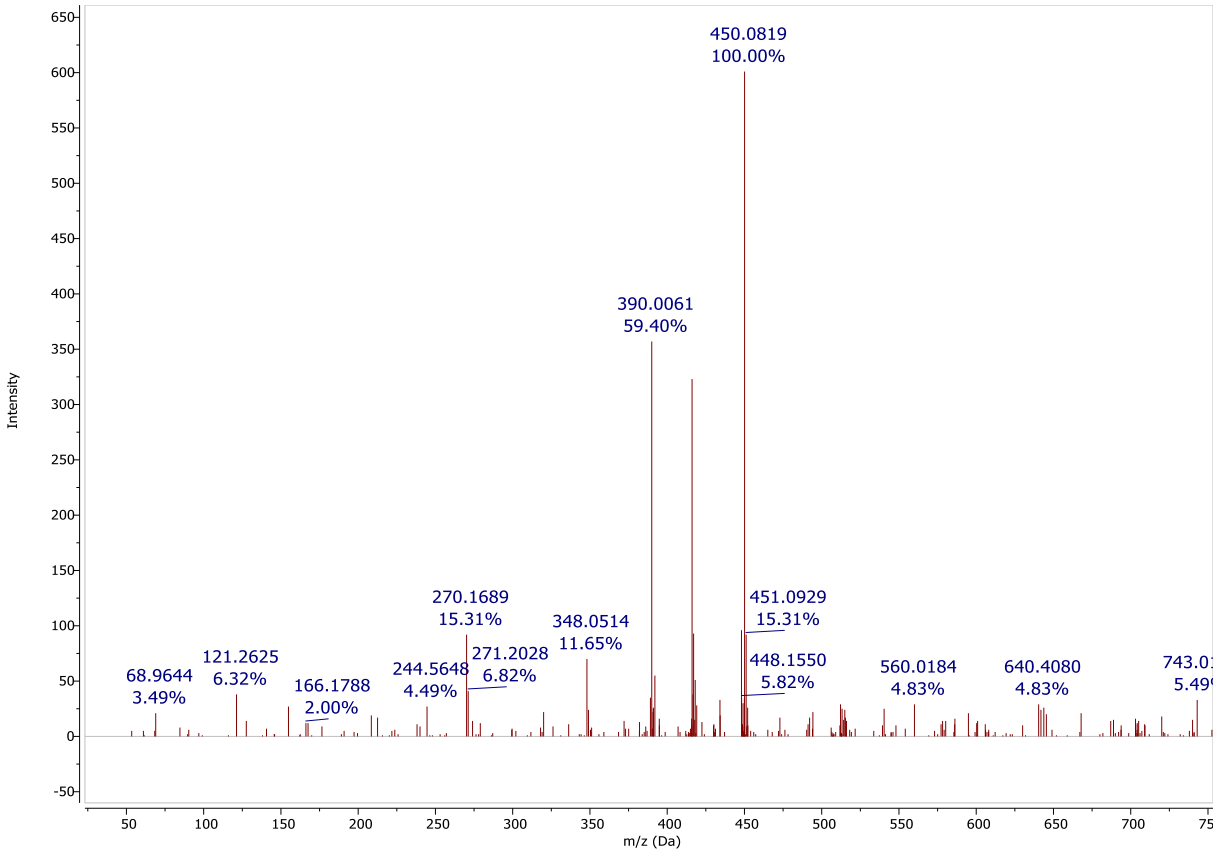

***Figure 77**: ESI MS of 3, positive mode*

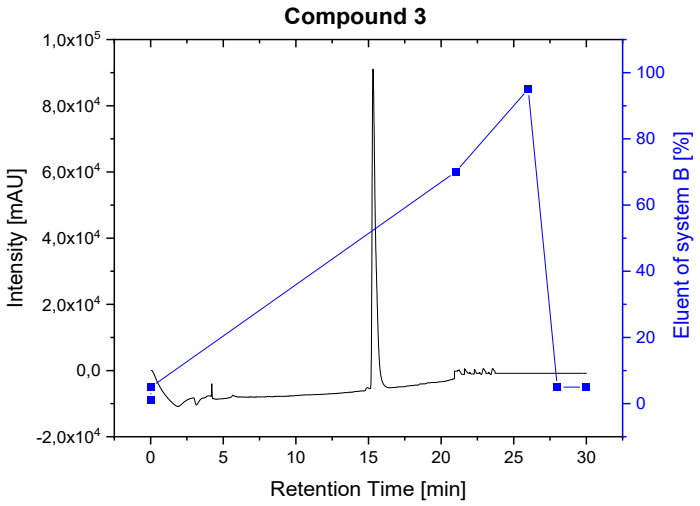

***Figure 78**: Analytic HPLC of 3, Nucleosil C18 (5 µm, 4.6 mm x 25 mm), H_2O with 0.1% TFA (system A) / 80% MeCN-20% H_2O and 0.1 % TFA (system B), 1 mL/min, 0.02 min - 5% eluent of system B, 21 min - 70% eluent of system B, t_R = 15.2 min*

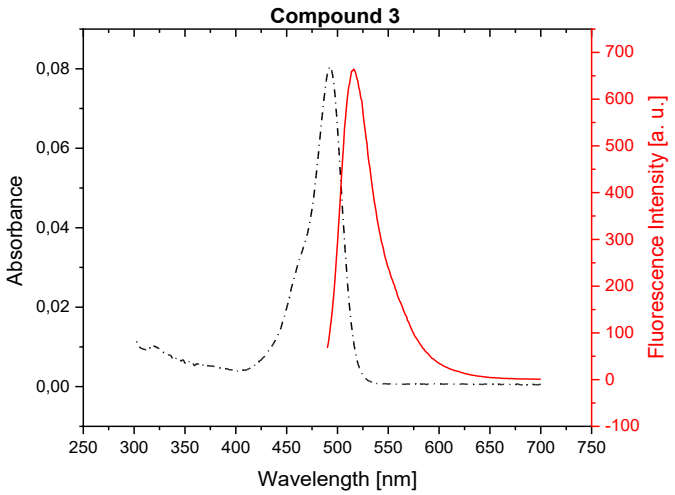

***Figure 79**: Absorbance and emission spectra of 1 µM of 3 in PBS (pH = 7.4) using 1 mL PMMA cuvettes. Dashed lines represent absorbance spectra, while solid lines correspond to emission spectra.*

9.7 Fluorescein-Oxime ether derivatives

9.7.1 Compound 4

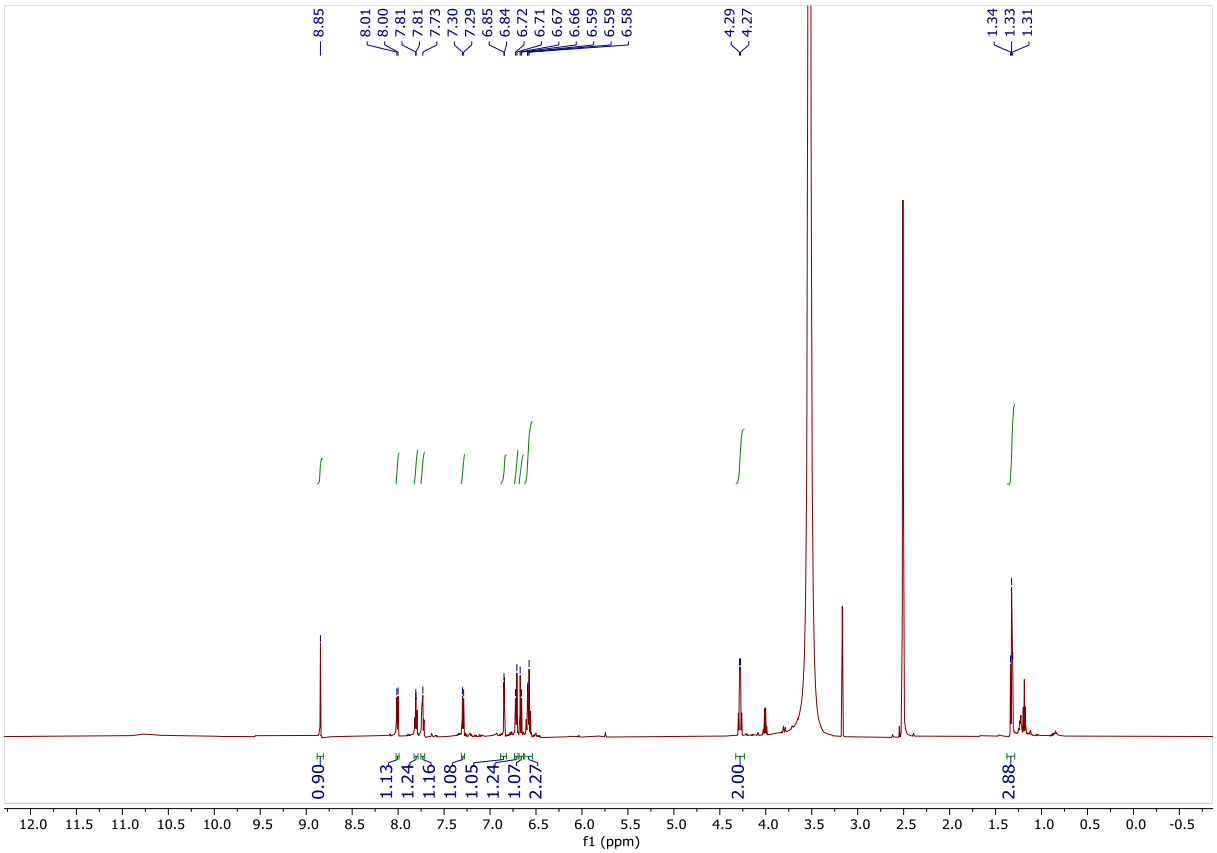

***Figure 80**: ^{1}H NMR of 4, 600 MHz, DMSO-d_6*

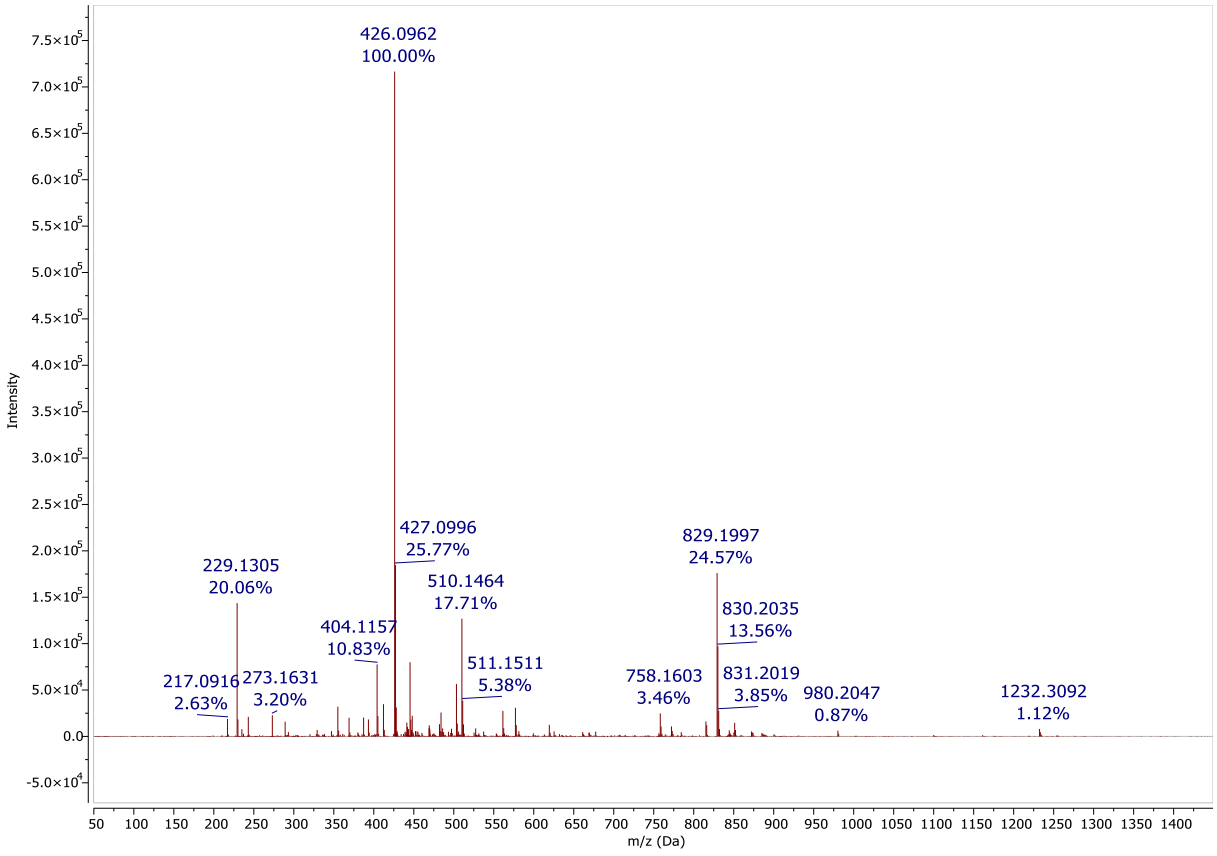

***Figure 81**: ESI MS of 4, positive mode*

9.7.2 Compound 5

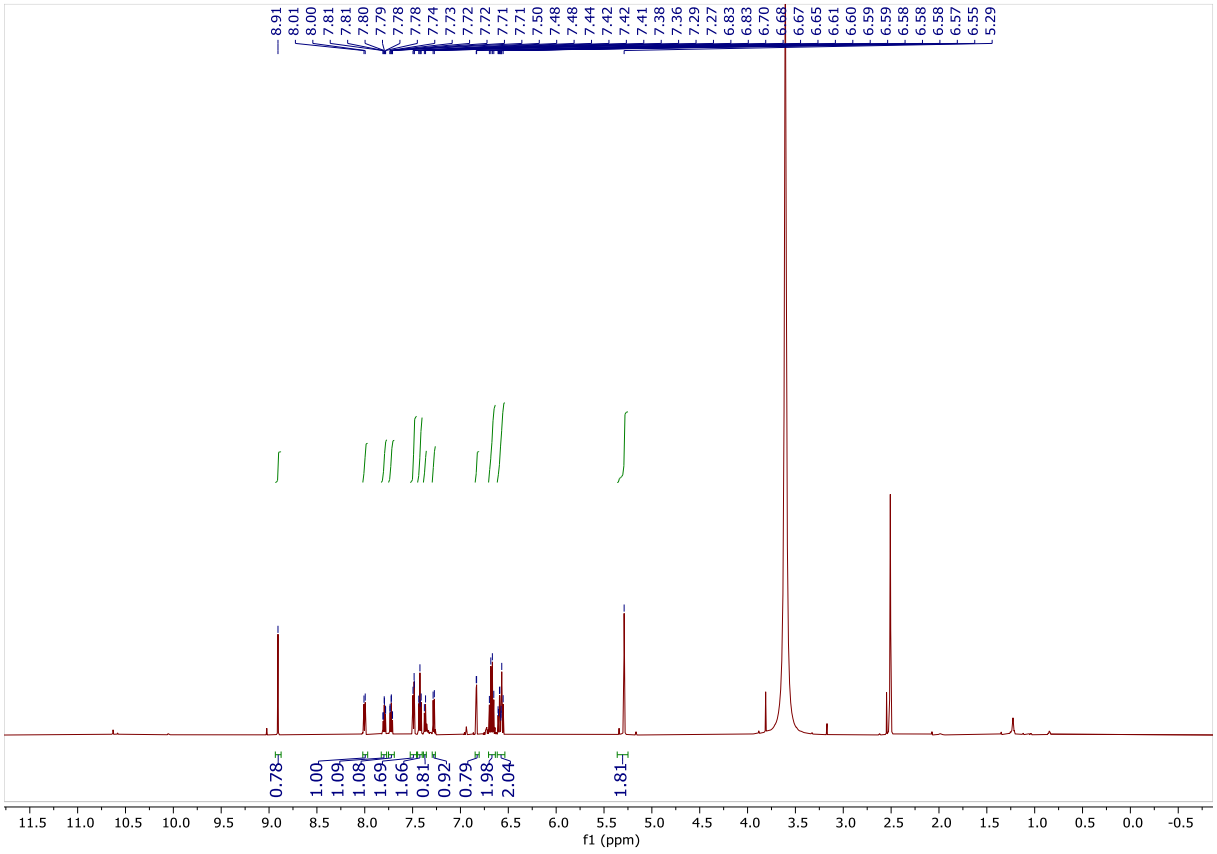

***Figure 82**: ^{1}H NMR of 5, 600 MHz, DMSO-d_6*

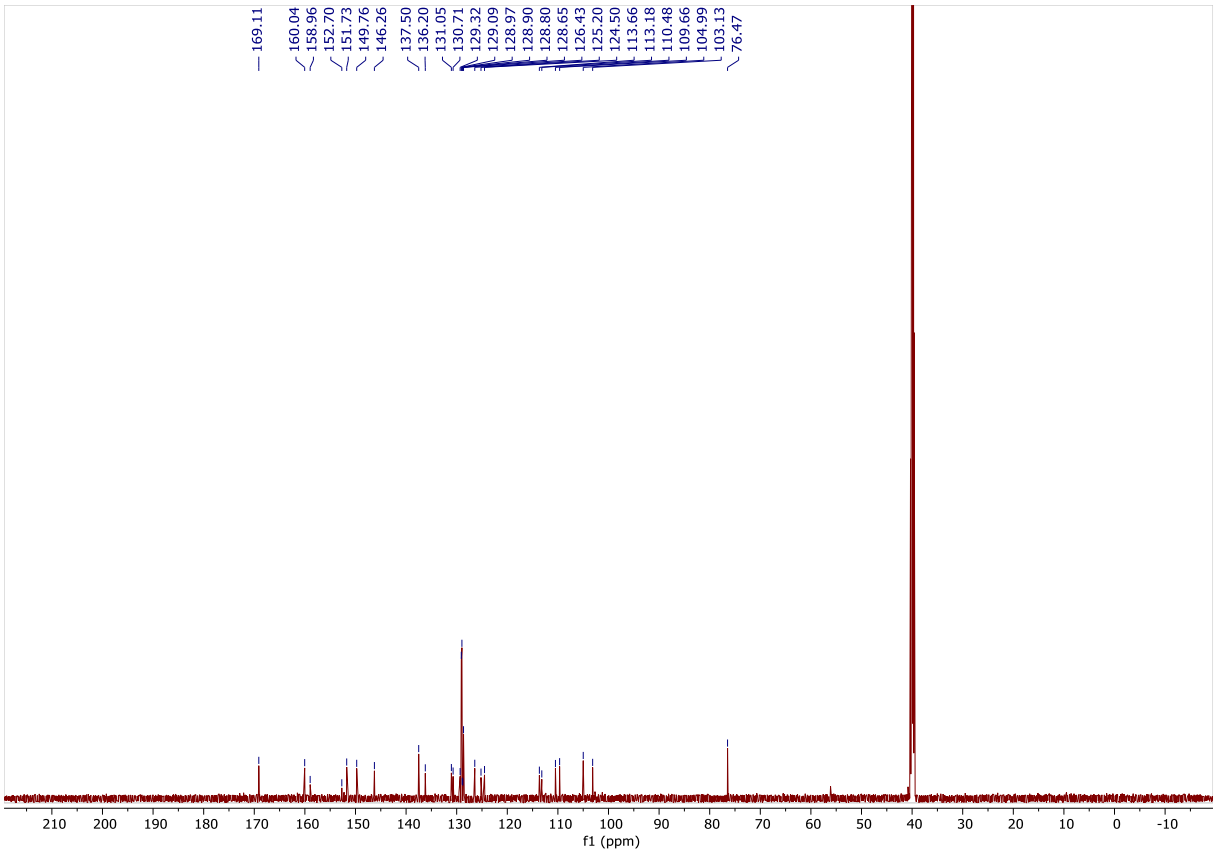

***Figure 83**: ^{13}C NMR of 5, 151 MHz, DMSO-d_6*

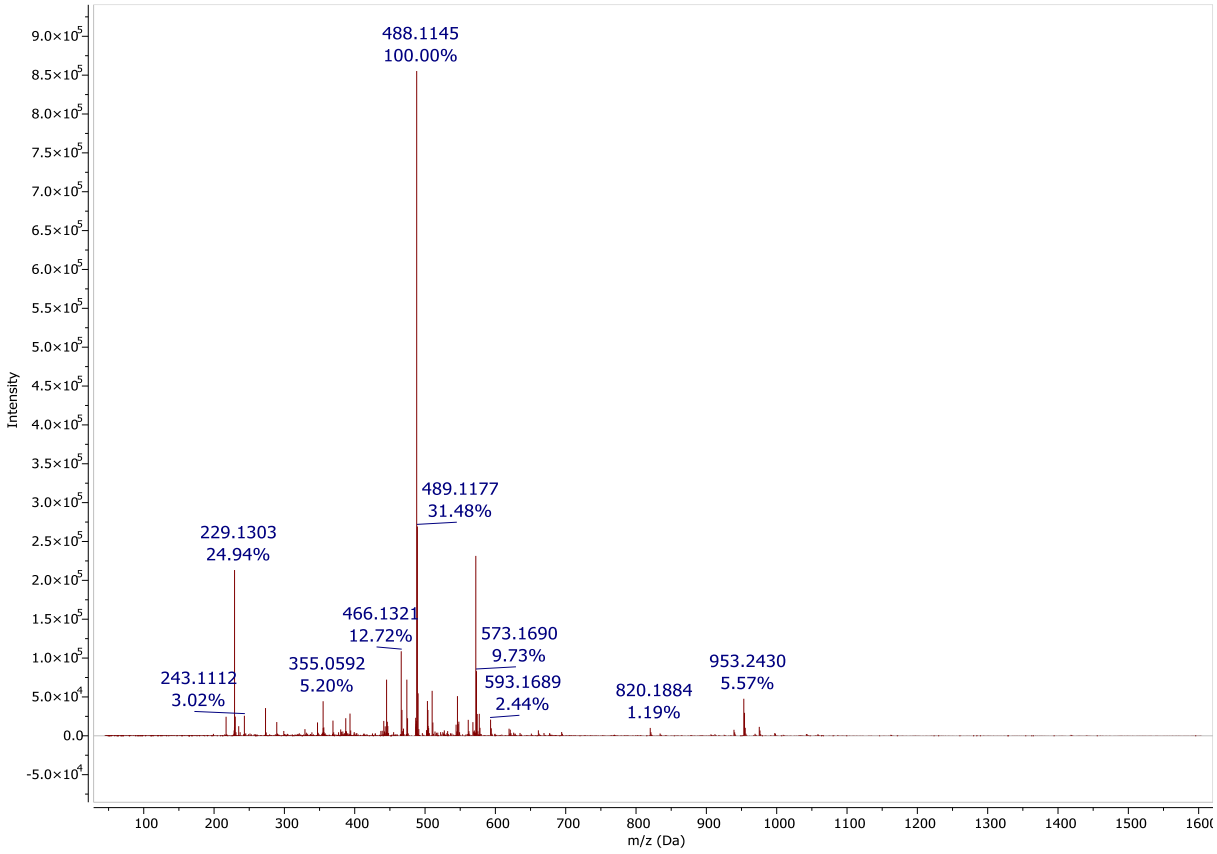

***Figure 84**: ESI MS of 5, positive mode*

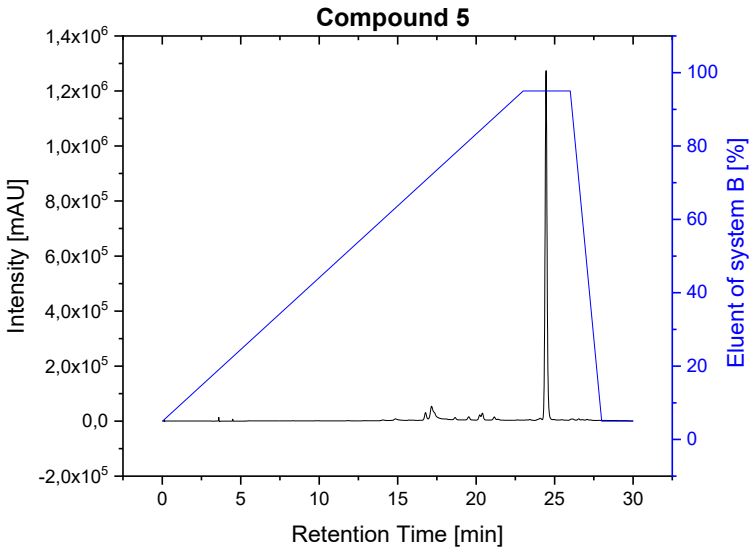

***Figure 85**: Analytical HPLC of 5, Nucleosil C18 (5 µm, 4.6 mm x 25 mm), H_2O with 0.1% TFA (system A) / 80% MeCN-20% H_2O and 0.1 % TFA (system B), 1 mL/min, 0.02 min - 5% eluent of system B, 23 min - 95% eluent of system B, (t_R = 24.4 min)*

9.7.3 Compound 6

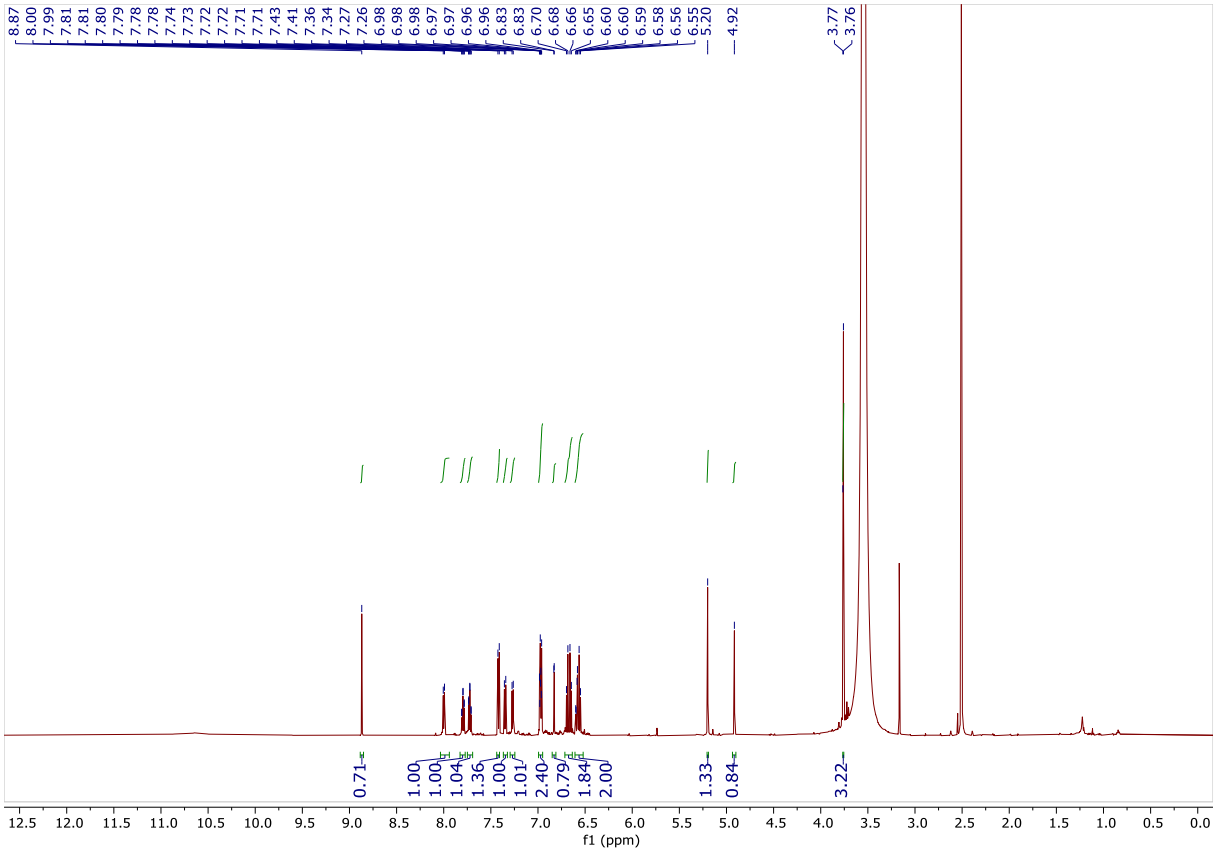

***Figure 86**: ^1H NMR of 6, 600 MHz, DMSO-d_6*

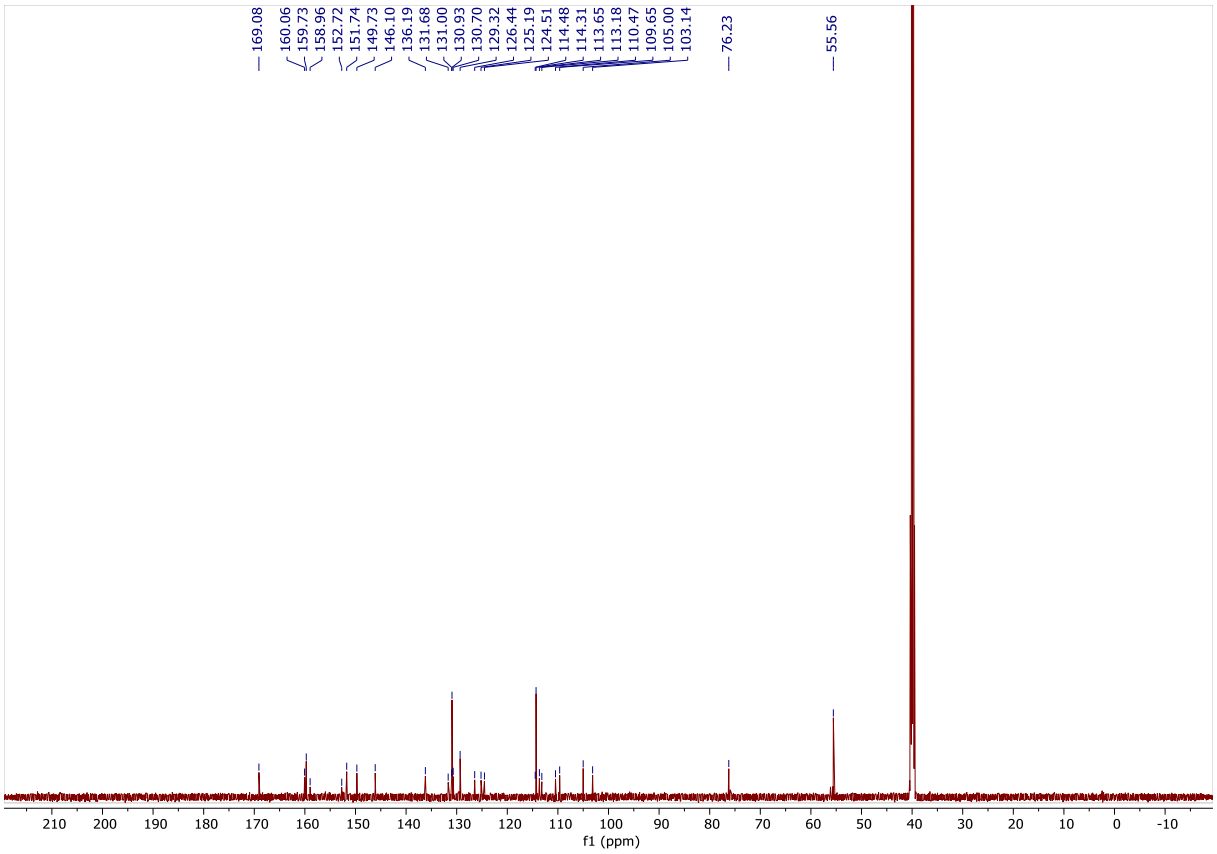

***Figure 87**: [13]C NMR of 6, 151 MHz, DMSO-d_6*

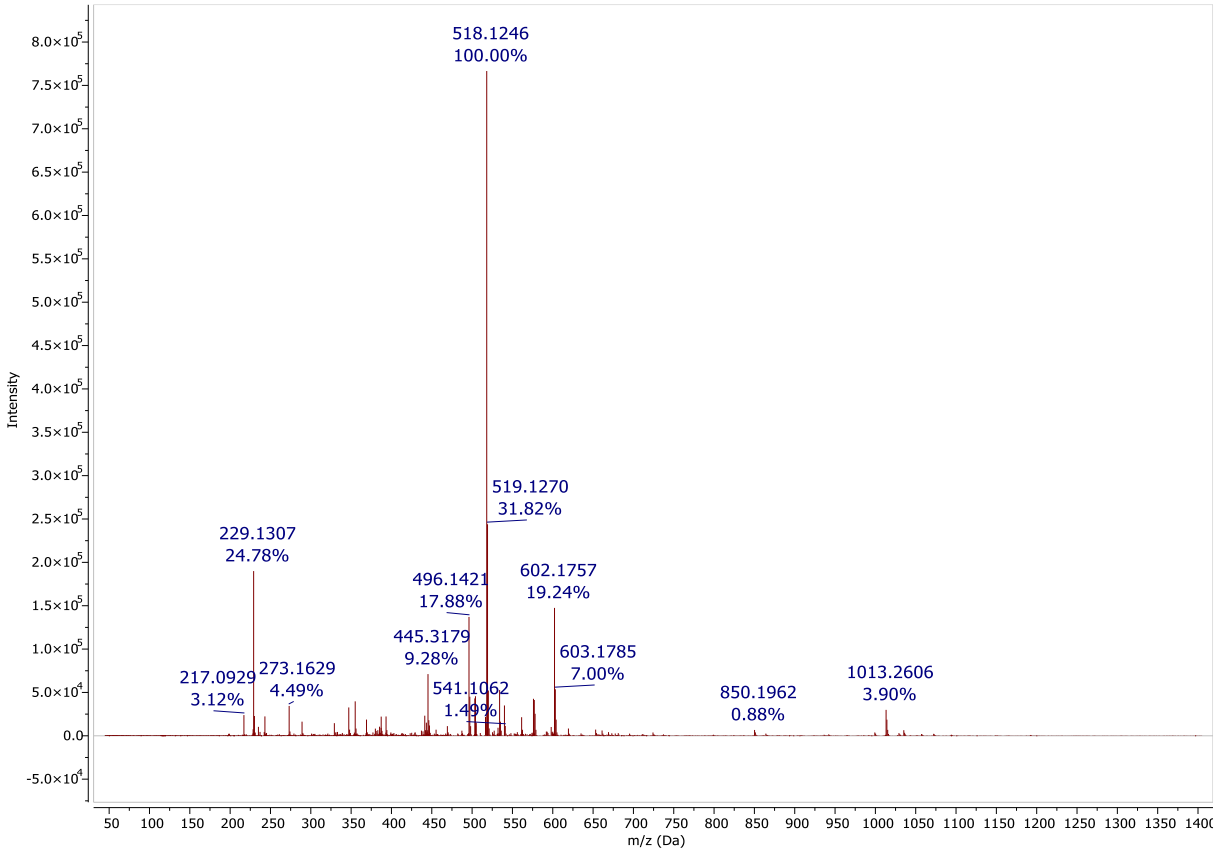

***Figure 88**: ESI MS of 6, positive mode*

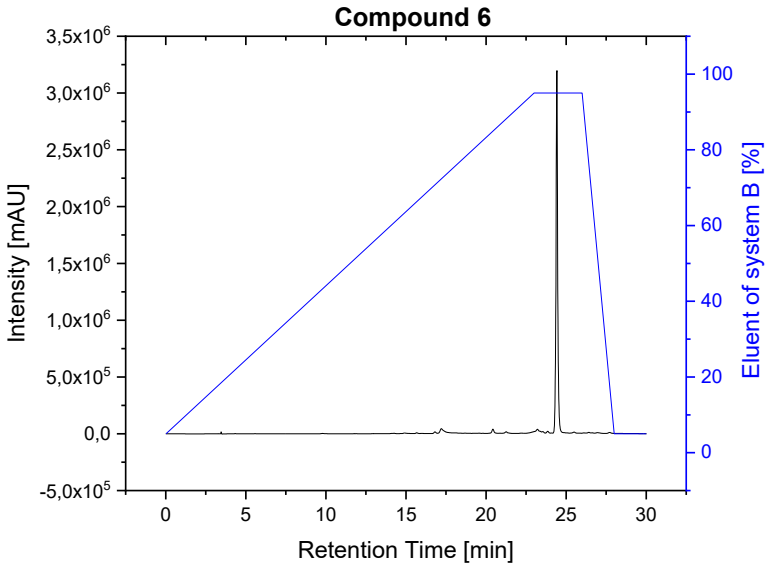

***Figure 89**: Analytical HPLC of 6, Nucleosil C18 (5 µm, 4.6 mm x 25 mm), H_2O with 0.1% TFA (system A) / 80% MeCN-20% H_2O and 0.1 % TFA (system B), 1 mL/min, 0.02 min - 5% eluent of system B, 23 min - 95% eluent of system B, (t_R = 24.3 min)*

9.7.4 Compound 7

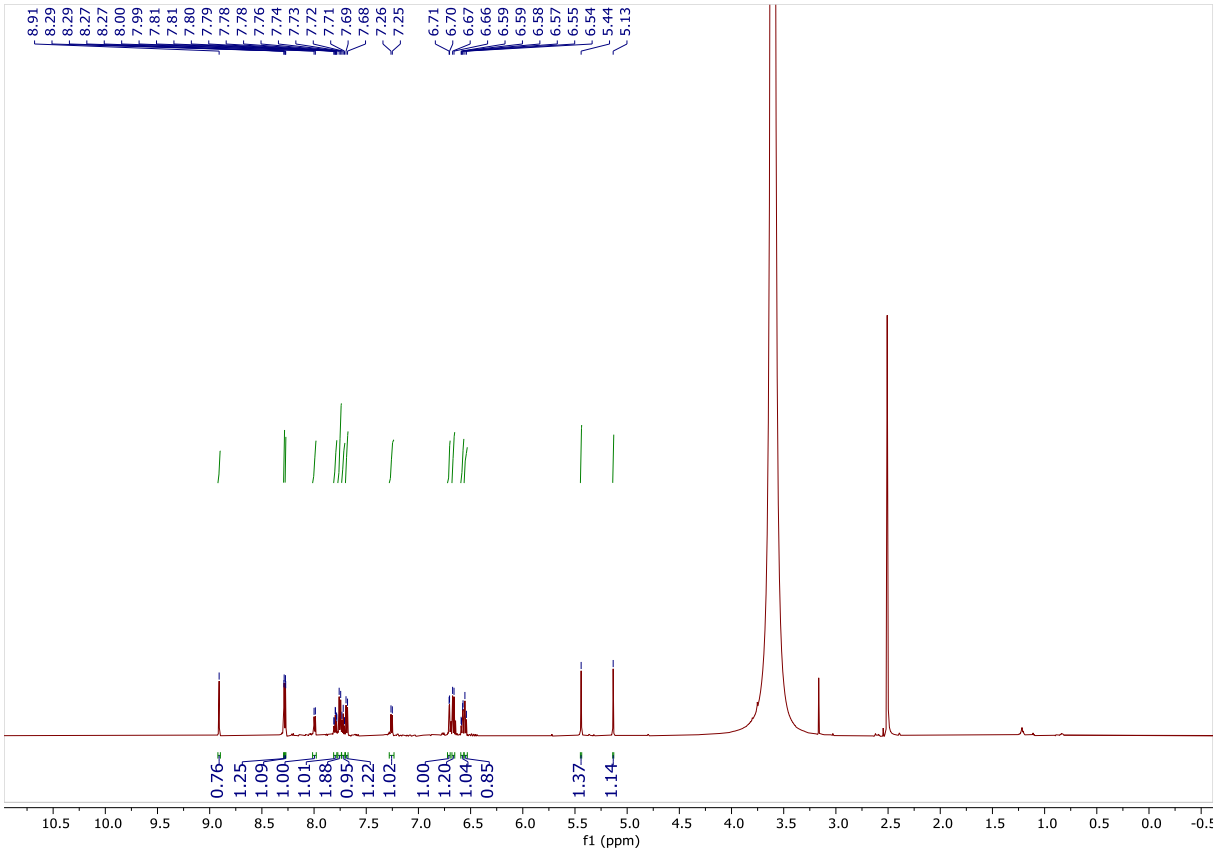

***Figure 90**: ^1H NMR of 7, 600 MHz, DMSO-d_6*

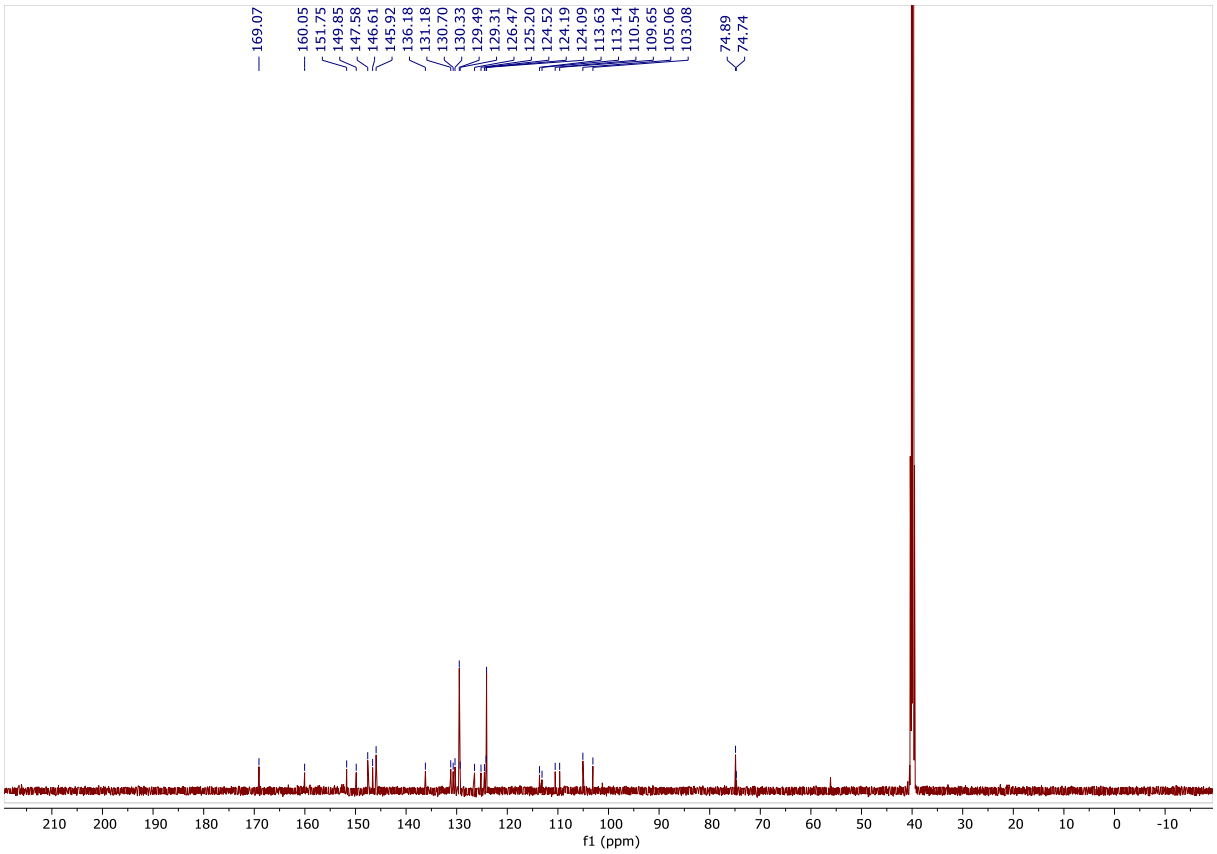

***Figure 91**: [13]C NMR of 7, 151 MHz, DMSO-d_6*

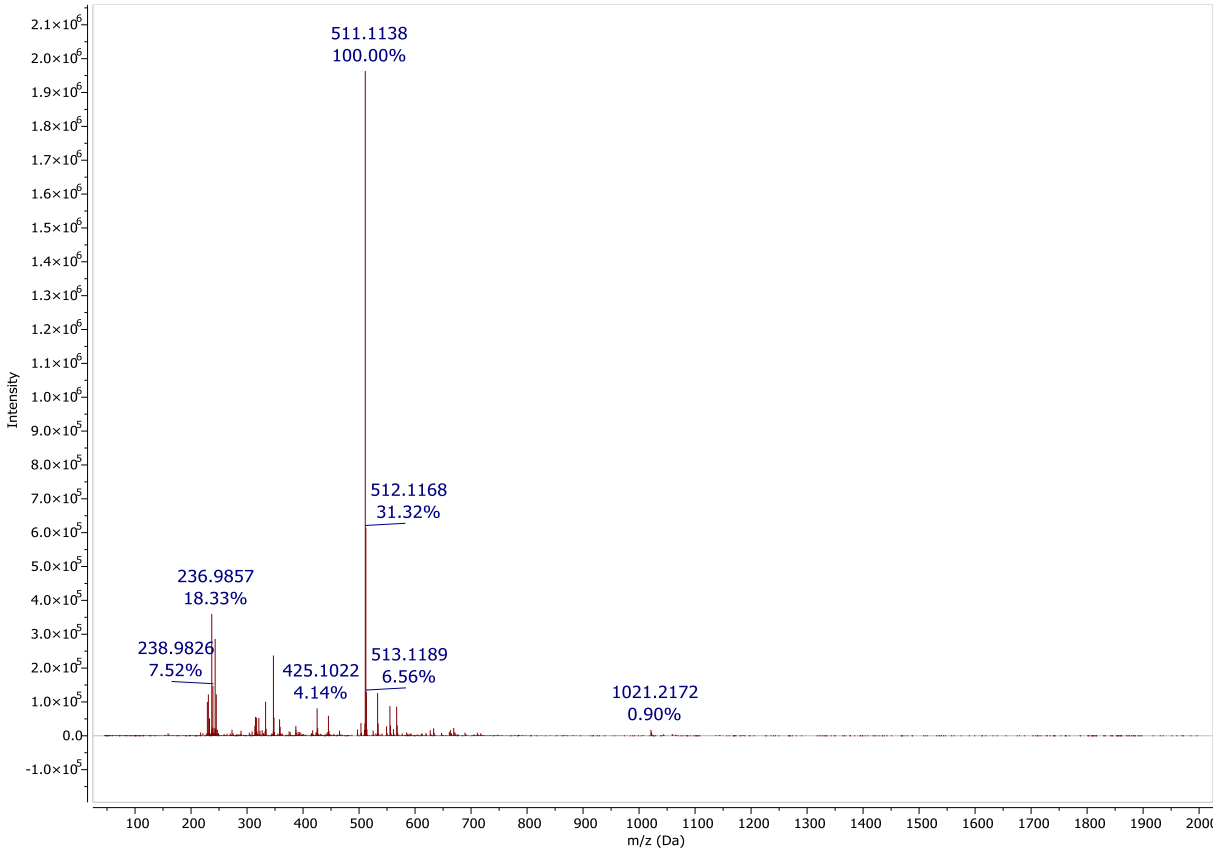

***Figure 92**: ESI MS of 7, positive mode*

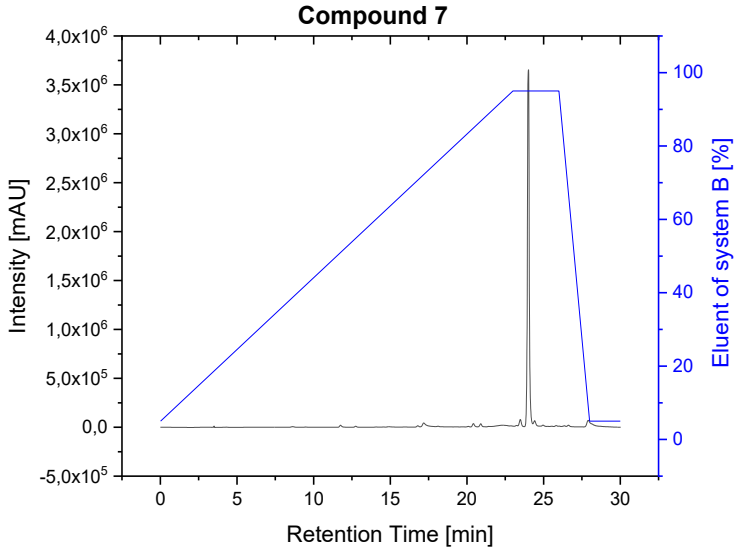

***Figure 93**: Analytical HPLC of 7, Nucleosil C18 (5 µm, 4.6 mm x 25 mm), H_2O with 0.1% TFA (system A) / 80% MeCN-20% H_2O and 0.1 % TFA (system B), 1 mL/min, 0.02 min - 5% eluent of system B, 23 min - 95% eluent of system B, (t_R = 23.9 min)*

9.7.5 Compound 8

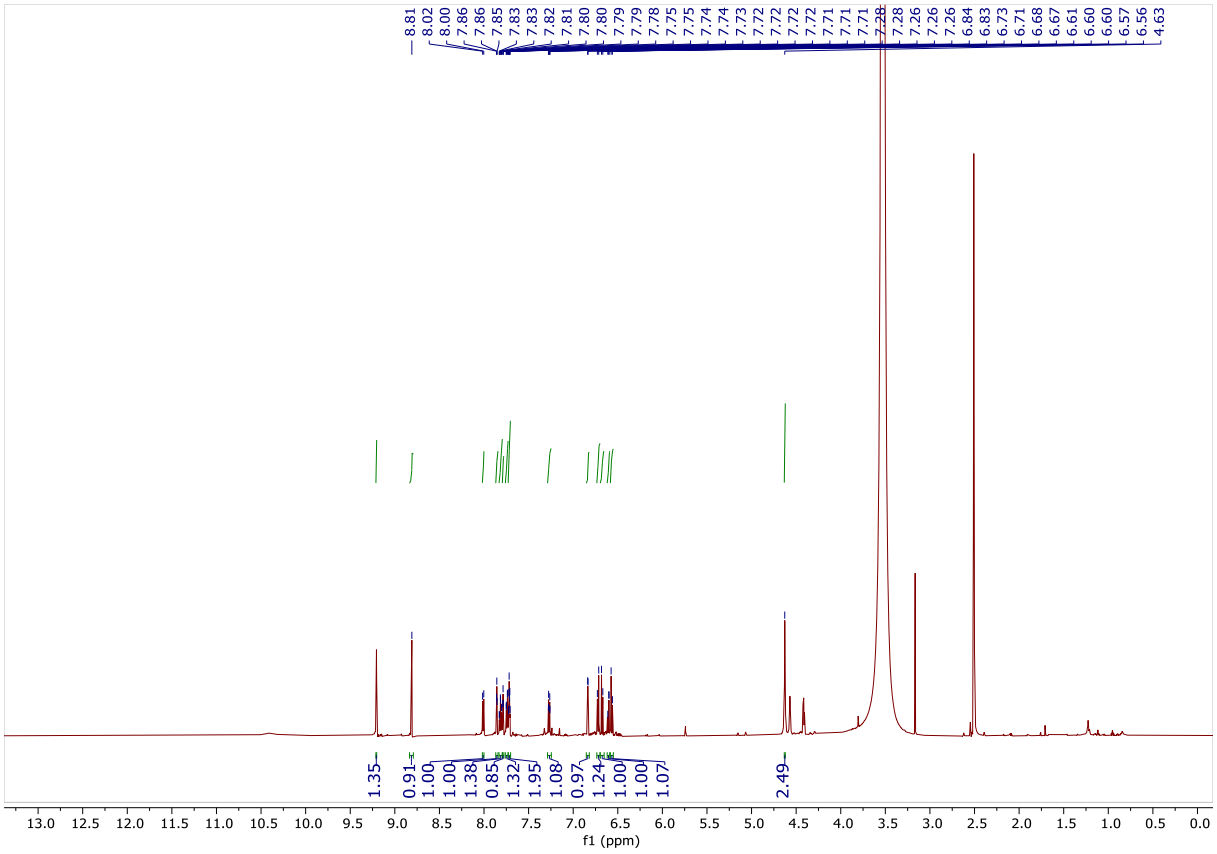

***Figure 94**: ^1H NMR of 8, 600 MHz, DMSO-d_6*

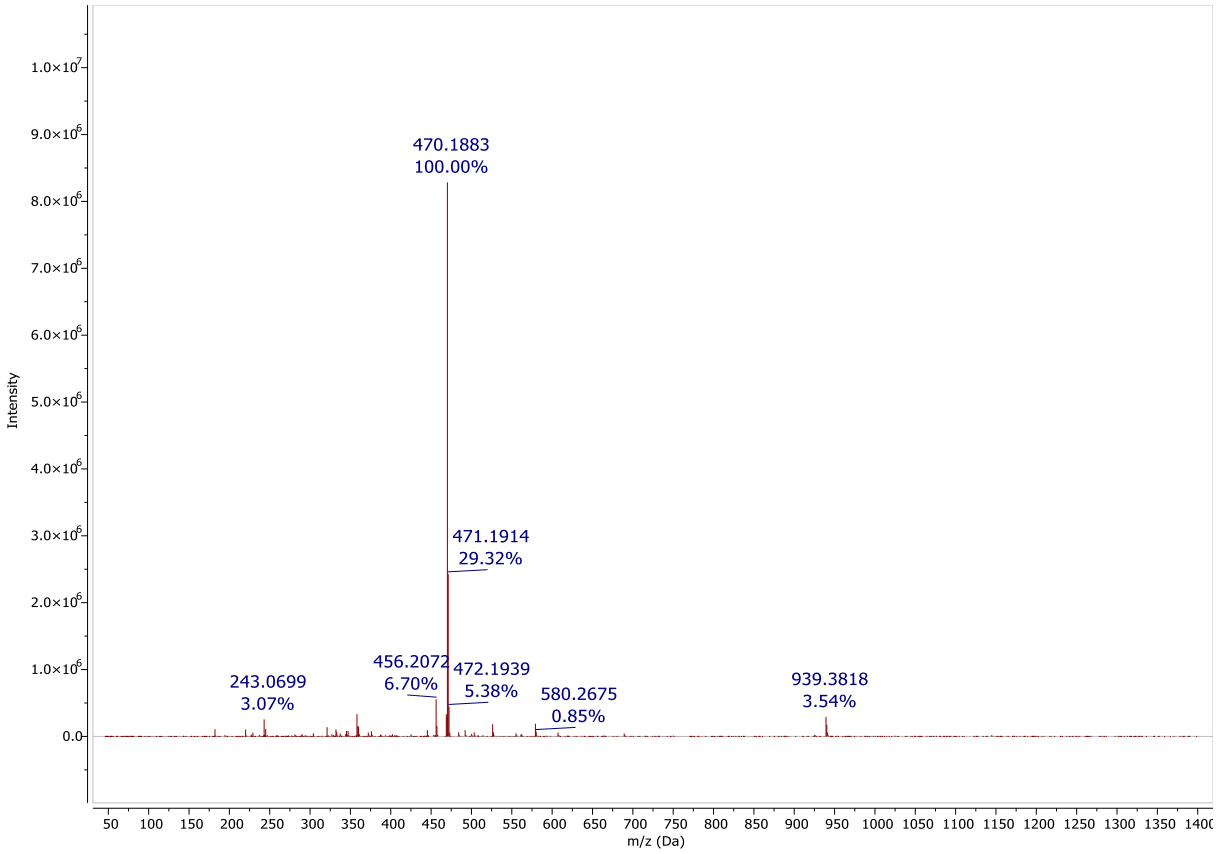

***Figure 95**: ESI MS of 8, positive mode*

9.8 Compound 9

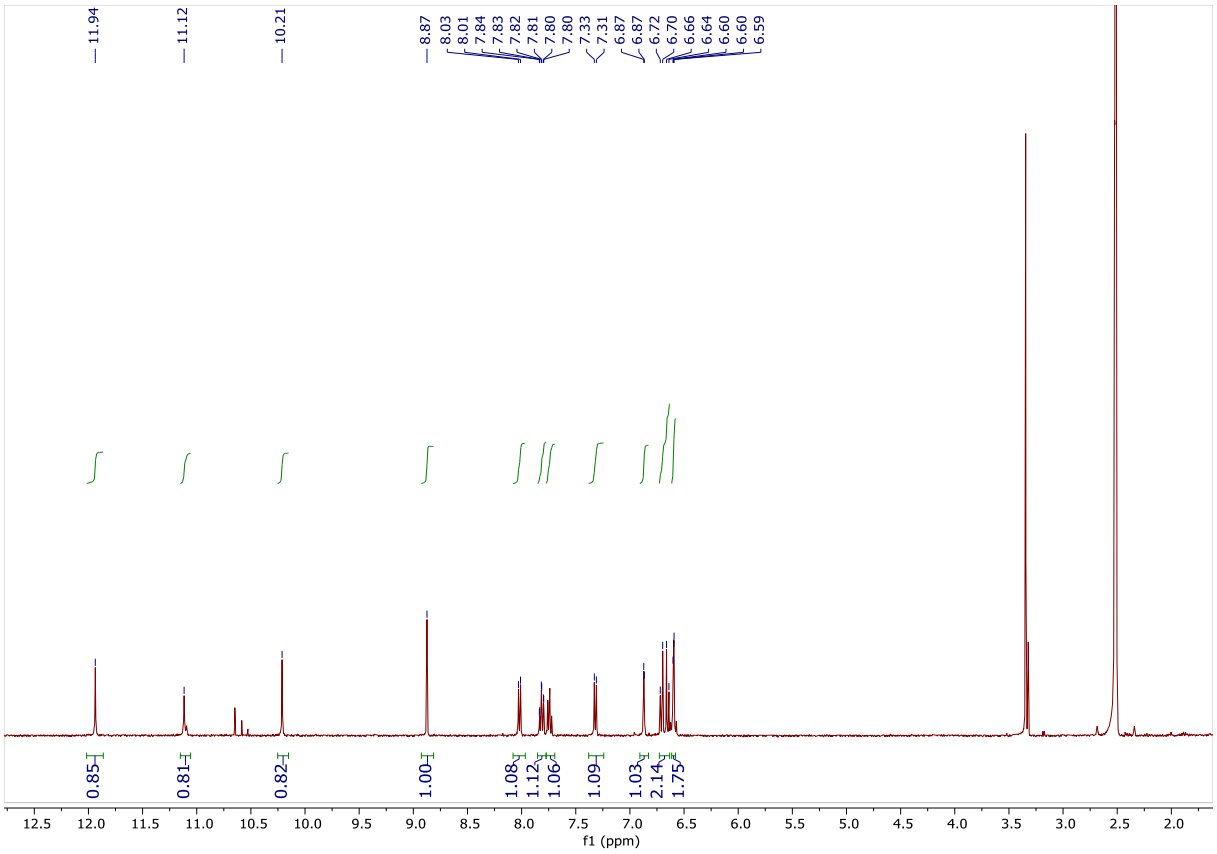

***Figure 96**: [1]H- NMR of 9, 400 MHz, DMSO-d_6*

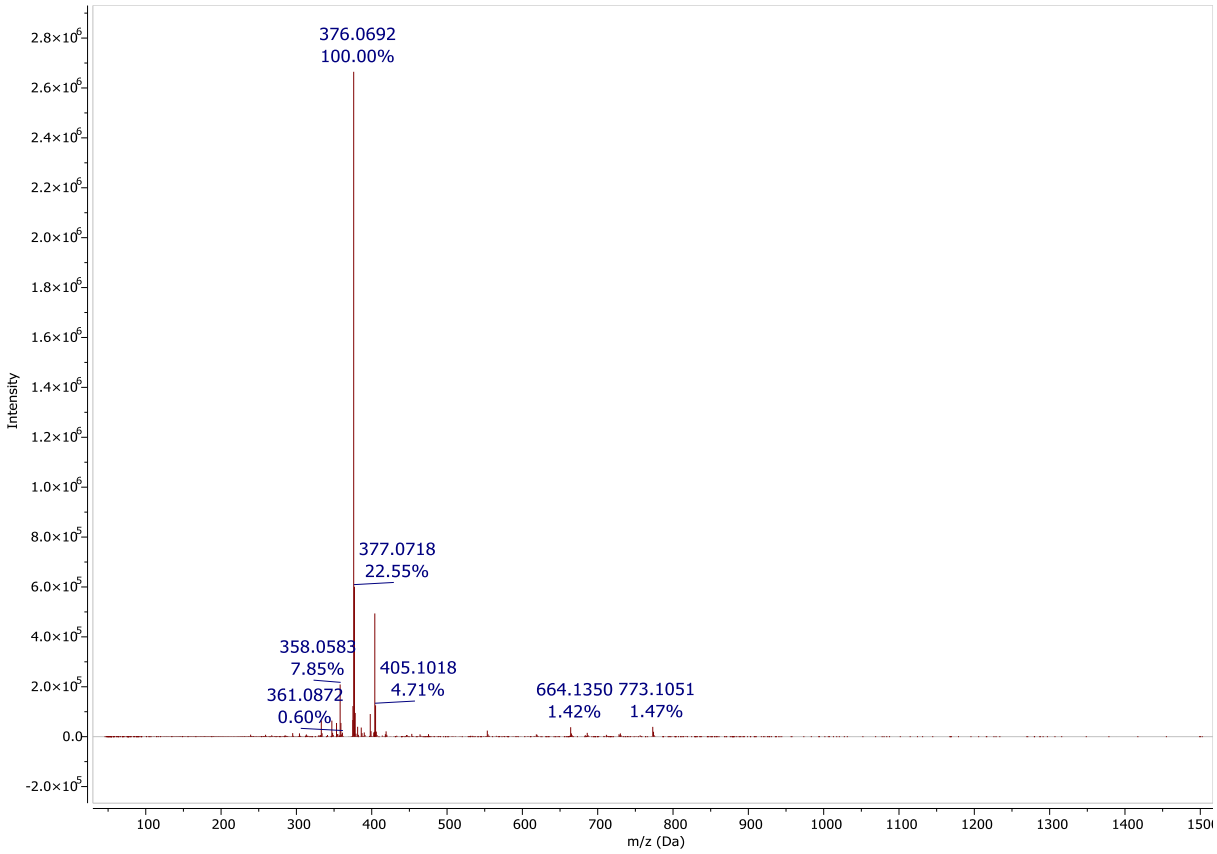

***Figure 97**: ESI- MS spectrum of 9, positive mode*

9.9 Fluorescein isoxazole

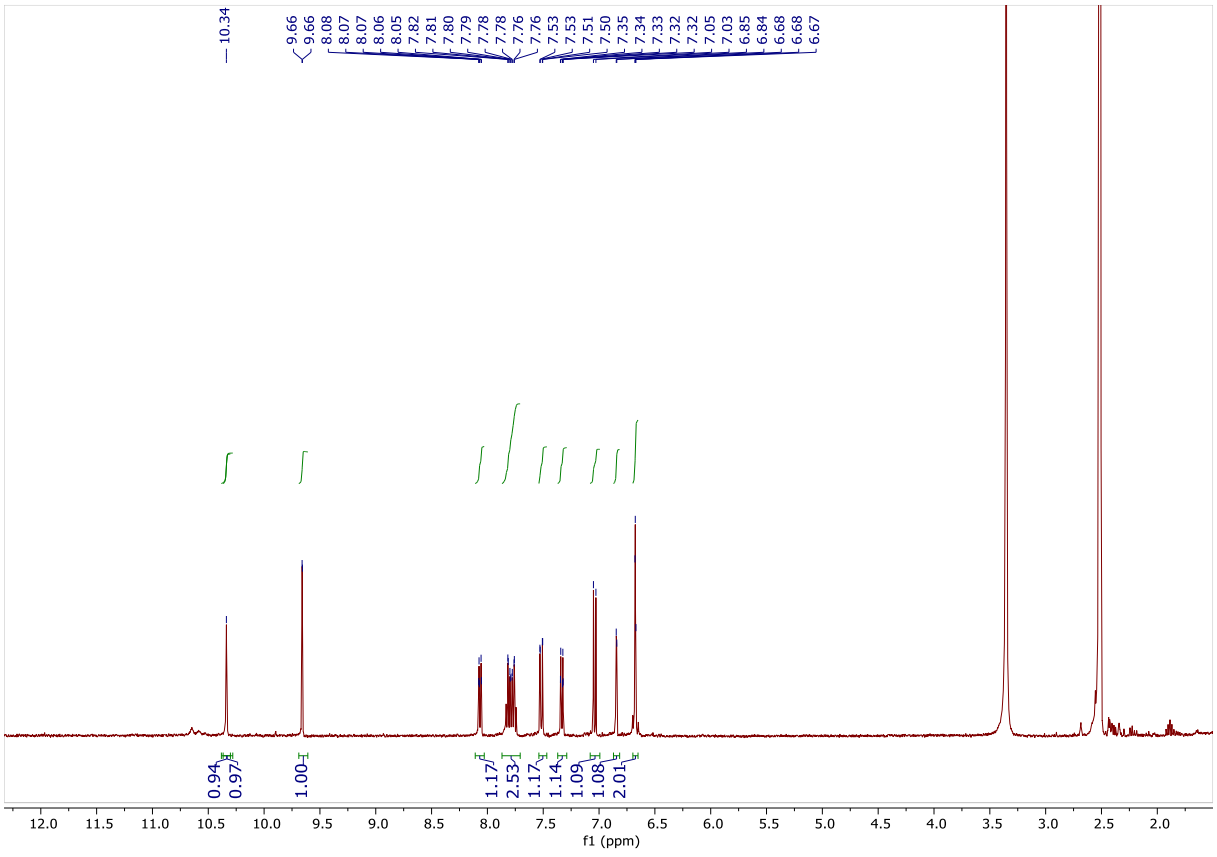

***Figure 98**: [1]H- NMR of Fluorescein isoxazole, 400 MHz, DMSO-d_6*

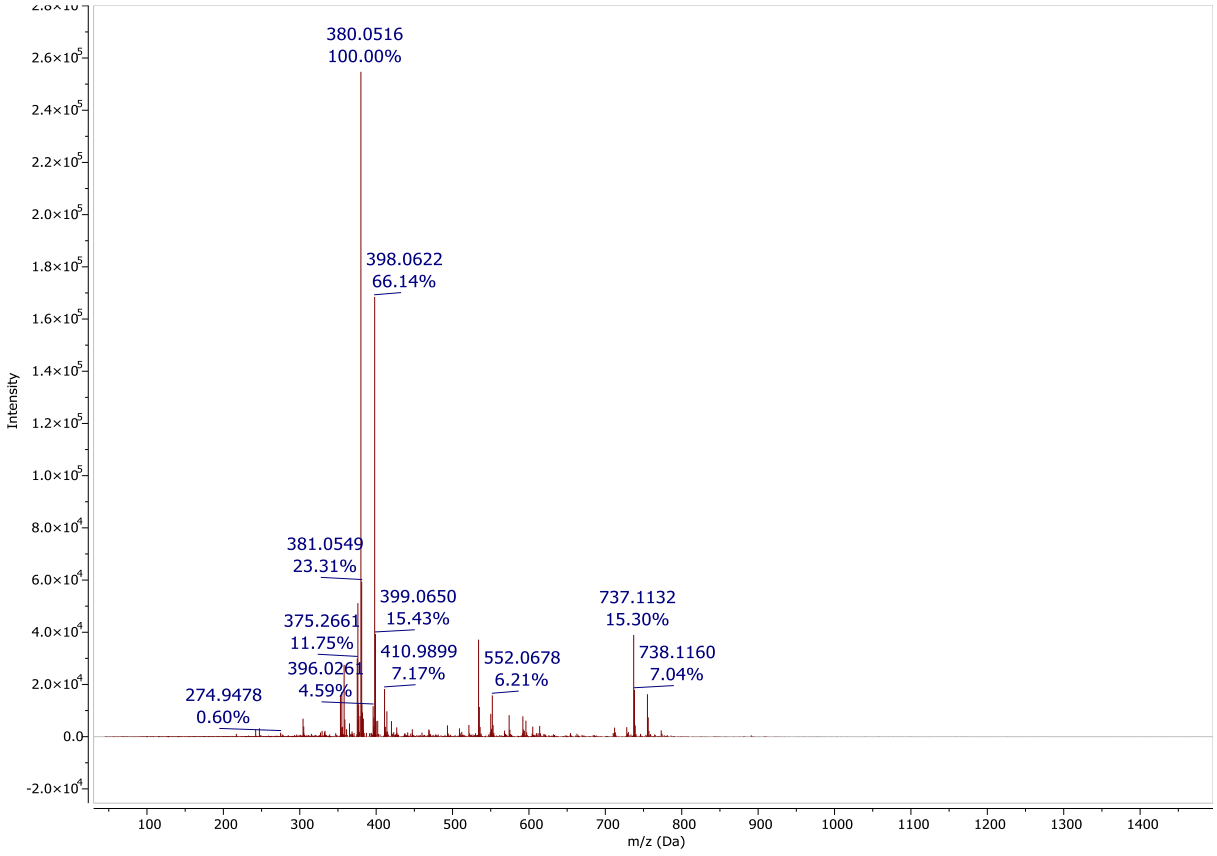

***Figure 99**: ESI- MS spectrum of Fluorescein isoxazole, positive mode*

9.10 Fluorescein nitrile*

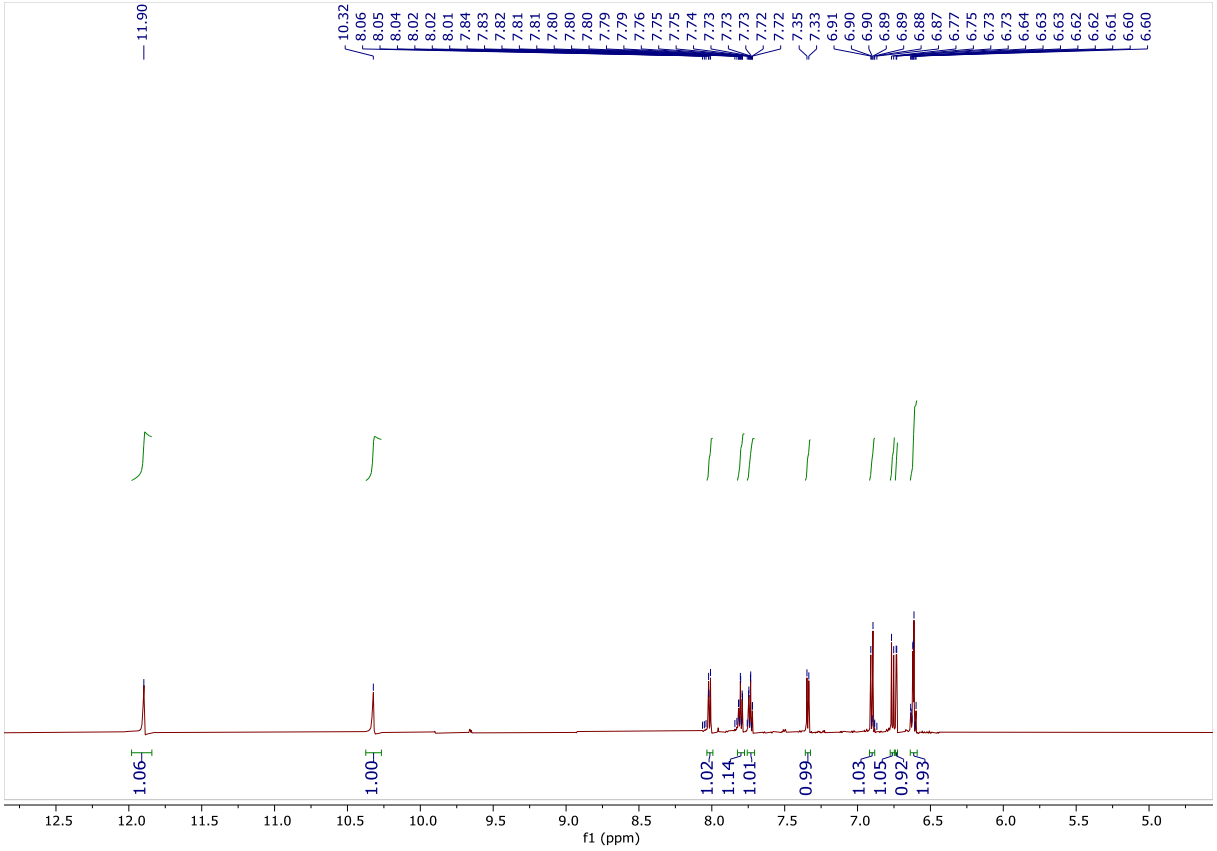

***Figure 100**: [1]H- NMR of Fluorescein nitrile, 600 MHz, DMSO-d_6*

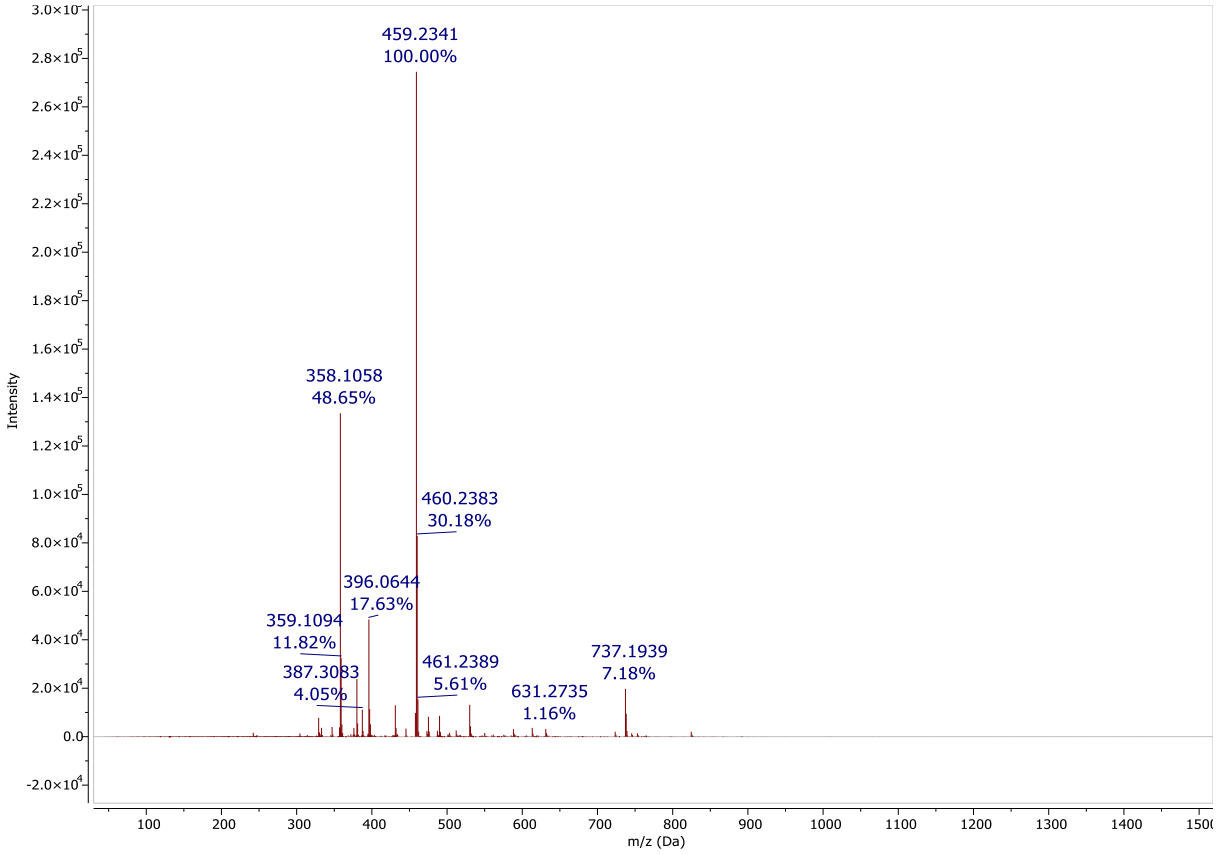

***Figure 101**: ESI- MS spectrum of Fluorescein nitrile, positive mode*

9.11 N-Boc-cystamine

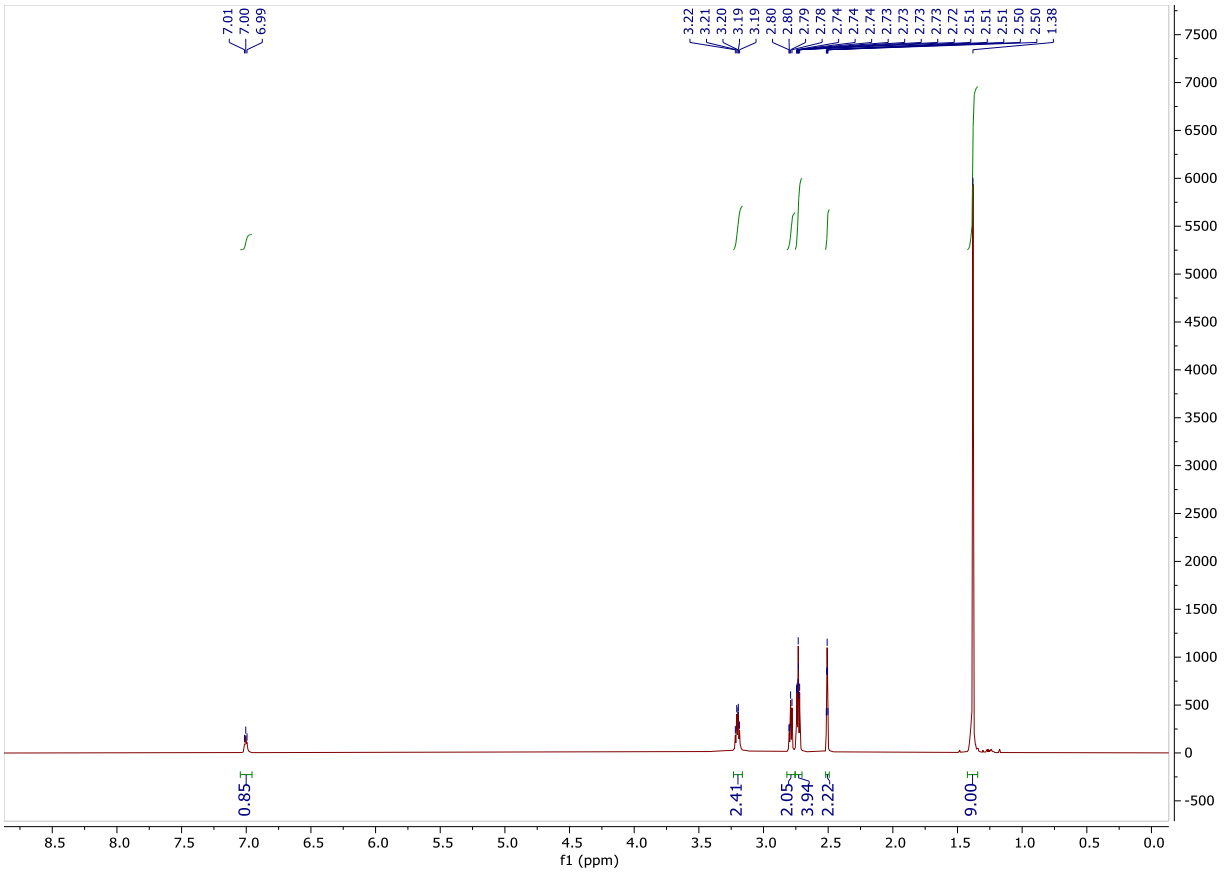

***Figure 102**: [1]H NMR spectra of N-Boc-cystamine*

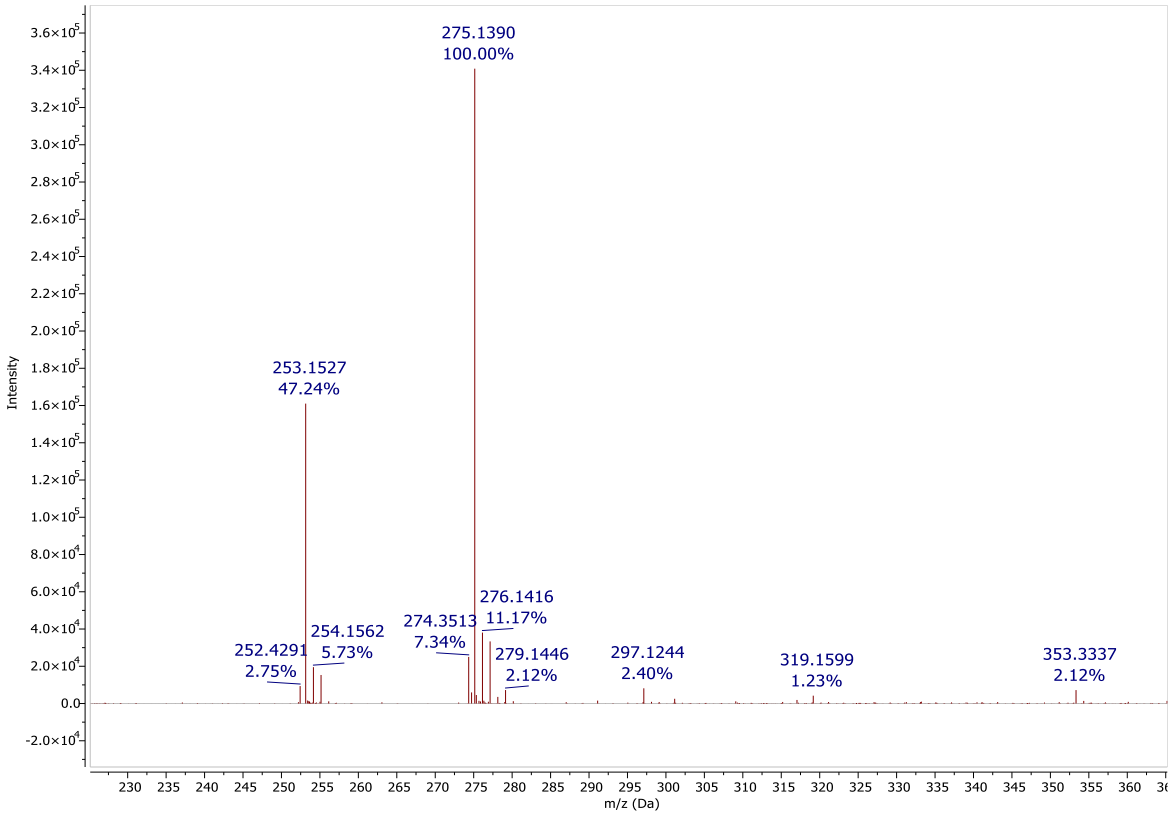

***Figure 103**: ESI MS of N-Boc-cystamine, positive mode*

9.12 Fol-cystamine

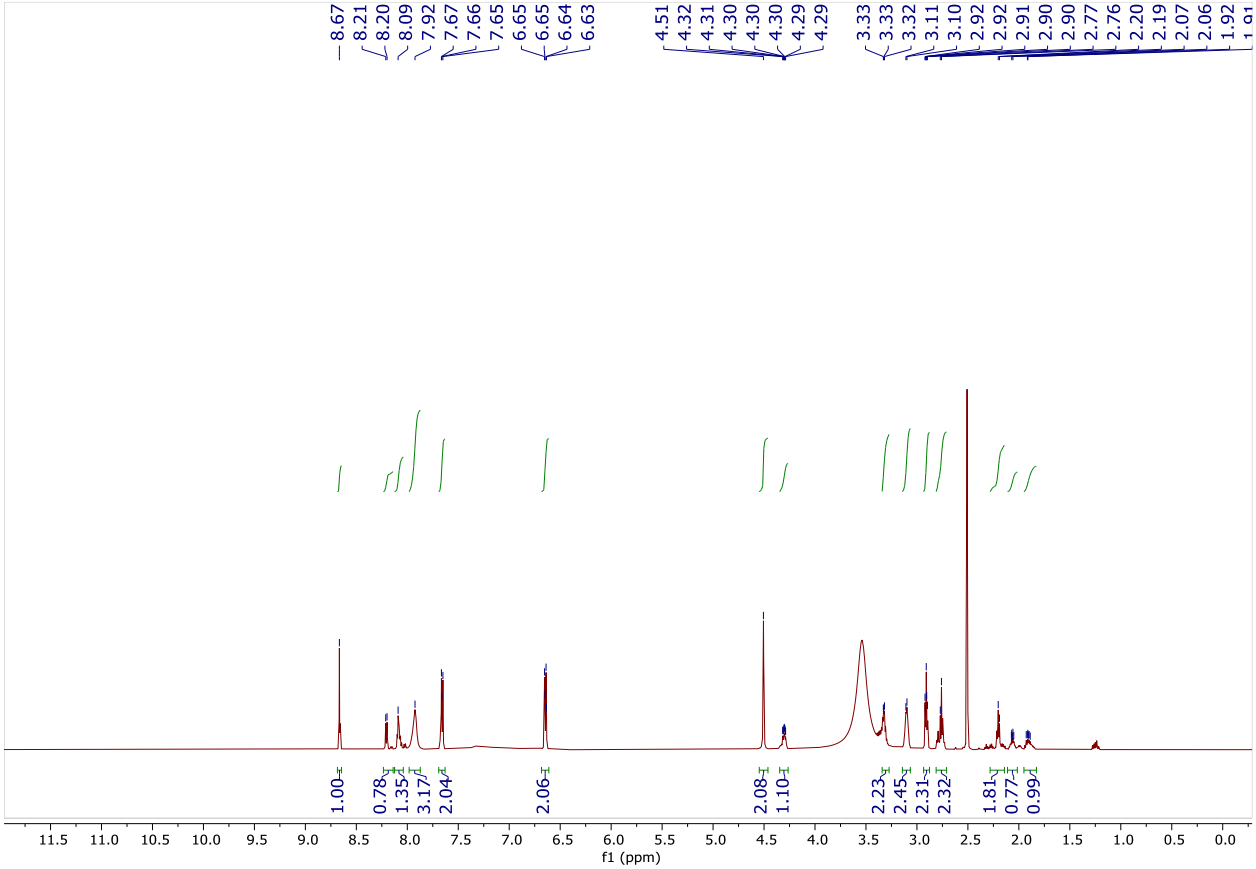

Figure 104: *^{1}H-NMR of γ-Fol-cystamine, 600 MHz, DMSO-d_6*

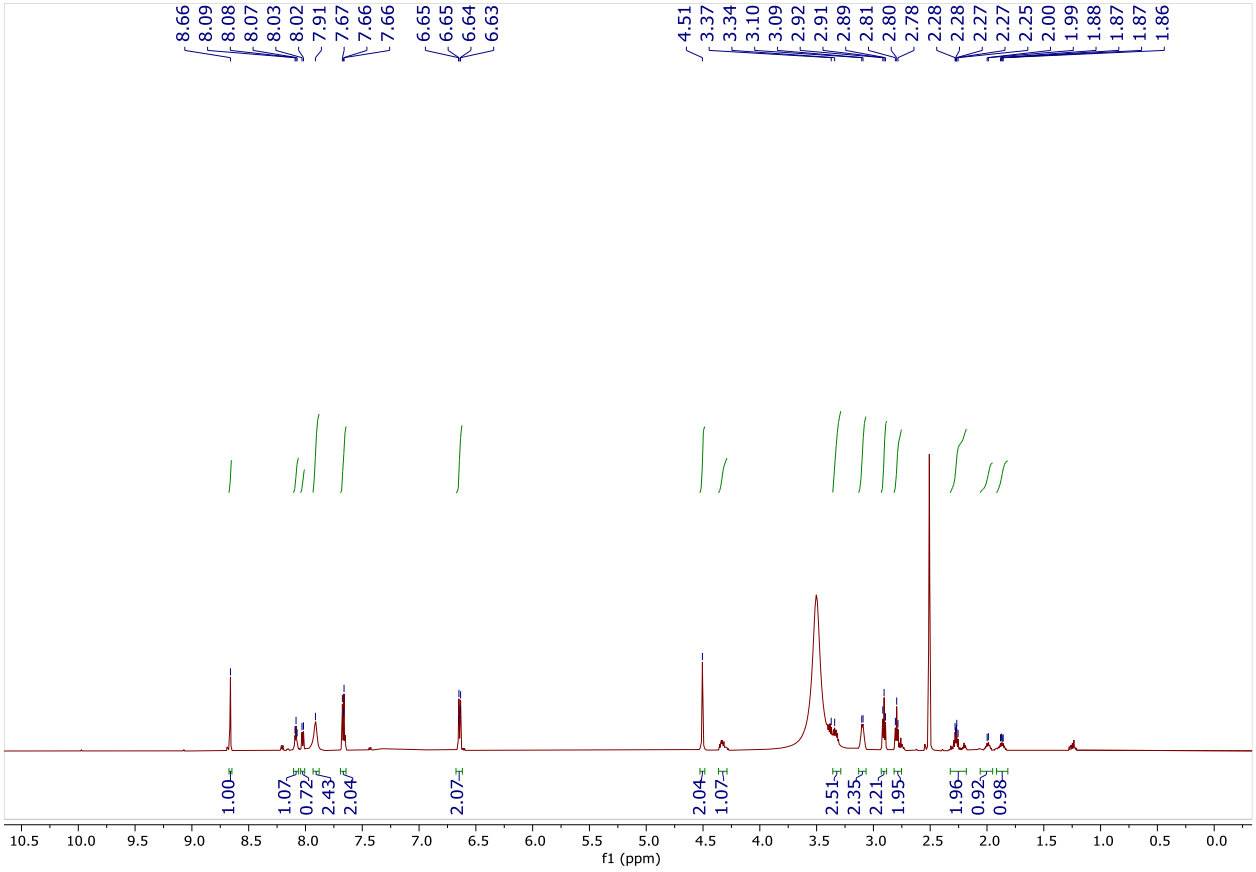

Figure 105: *^{1}H-NMR of α-Fol-cystamine, 600 MHz, DMSO-d_6*

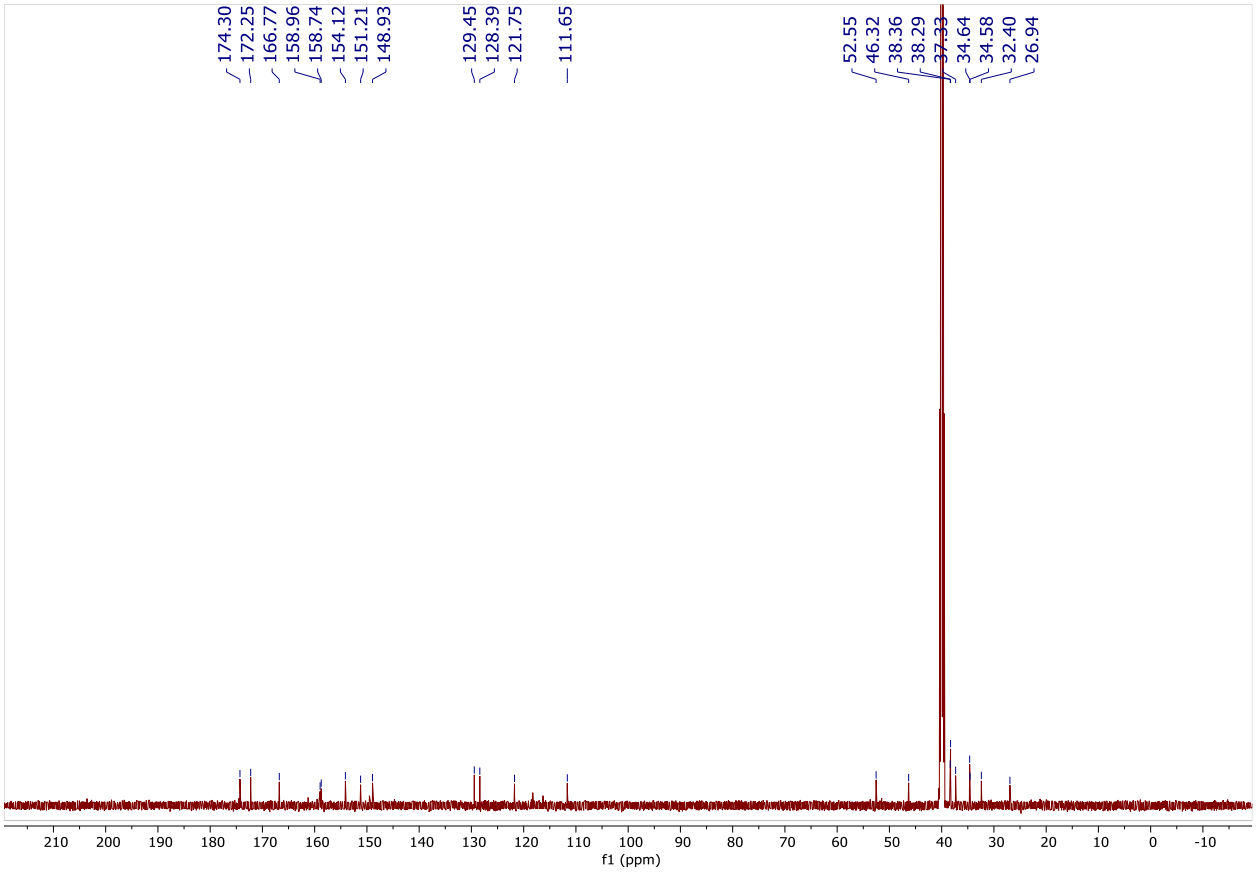

Figure 106*: ^{13}C-NMR of γ-Fol-cystamine, 151MHz, DMSO-d_6*

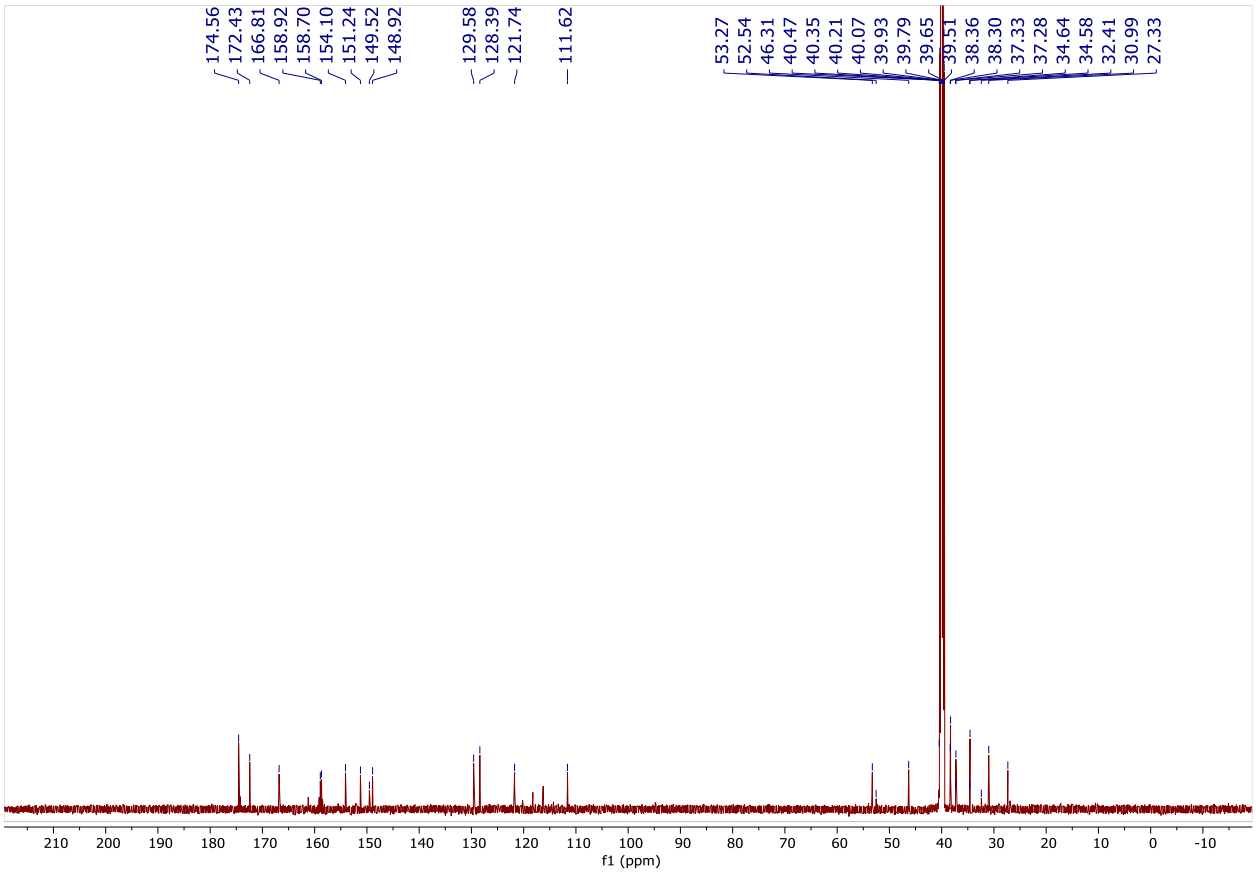

***Figure 107**: [13]C-NMR of α-Fol-cystamine, 151MHz, DMSO-d_6*

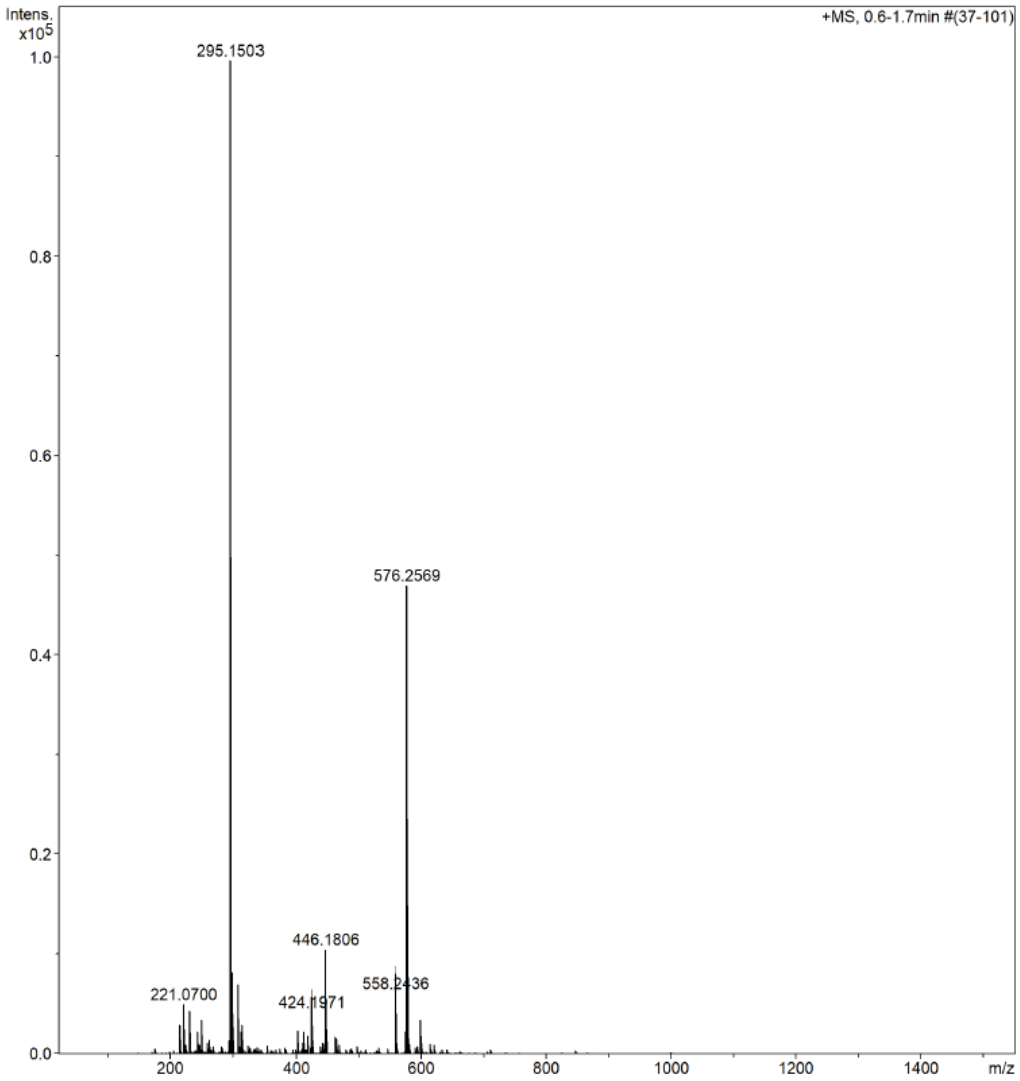

***Figure 108**: ESI MS of Fol-cystamine, positive mode*

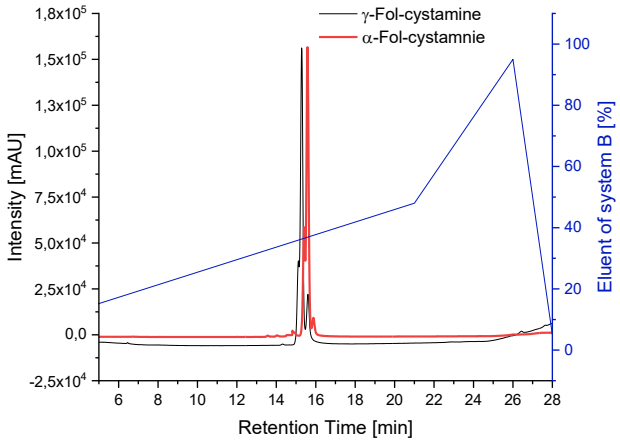

***Figure 109:** Analytical HPLC of α and γ isomers of Fol-cystamine, Nucleosil C18 (5 µm, 4.6 mm x 25 mm), H_2O with 0.1% TFA (system A) / 80% MeCN-20% H_2O and 0.1 % TFA (system B), 1 mL/min, 0.02 min - 5% eluent of system B, 21 min - 48% eluent of system B, (γ-isomer: t_R = 15.3 min, α- isomer: t_R = 15.6 min)*

9.13 FP 10

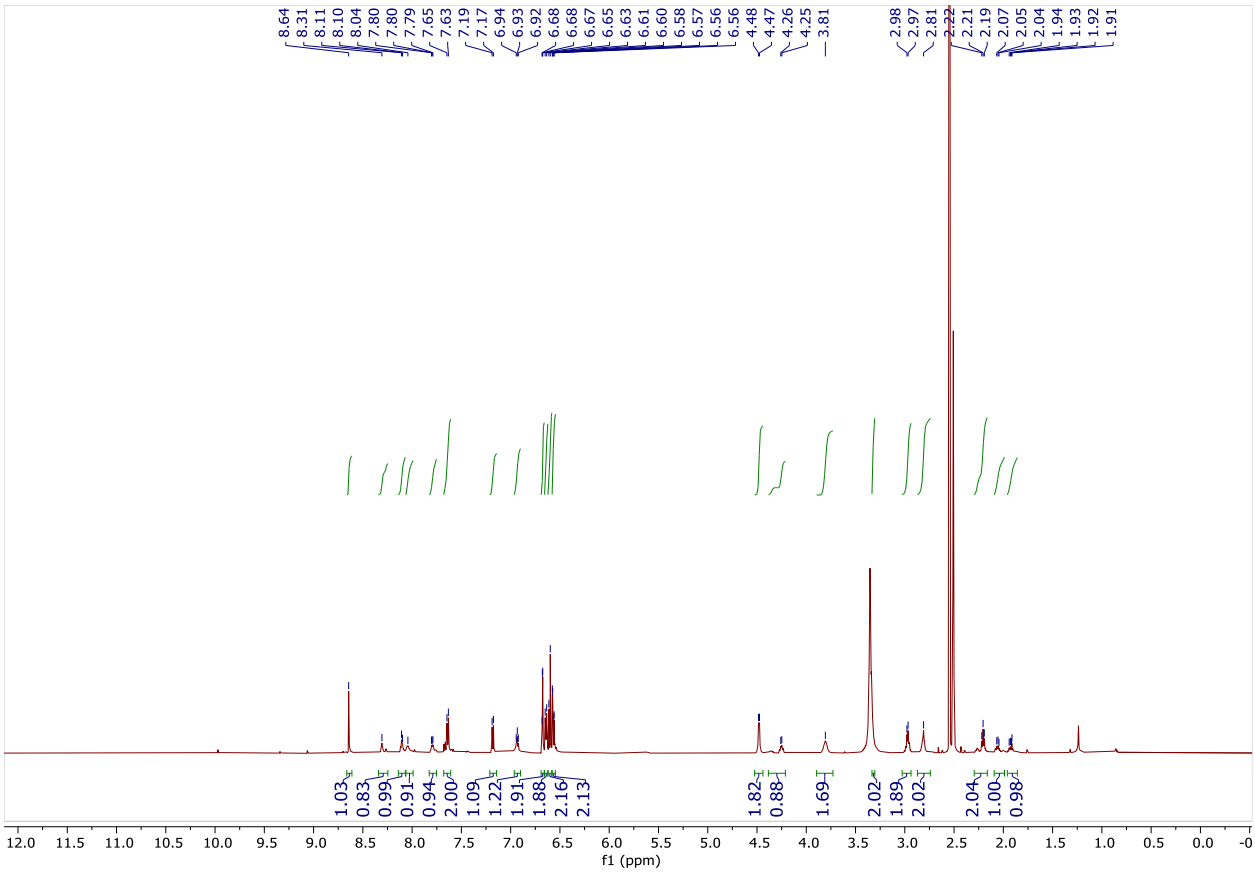

Figure 110: *^{1}H-NMR of FP 10, 600 MHz, DMSO-d_6*

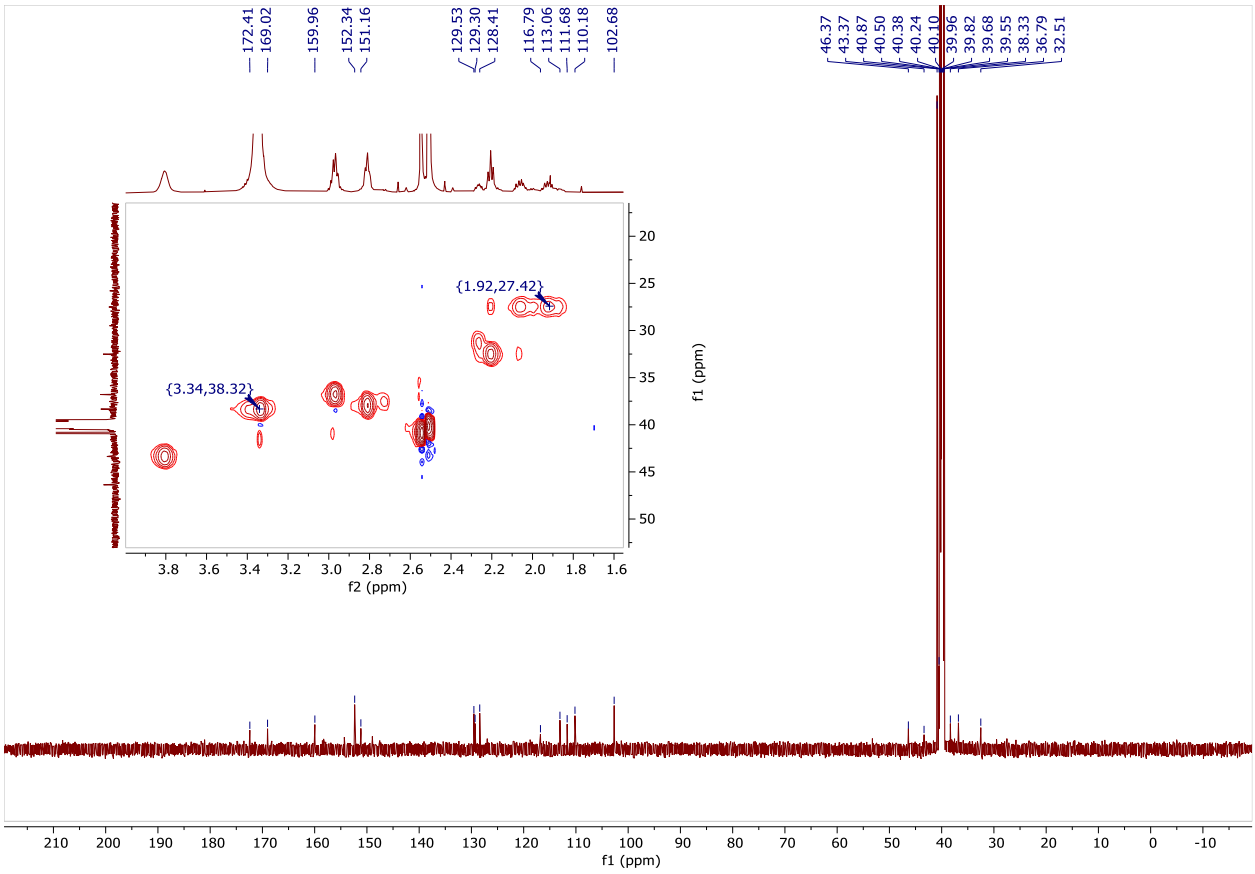

Figure 111: *^{13}C-NMR of FP 10, 151MHz, DMSO-d_6, with a 2D HSQC spectrum inset showing proton-carbon correlations.*

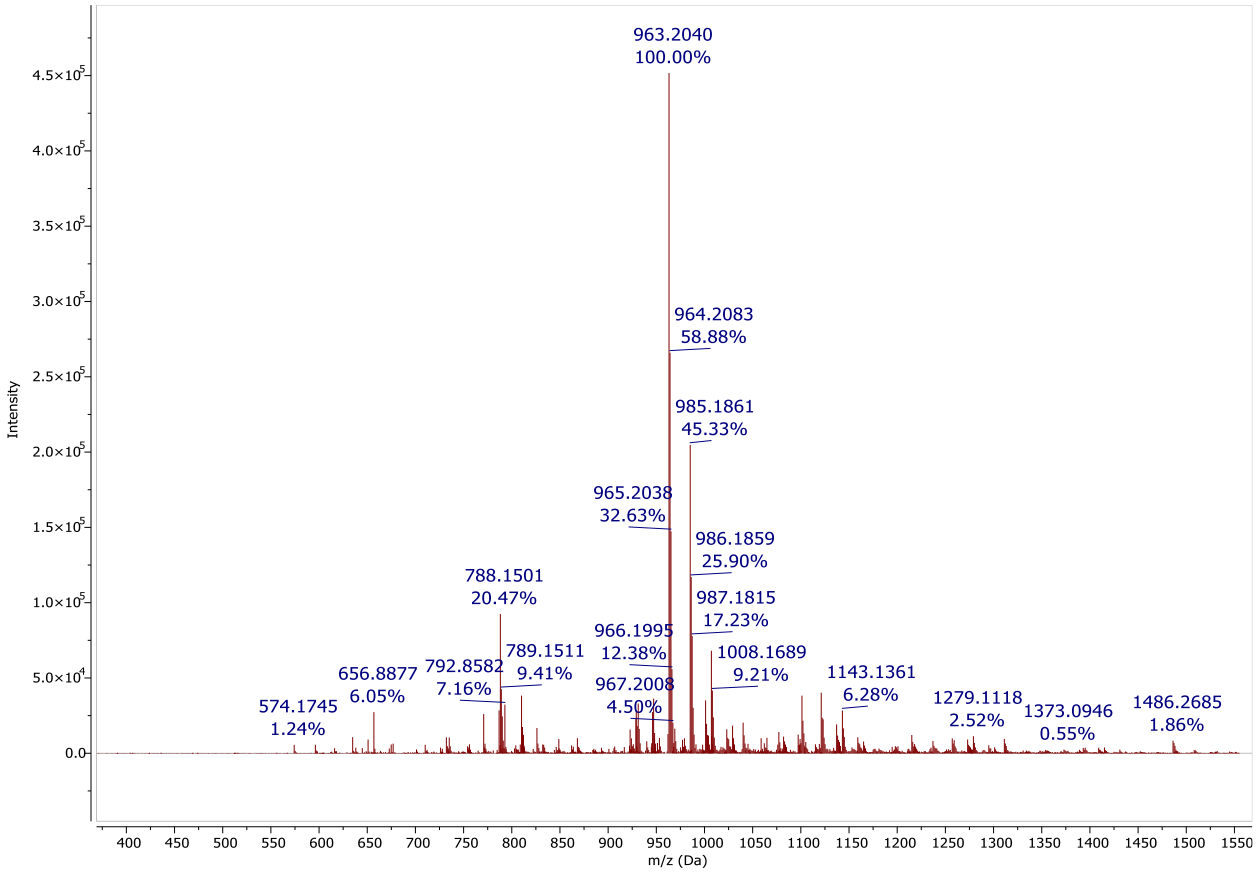

***Figure 112**: ESI MS of FP 10, negative mode*

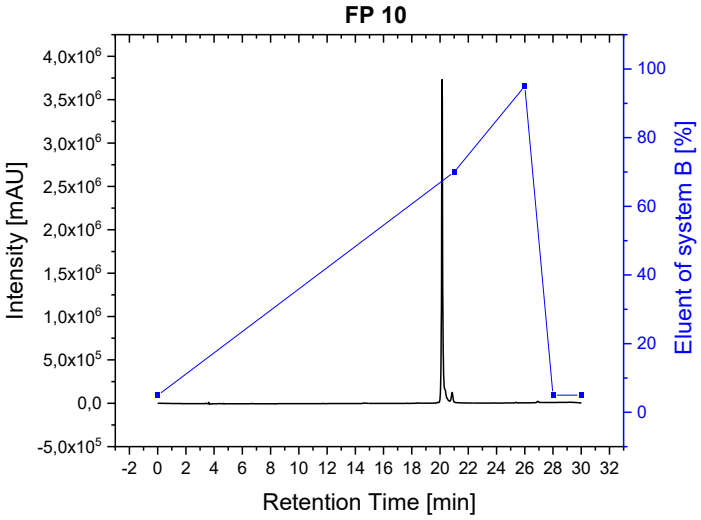

***Figure 113**: Analytical HPLC of α and γ isomers of FP 10, Nucleosil C18 (5 µm, 4.6 mm x 25 mm), H_2O with 0.1% TFA (system A) / 80% MeCN-20% H_2O and 0.1 % TFA (system B), 1 mL/min, 0.02 min - 5% eluent of system B, 21 min - 70% eluent of system B, (t_R = 20.1 min).*

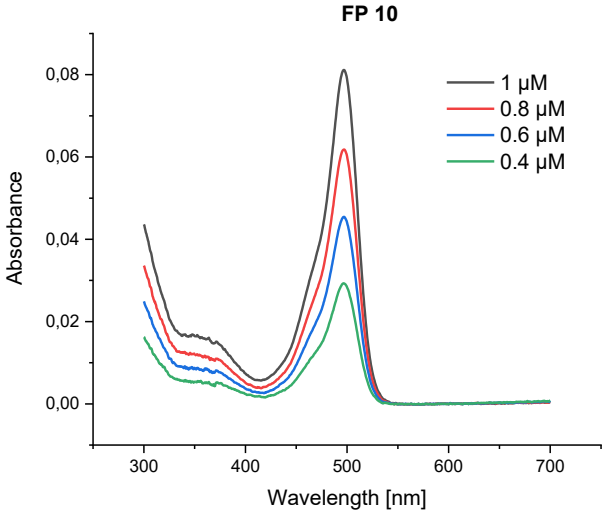

Figure 114: *Absorption spectra of* FP 10 *in 4 different concentrations, PBS (pH=7.4)*

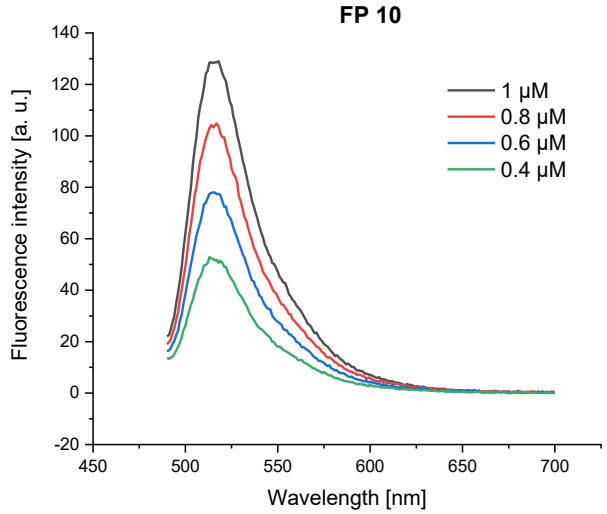

***Figure 115**: Fluorescence spectra of FP 10 in 4 different concentrations, PBS (pH=7.4), Excitation wavelength: 480 nm*

9.14 FP 11

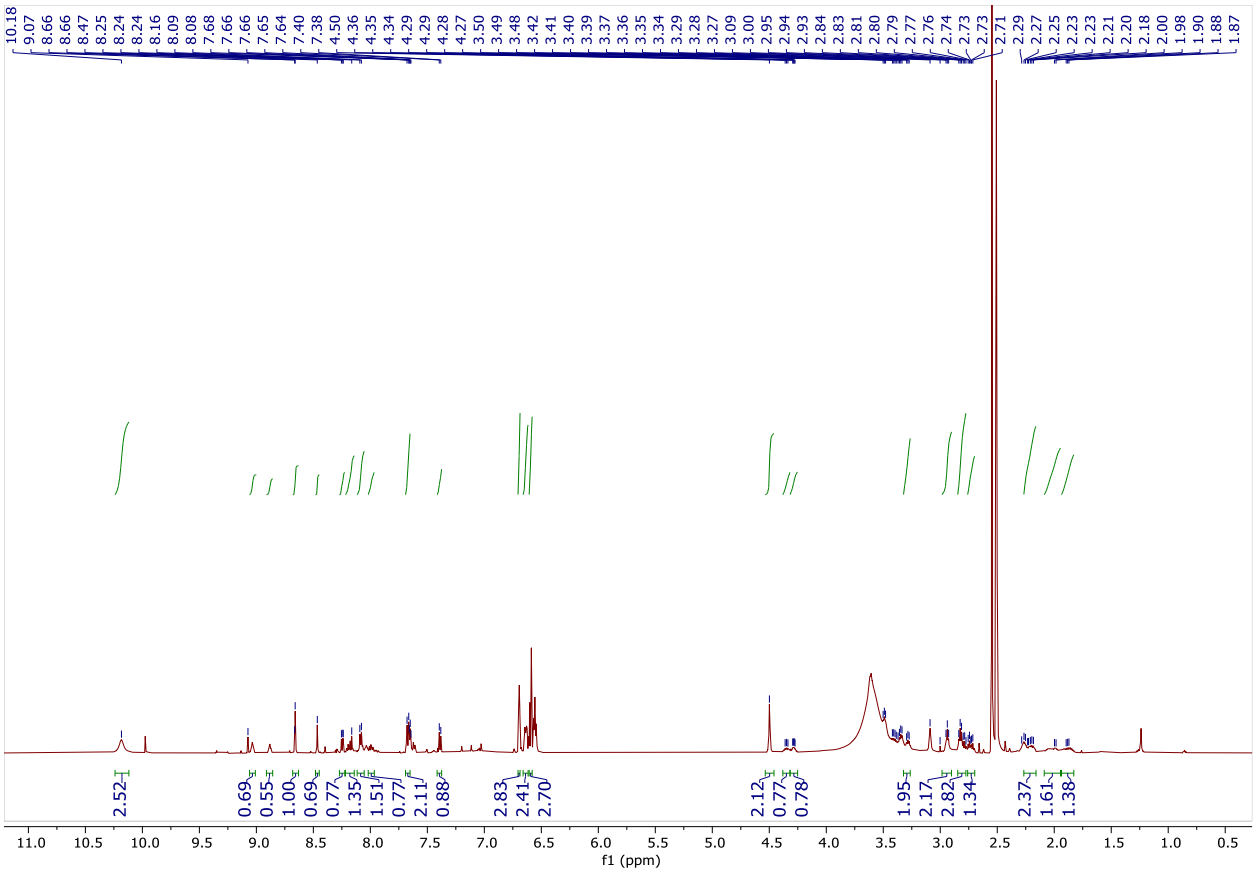

Figure 116: *^{1}H-NMR of FP 11, 600 MHz, DMSO-d_6*

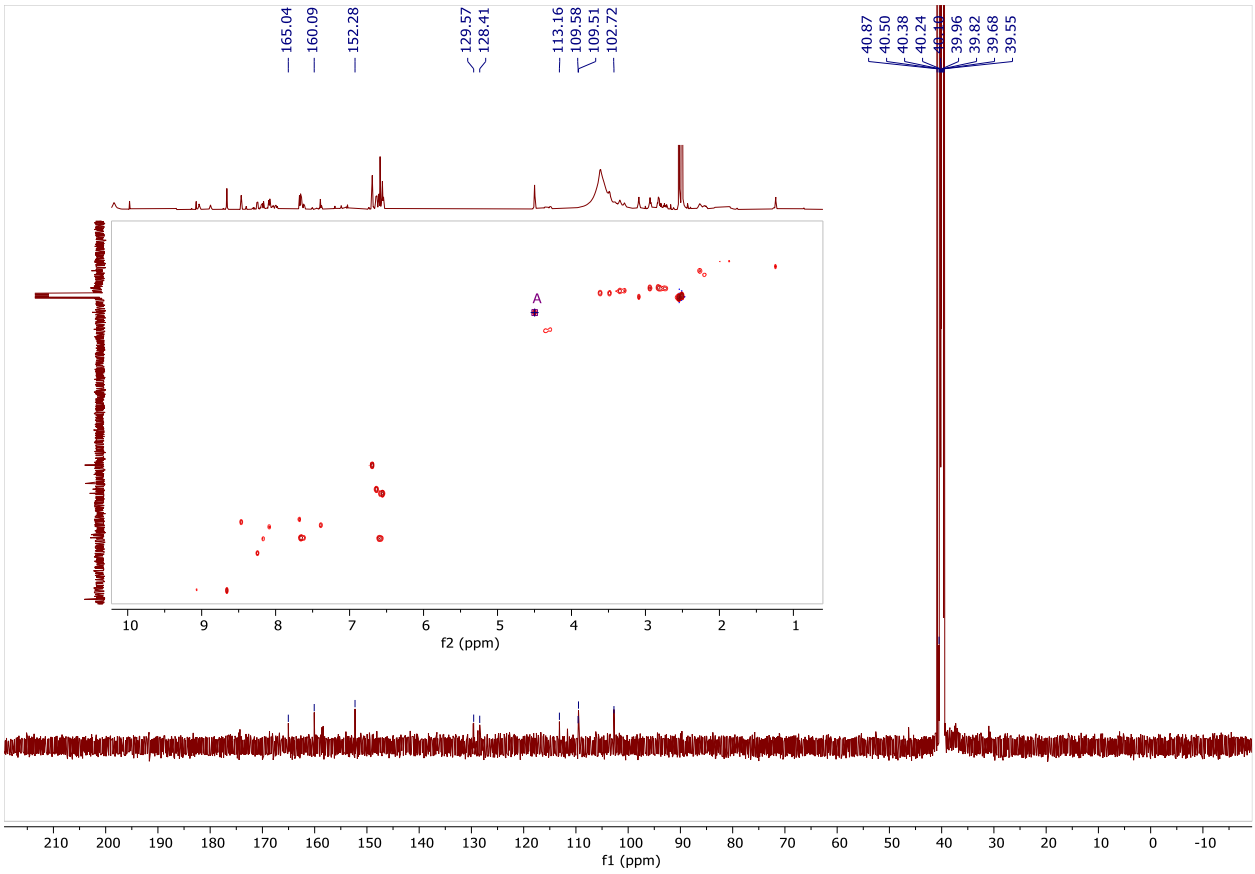

***Figure 117**: ^{13}C-NMR of FP 11, 151MHz, DMSO-d_6 with a 2D HSQC spectrum inset showing proton-carbon correlations.*

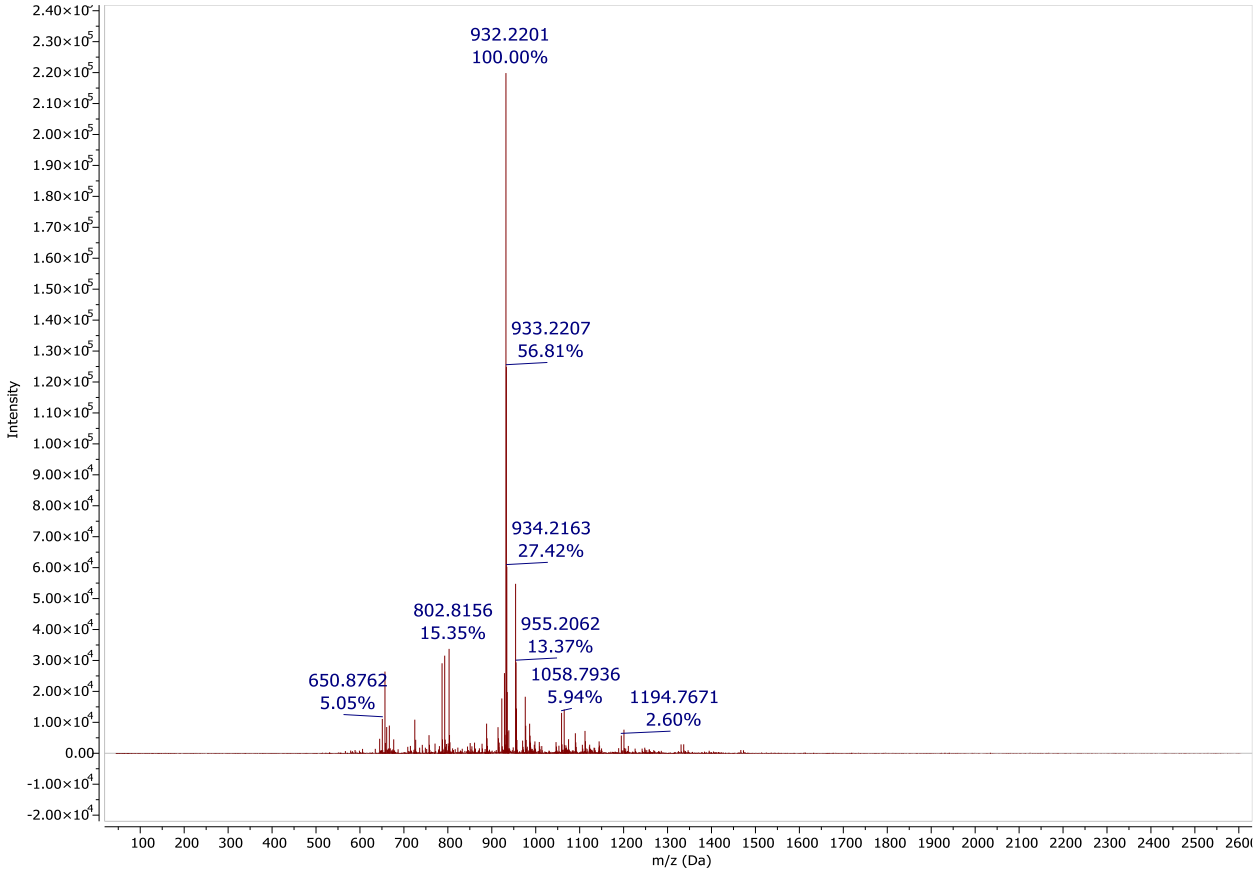

***Figure 118**: ESI MS of FP 11, negative mode*

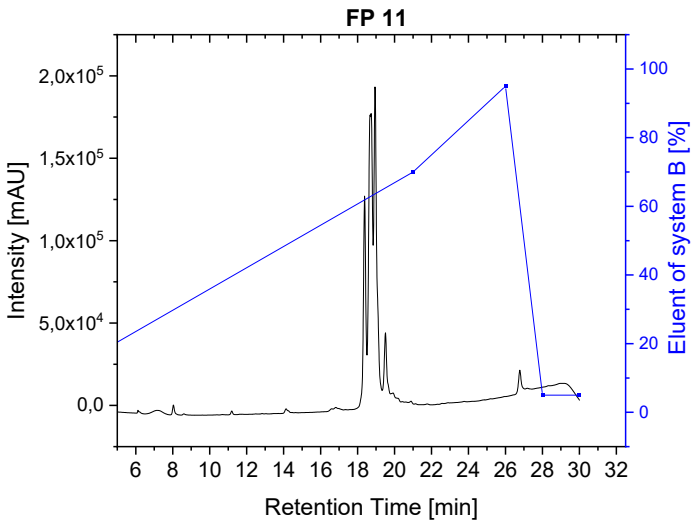

***Figure 119**: Analytical HPLC of α and γ isomers of FP 11, Nucleosil C18 (5 µm, 4.6 mm x 25 mm), H_2O with 0.1% TFA (system A) / 80% MeCN-20% H_2O and 0.1 % TFA (system B), 1 mL/min, 0.02 min - 5% eluent of system B, 21 min - 70% eluent of system B.*

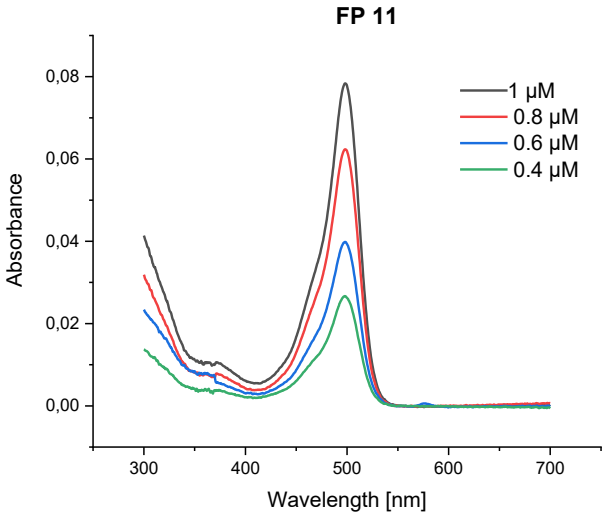

***Figure 120**: Absorption spectra of FP 11 in 4 different concentrations, PBS (pH=7.4)*

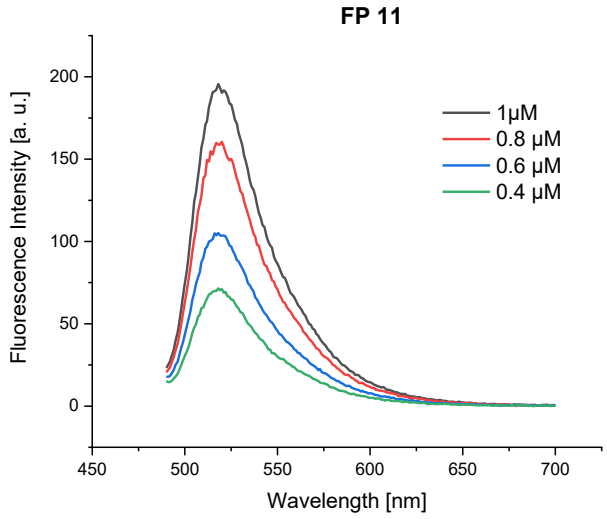

***Figure 121**: Fluorescence spectra of FP 11 in 4 different concentrations, PBS (pH=7.4), Excitation wavelength: 480 nm.*

9.15 N-(6-Aminohexyl)folic acid

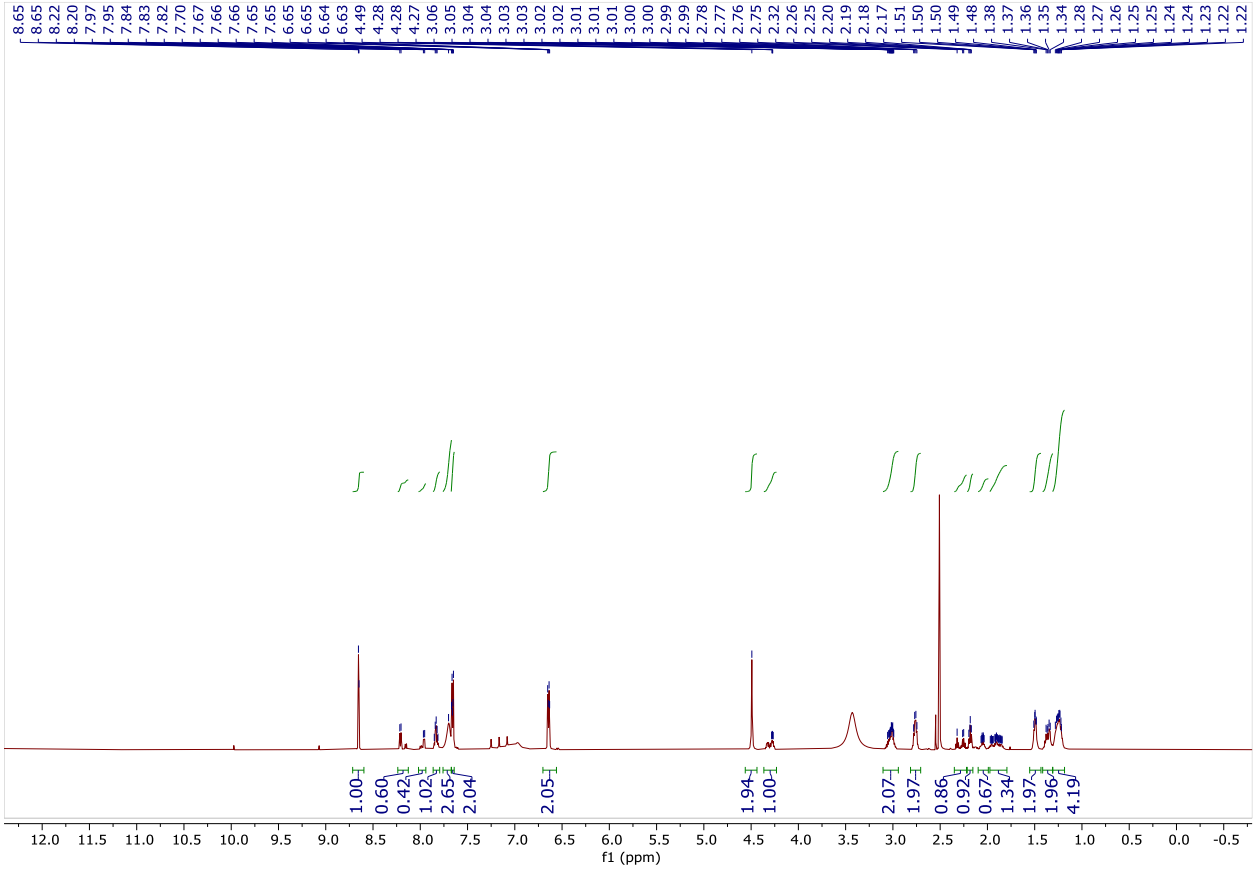

***Figure 122**: [1]H-NMR of N-(6-Aminohexyl)folic acid , 600 MHz, DMSO-d_6*

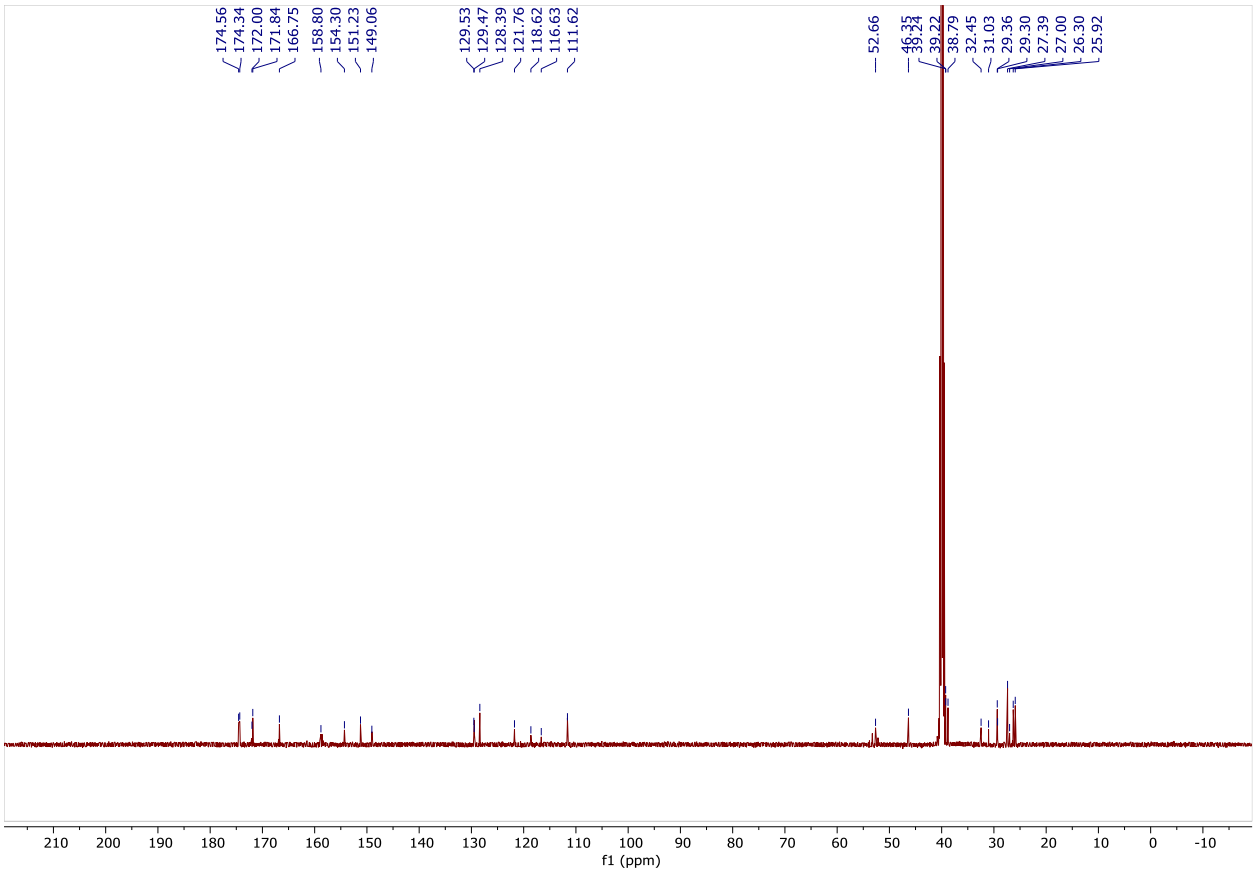

***Figure 123**: ^{13}C-NMR of N-(6-Aminohexyl)folic acid , 151MHz, DMSO-d_6*

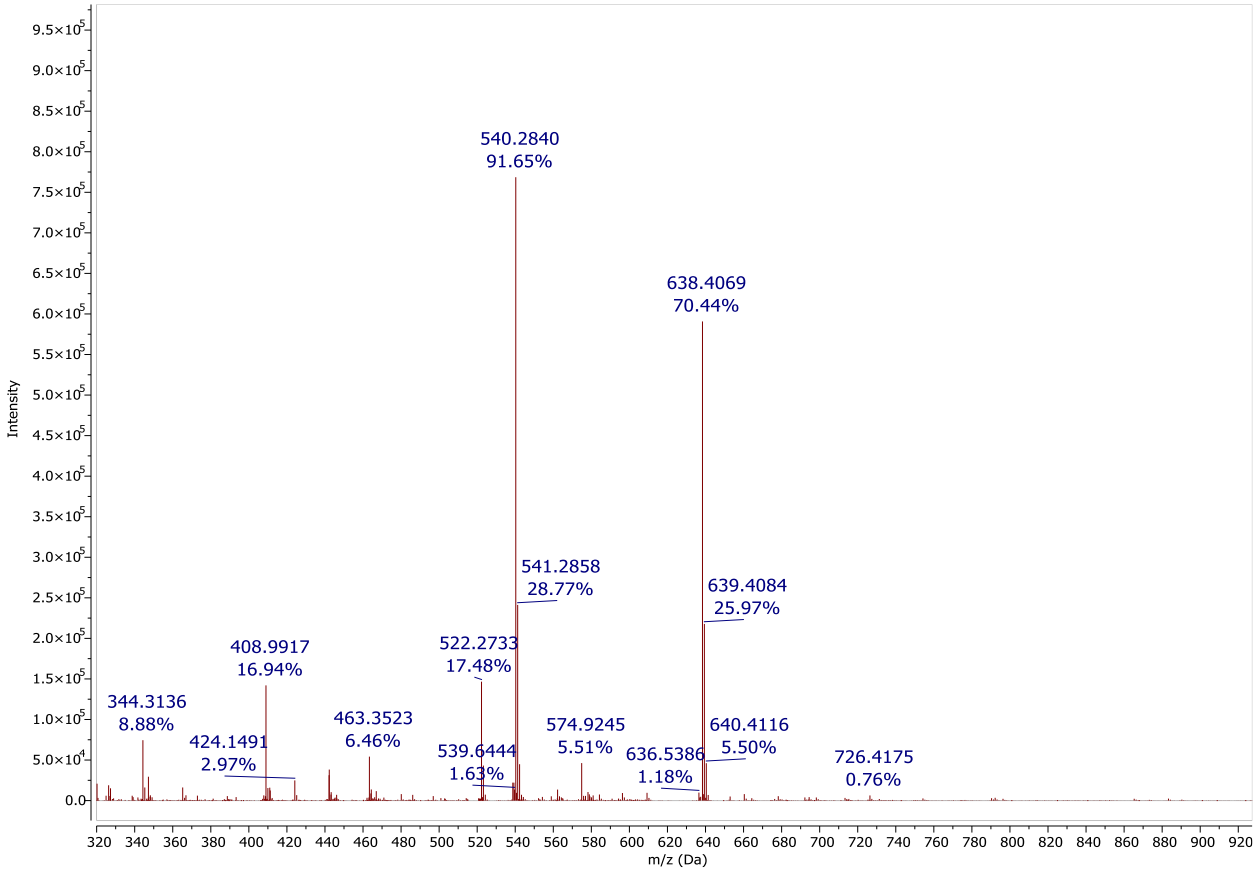

***Figure 124**: ESI MS of N-(6-Aminohexyl)folic acid , positive mode*

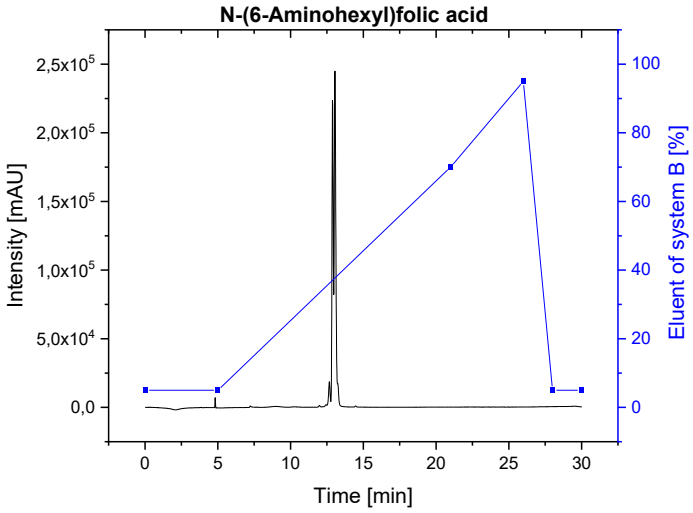

***Figure 125**: Analytical HPLC of α and γ isomers of N-(6-Aminohexyl)folic acid, Nucleosil C18 (5 µm, 4.6 mm x 25 mm), H_2O with 0.1% TFA (system A) / 80% MeCN-20% H_2O and 0.1 % TFA (system B), 1 mL/min, 0.02 – 5 min - 5% eluent of system B, 21 min - 70% eluent of system B (t_R =12.8 min for the first isomer, 13.0 min for the second isomer).*

9.16 FP 12

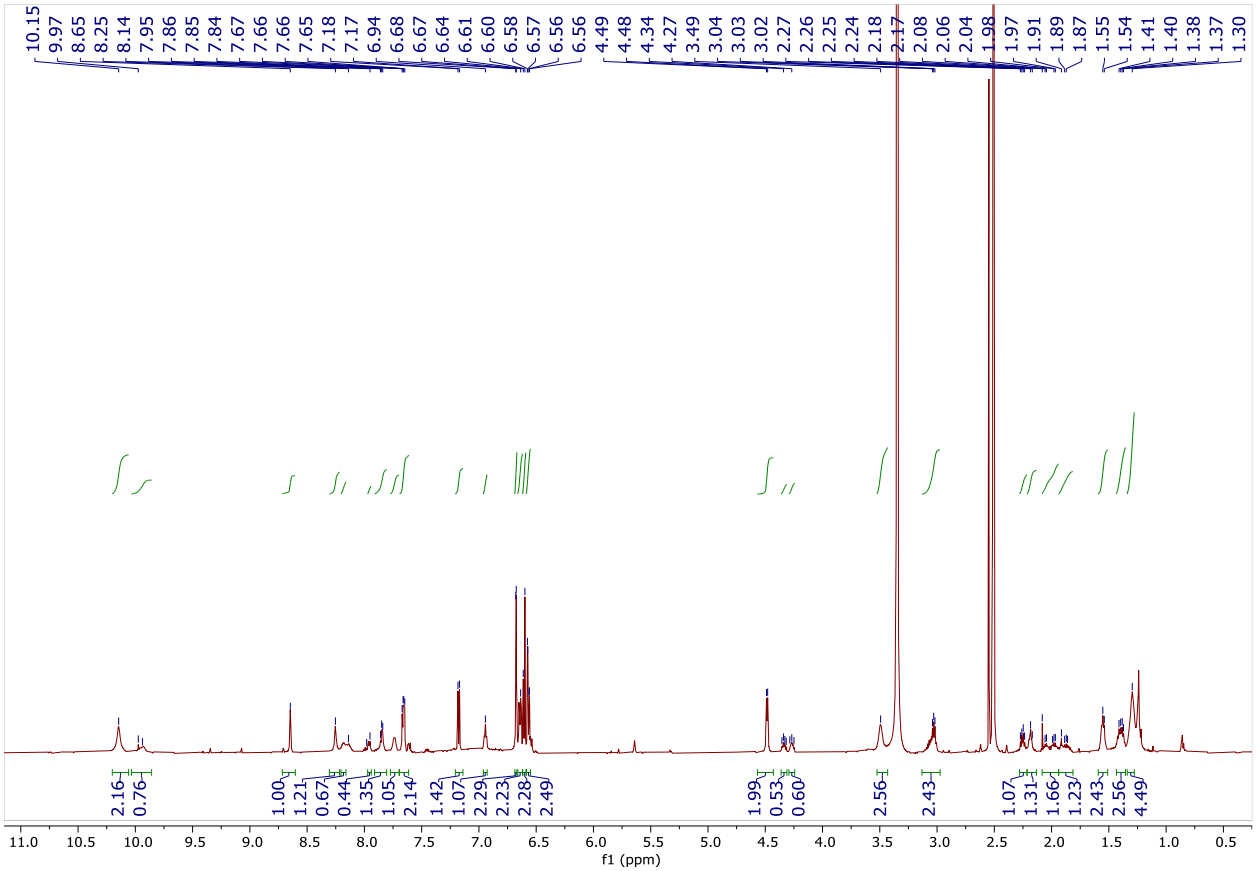

***Figure 126**: ^{1}H-NMR of FP 12, 600 MHz, DMSO-d_6*

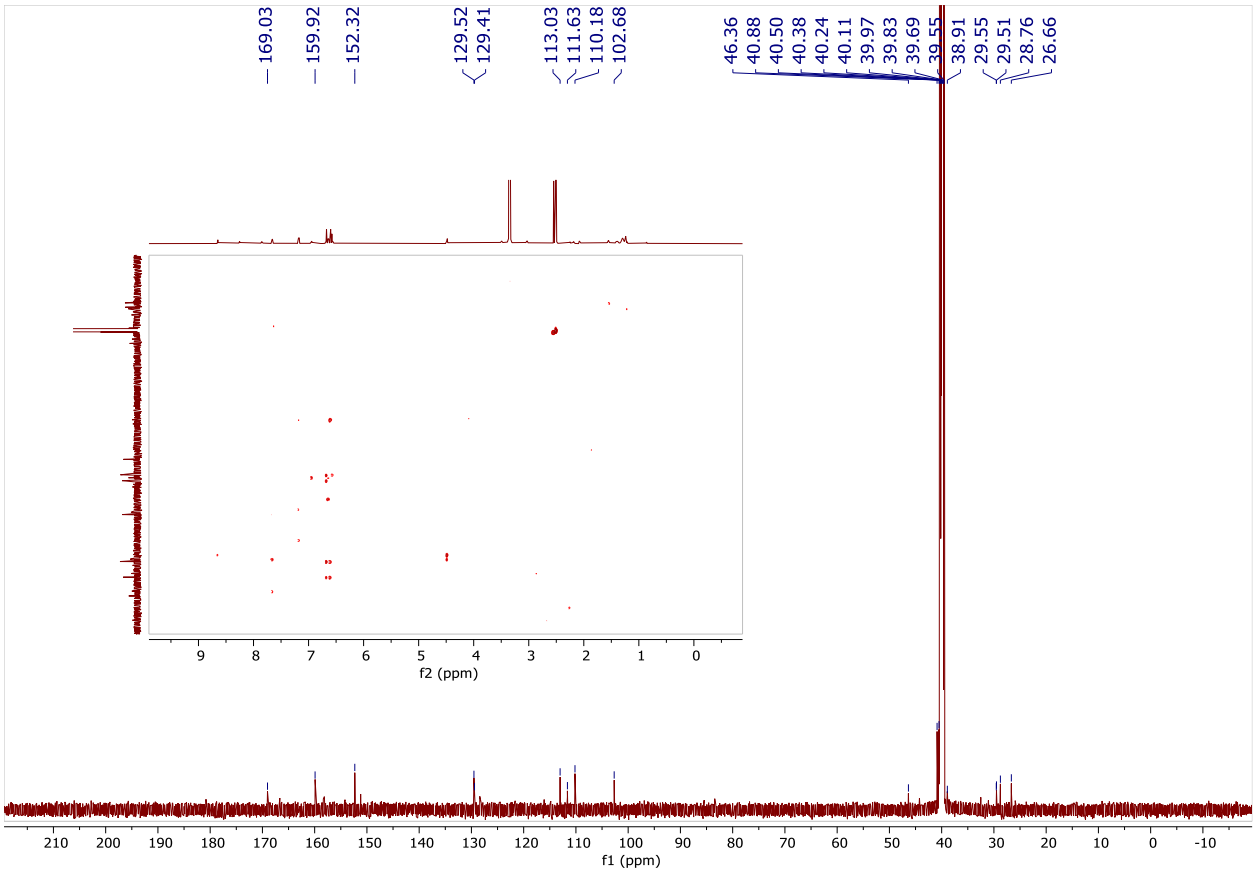

***Figure 127**: [13]C-NMR of FP 12, 151MHz, DMSO-d_6 with a 2D HMBC spectrum inset showing proton-carbon correlations.*

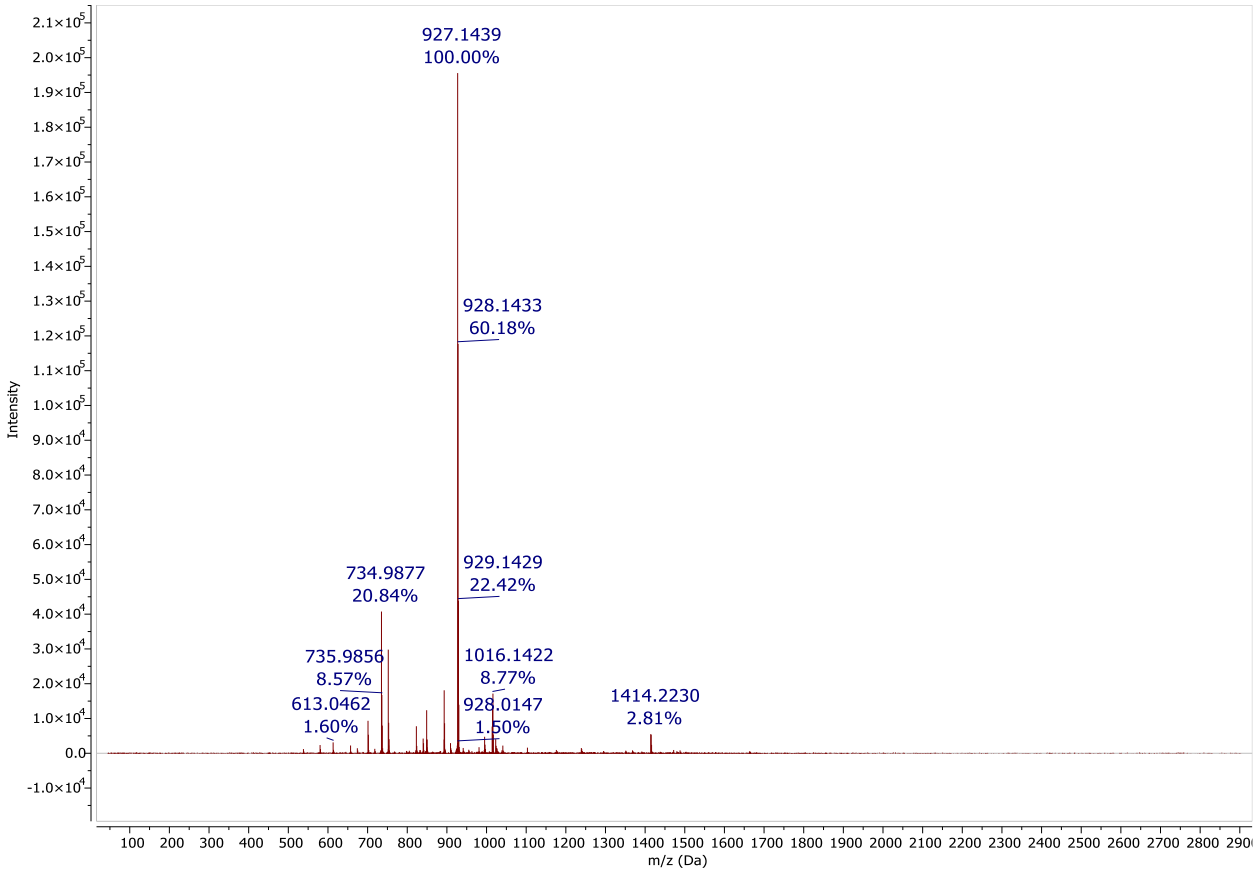

***Figure 128**: ESI MS of FP 12, negative mode*

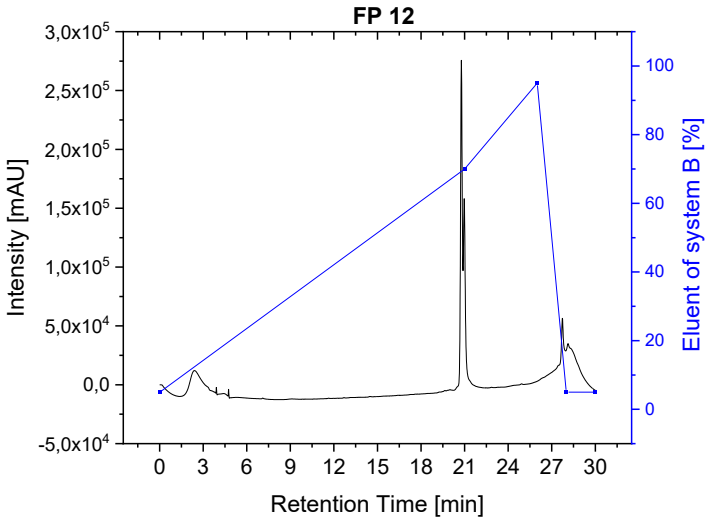

***Figure 129**: Analytical HPLC of α and γ isomers of FP 12, Nucleosil C18 (5 µm, 4.6 mm x 25 mm), H_2O with 0.1% TFA (system A) / 80% MeCN-20% H_2O and 0.1 % TFA (system B), 1 mL/min, 0.02 min - 5% eluent of system B, 21 min - 70% eluent of system B, (t_R =20.7 min for the first isomer, and 20.9 min for the second isomer).*

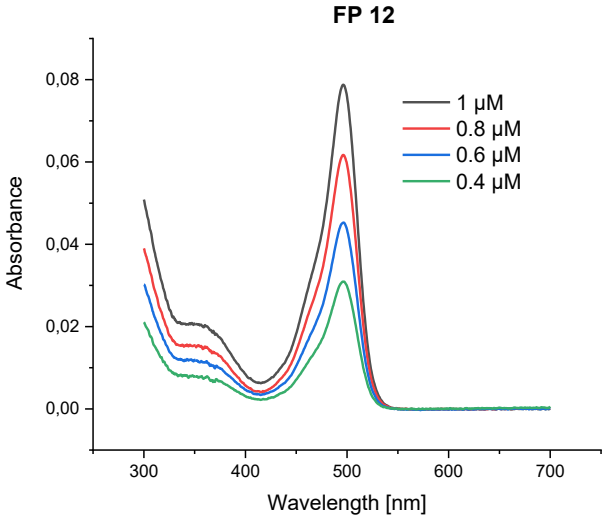

***Figure 130**: Absorption spectra of FP 12 in 4 different concentrations, PBS (pH=7.4)*

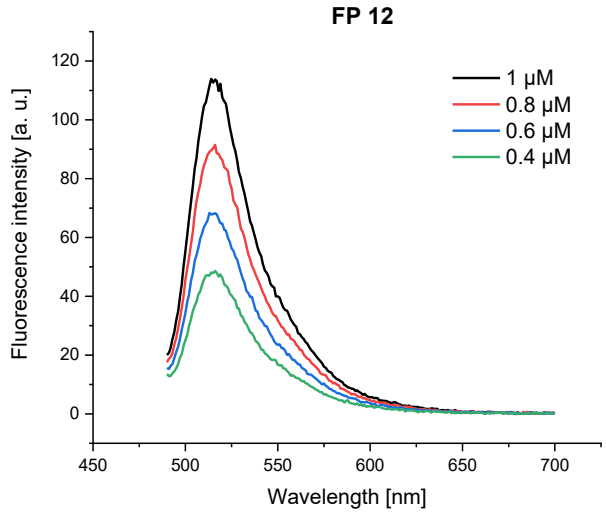

***Figure 131**: Fluorescence spectra of FP 12 in 4 different concentrations, PBS (pH=7.4), Excitation wavelength: 480 nm*

9.17 FP 13

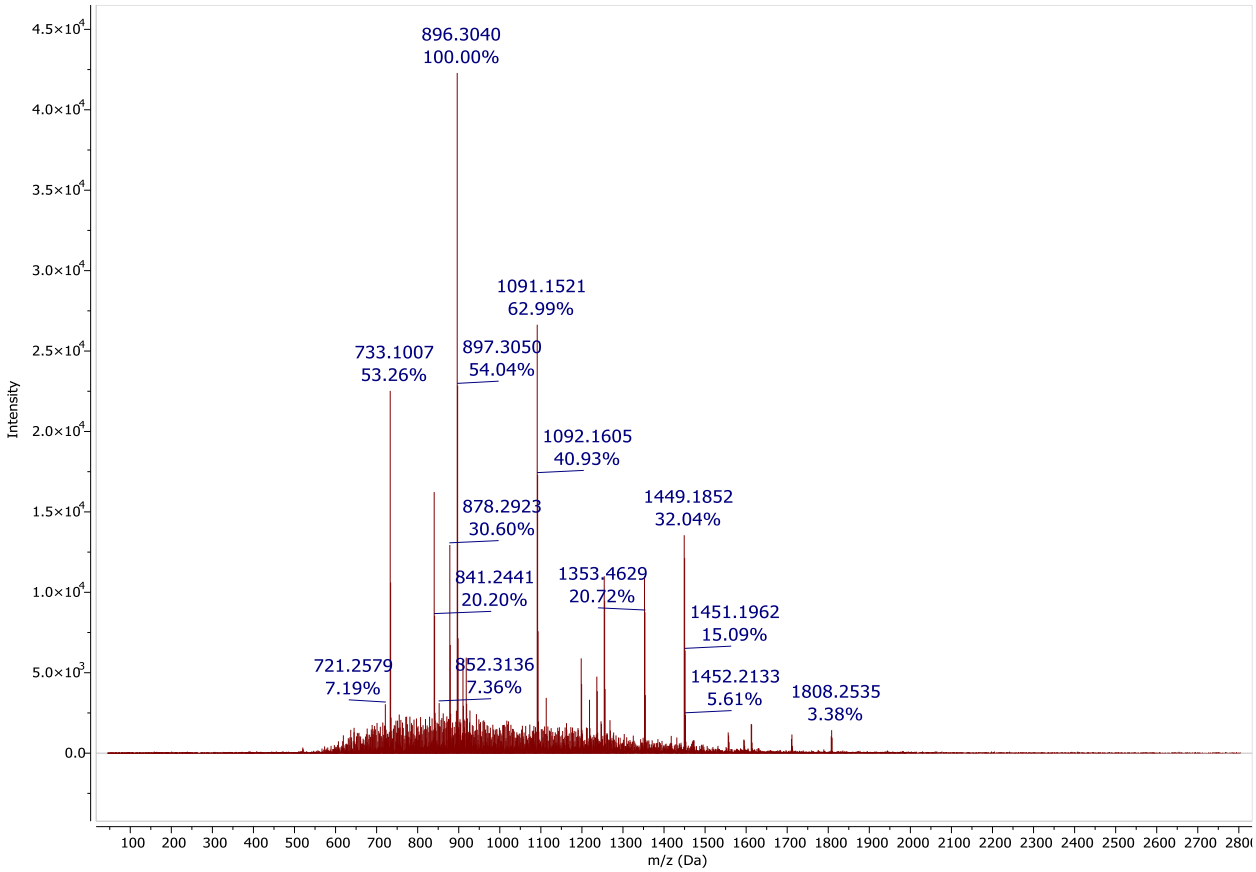

***Figure 132**: ESI MS of FP 13, negative mode*

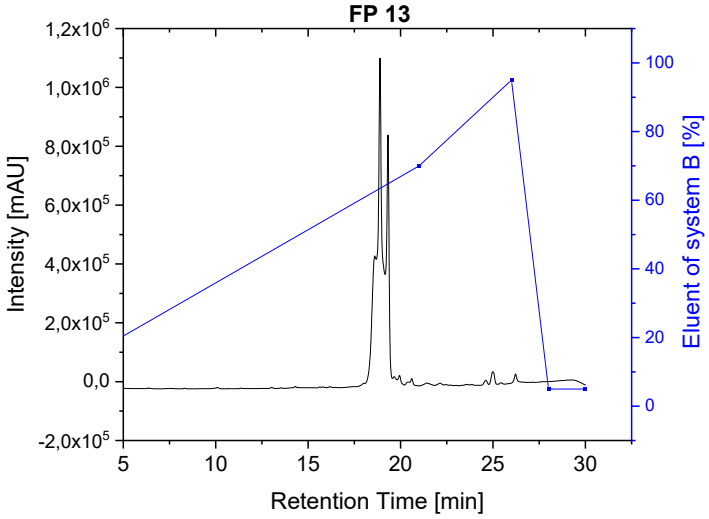

***Figure 133**: Analytical HPLC of FP 13, Nucleosil C18 (5 µm, 4.6 mm x 25 mm), H_2O with 0.1% TFA (system A) / 80% MeCN-20% H_2O and 0.1 % TFA (system B), 1 mL/min, 0.02 min - 5% eluent of system B, 21 min - 70% eluent of system B.*

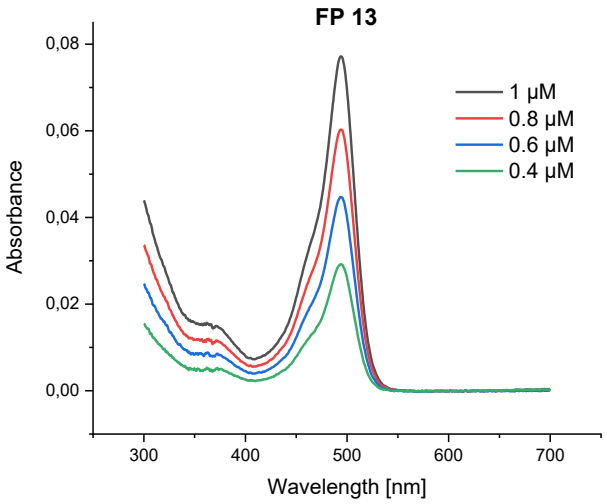

***Figure 134**: Absorption spectra of FP 13 in 4 different concentrations, PBS (pH=7.4)*

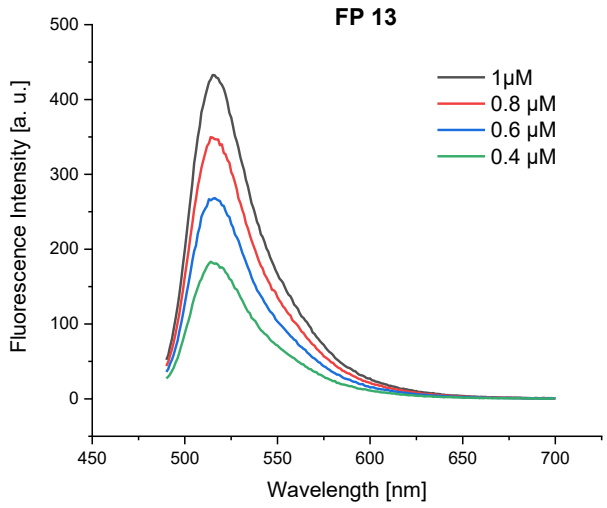

***Figure 135**: Fluorescence spectra of FP 13 in 4 different concentrations, PBS (pH=7.4), Excitation wavelength: 480 nm*

9.18 N-Boc-Cystine di-t-Boc

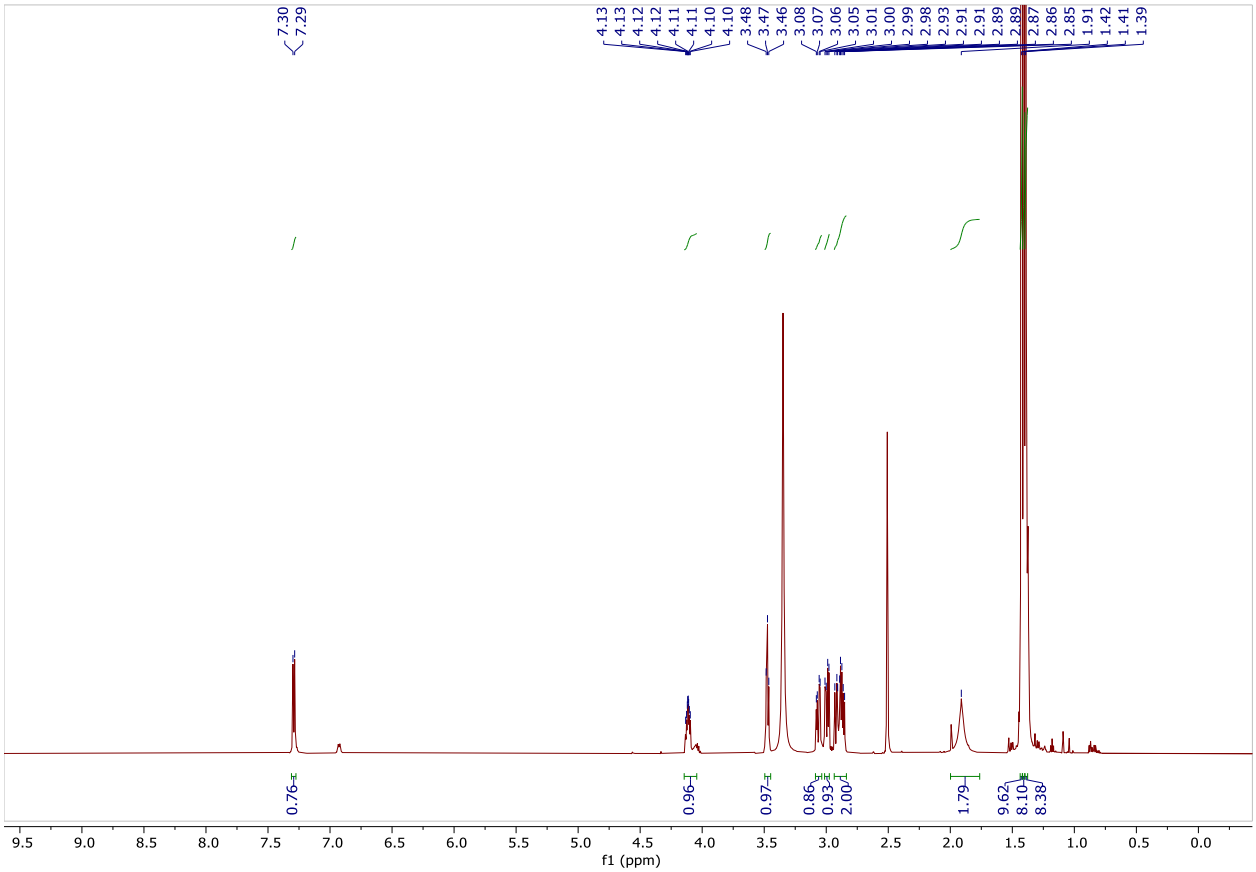

***Figure 136**: [1]H-NMR of N-Boc-Cystine di-t-But, 600 MHz, DMSO-d_6*

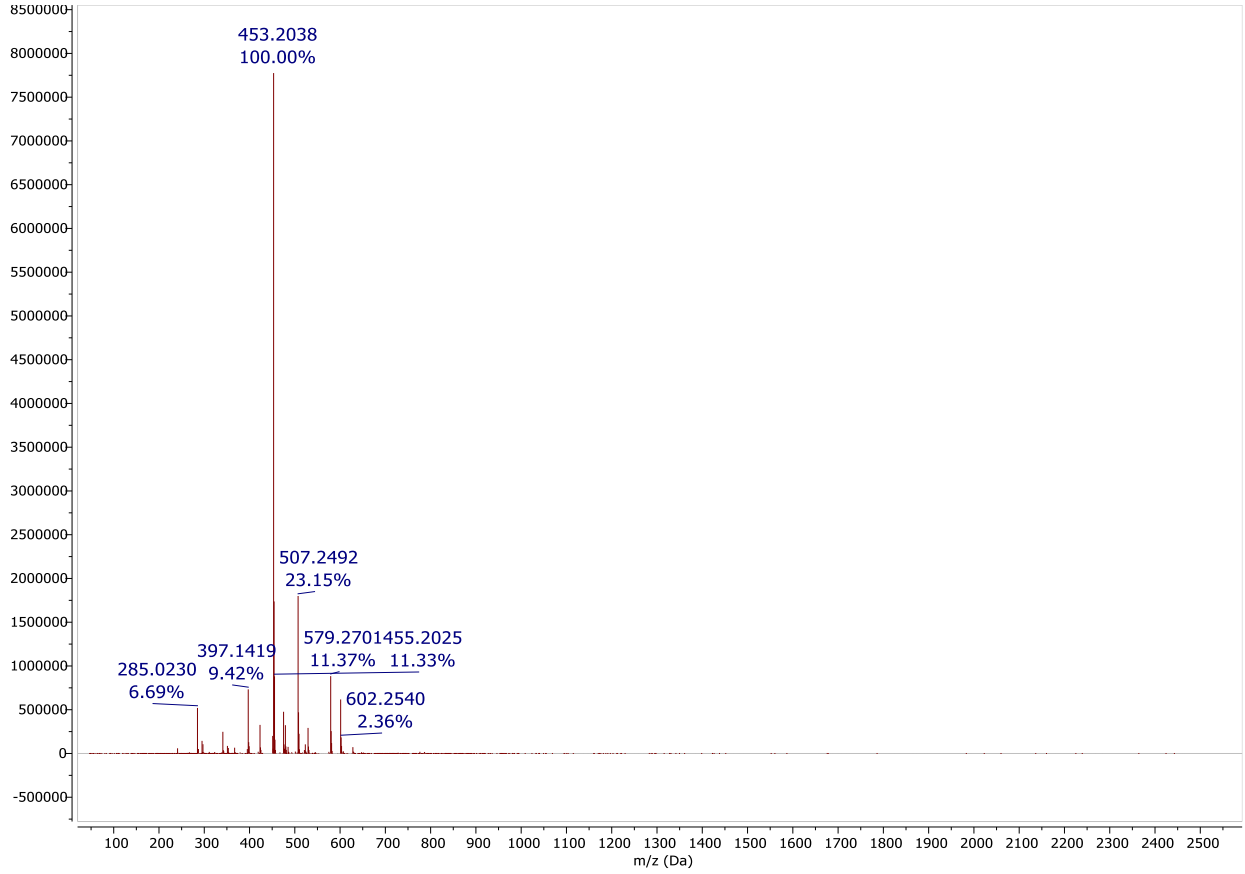

***Figure 137**: ESI MS of N-Boc-Cystine di-t-But, positive mode*

9.19 Fol-cystine

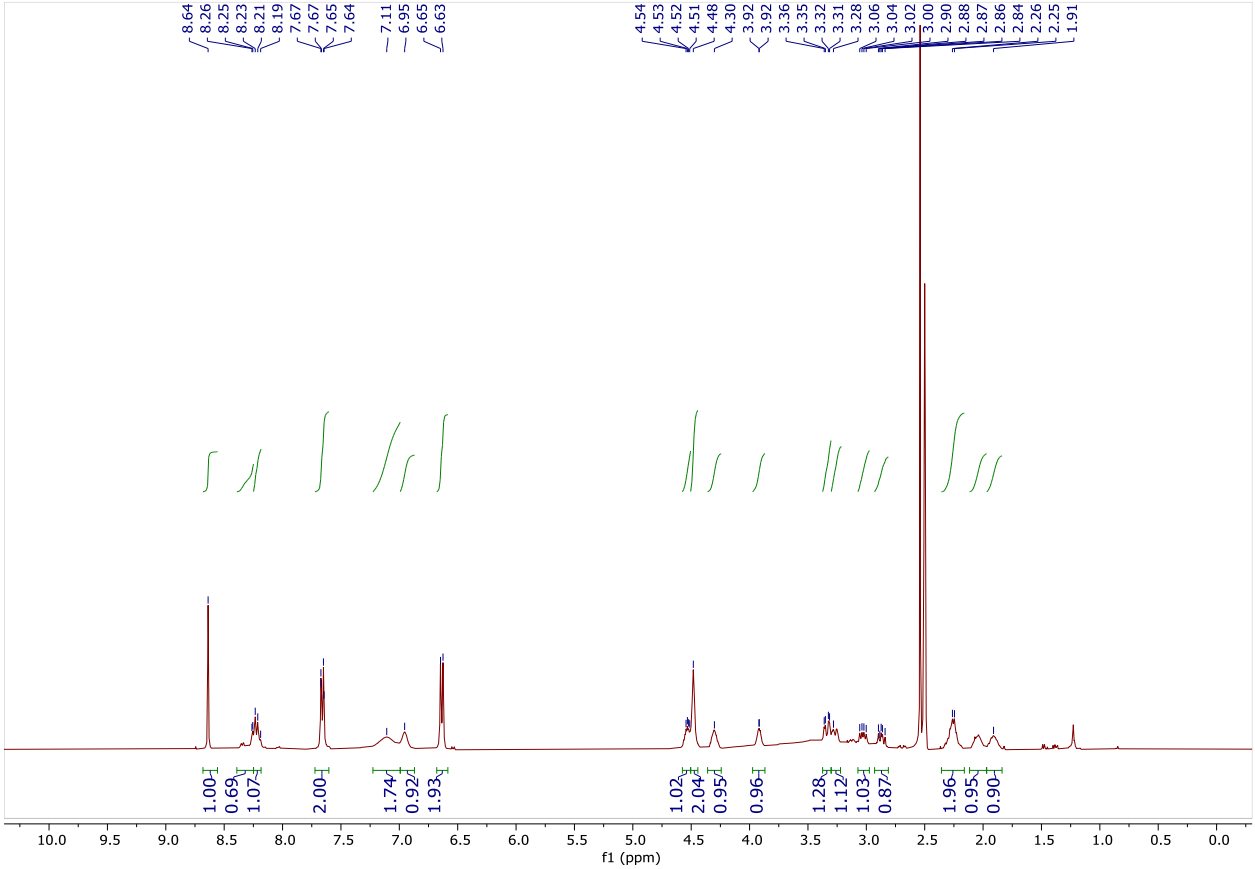

***Figure 138**: [1]H-NMR of γ-isomer of Fol-cystine, 400 MHz, DMSO-d_6*

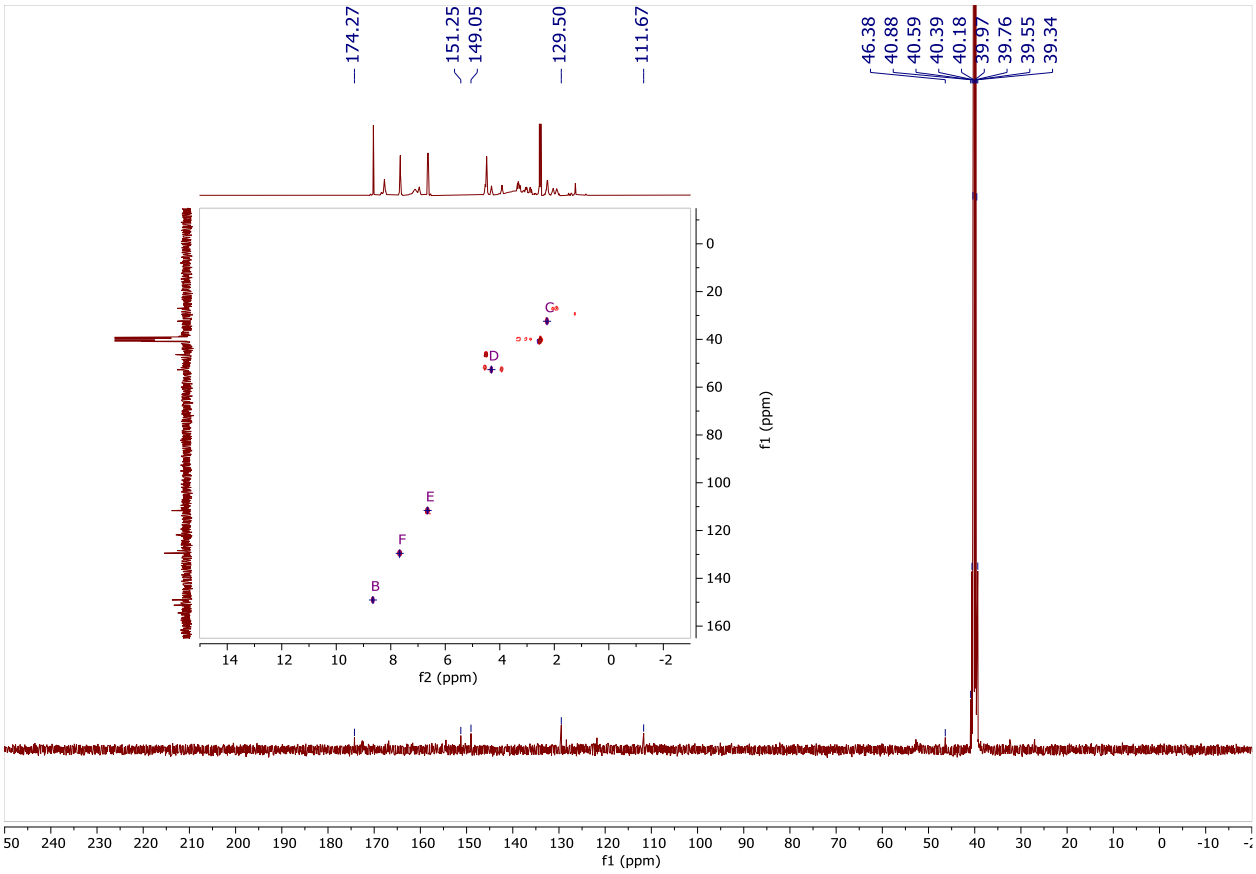

***Figure 139**: [13]C-NMR of Fol-cystine, 101MHz, DMSO-d_6 with a 2D HSQC spectrum inset showing proton-carbon correlations.*

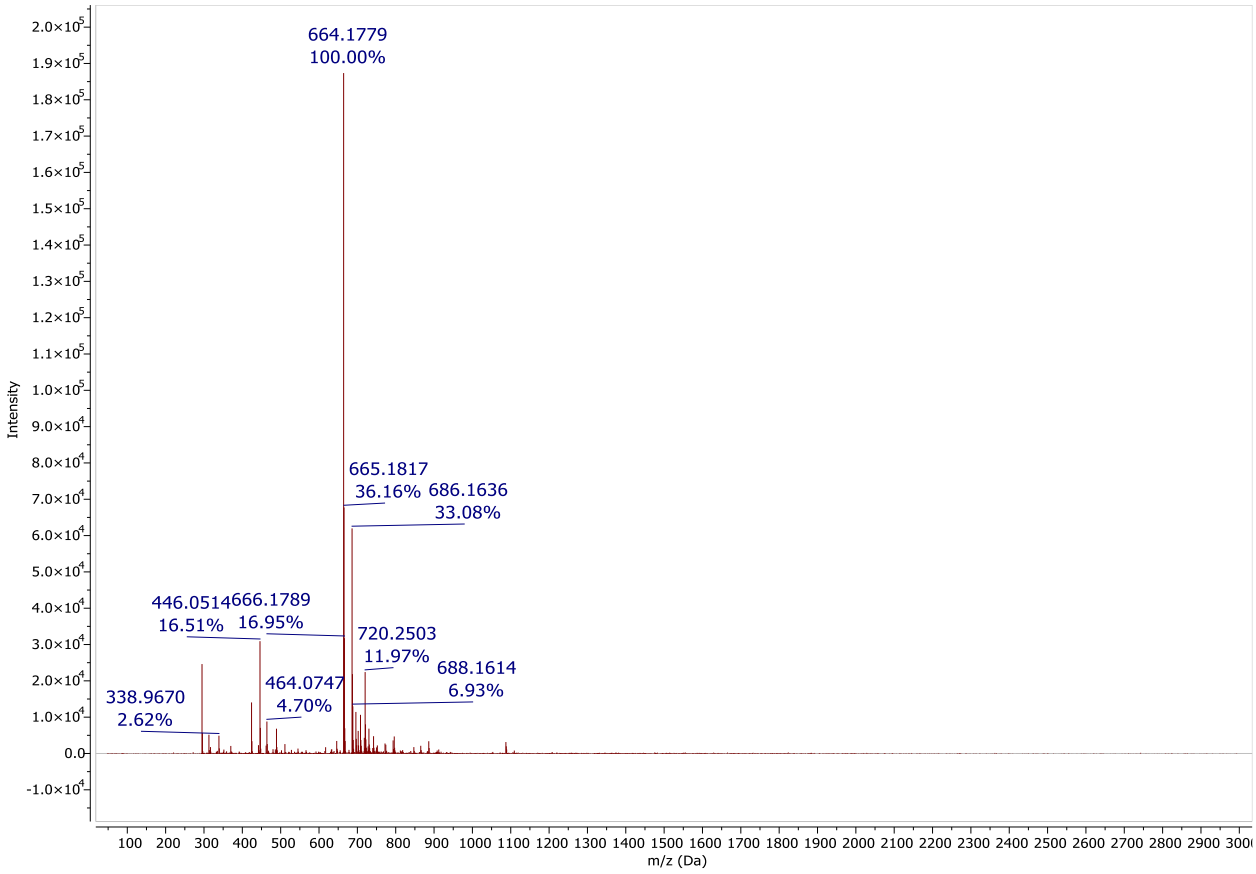

***Figure 140**: ESI MS of Fol-cystine, positive mode*

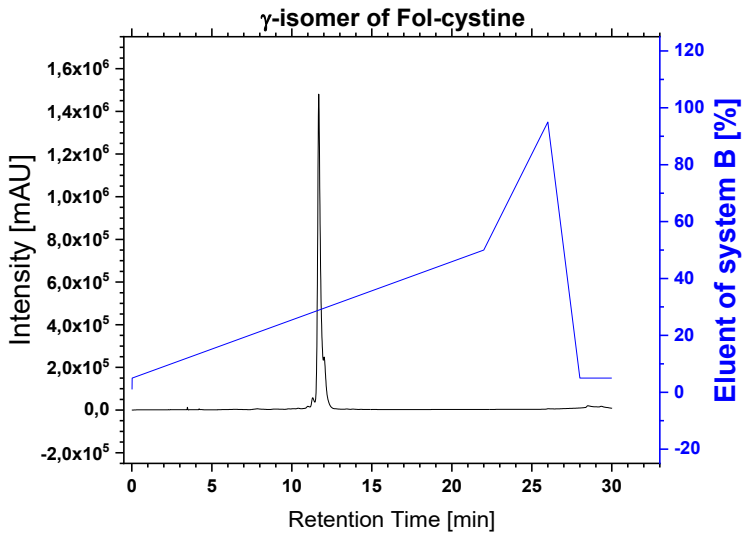

***Figure 141**: Analytical HPLC of Fol-cystine, Nucleosil C18 (5 µm, 4.6 mm x 25 mm), H_2O with 0.1% TFA (system A) / 80% MeCN-20% H_2O and 0.1 % TFA (system B), 1 mL/min, 0.02 min - 5% eluent of system B, 22 min - 50% eluent of system B (t_R =11.7 min).*

9.20 FP 14

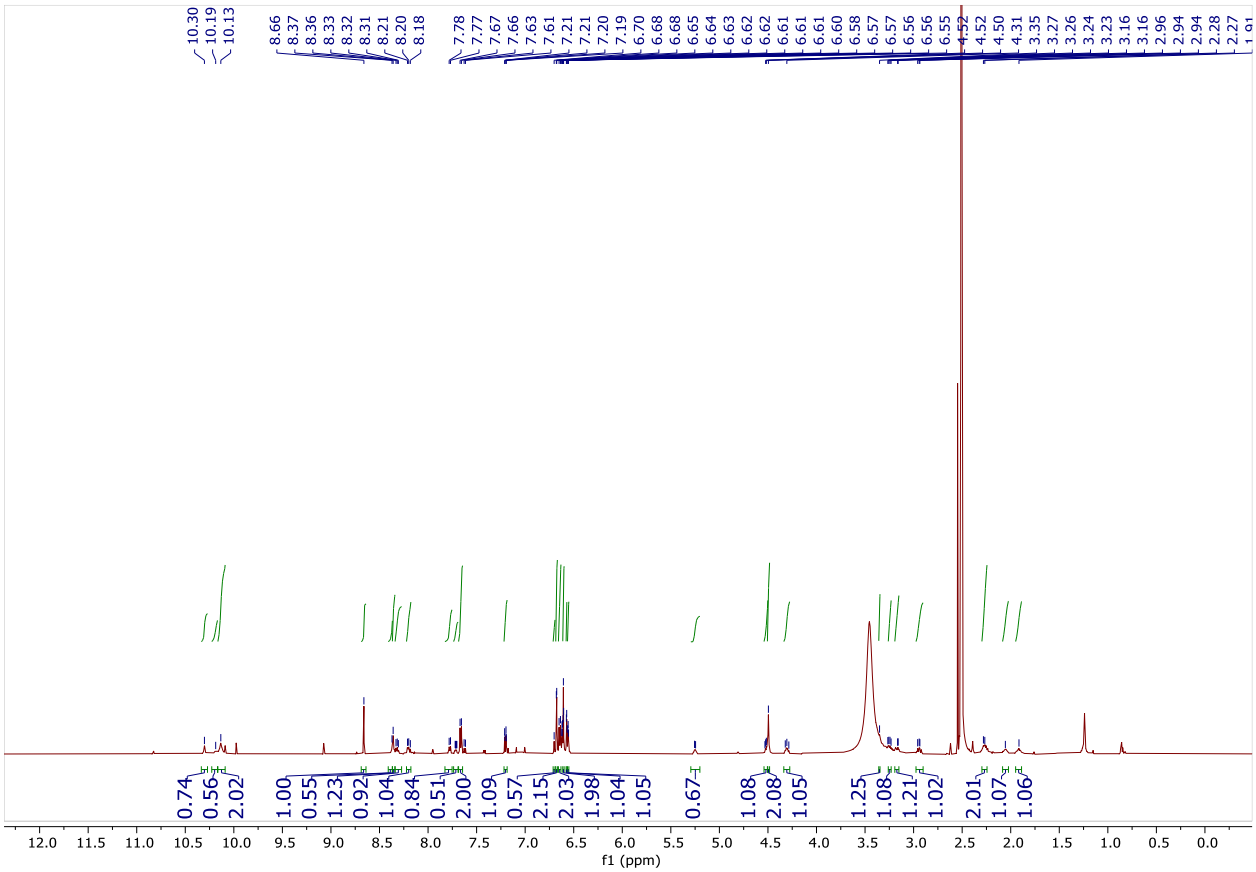

***Figure 142**: [1]H-NMR of FP 14, 600 MHz, DMSO-d_6*

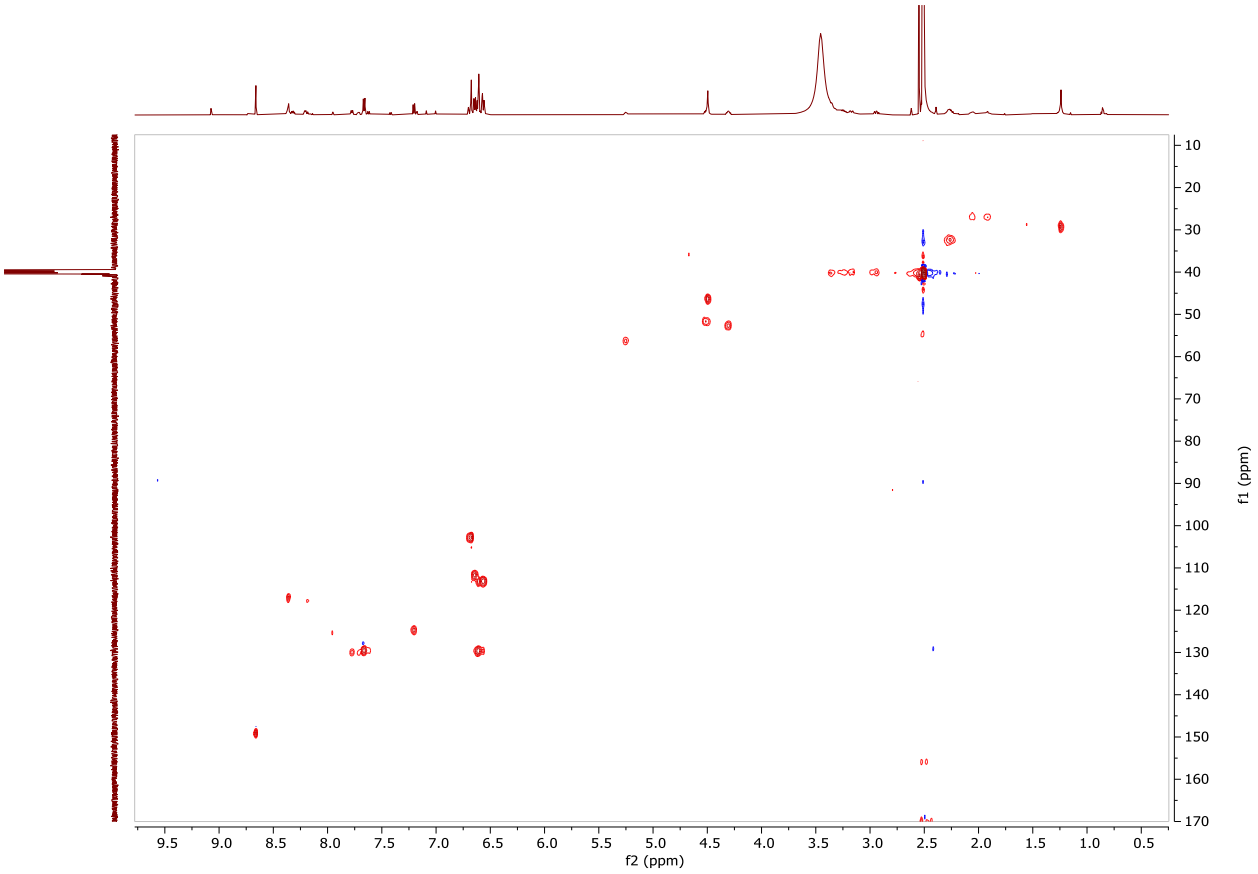

***Figure 143**: (^{1}H, ^{13}C) COSY - NMR of FP 14 in DMSO-d_6*

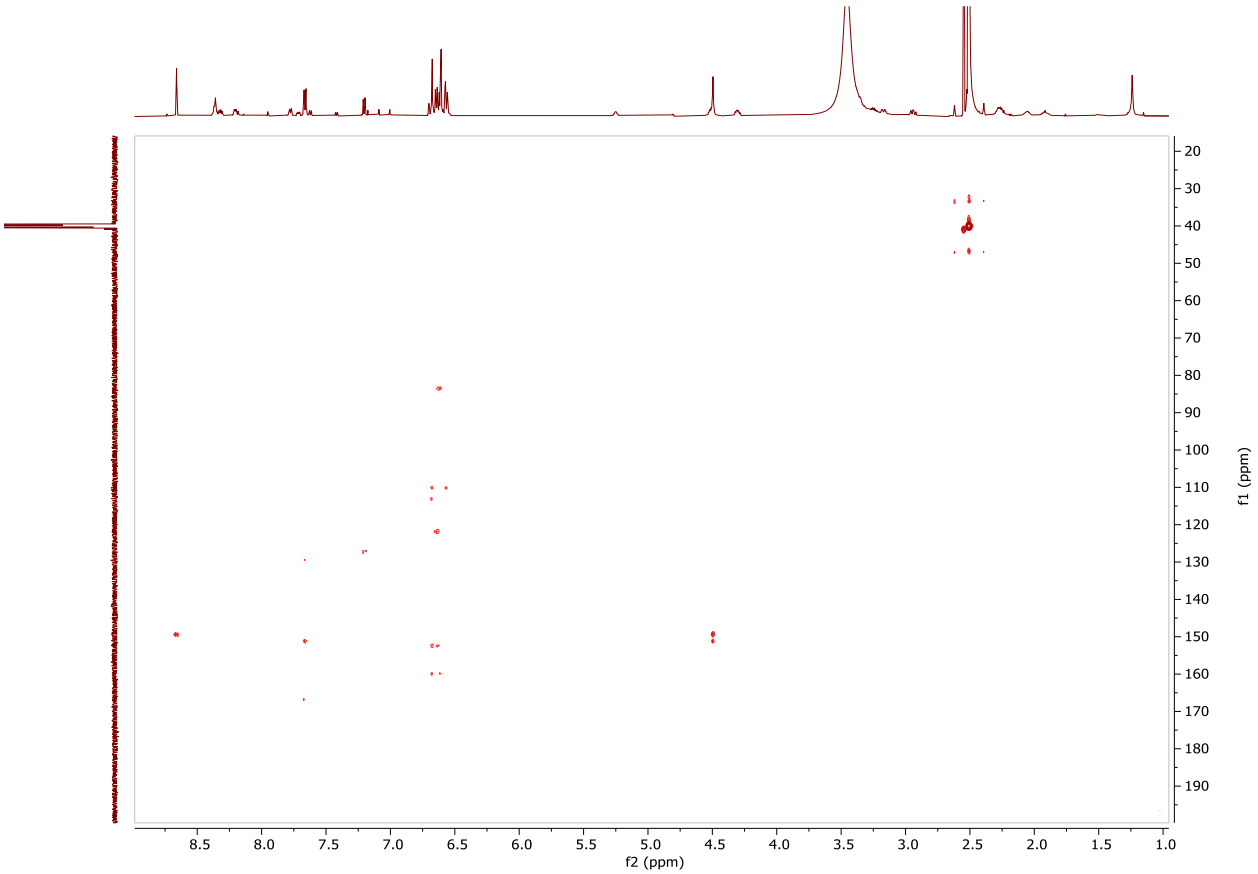

***Figure 144**: (^{1}H, ^{13}C) HMBC - NMR of FP 14 in DMSO-d_6*

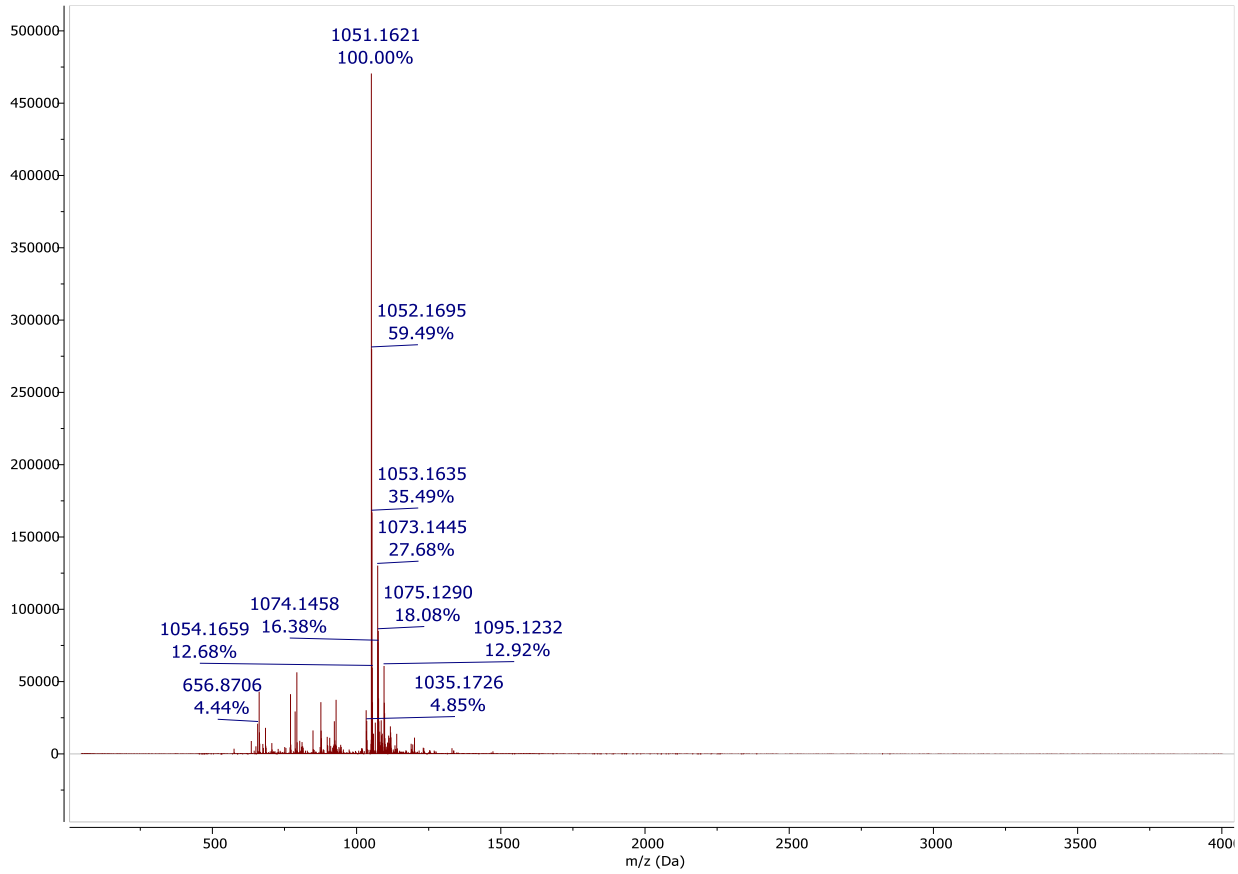

***Figure 145**: ESI MS of FP 14, negative mode*

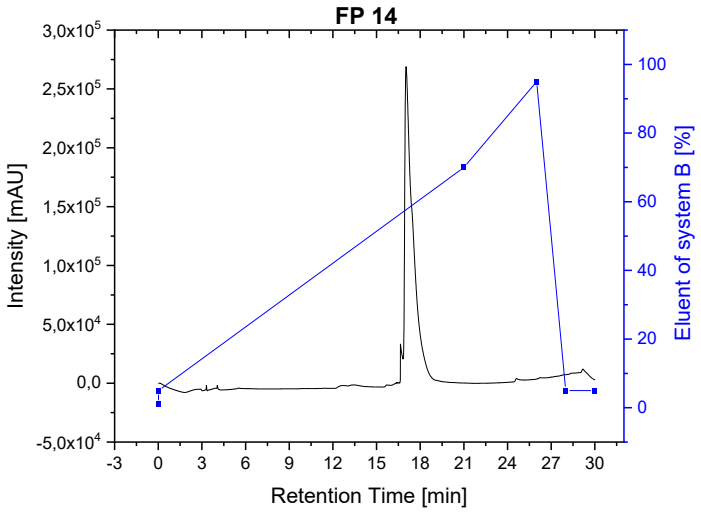

***Figure 146**: Analytical HPLC of FP 14, Nucleosil C18 (5 µm, 4.6 mm x 25 mm), H_2O with 0.1% TFA (system A) / 80% MeCN-20% H_2O and 0.1 % TFA (system B), 1 mL/min, 0.02 min - 5% eluent of system B, 21 min - 70% eluent of system B (t_R =17.1 min).*

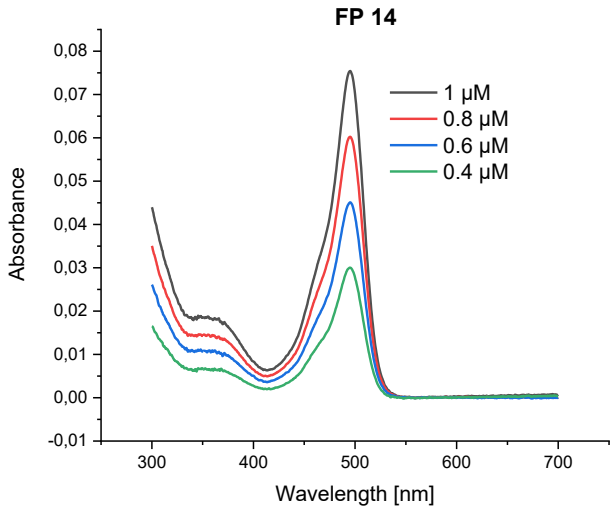

***Figure 147**: Absorption spectra of FP 14 in 4 different concentrations, PBS (pH=7.4)*

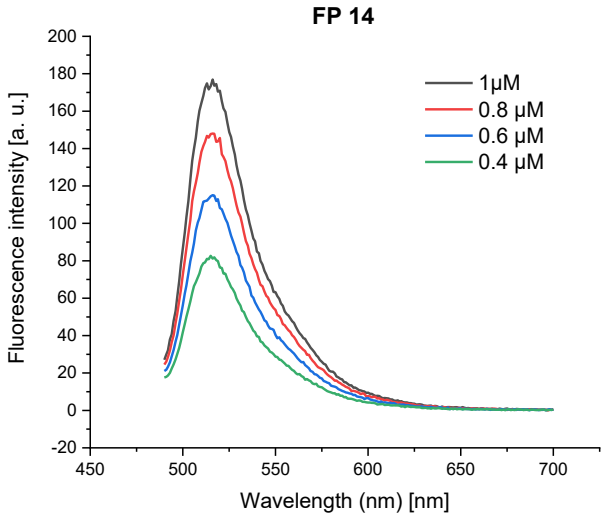

***Figure 148**: Fluorescence spectra of FP 14 in 4 different concentrations, PBS (pH=7.4), Excitation wavelength: 480 nm*

9.21 FP 15

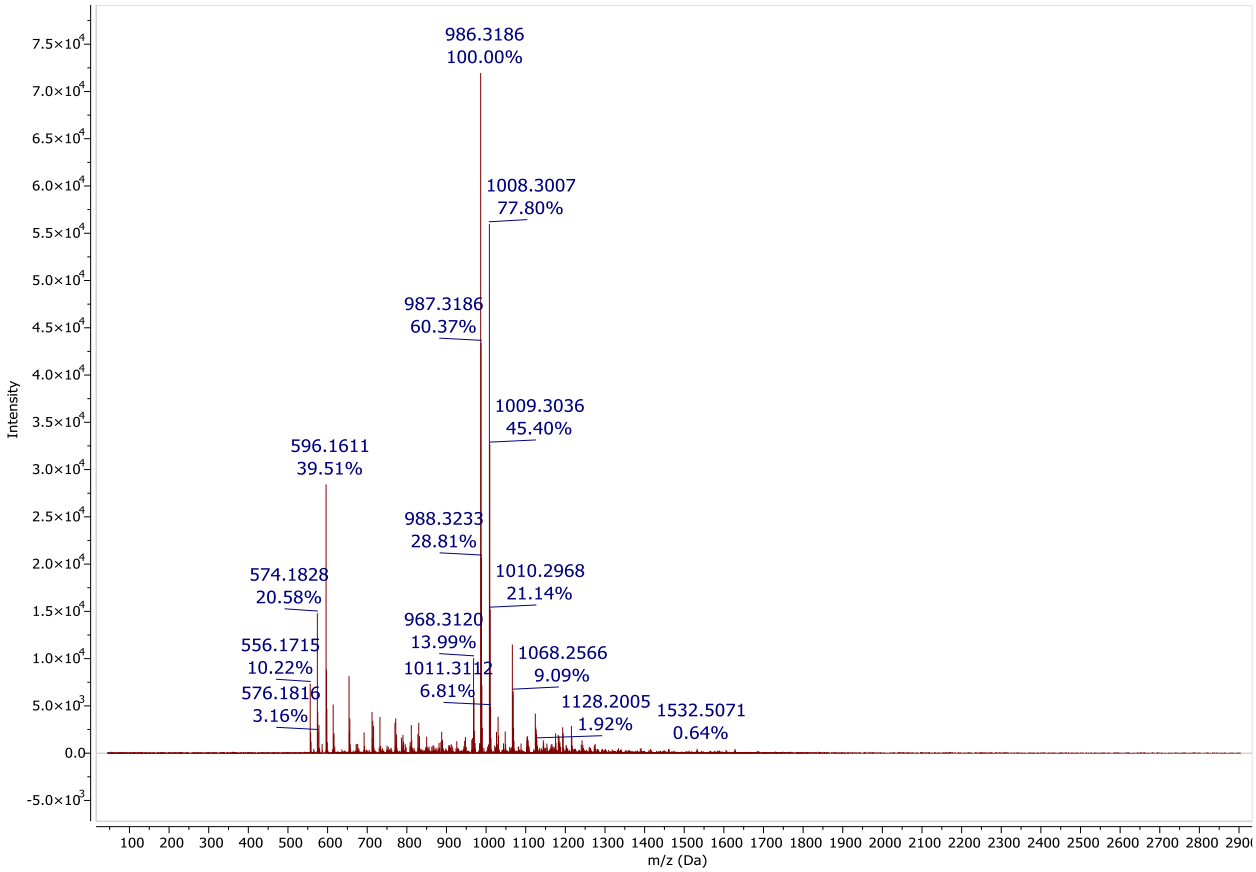

***Figure 149**: ESI MS of FP 15, negative mode*

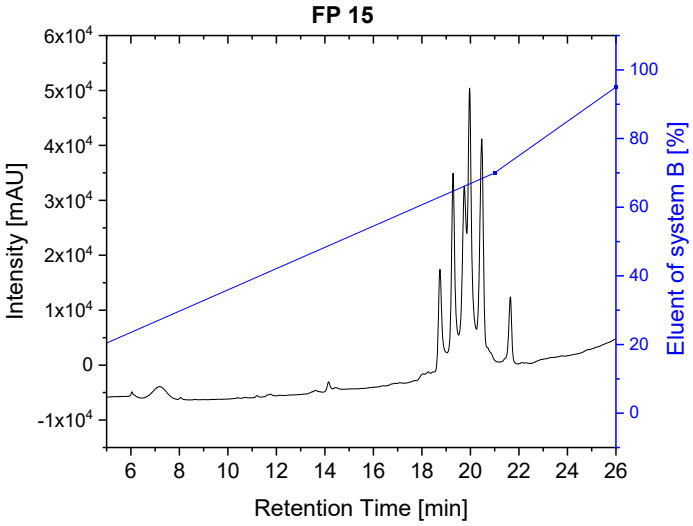

***Figure 150**: Analytical HPLC of α and γ isomers of FP 15, Nucleosil C18 (5 µm, 4.6 mm x 25 mm), H_2O with 0.1% TFA (system A) / 80% MeCN-20% H_2O and 0.1 % TFA (system B), 1 mL/min, 0.02 min - 5% eluent of system B, 21 min - 70% eluent of system B.*

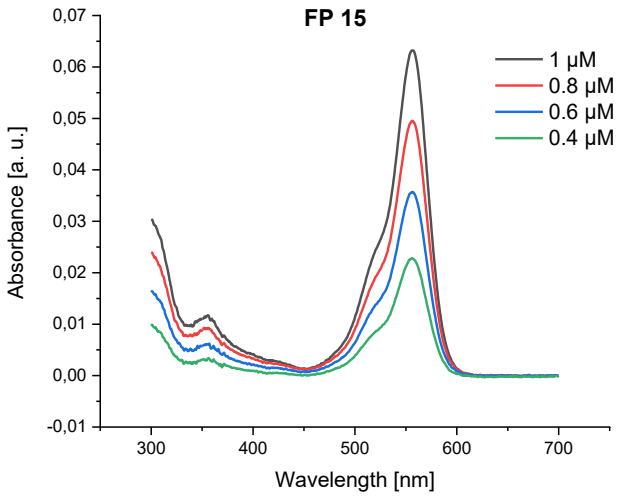

***Figure 151**: Absorption spectra of FP 15 in 4 different concentrations, PBS (pH=7.4)*

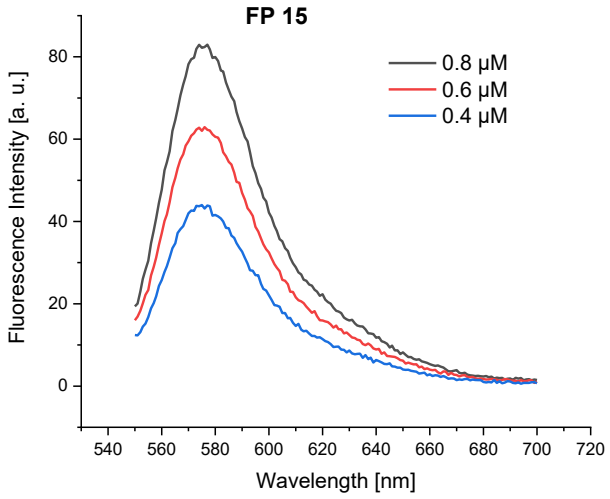

***Figure 152**: Fluorescence spectra of FP 15 in 3 different concentrations, PBS (pH=7.4), Excitation wavelength: 540 nm*

9.22 Compound 16

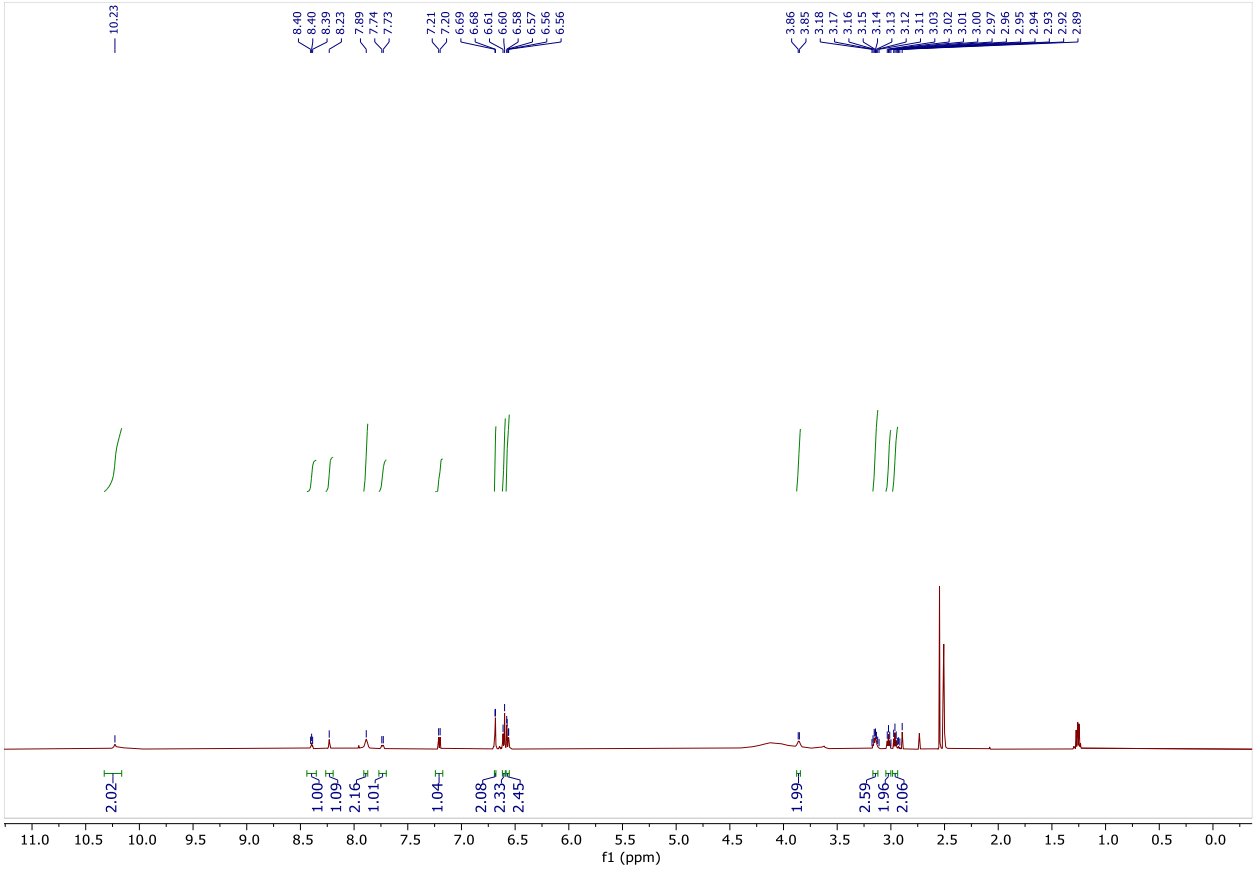

***Figure 153**: [1]H-NMR of 16, 600 MHz, DMSO-d_6*

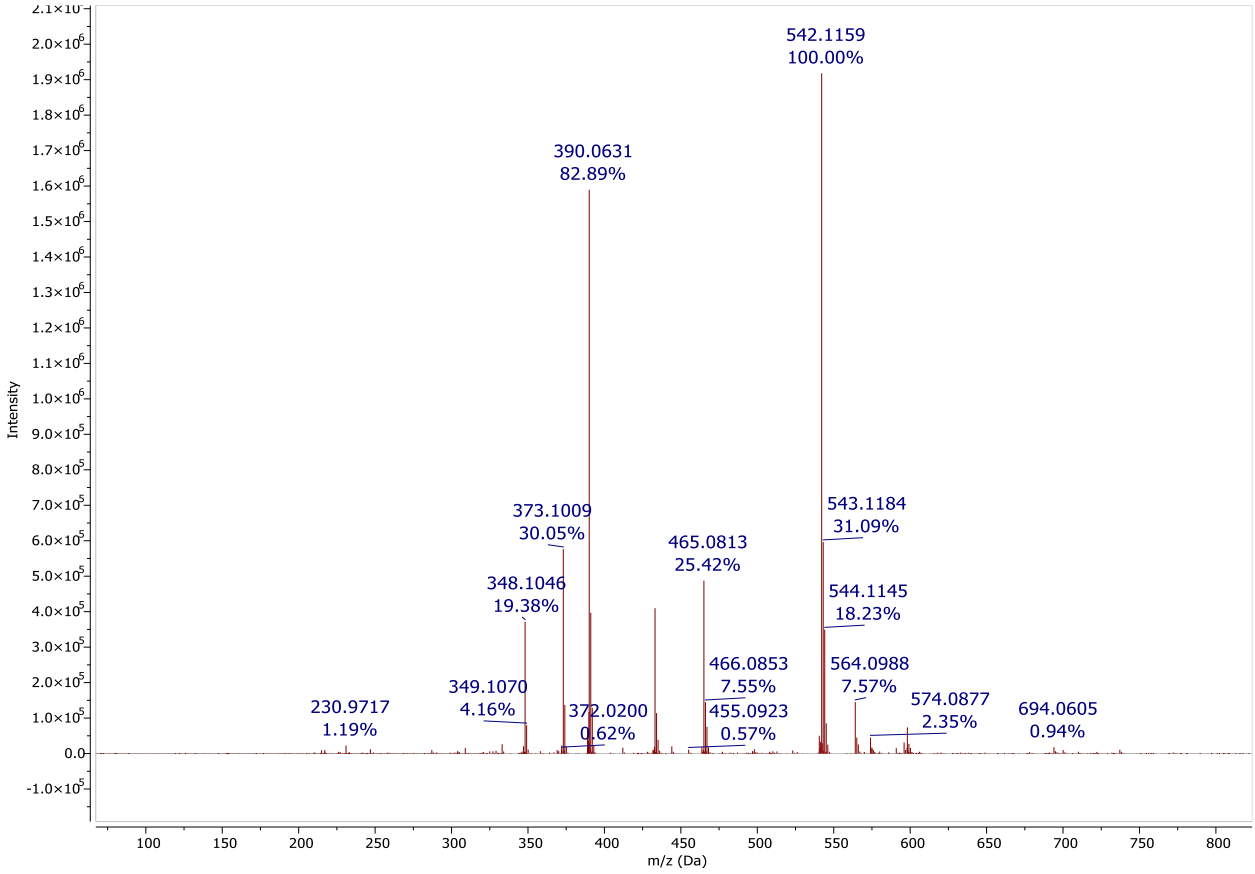

***Figure 154**: ESI MS of 16, positive mode*

9.23 Compound 17

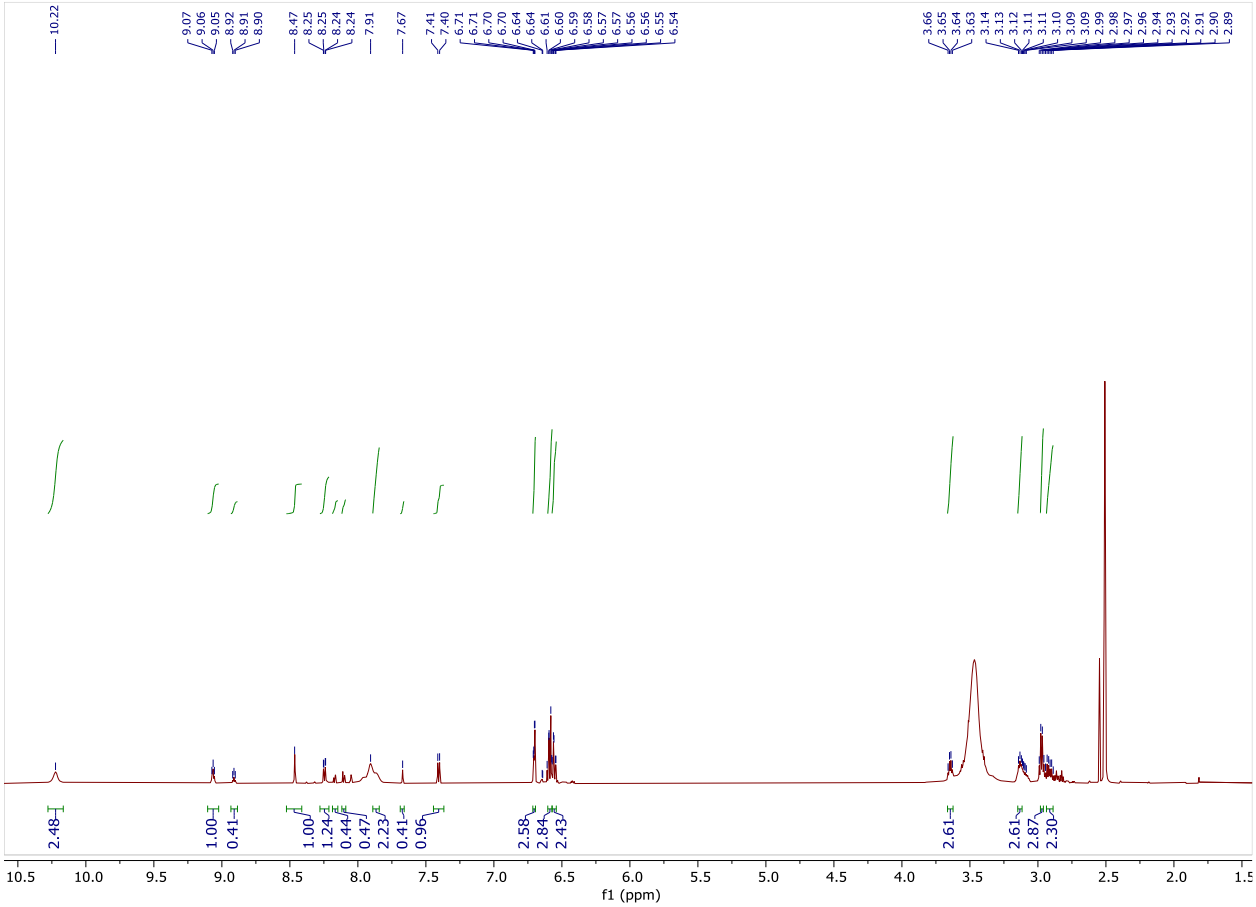

***Figure 155**: [1]H-NMR of 17, 600 MHz, DMSO-d_6. Additional peaks observed in the proton NMR spectrum, with lower integral values relative to the main peaks, are attributed to the presence of the 5- and 6-isomers of carboxyfluorescein, which exhibit distinct chemical shifts due to differences in their molecular environments.*

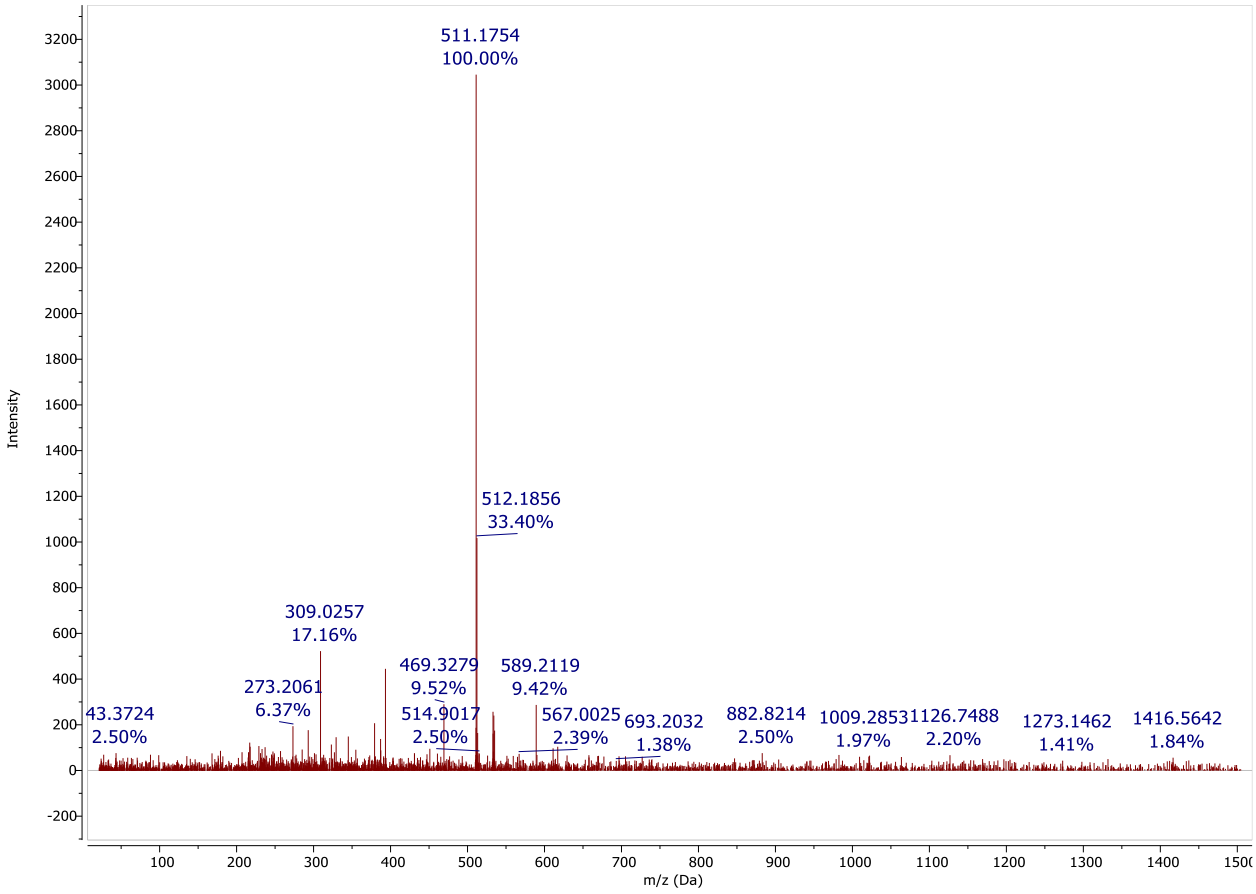

***Figure 156**: ESI MS of 17, positive mode*

9.24 FP 18

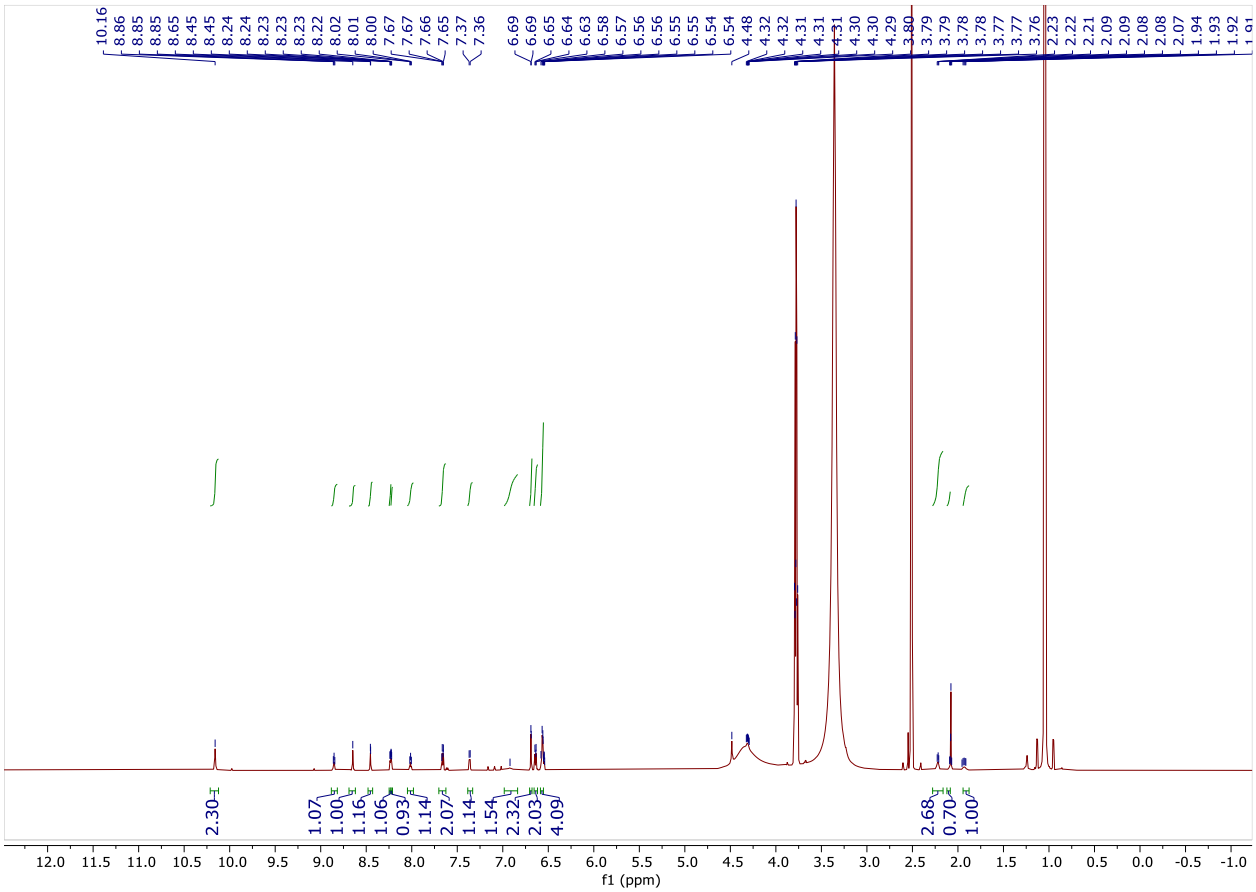

***Figure 157**: [1]H NMR of FP 18, 700 MHz-DMSO-d_6. The peak at 1.05 ppm and 3.78 ppm corresponds to isopropanol, which was used as a reference to determine the concentration of the product in the NMR tube. The analyte peaks at 3.35 ppm and 3.25 ppm overlap with the H_2O peak of the solvent. Additionally, the analyte peak at 4.30 ppm overlaps with the OH signal of isopropanol.*

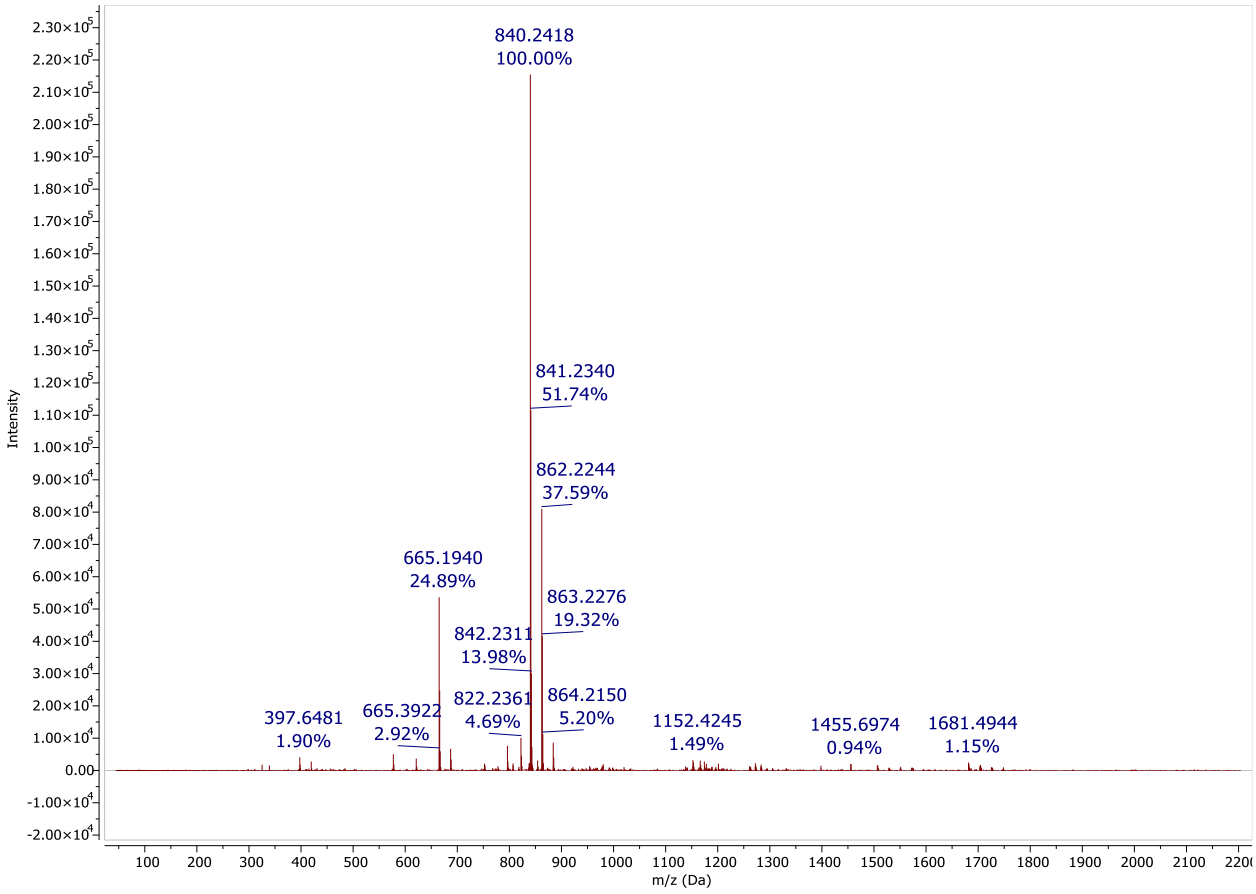

***Figure 158**: ESI MS of FP 18, negative mode*

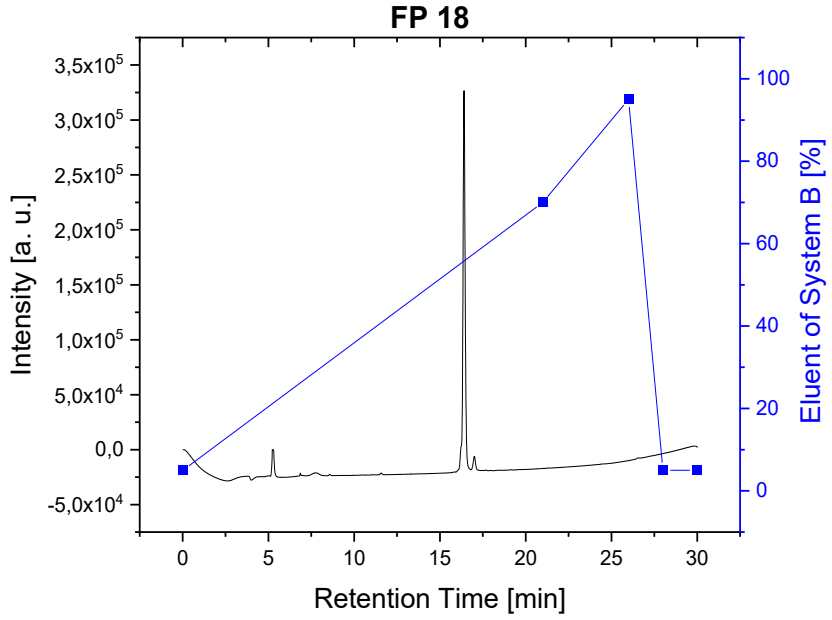

***Figure 159**: Analytical HPLC chromatograms of FP 18 with separated γ isomer. HPLC conditions: Nucleosil C18 column (5 µm, 4.6 mm x 25 mm); Mobile phase: (A) H_2O with 0.1% TFA, (B) 80% MeCN-20% H_2O with 0.1% TFA; Flow rate: 1 mL/min; Gradient: 5% eluent of system B at 0.02 min to 70% eluent of system B at 21 min (t_R=16.4 min)*

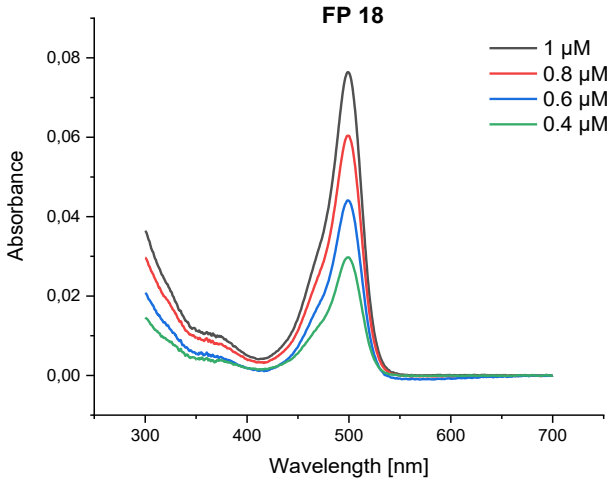

***Figure 160**: Absorption spectra of FP 18 in 4 different concentrations, PBS (pH=7.4)*

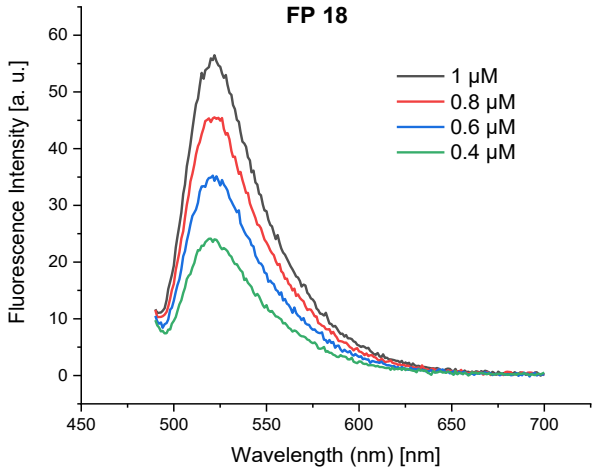

***Figure 161**: Fluorescence spectra of FP 18 in 4 different concentrations, PBS (pH=7.4), Excitation wavelength: 480 nm.*

9.25 FoI-6AF (FP 19)

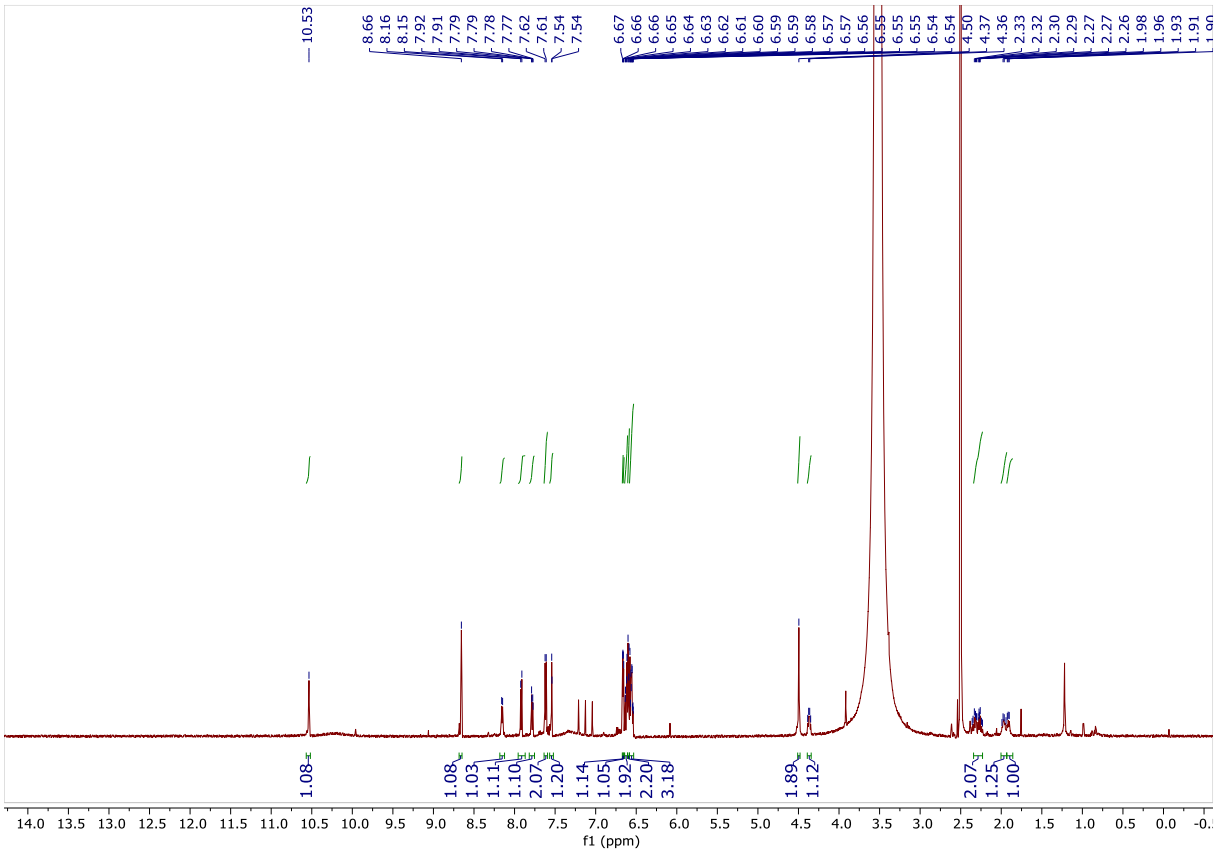

***Figure 162**: [1]H-NMR of FoI-6AF (FP 19), 600 MHz, DMSo-d_6, the peak at 2.50 ppm corresponds to the DMSO-d_6 solvent. The peak at 3.35 ppm is attributed to the water peak present in DMSO.*

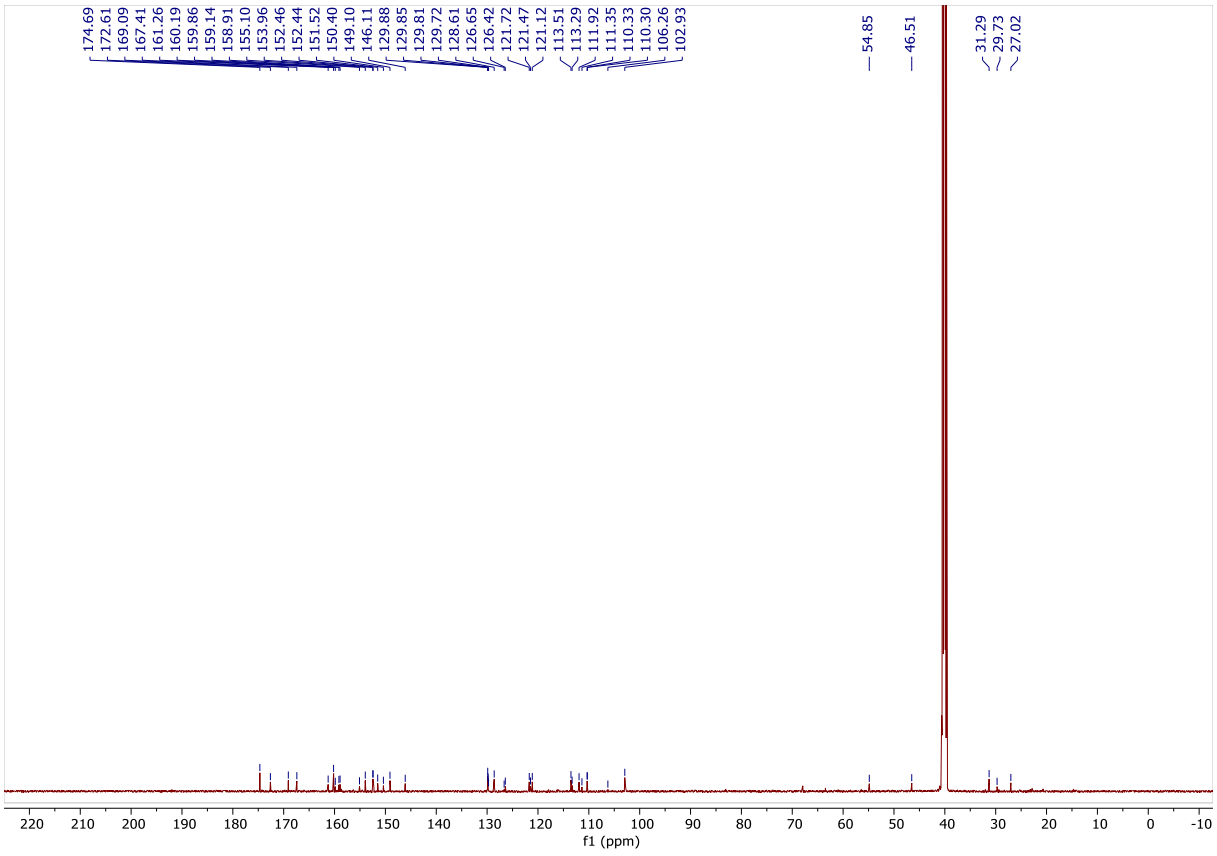

***Figure 163**:[13]C- NMR of FoI-6AF (FP 19), 151 MHz, DMSO-d_6.*

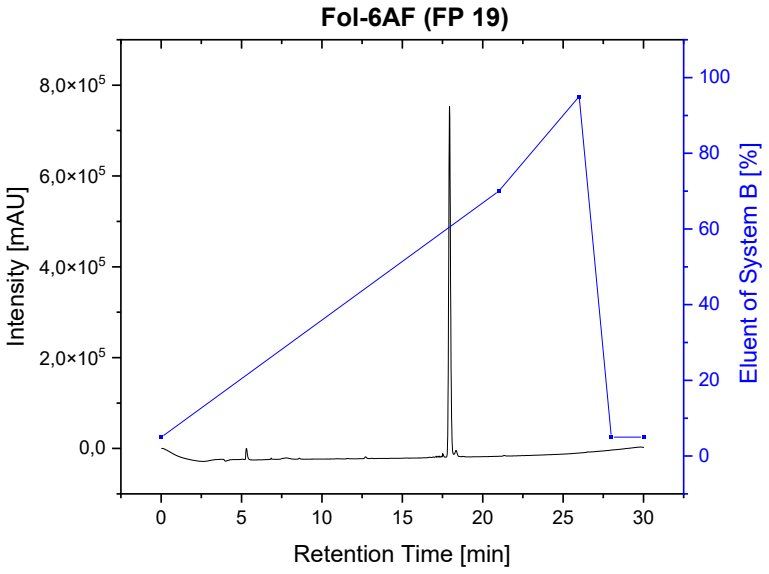

***Figure 164**:Analytical HPLC of FoI-6AF (FP 19), Nucleosil C18 (5 µm, 4.6 mm x 25 mm), H_2O with 0.1% TFA (system A) / 80% MeCN-20% H_2O and 0.1 % TFA (system B), 1 mL/min, 0.02 min - 5% eluent of system B, 21 min - 70% eluent of system B, t_R = 17.9 min.*

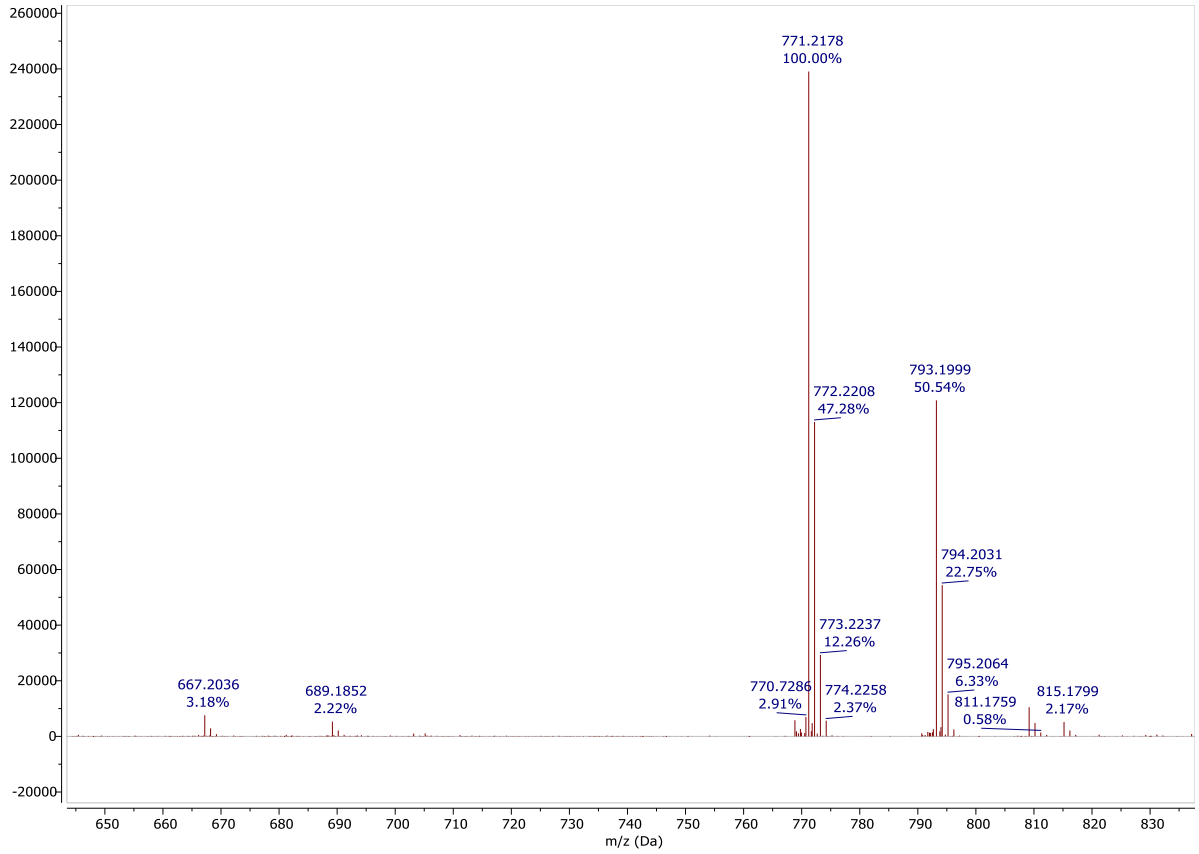

***Figure 165**: HR-ESI MS of Fol-6AF (FP 19), positive mode*

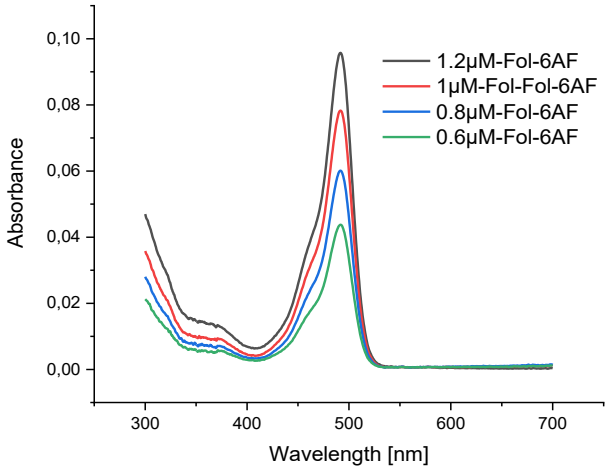

***Figure 166**: Absorption spectra of Fol-6AF (FP 19) in 4 different concentrations, PBS (pH=7.4)*

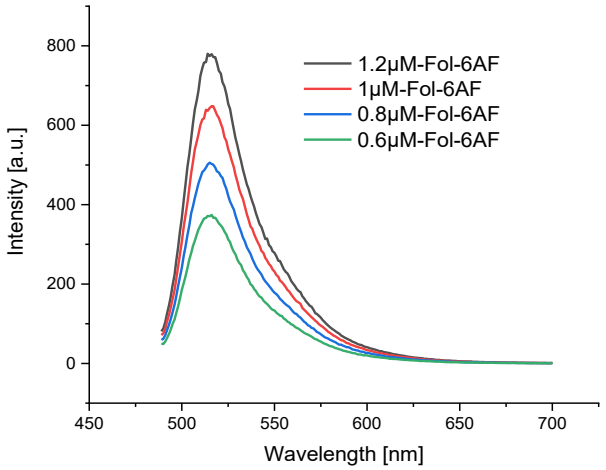

***Figure 167**: Fluorescence emission spectra of Fol-6AF (FP 19) in 4 different concentrations, PBS (pH=7.4), Excitation wavelength: 480 nm.*

9.26 Fol-5AF (FP 20)

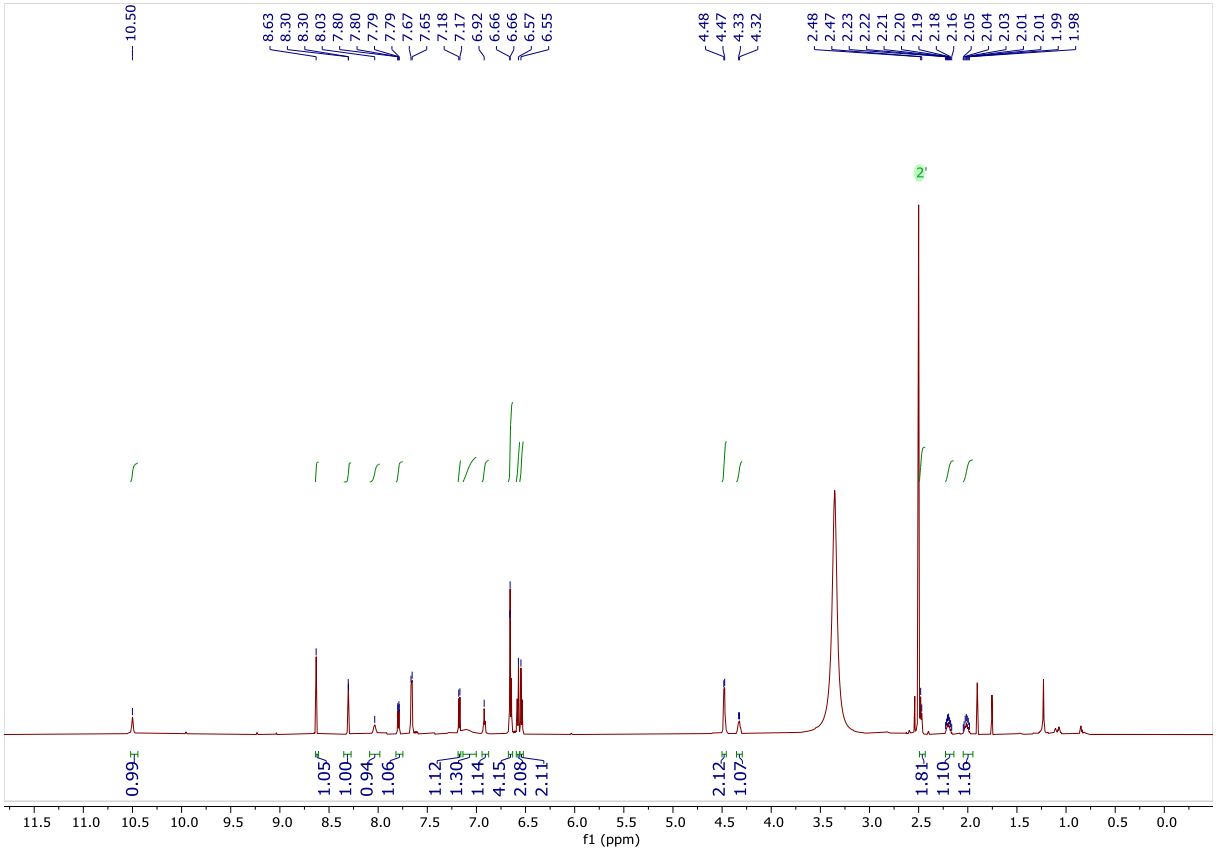

***Figure 168**: [1]H-NMR of Fol-5AF (FP 20), 700 MHz, DMSO-d_6. The aliphatic region of the spectrum exhibits additional signals due to the presence of acetate counter ions in the product.*

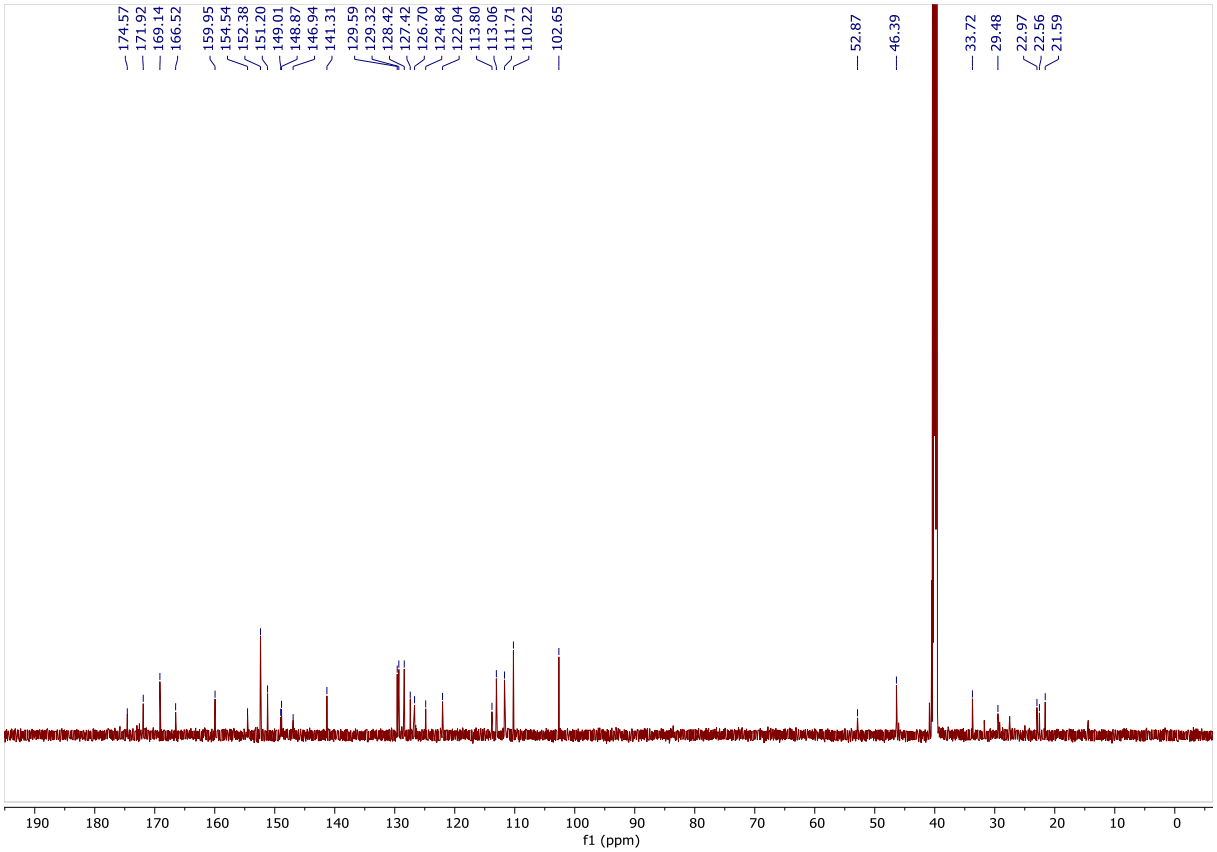

Figure 169: *^{13}C-NMR of Fol-5AF (FP 20), 176 MHz, DMSO-d_6, the aliphatic region of the spectrum exhibits additional signals due to the presence of acetic acid counter ions in the product.*

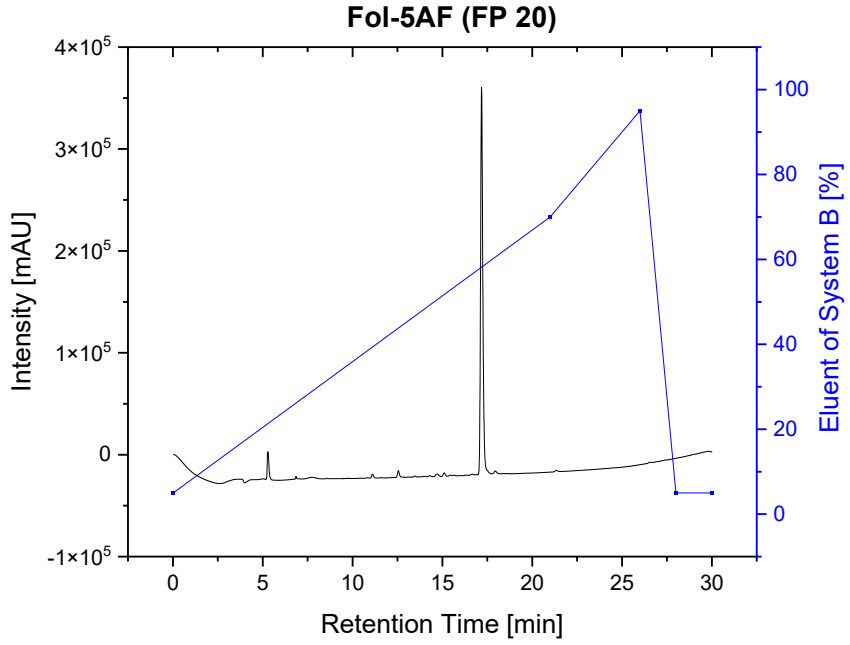

Figure 170: *Analytical HPLC of Fol-5AF (FP 20), Nucleosil C18 (5 µm, 4.6 mm x 25 mm), H_2O with 0.1% TFA (system A) / 80% MeCN-20% H_2O and 0.1 % TFA (system B), 1 mL/min, 0.02 min - 5% eluent of system B, 21 min - 70% eluent of system B, t_R = 17.1 min.*

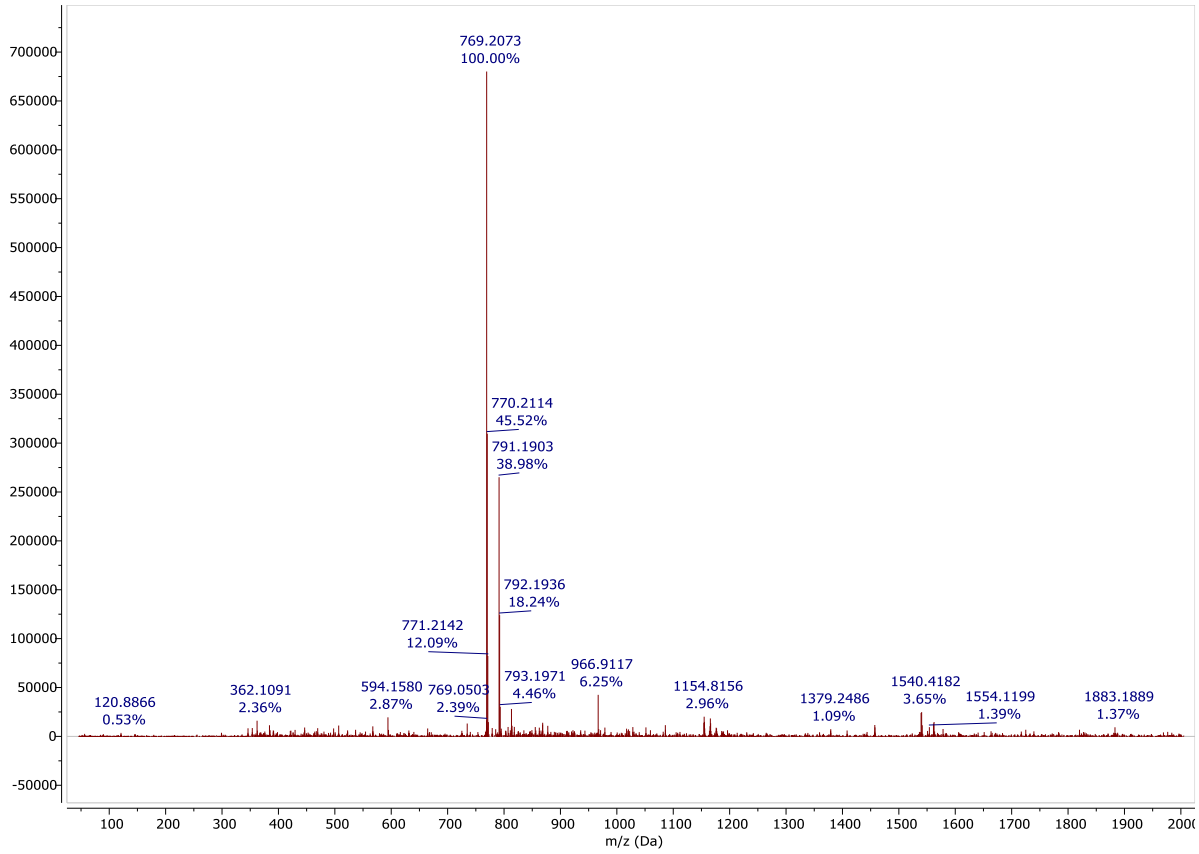

***Figure 171**: HR-ESI MS of FoI-5AF (FP 20), negative mode*

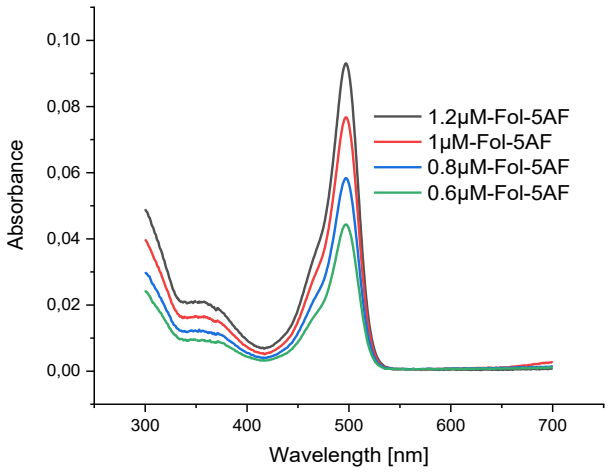

***Figure 172**: Absorption spectra of FoI-5AF (FP 20) in 4 different concentrations, PBS (pH=7.4).*

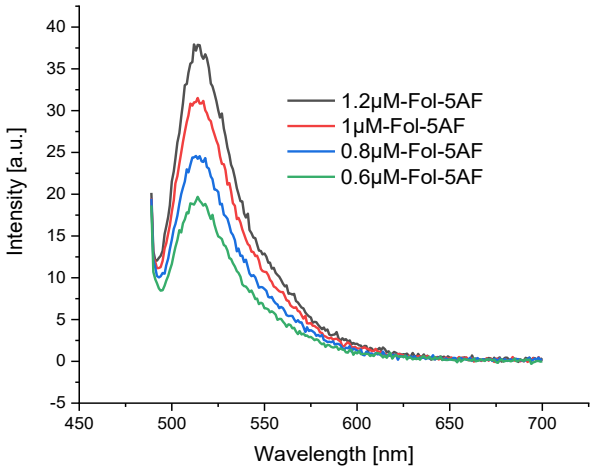

***Figure 173**: Fluorescence emission spectra of Fol-5AF (FP 20) in 4 different concentrations, PBS (pH=7.4), Excitation wavelength: 480 nm.*

9.27 βAla-5AF

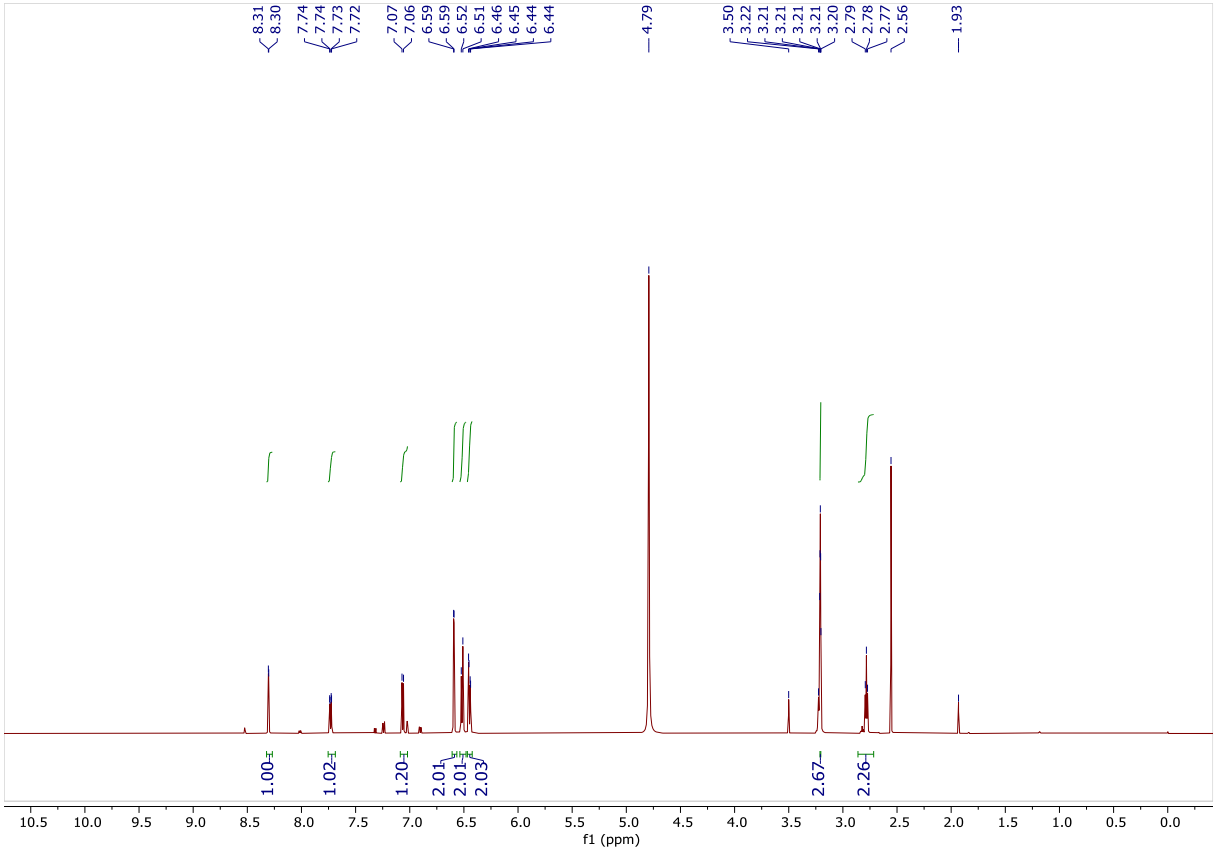

***Figure 174**: ^{1}H-NMR of βAla-5AF, 600 MHz, Methanol-d$_4$. The peak at 2.55 ppm corresponds to residual DMSO from the synthesis process. The peaks at 3.31 ppm and 4.78 ppm are attributed to methanol-d$_4$. The analyte peak at 3.31 ppm overlaps with the solvent peak. The peaks at 1.93 ppm and 3.50 ppm correspond to residual diisopropyl ether from the reaction workup.*

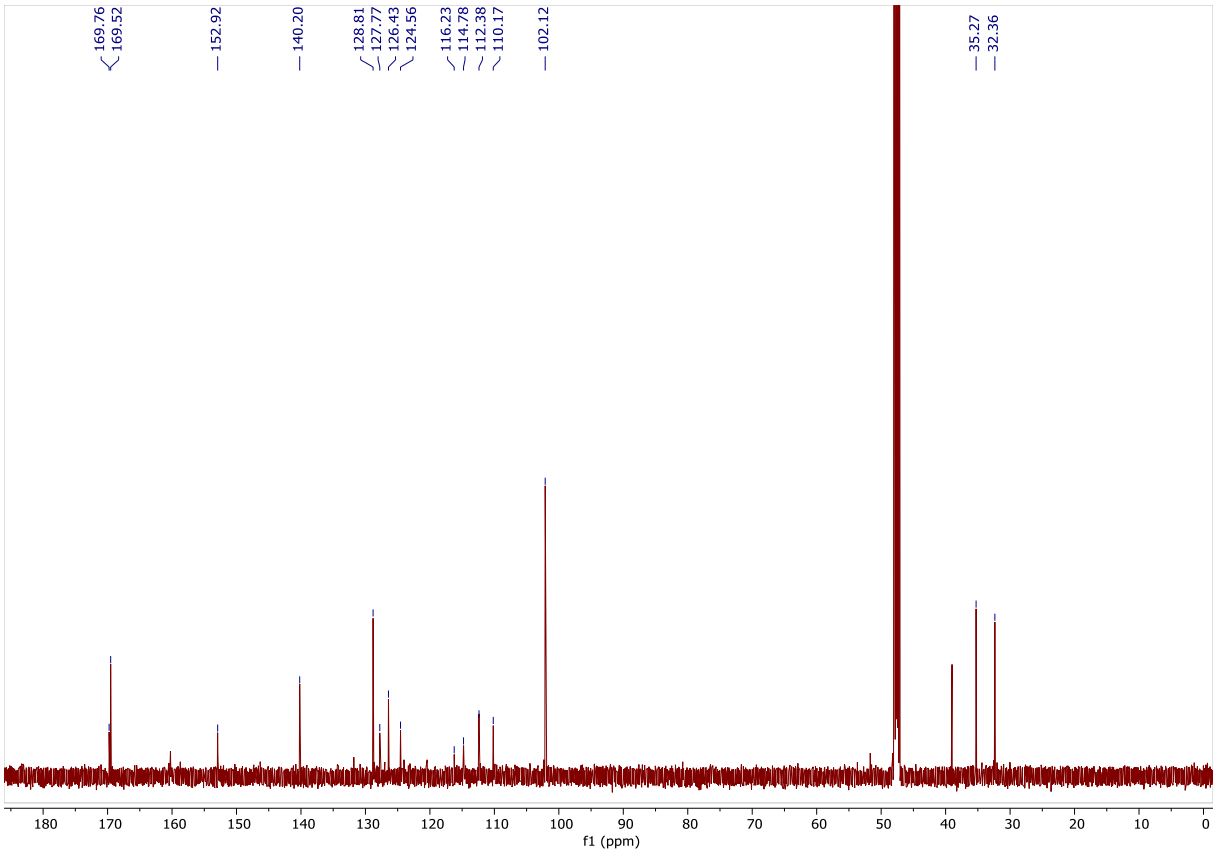

***Figure 175**: ^{13}C- NMR of βAla-5AF, 151 MHz, methanol-d_4. The peak at 39.5 ppm corresponds to DMSO, a residual solvent from the synthesis process. The peak at 51.8 ppm is attributed to the carbon of methanol-d_4.:*

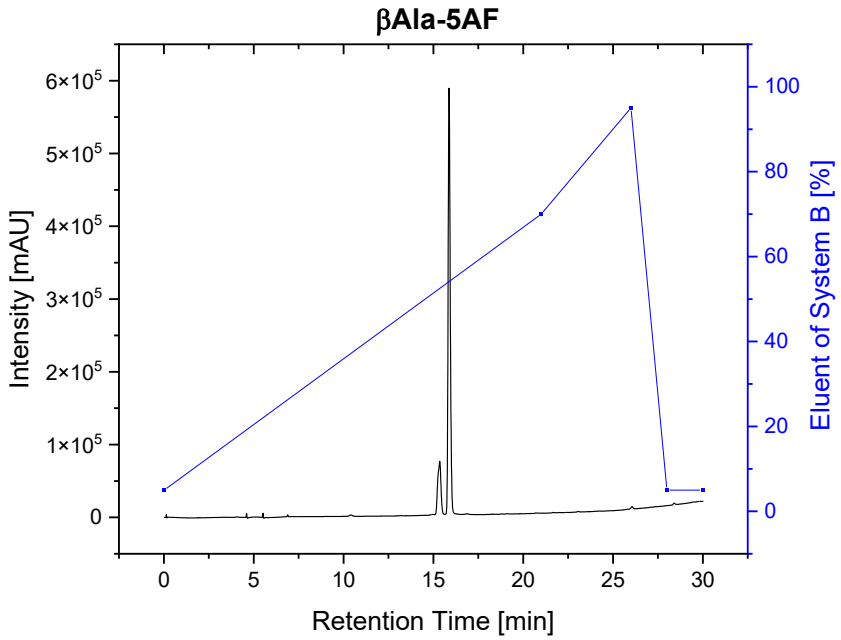

***Figure 176**: Analytical HPLC of βAla-5AF, Nucleosil C18 (5 µm, 4.6 mm x 25 mm), H_2O with 0.1% TFA (system A) / 80% MeCN-20% H_2O and 0.1 % TFA (system B), 1 mL/min, 0.02 min - 5% eluent of system B, 21 min - 70% eluent of system B, t_R = 15.9 min. The minor peak at t_R 15.2 min indicates the presence of an impurity with the same exact mass of the product.*

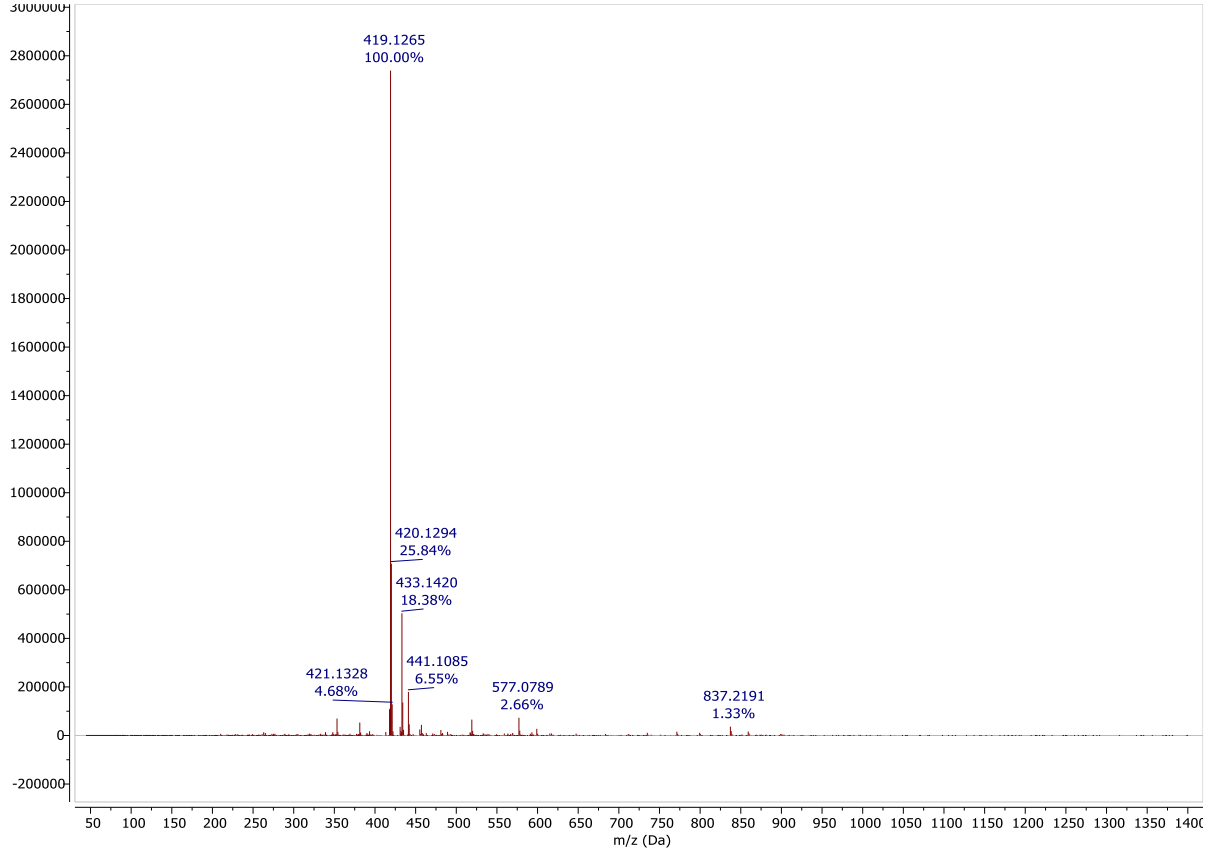

***Figure 177**: HR-ESI MS of βAla-5AF, positive mode*

9.28 Fol-βAla-5AF (FP 21)

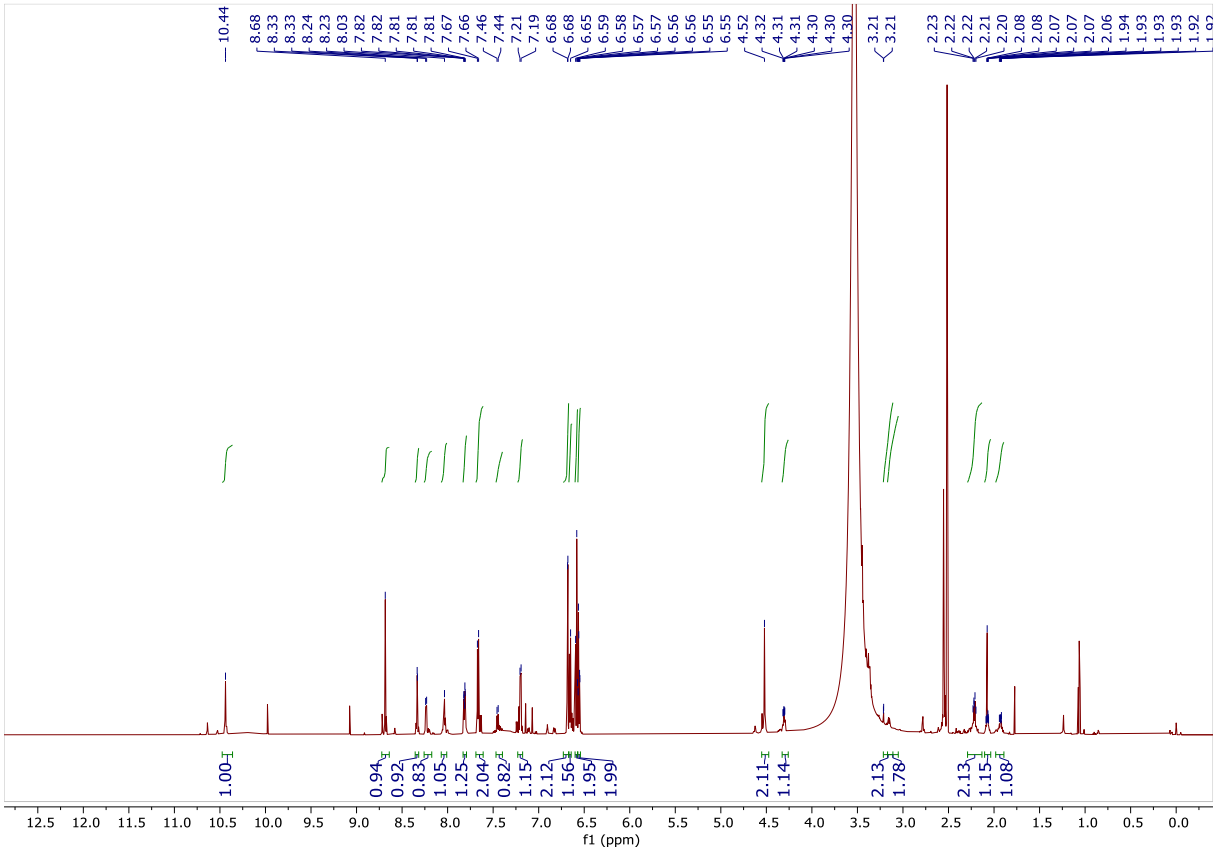

***Figure 178**: [1]H-NMR of Fol-βAla-5AF (FP 21), 700 MHz, DMSO-d_6*

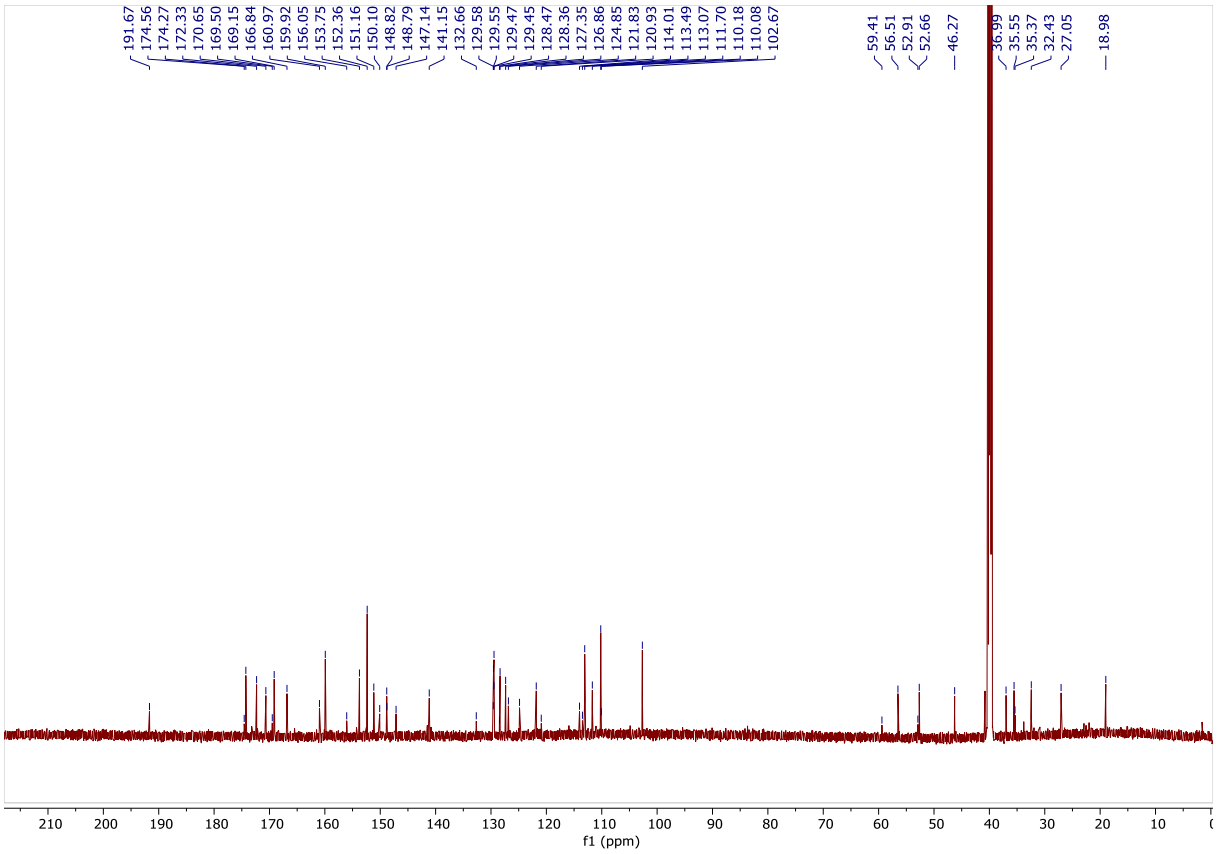

***Figure 179**: [13]C-NMR of Fol-βAla-5AF (FP 21), 176 MHz, DMSO-d_6, the aliphatic region of the spectrum exhibits additional signals due to the presence of γ and α isomers of the product.*

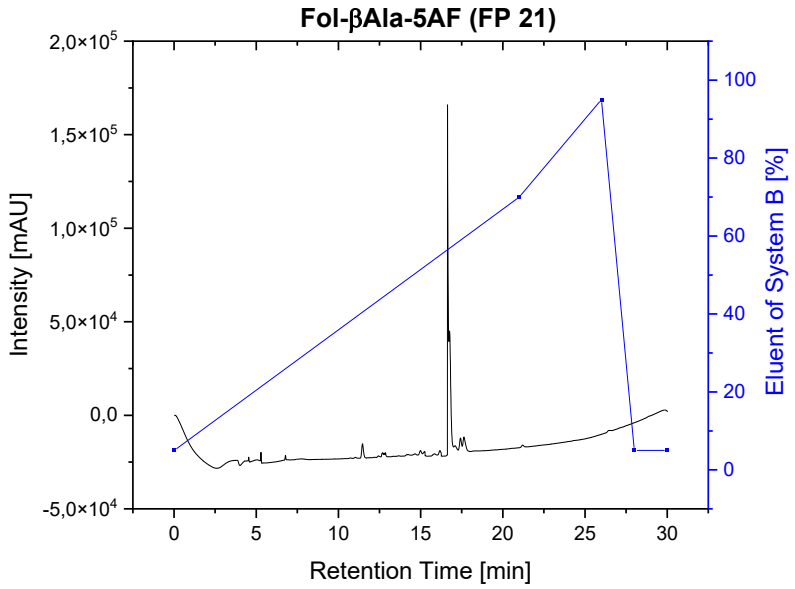

***Figure 180**: Analytical HPLC of Fol-βAla-5AF (FP 21), Nucleosil C18 (5 µm, 4.6 mm x 25 mm), H_2O with 0.1% TFA (system A) / 80% MeCN-20% H_2O and 0.1 % TFA (system B), 1 mL/min, 0.02 min - 5% eluent of system B, 21 min - 70% eluent of system B, t_R = 16.6 min.*

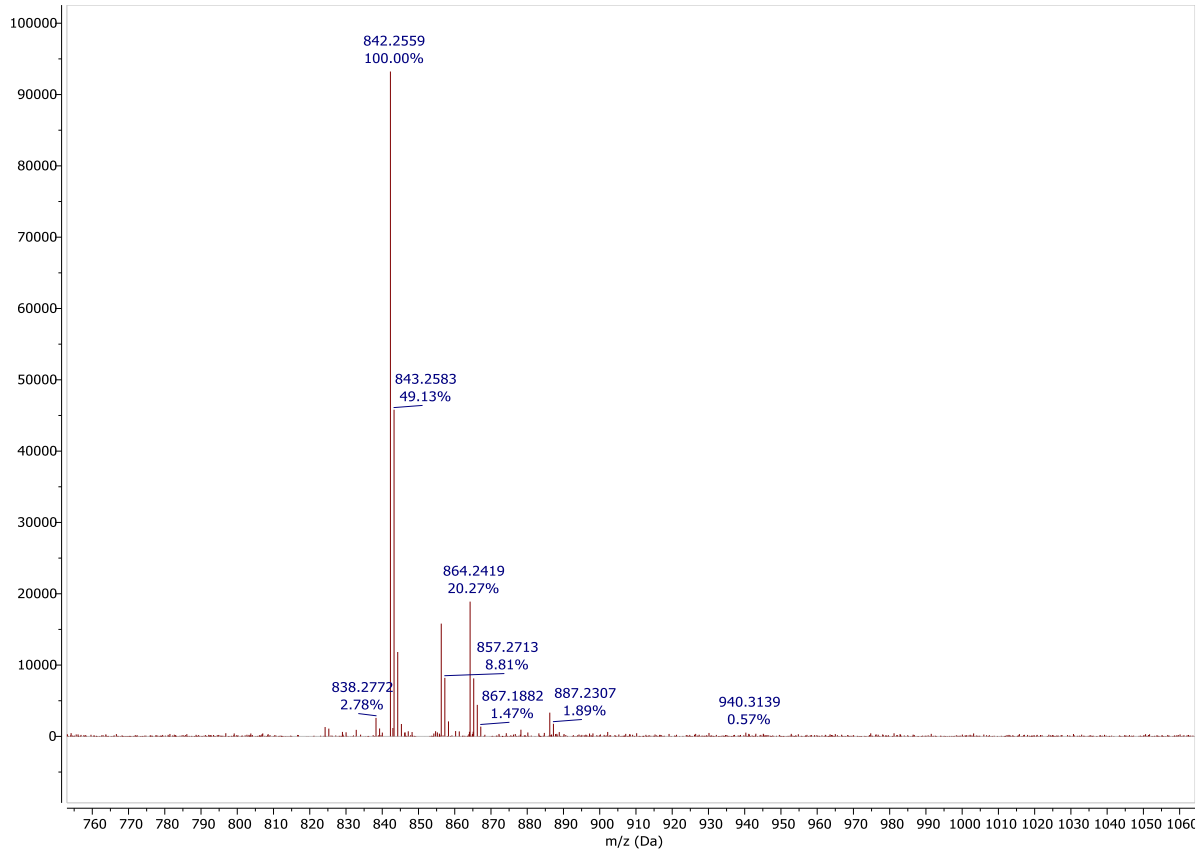

***Figure 181**: HR-ESI MS of Fol-βAla-5AF (FP 21), positive mode*

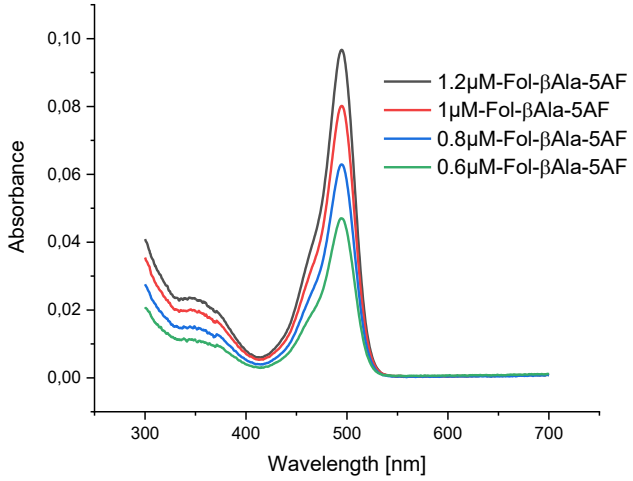

***Figure 182**: Absorption spectra of Fol-βAla-5AF (FP 21) in 4 different concentrations, PBS (pH=7.4)*

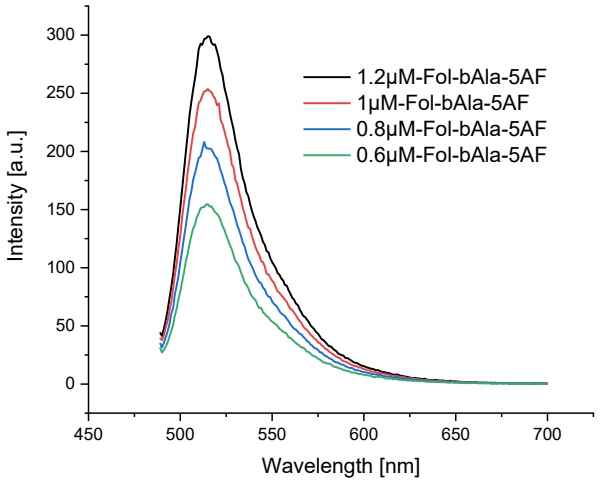

***Figure 183**: Fluorescence emission spectra of Fol-βAla-5AF (FP 21) in 4 different concentrations, PBS (pH=7.4), Excitation wavelength: 480 nm.*

10. List of References

[1] Nawaz, F. Z.; Kipreos, E. T. Emerging roles for folate receptor FOLR1 in signaling and cancer. *Trends Endocrinol Metab* **2022**, *33* (3), 159-174. DOI: 10.1016/j.tem.2021.12.003 From NLM Medline.
[2] Donkor, M.; Choe, J. Y.; Reid, D. M.; Fiadjoe, H. K.; Quinn, B.; Ranjan, A.; Pulse, M.; Chaudhary, P.; Basha, R.; Jones, H. P. Surgical Primary Tumor Resection Reduces Accumulation of CD11b(+) Myeloid Cells in the Lungs Augmenting the Efficacy of an Intranasal Cancer Vaccination against Secondary Lung Metastasis. *Pharmaceuticals (Basel)* **2023**, *17* (1). DOI: 10.3390/ph17010051 From NLM PubMed-not-MEDLINE.
[3] Parrish-Novak, J.; Holland, E. C.; Olson, J. M. Image-Guided Tumor Resection. *Cancer Journal* **2015**, *21* (3), 206-212. DOI: 10.1097/Ppo.0000000000000113.
[4] Detterbeck, F. C.; Ostrowski, M.; Hoffmann, H.; Rami-Porta, R.; Osarogiagbon, R. U.; Donnington, J.; Infante, M.; Marino, M.; Marom, E. M.; Nakajima, J.; et al. The International Association for the Study of Lung Cancer Lung Cancer Staging Project: Proposals for Revision of the Classification of Residual Tumor After Resection for the Forthcoming (Ninth) Edition of the TNM Classification of Lung Cancer. *J Thorac Oncol* **2024**, *19* (7), 1052-1072. DOI: 10.1016/j.jtho.2024.03.021 From NLM Medline.
[5] Chaubal, R.; Gardi, N.; Joshi, S.; Pantvaidya, G.; Kadam, R.; Vanmali, V.; Hawaldar, R.; Talker, E.; Chitra, J.; Gera, P.; et al. Surgical Tumor Resection Deregulates Hallmarks of Cancer in Resected Tissue and the Surrounding Microenvironment. *Mol Cancer Res* **2024**, *22* (6), 572-584. DOI: 10.1158/1541-7786.MCR-23-0265 From NLM Medline.
[6] Pal, K.; Heinsch, A.; Berkessel, A.; Koner, A. L. Differentiation of Folate-Receptor-Positive and -Negative Cells Using a Substrate-Mimicking Fluorescent Probe. *Chemistry* **2017**, *23* (60), 15008-15011. DOI: 10.1002/chem.201703305 From NLM PubMed-not-MEDLINE.
[7] Bellotti, E.; Cascone, M. G.; Barbani, N.; Rossin, D.; Rastaldo, R.; Giachino, C.; Cristallini, C. Targeting Cancer Cells Overexpressing Folate Receptors with New Terpolymer-Based Nanocapsules: Toward a Novel Targeted DNA Delivery System for Cancer Therapy. *Biomedicines* **2021**, *9* (9). DOI: 10.3390/biomedicines9091275 From NLM PubMed-not-MEDLINE.
[8] Maurer, A. H.; Elsinga, P.; Fanti, S.; Nguyen, B.; Oyen, W. J.; Weber, W. A. Imaging the folate receptor on cancer cells with 99mTc-etarfolatide: properties, clinical use, and future potential of folate receptor imaging. *J Nucl Med* **2014**, *55* (5), 701-704. DOI: 10.2967/jnumed.113.133074 From NLM Medline.
[9] Duthie, S. J.; Narayanan, S.; Blum, S.; Pirie, L.; Brand, G. M. Folate deficiency in vitro induces uracil misincorporation and DNA hypomethylation and inhibits DNA excision repair in immortalized normal human colon epithelial cells. *Nutr Cancer* **2000**, *37* (2), 245-251. DOI: 10.1207/S15327914NC372_18 From NLM Medline.
[10] Duthie, S. J. Folate and cancer: how DNA damage, repair and methylation impact on colon carcinogenesis. *J Inherit Metab Dis* **2011**, *34* (1), 101-109. DOI: 10.1007/s10545-010-9128-0 From NLM Medline.
[11] Cao, X.; Xu, J.; Lin, Y. L.; Cabrera, R. M.; Chen, Q.; Zhang, C.; Steele, J. W.; Han, X.; Gross, S. S.; Wlodarczyk, B. J.; et al. Excess folic acid intake increases DNA de novo point mutations. *Cell Discov* **2023**, *9* (1), 22. DOI: 10.1038/s41421-022-00512-0 From NLM PubMed-not-MEDLINE.
[12] Carron, P. M.; Crowley, A.; O'Shea, D.; McCann, M.; Howe, O.; Hunt, M.; Devereux, M. Targeting the Folate Receptor: Improving Efficacy in Inorganic

Medicinal Chemistry. *Curr Med Chem* **2018**, *25* (23), 2675-2708. DOI: 10.2174/0929867325666180209143715 From NLM Medline.
[13] Revuelta, J. L.; Serrano-Amatriain, C.; Ledesma-Amaro, R.; Jiménez, A. Formation of folates by microorganisms: towards the biotechnological production of this vitamin. *Applied Microbiology and Biotechnology* **2018**, *102* (20), 8613-8620. DOI: 10.1007/s00253-018-9266-0.
[14] Ewa Cieślik, I. C. Occurrence and significance of folic acid. *De Gruyter* **2018**, *29*.
[15] Chen, C.; Ke, J.; Zhou, X. E.; Yi, W.; Brunzelle, J. S.; Li, J.; Yong, E. L.; Xu, H. E.; Melcher, K. Structural basis for molecular recognition of folic acid by folate receptors. *Nature* **2013**, *500* (7463), 486-489. DOI: 10.1038/nature12327 From NLM Medline.
[16] Bettio, A.; Honer, M.; Muller, C.; Bruhlmeier, M.; Muller, U.; Schibli, R.; Groehn, V.; Schubiger, A. P.; Ametamey, S. M. Synthesis and preclinical evaluation of a folic acid derivative labeled with 18F for PET imaging of folate receptor-positive tumors. *J Nucl Med* **2006**, *47* (7), 1153-1160. From NLM Medline.
[17] Frigerio, B.; Bizzoni, C.; Jansen, G.; Leamon, C. P.; Peters, G. J.; Low, P. S.; Matherly, L. H.; Figini, M. Folate receptors and transporters: biological role and diagnostic/therapeutic targets in cancer and other diseases. *J Exp Clin Cancer Res* **2019**, *38* (1), 125. DOI: 10.1186/s13046-019-1123-1 From NLM Medline.
[18] Gonzalez, T.; Muminovic, M.; Nano, O.; Vulfovich, M. Folate Receptor Alpha-A Novel Approach to Cancer Therapy. *Int J Mol Sci* **2024**, *25* (2). DOI: 10.3390/ijms25021046 From NLM Medline.
[19] Fernandez, M.; Javaid, F.; Chudasama, V. Advances in targeting the folate receptor in the treatment/imaging of cancers. *Chem Sci* **2018**, *9* (4), 790-810. DOI: 10.1039/c7sc04004k From NLM PubMed-not-MEDLINE.
[20] Madduri Srinivasarao, C. V. G. P. S. L. Principles in the design of ligandtargeted cancer therapeutics and imaging agents. *Nature Reviews Drug Discovery* **2015**.
[21] Tummers, Q. R.; Hoogstins, C. E.; Gaarenstroom, K. N.; de Kroon, C. D.; van Poelgeest, M. I.; Vuyk, J.; Bosse, T.; Smit, V. T.; van de Velde, C. J.; Cohen, A. F.; et al. Intraoperative imaging of folate receptor alpha positive ovarian and breast cancer using the tumor specific agent EC17. *Oncotarget* **2016**, *7* (22), 32144-32155. DOI: 10.18632/oncotarget.8282 From NLM Medline.
[22] De Jesus, E.; Keating, J. J.; Kularatne, S. A.; Jiang, J.; Judy, R.; Predina, J.; Nie, S.; Low, P.; Singhal, S. Comparison of Folate Receptor Targeted Optical Contrast Agents for Intraoperative Molecular Imaging. *Int J Mol Imaging* **2015**, *2015*, 469047. DOI: 10.1155/2015/469047 From NLM PubMed-not-MEDLINE.
[23] Ullah, Z.; Roy, S.; Muhammad, S.; Yu, C.; Huang, H.; Chen, D.; Long, H.; Yang, X.; Du, X.; Guo, B. Fluorescence imaging-guided surgery: current status and future directions. *Biomater Sci* **2024**, *12* (15), 3765-3804. DOI: 10.1039/d4bm00410h From NLM Medline.
[24] Predina, J. D.; Newton, A. D.; Keating, J.; Dunbar, A.; Connolly, C.; Baldassari, M.; Mizelle, J.; Xia, L.; Deshpande, C.; Kucharczuk, J.; et al. A Phase I Clinical Trial of Targeted Intraoperative Molecular Imaging for Pulmonary Adenocarcinomas. *Ann Thorac Surg* **2018**, *105* (3), 901-908. DOI: 10.1016/j.athoracsur.2017.08.062 From NLM Medline.
[25] Trials.gov, C. Intra-op Detection of Occult Ovarian Carcinoma Using a Folate-Alpha Receptor Specific Fluorescent Ligand. *U. S. Natinal Libarary of Medicine* **Last Update Posted 2020-11-12**. (acccessed 14.08.2024).
[26] Roshani A Patil, M. S., Mansoor M Amiji, Philip S Low, Mark Niedre. Fluorescence Labeling of Circulating Tumor Cells with a Folate Receptor-Targeted Molecular Probe for Diffuse In Vivo Flow Cytometry. *Mol Imaging Biol.*

2020, *22 (5)*. DOI: 10.1007/s11307-020-01505-9.
[27] Trials.gov, C. *OTL38 for Intraoperative Imaging of Folate Receptor Positive Lung Nodules*; U.S. National Library of Medicine, Last Update Posted 2023-03-23. https://clinicaltrials.gov/ct2/show/NCT04241315 (accessed 14.08.2024).
(28) Low, P. S.; Henne, W. A.; Doorneweerd, D. D. Discovery and development of folic-acid-based receptor targeting for imaging and therapy of cancer and inflammatory diseases. *Acc Chem Res* **2008**, *41* (1), 120-129. DOI: 10.1021/ar7000815 From NLM Medline.
[29] Wang, Q.; Guan, J. K.; Wan, J. L.; Li, Z. F. Disulfide based prodrugs for cancer therapy. *Rsc Adv* **2020**, *10* (41), 24397-24409. DOI: 10.1039/d0ra04155f.
[30] Feng, D.; Song, Y. C.; Shi, W.; Li, X. H.; Ma, H. M. Distinguishing Folate-Receptor-Positive Cells from Folate-Receptor-Negative Cells Using a Fluorescence Off-On Nanoprobe. *Anal Chem* **2013**, *85* (13), 6530-6535. DOI: 10.1021/ac401377n.
[31] Zhang, Y.; Zhou, J.; Yang, C.; Wang, W.; Chu, L.; Huang, F.; Liu, Q.; Deng, L.; Kong, D.; Liu, J.; et al. Folic acid-targeted disulfide-based cross-linking micelle for enhanced drug encapsulation stability and site-specific drug delivery against tumors. *Int J Nanomedicine* **2016**, *11*, 1119-1130. DOI: 10.2147/IJN.S101649 From NLM Medline.
[32] Yang, Z.; Lee, J. H.; Jeon, H. M.; Han, J. H.; Park, N.; He, Y.; Lee, H.; Hong, K. S.; Kang, C.; Kim, J. S. Folate-based near-infrared fluorescent theranostic gemcitabine delivery. *J Am Chem Soc* **2013**, *135* (31), 11657-11662. DOI: 10.1021/ja405372k From NLM Medline.
[33] Lee, M. H.; Sessler, J. L.; Kim, J. S. Disulfide-Based Multifunctional Conjugates for Targeted Theranostic Drug Delivery. *Accounts Chem Res* **2015**, *48* (11), 2935-2946. DOI: 10.1021/acs.accounts.5b00406.
[34] Atkins. *Physikalische Chemie*; Wiley-VCH Verlag, 2013.
[35] Lakowicz, J. R. *Principles of Fluorescence Spectroscopy*; Springer US, 2006.
[36] Photophysics of fluorescent proteins,. https://www.ibs.fr/fr/recherche/assemblage-dynamique-et-reactivite/groupe-imagerie-integree-de-la-reponse-au-stress/equipe-pixel/methodes/fluorescent-proteins?lang=fr. 05.08.2024.
[37] Jiwoong Kwon, M. S. E., and Sang-Hee Shim. Bleaching-Resistant Super-resolution Fluorescence Microscopy. *Adv Sci* **2022 Mar**, *9(9): 2101817*.
[38] Kalies, S.; Kuetemeyer, K.; Heisterkamp, A. Mechanisms of high-order photobleaching and its relationship to intracellular ablation. *Biomed Opt Express* **2011**, *2* (4), 805-816. DOI: 10.1364/boe.2.000816 From NLM.
[39] Green, C. M.; Sementa, D.; Mathur, D.; Melinger, J. S.; Deshpande, P.; Elbaum-Garfinkle, S.; Medintz, I. L.; Ulijn, R. V.; Diaz, S. A. Sequestration within peptide coacervates improves the fluorescence intensity, kinetics, and limits of detection of dye-based DNA biosensors. *Commun Chem* **2024**, *7* (1), 49. DOI: 10.1038/s42004-024-01124-3 From NLM PubMed-not-MEDLINE.
[40] Kwon, J.; Elgawish, M. S.; Shim, S. H. Bleaching-Resistant Super-Resolution Fluorescence Microscopy. *Adv Sci (Weinh)* **2022**, *9* (9), e2101817. DOI: 10.1002/advs.202101817 From NLM Medline.
[41] Tang, Y.; Zhao, Y.; Lin, W. Preparation of robust fluorescent probes for tracking endogenous formaldehyde in living cells and mouse tissue slices. *Nature Protocols* **2020**, *15* (10), 3499-3526. DOI: 10.1038/s41596-020-0384-7.
[42] Panchuk-Voloshina, N.; Haugland, R. P.; Bishop-Stewart, J.; Bhalgat, M. K.; Millard, P. J.; Mao, F.; Leung, W. Y.; Haugland, R. P. Alexa dyes, a series of new fluorescent dyes that yield exceptionally bright, photostable conjugates. *J Histochem*

Cytochem **1999**, *47* (9), 1179-1188. DOI: 10.1177/002215549904700910 From NLM.
[43] Drummen, G. P. C. Fluorescent Probes and Fluorescence (Microscopy) Techniques-Illuminating Biological and Biomedical Research. *Molecules* **2012**.
[44] Patterson, G.; Davidson, M.; Manley, S.; Lippincott-Schwartz, J. Superresolution imaging using single-molecule localization. *Annu Rev Phys Chem* **2010**, *61*, 345-367. DOI: 10.1146/annurev.physchem.012809.103444 From NLM.
[45] Fukaminato, T.; Ishida, S.; Métivier, R. Photochromic fluorophores at the molecular and nanoparticle levels: fundamentals and applications of diarylethenes. *Npg Asia Mater* **2018**, *10*, 859-881. DOI: 10.1038/s41427-018-0075-9.
[46] Tanifuji, N.; Irie, M.; Matsuda, K. New photoswitching unit for magnetic interaction: diarylethene with 2,5-bis(arylethynyl)-3-thienyl group. *J Am Chem Soc* **2005**, *127* (38), 13344-13353. DOI: 10.1021/ja053200p From NLM Medline.
[47] Mostaghimi, M.; Pacheco Hernandez, H.; Jiang, Y.; Wenzel, W.; Heinke, L.; Kozlowska, M. On-off conduction photoswitching in modelled spiropyran-based metal-organic frameworks. *Commun Chem* **2023**, *6* (1), 275. DOI: 10.1038/s42004-023-01072-4 From NLM PubMed-not-MEDLINE.
[48] Rad, J. K.; Balzade, Z.; Mahdavian, A. R. Spiropyran-based advanced photoswitchable materials: A fascinating pathway to the future stimuli-responsive devices. *J Photoch Photobio C* **2022**, *51*. DOI: ARTN 100487

10.1016/j.jphotochemrev.2022.100487.
[49] Fleming, C. L.; Li, S.; Grotli, M.; Andreasson, J. Shining New Light on the Spiropyran Photoswitch: A Photocage Decides between cis- trans or Spiro-Merocyanine Isomerization. *J Am Chem Soc* **2018**, *140* (43), 14069-14072. DOI: 10.1021/jacs.8b09523 From NLM PubMed-not-MEDLINE.
[50] Benôit Roubinet; Matthias Bischoff; Shamil Nizamov; Sergey Yan; Claudia Geisler; Hell, a. S. W. Photoactivatable Rhodamine Spiroamides and DiazoketonesDecorated with “Universal Hydrophilizer” or Hydroxyl Groups. *American Chemical Society* **2018**. DOI: 10.1021/acs.joc.8b00756J.
[51] Belov, V. N.; Bossi, M. L.; Folling, J.; Boyarskiy, V. P.; Hell, S. W. Rhodamine spiroamides for multicolor single-molecule switching fluorescent nanoscopy. *Chemistry* **2009**, *15* (41), 10762-10776. DOI: 10.1002/chem.200901333 From NLM Medline.
[52] Sarwat B. Rizvi, S. G., Mo Keshtgar & Alexander M. Seifalian. Semiconductor quantum dots as fluorescent probes for in vitro and in vivo bio-molecular and cellular imaging. *Nano Reviews* **2010**. DOI: 10.3402/nano.v1i0.5161.
[53] Barroso, M. M. Quantum Dots in Cell Biology. *Journal of Histochemistry & Cytochemistry* **2010**, *59(3)*. DOI: 10.1369/0022155411398487.
[54] Zeng, M.-X. Z. a. E.-Z. Application of functional quantum dot nanoparticles as fluorescence probes in cell labeling and tumor diagnostic imaging. *Nanoscale Research Letters* **2015**. DOI: 10.1186/s11671-015-0873-8.
[55] Xiaohu Gao, Y. C., Richard M Levenson, Leland W K Chung & Shuming Nie. In vivo cancer targeting and imaging with semiconductor quantum dots. *nature biotechnology* **2004**, *22*.
[56] Sulaxna Pandey, D. B. High-quality quantumdots for multiplexed bioimaging: A critical review. *Advances in Colloid and Interface Science* **2020**, *278*. DOI: https://doi.org/10.1016/j.cis.2020.102137.
[57] Dootz, K. Folaterezeptor-vermittelte,selektive Markierung von Krebszellen. Disseration, Heidelberg, 2017-2020.

[58] Zhang, X. F.; Zhang, J.; Liu, L. Fluorescence properties of twenty fluorescein derivatives: lifetime, quantum yield, absorption and emission spectra. *J Fluoresc* **2014**, *24* (3), 819-826. DOI: 10.1007/s10895-014-1356-5 From NLM PubMed-not-MEDLINE.
[59] Lee, H.; Kim, J.; Kim, H.; Kim, Y.; Choi, Y. A folate receptor-specific activatable probe for near-infrared fluorescence imaging of ovarian cancer. *Chem Commun (Camb)* **2014**, *50* (56), 7507-7510. DOI: 10.1039/c4cc02301c From NLM Medline.
[60] Kellnerova, S.; Huber, S.; Massri, M.; Fleischer, V.; Losso, K.; Sarg, B.; Kremser, L.; Talasz, H.; He, X.; Varrone, E.; et al. Enzymatic Cleavage of Stx2a in the Gut and Identification of Pancreatic Elastase and Trypsin as Possible Main Cleavers. *Microorganisms* **2023**, *11* (10). DOI: 10.3390/microorganisms11102487 From NLM PubMed-not-MEDLINE.
[61] He, H.; Wang, J.; Wang, H.; Zhou, N.; Yang, D.; Green, D. R.; Xu, B. Enzymatic Cleavage of Branched Peptides for Targeting Mitochondria. *J Am Chem Soc* **2018**, *140* (4), 1215-1218. DOI: 10.1021/jacs.7b11582 From NLM Medline.
[62] Farahani, P. E.; Adelmund, S. M.; Shadish, J. A.; DeForest, C. A. Photomediated oxime ligation as a bioorthogonal tool for spatiotemporally-controlled hydrogel formation and modification. *J Mater Chem B* **2017**, *5* (23), 4435-4442. DOI: 10.1039/c6tb03400d From NLM PubMed-not-MEDLINE.
[63] Hering, A.; Braga Emidio, N.; Muttenthaler, M. Expanding the versatility and scope of the oxime ligation: rapid bioconjugation to disulfide-rich peptides. *Chem Commun (Camb)* **2022**, *58* (65), 9100-9103. DOI: 10.1039/d2cc03752a From NLM Medline.
[64] Datta, D.; Mori, S.; Madaoui, M.; Wassarman, K.; Zlatev, I.; Manoharan, M. Aminooxy Click Chemistry as a Tool for Bis-homo and Bis-hetero Ligand Conjugation to Nucleic Acids. *Org Lett* **2022**, *24* (25), 4496-4501. DOI: 10.1021/acs.orglett.2c00988 From NLM Medline.
[65] Kolmel, D. K.; Kool, E. T. Oximes and Hydrazones in Bioconjugation: Mechanism and Catalysis. *Chem Rev* **2017**, *117* (15), 10358-10376. DOI: 10.1021/acs.chemrev.7b00090 From NLM Medline.
[66] Collins, J.; Xiao, Z. Y.; Müllner, M.; Connal, L. A. The emergence of oxime click chemistry and its utility in polymer science. *Polym Chem-Uk* **2016**, *7* (23), 3812-3826. DOI: 10.1039/c6py00635c.
[67] Bahta, M.; Burke, T. R., Jr. Oxime-based click chemistry in the development of 3-isoxazolecarboxylic acid containing inhibitors of Yersinia pestis protein tyrosine phosphatase, YopH. *ChemMedChem* **2011**, *6* (8), 1363-1370. DOI: 10.1002/cmdc.201100200 From NLM Medline.
[68] Wang, L.; Wang, S.; Tang, J.; Espinoza, V. B.; Loredo, A.; Tian, Z.; Weisman, R. B.; Xiao, H. Oxime as a general photocage for the design of visible light photo-activatable fluorophores. *Chem Sci* **2021**, *12* (47), 15572-15580. DOI: 10.1039/d1sc05351e From NLM PubMed-not-MEDLINE.
[69] Wan, Z.; Yu, S.; Wang, Q.; Sambath, K.; Harty, R.; Liu, X.; Chen, H.; Wang, C.; Liu, X.; Zhang, Y. Far-red BODIPY-based oxime esters: photo-uncaging and drug delivery. *J Mater Chem B* **2023**, *11* (41), 9889-9893. DOI: 10.1039/d3tb01867a From NLM Medline.
[70] Anger, P.; Bharadwaj, P.; Novotny, L. Enhancement and quenching of single-molecule fluorescence. *Phys Rev Lett* **2006**, *96* (11), 113002. DOI: 10.1103/PhysRevLett.96.113002 From NLM PubMed-not-MEDLINE.
[71] Lee, H.; Kim, H. J. Novel fluorescent probe for the selective detection of organophosphorous nerve agents through a cascade reaction from oxime to nitrile

via isoxazole. *Tetrahedron* **2014**, *70* (18), 2966-2970. DOI: 10.1016/j.tet.2014.03.026.
[72] Okamura, H.; Iida, M.; Kaneyama, Y.; Nagatsugi, F. o-Nitrobenzyl Oxime Ethers Enable Photoinduced Cyclization Reaction to Provide Phenanthridines under Aqueous Conditions. *Organic Letters* **2023**, *25* (3), 466-470. DOI: 10.1021/acs.orglett.2c04015.
[73] Yin, W. Q.; Wang, X. L. Recent advances in iminyl radical-mediated catalytic cyclizations and ring-opening reactions. *New J Chem* **2019**, *43* (8), 3254-3264. DOI: 10.1039/c8nj06165c.
[74] Shi, W. J.; Lo, P. C.; Zhao, S.; Wong, R. C.; Wang, Q.; Fong, W. P.; Ng, D. K. A biotin-conjugated glutathione-responsive FRET-based fluorescent probe with a ferrocenyl BODIPY as the dark quencher. *Dalton Trans* **2016**, *45* (44), 17798-17806. DOI: 10.1039/c6dt03141b From NLM Medline.
[75] Zhang, Y.; Xia, S.; Wan, S.; Steenwinkel, T. E.; Vohs, T.; Luck, R. L.; Werner, T.; Liu, H. Ratiometric Detection of Glutathione Based on Disulfide Linkage Rupture between a FRET Coumarin Donor and a Rhodamine Acceptor. *Chembiochem* **2021**, *22* (13), 2282-2291. DOI: 10.1002/cbic.202100108 From NLM Medline.
[76] Solidoro, R.; Centonze, A.; Miciaccia, M.; Baldelli, O. M.; Armenise, D.; Ferorelli, S.; Perrone, M. G.; Scilimati, A. Fluorescent imaging probes for in vivo ovarian cancer targeted detection and surgery. *Medicinal Research Reviews n/a* (n/a). DOI: https://doi.org/10.1002/med.22027.
[77] Kralova, J.; Jurasek, M.; Miksatkova, L.; Maresova, A.; Fahnrich, J.; Cihlarova, P.; Drasar, P.; Bartunek, P.; Kral, V. Influence of fluorophore and linker length on the localization and trafficking of fluorescent sterol probes. *Sci Rep* **2020**, *10* (1), 22053. DOI: 10.1038/s41598-020-78085-9 From NLM PubMed-not-MEDLINE.
[78] Figliola, C.; Marchal, E.; Groves, B. R.; Thompson, A. A step-wise synthetic approach is necessary to access gamma-conjugates of folate: folate-conjugated prodigiosenes. *Rsc Adv* **2019**, *9* (25), 14078-14092. DOI: 10.1039/c9ra01435g From NLM PubMed-not-MEDLINE.
[79] Organization, W. H. *Serum and red blood cell folate concentrations for assessing folate status in populations*; 2012. http://apps.who.int/iris/bitstream/10665/75584/1/WHO_NMH_NHD_EPG_12.1_eng.pdf.
[80] Konig, S. G.; Kramer, R. Accessing Structurally Diverse Near-Infrared Cyanine Dyes for Folate Receptor-Targeted Cancer Cell Staining. *Chemistry* **2017**, *23* (39), 9306-9312. DOI: 10.1002/chem.201700026 From NLM Medline.
[81] Ettenauer, J.; Semak, V.; Brandl, M.; . Synthesis of Fluorescein Aldehydes for the Sensitive Detection of L-Cysteine. *proceedings* **2018**. DOI: doi:10.3390/proceedings2130895.
[82] Kulak*a, C. W. a. N. Fluorophore ATCUN complexes: combining agent and probe for oxidative DNA cleavage. *chemical comunications* **2015**.
[83] Gasparini, G.; Sargsyan, G.; Bang, E. K.; Sakai, N.; Matile, S. Ring Tension Applied to Thiol-Mediated Cellular Uptake. *Angew Chem Int Ed Engl* **2015**, *54* (25), 7328-7331. DOI: 10.1002/anie.201502358 From NLM Medline.
[84] Gentsch, R.; Pippig, F.; Nilles, K.; Theato, P.; Kikkeri, R.; Maglinao, M.; Lepenies, B.; Seeberger, P. H.; Börner, H. G. Modular Approach toward Bioactive Fiber Meshes Carrying Oligosaccharides. *Macromolecules* **2010**, *43* (22), 9239-9247. DOI: 10.1021/ma101607a.
[85] Nie, Y. Near infrared fluorescent dye based on cyanine dye fluorescent group as skeleton, and preparing method and application thereof. China, CN107266929 2017-10-20.

[86] Zhao, F.; Yin, H.; Zhang, Z.; Li, J. Folic acid modified cationic gamma-cyclodextrin-oligoethylenimine star polymer with bioreducible disulfide linker for efficient targeted gene delivery. *Biomacromolecules* **2013**, *14* (2), 476-484. DOI: 10.1021/bm301718f From NLM Medline.
[87] Zhukova, O. V.; Bulgakova, S. A. Synthesis of a Polymeric Doxorubicin Derivative and its Evaluation Using IR and UV Spectroscopy. *Pharm Chem J+* **2015**, *48* (12), 830-834. DOI: 10.1007/s11094-015-1204-1.
[88] Yamamoto, S.; Kitahata, S.; Shimomura, A.; Tokuda, K.; Nishino, T.; Maruyama, T. Surfactant-induced polymer segregation to produce antifouling surfaces via dip-coating with an amphiphilic polymer. *Langmuir* **2015**, *31* (1), 125-131. DOI: 10.1021/la5043712.

11. Acknowledgment

I would like to take this opportunity to thank all the individuals who contributed to the successful completion of this dissertation.

First, I want to thank **Prof. Dr. Roland Krämer** for welcoming me into his research group, providing excellent working conditions, and guiding me with a fascinating research topic. His support, insights, and the freedom he allowed me in my work were invaluable for my growth as a scientist and as a person.

I am also deeply grateful to **Prof. Dr. Peter Comba** for accepting to be my second reviewer and for providing me with the opportunity to collaborate on the computational calculations of the photophysical properties of FP 19 and FP 20.

I would like to thank **Dr. Dumitru Arian** for his exceptional support and guidance throughout my doctoral research. His scientific expertise and constant help during difficult moments were invaluable. I am especially grateful for the time he dedicated to reviewing and for proofreading my thesis. His support has been truly decisive in my progress.

I am truly thankful to **Dr. Matthias Hofmann** for his excellent organization of the Lehramtspraktikum and for his amazing Christmas baking, which brightened every holiday season. I also want to thank **Prof. Dr. Franziska Thomas** for her thoughtful advice, encouragement, and positive attitude, which were always inspiring.

I am deeply grateful to my colleague **Claudia Dienemann** for her unwavering support, insightful conversations, and help with numerous ESI measurements. I also want to thank her for the fun moments we shared, which I truly miss. Her presence made the work environment much brighter and more enjoyable.

I would also like to thank **Christina Giese**, for the great collaboration in the lab. I am especially grateful for the delicious baked almonds she always made for me, such a kind and thoughtful gesture that I truly appreciated.

I am thankful to **Ulrich Warttinger**, and **Jeannette Grosse** for their kind conversations and support throughout this work. My appreciation also extends to my colleagues, **Kathrin**, **Nora**, **Mahmud, Marlin, Maryam, Miles, Ramin, Sara**, and **Stefan.** The enjoyable moments we shared, particularly our conversations in the coffee room, made lunch breaks some of the happiest and most memorable parts of my day. Special

thanks to **Ramin** for proofreading my thesis and offering valuable feedback that greatly enhanced its quality.

I would also like to thank **Frau Beate Termin** for conducting countless NMR measurements. My thanks also go to the **Nikon Imaging Center** at Heidelberg University, particularly **Dr. Christian Ackermann**, for their assistance with confocal microscopy.

I am also grateful to **Dr. Barbara Schamberger** for sharing her expertise in confocal microscopy, answering my questions, and offering practical tips that significantly improved my work.

Furthermore, I would like to thank my Bachelor students **Leonie** and **Moritz**, as well as my research interns **Elisabeth**, **Miguel**, **Lars**, **Fabricio**, **Ronja**, and **Maedeh**, for their excellent collaboration and the enjoyable time we shared in the lab.

I am deeply thankful to my close friends **Rafat**, **Kianush**, **Elham**, and **Farbod**. Their support and encouragement provided me with strength and balance during this journey. The time spent with them brought immense joy and comfort.

Finally, I would like to express my profound gratitude to **my parents** and especially to my husband, **Amir**, whose love and support were the foundation of this achievement. Without his encouragement and understanding, this work would not have been possible.

12. Sworn Affidavit according to § 8 of the doctoral degree regulations of the Combined Faculty of Mathematics, Engineering and Natural Sciences at the Heidelberg University

1. The thesis I have submitted entitled …**Folate-Conjugated Fluorescent Probes for Enhanced Selective Labeling of Cancer Cells** is my own work.

2. I have only used the sources indicated and have not made unauthorised use of services of a third party. Where the work of others has been quoted or reproduced, the source is always given.

3. I have not yet presented this thesis or parts thereof to a university as part of an examination or degree.

4. I confirm that the declarations made above are correct.

5. I am aware of the importance of a sworn affidavit and the criminal prosecution in case of a false or incomplete affidavit.

I affirm that the above is the absolute truth to the best of my knowledge and that I have not concealed anything.

……

Place and date Signature